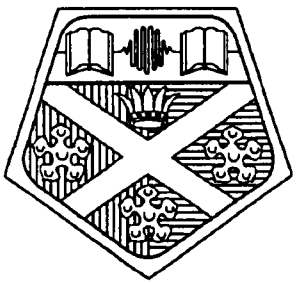

UNIVERSITY OF STRATHCLYDE

DIVISION OF MECHANICS OF MATERIALS
DEPARTMENT OF MECHANICAL ENGINEERING
GLASGOW, SCOTLAND

SOME PLASTICITY STUDIES RELATING TO THIN-WALLED BEAMS

Thesis Presented For The
Degree of Doctor of Philosophy

By

Thiam Huat **Lim** , BEng.(Hons)

July 1995

ABSTRACT

In the field of cold formed structural steels, in which the load carrying members consist of thin-walled sections, failure often occurs due to the development of local buckles which are initiated in the compression elements. The work presented in this thesis details experimental and theoretical investigations conducted to study the behaviour of some thin-walled beams which fail mainly due to local buckling. The ultimate load carrying capacity and collapse behaviour of plain channel, lipped channel and zed section beams in simple bending were examined and the results were then used in an extension of the theory to predict the behaviour of indeterminate beams of similar cross-section which experience plastic moment redistribution before ultimate collapse. The findings from an experimental investigation on the effects of strain hardening on the material strength of cold formed sections are also included in this thesis.

The thesis begins with a short introduction, followed by a review of relevant published literature, which focuses mainly on the use of the plastic mechanism approach in the theoretical analysis of failure modes in thin-walled structures.

The theoretical method of using an elastic buckling analysis in conjunction with a separate plastic analysis to estimate the behaviour of thin-walled beams in the entire range of loading history, from the initial linear elastic characteristics to the collapse behaviour of the beams as they are loaded beyond the ultimate load carrying capacities, is described in chapter 2. Two theoretical methods of using the results from the study of the collapse characteristics of beams in simple bending to predict the behaviour of multi-spanning beams are presented in chapters 2 and 3. These theories are then applied in models for plain channel, lipped channel and zed section beams in chapters 3, 4, and 5 respectively.

Details of the rather extensive experimental investigations carried out to examine the behaviour of beams of the selected sections are then presented in chapter 6. The resulting predictions generated by the theoretical models which are based on the findings from these experiments are compared with the experimental load-deflection results in chapter 7 of this thesis. Results based on conventional simple elastic and plastic theories and the BS 5950 : Part 5 : 1987 are also presented for comparison. Generally, good agreement was found between the results of current theory and the experimental findings.

The experimental work on the effects of strain hardening on the yield strength of cold formed sections is detailed in chapter 8 where the results and observations are included.

Discussion of the presented work is carried out in detail in chapter 9, which also summarises the conclusions drawn from the studies and some recommendations for further research and extension of the analysis.

The publications cited in this thesis are listed in a bibliography. These are arranged in alphabetical order with reference to the authors. The thesis is then concluded by three appendices which supplement the main text.

ACKNOWLEDGEMENTS

I wish to express my grateful appreciation to Prof. John Spence, Vice Principal (Elect), University of Strathclyde and Prof. Thomas Gray, Head of Division of Mechanics of Materials, Head of Department of Mechanical Engineering, University of Strathclyde, for their kindness and the use of the Department's facilities.

It is with great pleasure that I express my sincere gratitude and acknowledge the efforts of my Supervisor Prof. James Rhodes, Professor in the Division of Mechanics of Materials, Department of Mechanical Engineering, University of Strathclyde, whose inspiring guidance, valuable suggestions and encouragement throughout the course of this research program have contributed much to the completion of this thesis and his ever cheerful and warm nature has made my work in the department a most uplifting experience.

A special thanks to Miss Janet Harbidge, Administrative Assistant of the Department, for her advise and assistance in numerous matters and for her warm and caring encouragement that have made my stay in the University most enriching.

My sincere thanks to the technical staff of the Division of Mechanics of Materials, Mr Chris Cameron, Mr John Low, Mr Ronnie Mckenzie, Mr John Barnes and Mr Andrew Crocket for their valuable assistance in the experimental aspects of the work.

I am grateful to the staff of the drawing office and secretaries of the department for their help in many ways.

The financial support given by the Committee of Vice-Chancellors and Principals of the Universities of the United Kingdom and the University of Strathclyde throughout the duration of this research project is gratefully acknowledged.

My gratitude to Metal Sections Limited of West Midlands for graciously allowing the results of several beam experiments they commissioned for the purpose of product certification to be used in this thesis.

Many thanks to all the friends and colleagues I have found in Scotland whose contributions to my knowledge and experiences are invaluable and have added much to my appreciation of this chapter of my spiritual journey through life.

Finally, I would like to thank my family members and friends who have supported me in various ways throughout my studies at the University of Strathclyde.

NOMENCLATURE

All symbols are defined where they first appear in the text. In most cases, only one meaning has been assigned to each symbol, but where this is not the case, the interpretation will be evident from the context. For convenience, the notation is listed below.

A	Cross-sectional area.
a	Plastic hinge travel distance.
B	Width of vacuum box.
b	Elemental plate width.
b_{ef}	Effective width.
b_{eff}	Effective width of a stiffened element.
b_{eu}	Effective width of an unstiffened element.
c	Plastic mechanism size.
D	Plate flexural rigidity. (= $\frac{E \cdot t^3}{12[1-\upsilon^2]}$)
d	Depth of beam section.
E	Young's modulus of elasticity.
E_p	Plastic modulus for strain hardening materials.
$F_{( )}$	Equivalent forces.
f_c	Compressional stress on the effective element.
g	Gravitational acceleration. (=9.81 m/sec^2)
H	Manometer head in (cm H_2O).
H_v	Vickers hardness number.
h	Position of the neutral axis of bending.
I	Second moment of area.
I_{eff}	Second moment of area based on the effective section.
K	Local buckling coefficient.
k	Strength coefficient.
L	Length of beam span.
l_b	Plastic hinge length which is dependent on the bolt positions.
M	General symbol for bending moment.
M_{eb}	Bending moment considering elastic buckling.
M_u	Section ultimate bending moment capacity.
$M(\mu)$	Bending moment of the global plastic hinge at the hinge angle of μ.
m_p	Plate fully plastic bending moment capacity.
m_p'	Reduced bending moment capacity of a plate subjected to axial compression.

m_p''	Reduced moment capacity of an inclined plastic hinge.
m_{psh}	Plate plastic bending moment for strain hardening materials.
N	General symbol for stress resultants in N/mm. ($= \sigma \cdot t$)
n	Position of the neutral axis of bending.
P, p	Applied load.
P_{cr}	Local buckling stress.
P_o	Section squash load.
Q	Applied pressure.
R	General symbol for radius of curvature.
r	Mean radius at plastic hinges.
t	Plate thickness.
U	Applied uniformly distributed load.
v	General symbol for beam deflection.
v_{ms}	Mid-span beam deflection.
vol	Volume.
W	General symbol for energy dissipation.
w	Lip size.
x, y, z	Components describing position with reference to a co-ordinate axis.
Z_p	Plastic section modulus.
$\alpha, \beta, \gamma, \theta, \xi, \varphi$	Plastic mechanism hinge angles.
$\delta( )$	Virtual quantity.
ε	General symbol for strain.
μ	Angle of global plastic hinge rotation.
ρ	Density of H_2O. (=1000 kg/m^3)
σ	General symbol of stress.
σ_{avo}	Compressional stress on the effective element.
σ_e	Extreme fibre stress.
σ_o	Material yield stress.
σ_{sh}	Stress in the strain hardening region of material behaviour.
σ_t	Tensile extreme fibre stress.
σ_{yc}	Corner average yield strength.
$\sigma_{1,2}$	Principle stresses.
υ	Poisson's ratio.
τ	General symbol for shear stress.
$\bar{\varepsilon}$	Generalised strain.
$\bar{\sigma}$	Generalised stress.

CONTENTS

Chapter One

Introduction and Literature Survey

1.1 INTRODUCTION

The evolution of structural form has brought about much change since the early days when structures were often comprised of stout stone columns and massive arches. The introduction of metals into structural engineering in the late eighteenth century started a trend towards structural members of ever increasing slenderness. With the development of mild steel in the later part of the nineteenth century, came the ability to produce thin-walled structural elements made of a strong ductile material. These thin-walled members have since become very important in present day structural designs, not just in building construction, but in fields ranging from the aerospace industry to the manufacture of office furniture and home appliances.

The success of thin-walled structural steel is mainly due to the advantages of high structural efficiency and high strength to weight ratio which comes with the usage of these steel members, these factors being of upmost importance in applications such as vehicle construction, ships, bridges and cranes where self-weight of the structure has to be a minimum. Minimising metal content can also prove to be very economically advantageous, not just in the savings in material cost but also in handling and transportation. By replacing the traditionally used timber with thin-walled steel sections in the construction of houses, some enterprising North American builders have also been able to replace large work crews with only a few men armed with some simple power tools, making huge savings in labour costs. Cold forming production methods allows thin-walled sections to be produced in a wide variety of shapes and dimensions, with the additional options such as protective coatings and insulating fillers, adding to the versatility and popularity of this family of structural products.

Thin-walled structural members do however come with their own perculiar problems which have to be taken into consideration during design, one of the most prominent of these problems being their tendency to buckle. The need for control of buckling is a major factor that dictates the final structural form. This has been the subject of much research in the past decades, but in spite of the numerous investigations, work in this specialised field has by no means reached finality. Books such as that of Walker et al [78] presents a good overall introduction to the subject, and go on to discuss some useful analytical solutions for the problems usually faced in the designing of cold formed structural steel components.

It would be impossible to address all the possible problems that could be encountered in the field of thin-walled structures in this introduction, so only a very brief discussion shall be presented in this section on the most prominent failure mechanisms that usually operate on thin-walled structural members. The thinness of the material in this class of structural members gives rise to behavioural phenomena not usually encountered by the thicker hot-rolled sections and there are several important modes of failure which thin-walled sections may be prone to. Slender columns are likely to experience overall column buckling, a common occurrence even in some heavier sections of sufficient length. Certain thin-walled sections with low torsional stiffness may fail due to torsional flexural buckling in which all the cross-sections along the member retains ~~it's~~ their original shape but there is twisting of cross-sections relative to their neighbours. Sections with relatively thin wide component plates tend to be susceptible to local buckling, an important design consideration in this field. These local buckles can be easily identified by the wavelike deflections in the elements of the section which experience compression, the wavelength of the deformation being in the same order as the width of the element. In beams, local buckling may take effect as local buckling of compression flanges in which buckles form on the plates under compressive stress reducing the beam stiffness and overall load carrying capacity. A more devastating form of local instability in beams is web crippling which occurs in

areas of the beam subjected to concentrated loads and at support points. It is not unusual for thin-walled structures to fail with a combination of two or more of the mentioned buckling modes, this can sometimes prove to be extremely dangerous like in the case where the critical loads to cause local buckling are very close to the overall buckling load in a strut, such a member would collapse very suddenly with little load carrying capacity after initial failure. On the other hand, the engineer may want to design the member to this effect for the optimisation of the design, when there is an alternative load path and the collapse of that member does not compromise the safety of the structure as a whole. Interaction between local and overall buckling generally reduces the buckling load to a value below that of each of the buckling modes acting alone, this interaction must hence be taken into account during design.

1.1.1 Scope and Objectives

The present study is concerned primarily with cold-formed thin gauge steel beams in which ultimate failure is brought about by local buckling of compressed plate elements at the portions along the beams where the effects of bending moments are most adverse. The main subjects of this study are plain and lipped channel section beams, and some work is presented on zed sections subjected to similar treatment.

Although local buckles may not cause immediate failure, they can drastically alter the stress system within the member, reducing the stiffness of the compressed elements against further compression, thus hastening the ultimate failure of the beam. It is one of the primary objectives of this thesis to investigate the behaviour of thin-walled statically determinate beams of the selected sections subjected to bending in the full range of loading, covering the pre-buckling state, initialisation of buckling, post-buckling behaviour preceding the ultimate load and the final phase of bending collapse and to develop theoretical models that can closely approximate the behaviour through relatively simple means. The beam characteristic behaviours are represented

in load-deflection or bending moment-rotation plots, which shows the important characteristics of collapse load and the collapse behaviour after failure has been initiated.

With comprehensive information of the collapse behaviour of the beams with a single failure section, the behaviour of statically indeterminate beams of similar cross-sections, in which multiple failure sections along it's length has to develop before collapse is possible, is then predicted. The case of multi-spanning beams is an example of this type of situation and it is the other primary objective of the current work to study the behaviour of thin-walled beams with multiple spans as they are loaded beyond the initiation of failure. With such beams, as the loads are increased, bending moments throughout the beam increases proportionally in the elastic domain up to such time when buckling occurs at the points along the beam where the effects of bending moment are most severe. These initial failure points are usually found at the location of the supports between spans where moments are maximum. Although buckling and perhaps plasticity would have caused these sections of the beam to lose some of their moment carrying capacity at this point, the applied loads can still be increased since the other portions of the beam have yet to reach their ultimate loading conditions. The failing sections over the supports can be said to shed some of the load carrying responsibility as they lose their ability to maintain resisting moments, the additional loads are hence taken up by other portions of the beam. On further increases of the applied loads, the ultimate moment capacity of the next most severely loaded beam portions would eventually be reached and when sufficient failure points have formed, the beam will collapse. This phenomenon is known as 'moment redistribution' and is the subject of study for much of this thesis.

Murray [40,41,42] has defined the "toughness" of a structure as it's ability to withstand limited amounts of overload, initial imperfections, load eccentricity and so on. It is an important concept in structural design. The toughness of a structure could

be increased by increasing it's ductility, by introducing alternative load paths, choosing shapes of cross-sections that do not lead to sudden (brittle) collapse. To determine whether a structure has these desirable properties, it is necessary to study it's post-collapse behaviour. Collapse characteristics of thin-walled structures can be obtained by analysing the behaviour of the local plastic mechanism that develop during the collapse of the structure. Such information can be very useful in certain applications. One such application is in the design of structures in earthquake zones, where the ductility of the collapsing structure is of upmost importance in the event of severe tremors, it has to collapse slow enough for the occupants to have time to escape. Another important application is in energy absorbing devices such as in the safety of car structures, the ability for the car structure to control the deceleration of the impacting bodies in a crash situation, in this case called the vehicle crashworthiness, can mean the saving of lifes. In the design of bus superstructures, passenger cabins of trucks and vehicles with roll bars, knowledge of the collapse behaviour of the structure can be used to predict the loss of survival space in the vehicle in roll-over situations as it collapses inwards with an ever decreasing load carrying capacity.

Although the present work is mostly directed towards the study of cold formed steel beams as applied in building construction, it is hoped that the techniques developed and observations documented in this thesis will be useful to further work in other applications of thin-walled structures as well.

The long known fact that the mechanical properties of steel can be changed when the material is subjected to large plastic strains is an important advantage for cold formed structural steel, since the mechanical strength is usually improved in the process. As a secondary objective, an experimental investigation into this phenomenon was undertaken and this work is presented in chapter 8 of this thesis.

1.1.2 Work presented in this thesis

Theoretical models of plastic collapse mechanisms are used with an energy approach to generate predictions of post failure load-deflection behaviour of the beams of selected cross-sections, as they are subjected to loads in the full range of loading and some ways through the collapse. Two separate theories will be used to construct the full range of behaviour, an elastic analysis incorporating an effective width approach will be used to obtain the elastic loading lines and collapse curves based on a plastic mechanism method will be superimposed onto the elastic lines. The intersection of the two lines will provide the estimation of the ultimate load of the beam and the part of the collapse curve after the intersection will show the collapse characteristics. A full description of the technique is presented in chapter 2 of this thesis.

Experimental investigations of the problem are presented, in which samples of the selected beam sections were tested as single and double span beams, supported through cleats. The theoretical plastic collapse mechanisms are modelled to closely resemble the fold line patterns observed in the laboratory but certain simplifying idealisations have been used so as to allow relatively simple and quick analysis that does not require the solving of complicated non-linear mathematical expressions or a tremendous amount of computing time and power, usually intrinsic to numerical methods. The load-deflection data collected from the experiments are subsequently used to verify the theoretical models.

This study starts with a brief survey of the existing literature on the subject, which will be presented in the remainder of this chapter. This literature survey presented in the following sections begins with a brief look at the more popular methods that have been used to analyse elastic plate buckling. The next section takes a quick look at the effective width approach which has been widely used in numerous design codes. The third section reviews the methods used in predicting plate behaviour in the elasto-plastic range followed by a small section on the behaviour of thin-walled beams. The review then looks at the research relating to the use of the plastic mechanism approach which is the method employed in the thesis and ends with some concluding remarks to the literature survey.

1.2 BUCKLING OF PLATES

Investigations into the behaviour of thin-walled structures have led many researchers to study the behaviour of plates in buckling, since these are the elements from which thin-walled structures are constructed. The following paragraphs summarises some of the contributions made in this field of study.

St Venant [75] in 1883, derived the differential equation for the elastic buckling of a plate subjected to in-plane stresses, shown below as equation 1.2.1.

$$\frac{\partial^4 w}{\partial x^4} + 2\frac{\partial^4 w}{\partial x^2 \partial y^2} + \frac{\partial^4 w}{\partial y^4} + \frac{\sigma t}{D}\frac{\partial^2 w}{\partial x^2} = 0 \qquad \text{Eqn.(1.2.1)}$$

In the equation, D is the flexural rigidity of the plate, t the plate thickness, σ the stress in the x direction and w the plate deflection.

Bryan [10] in 1891, presented the first solution to this equation for a square simply supported plate in uniaxial compression. The non-linear differential equations governing the post-buckling behaviour of an initially perfect plate were derived by von Kàrmàn in 1910 and these were developed further by Marguerre to include initial plate geometric imperfections in 1939, these equations are commonly referred to nowadays as the von Kàrmàn or Marguerre equations.

Since those early solutions, a number of investigators have developed solutions and methods to analyse the buckling behaviour of plates, a number of which have been presented in textbooks by Bleich [6] and Timoshenko and Gere [73]. Some of the more popular methods are briefly highlighted in the following paragraphs.

Based on the principle of conservation of energy, the Rayleigh's method allows simple approximations to be obtained through the use of a single algebraic expression which describes the shape of the buckled member. This method was improved upon by Ritz who used the principle of minimum potential energy. This improved technique is commonly known as the Rayleigh-Ritz method.

Galerkin's method is another means of obtaining approximations. In the method, the postulated deflection form must satisfy all boundary conditions, compatibility and equilibrium. Solutions are found through putting the deflection expressions into the governing differential equation to express the total potential energy of the system and solving the resulting equations.

The first exact solution to the von Kàrmàn equations was obtained by Levy [29] in 1942, this solution . *is* for square simply supported plates subjected to compressive stress on two opposing edges. The stress function series was derived from the von Kàrmàn compatibility equation and by substituting that and a double Fourier sine series, for the deflection, into the equilibrium equation, the coefficients for the deflection series were obtained. This method has since been adopted by other investigators.

Yamaki [81] also used a Fourier series for deflections, solving the equilibrium equation through Galerkin's method, obtained solutions for initially imperfect plates with several sets of boundary conditions.

Rhodes and Harvey [60,61,62], presented a series of papers aimed to address the problem of uniaxially compressed plates with the loaded edges restrained elastically from rotation which was applicable to more cases in practical structures than the simply supported or clamped boundary assumptions which were actually the limiting

conditions for the compressed plate. The first of these papers, [60], detailed a theoretical analysis of the post-buckling behaviour of uniformly compressed, initially perfectly flat plates, simply supported at the loaded edges and elastically restrained from rotation to an equal degree on both unloaded edges. The general approach was to postulate a series of functions for the deflection form of the buckled plate, to obtain the corresponding stress system within the plate by solving von Kàrmàn's compatibility equation exactly for those deflection functions and to apply the principle of minimum potential energy to evaluate the values for the coefficients in the deflection series for given values of end compression, hence obtaining the final deflection and stress system of the plate. The results obtained generally compared well with those from other authors and experimental data. The second paper, [61], utilised the same general analysis method to deal with uniformly compressed plates that had the unloaded boundaries in either elastic restraints against rotation to an equal or unequal degree on both edges, or rotational restraints on one edge with the other edge free. Using four terms in the postulated deflection series, gave accurate results for cases where the loads were not higher than twice the buckling load. However, the lost of accuracy as the load was increased beyond the buckling load could be prevented by introducing more terms into the deflection series of the post-buckling analysis. The third publication, [62], was an extension of the method which considered plates that were either compressed eccentrically or loaded eccentrically. It was found that the behaviour of compressed plates is extremely sensitive to the method of load application.

Treating a lipped channel section as a system of thin plates joined at the edges, Loughlan and Rhodes [33,34] studied the interaction buckling of pin-ended lipped channel columns under combined compression and bending. The semi-energy method of the theoretical analyses were based on a method which included a post-buckling analysis using the Rayleigh-Ritz solution of the von Kàrmàn plate equations for the local buckles in conjunction with a simple column analysis. Using a two term

deflection series for the post-local buckling analysis provided a continually changing locally buckled form during the loading. The overall behaviour was determined by using the differential equation for an eccentrically loaded simply supported column, the flexural rigidity of the column and the eccentricity of the applied load were based on the properties of the locally buckled column. Similar analyses were used in more recent publications by Loughlan and Upadhya [35] and Loughlan and Nabavian [36] which dealt with plain channel and I-section columns respectively.

Amongst the various techniques developed to analyse buckling problems, there are numerical methods which facilitate the solving of cases with relatively more complicated geometry, boundary conditions and loading configurations through the use of micro-computers. Three such techniques are the Finite Difference, the Finite Element and the Finite Strip methods, which shall be briefly reviewed in the following paragraphs.

The Finite Difference Method first introduced by L.F. Richardson in 1911 and later worked on by L. Collatz and M.G. Salvadori, is an approximate numerical method for evaluating buckling loads. It is based on the use of approximate expressions for the derivatives in the governing differential equation and boundary conditions and iterates for the buckling load through successive approximation. Detailed discussion of this method is presented in textbooks such as Bleich [6] and Timoshenko and Woinowsky-Krieger [74].

The Finite Element Method may be based upon the principle of virtual work or the minimisation of potential energy in a theoretical structure made up of "Finite Elements". With the stiffness matrix of the chosen "Element" defining the elemental load-displacement characteristics, strain energy in the structure is worked out from nodal displacements. The results from this method is sensitive to the stiffness matrix formulation of the "Elements" and the choice of size and formation of the "Finite

Elements" that make up the theoretical model. This technique can be very powerful, enabling the solving of complicated problems in buckling. Introduction to this method can be found in various textbooks such as Zienkiewicz [84], but effective application of this technique to real problems requires much experience.

The Finite Strip approach is a specialised technique adapted from the Finite Element method for buckling problems. Instead of constructing the theoretical model out of the usual "Finite Elements", "Finite Strips" are used, each strip having constant cross sectional properties along it's length. By taking the deflections of the structure in the longitudinal direction of the strips as being of a specified form, the problem becomes unidirectional.

A review of the developments in plate buckling research presented by Walker [77], highlights some of the important landmarks in the history of the subject and discusses in some detail, the more recent work that has been the basis of new design codes including that for the analysis of cold-formed steel sections. This review concentrates on the behaviour of rectangular plates subjected to relatively simple forms of in-plane loading.

1.3 THE EFFECTIVE WIDTH APPROACH

The Effective Width concept has become very important in the subject of post-buckling behaviour of thin-walled structures. This concept is usually applied as a semi-empirical method that allows the consideration of buckled components with relatively simple analysis, making it ideal for application in the design of practical structures. Effective width equations in various forms have been adopted in most cold-formed steel design specifications on both sides of the Atlantic. Much have been written about this topic in the past , it is not the intention of the author to review the numerous published literature but to take a very brief and somewhat historical look at the subject.

L. Schuman and G. Back, in 1930 conducted a large series of tests on compressed plates and discovered that the ultimate load capacity of plates, wide and thin enough to buckle under load, is relatively insensitive to increases in width. The conclusion drawn from that observation is that after buckling, a plate behaves as though only part of it's width is effective in carrying load.

In investigating this phenomenon in 1932, T. von Kàrmàn, E. Sechler and L. Donnel developed the first Effective Width expression for an initially perfect plate. The expression was developed further to include the effects of initial imperfections by G. Winter who had been a major contributor to the field of cold-formed sections in the USA. Winter [80] used experimental findings to extend von Kàrmàn's effective width equation into a more practical semi-empirical approach for the design of cold formed steel components and this work still forms the basis of the effective width equations adopted by the AISI standard at present.

A detailed review of the Effective Width approach was presented by Rhodes [54], which includes a brief historical overview of the topic. The various forms of effective width and their application in various situations are explained in this reference, along with some recommendations on the subject. The various equations adopted by the cold formed steel design codes in a number of different countries are also discussed.

1.4 PLATE BEHAVIOUR IN THE ELASTO-PLASTIC RANGE

Moxham [39] employed the Rayleigh-Ritz method to obtain the first rigorous elasto-plastic analysis for rectangular plates in compression with the unloaded edges simply supported and free to pull in. The analysis used a flow theory to model the inelastic material behaviour and included discretisation through the plate thickness to allow for gradual spread of plasticity.

Crisfield [13,14] used a Finite Element analysis to study the inelastic behaviour of plates. A full section yield criterion as derived by Ilyushin in 1956, was used in conjunction with the Prandtl-Reuss flow rule for the constitutive relations. By using the full section yield criterion, discretisation through the plate thickness was not required but this approximate approach caused the slopes in the resulting load-shortening curves to be excessively steep in the region after the ultimate load. Frieze et al. [16] used a similar approach in a Finite Difference analysis in 1976.

Little [31,32] utilised an approach which is very similar to that of Moxham, except that Little used a variational principle in which a particular energy function was minimised. This approach was able to produce quick solutions that were in fair agreement with those of Moxham and Crisfield.

Rhodes [53] suggested a simple and computationally efficient approach in predicting the load-end shortening behaviour of plates subjected to in-plane compression and in the elastic-plastic range. The method used the elastically derived effective width of a buckled plate and the hypothesis that this effective width adequately described post-yield behaviour. Although the basis of the method was not mathematically proven, the consistently high accuracy of prediction for plates with various boundary conditions considered in the paper proved the validity of the method, in those cases.

The research into elasto-plastic plate buckling behaviour in the United Kingdom was reviewed by Bradfield [7] in 1982. Mofflin & Dwight [38] using Little's energy minimisation approach, developed a method for inelastic plates and plate assemblies based on the Finite Strip. Key & Hancock [26] later used a similar Finite Strip approach and a modified Newton-Raphson technique for the problem.

1.5 BUCKLING BEHAVIOUR IN THIN-WALLED BEAMS

The analysis of thin-walled sections subjected to bending is slightly more complicated in comparison to compressed members, for this reason, most of the earlier works put forward to describe post-buckling behaviour in thin-walled beams are of an empirical nature.

Winter [80], in the late nineteen forties, was the first to provide a means to analyse problems of this nature. Winter considered the stiffened and unstiffened compression flanges of beams as individual plates that had the unloaded edges simply supported and simply supported-free respectively, and used the Effective Width approach to describe the behaviour of the buckled beam. In a large set of beam experiments, strain readings on the tension and compression flange were taken as the applied moments increased, this enabled the monitoring of the changes in the position of the neutral axis and the subsequent evaluation of the effective width of the compression flange. In this work, it is interesting to note that it was assumed that the stress distribution was fully plastic over the section during collapse.

The study of the interaction of the plate components in thin-walled beams was first undertaken by Harvey [20], who provided another empirical approach to the problem. The effective width of the compression flange at failure was found by rearrangement of the plate buckling formula and assuming that the buckling stress was equal in magnitude to the material yield stress.

Graves-Smith [17] developed a numerical procedure for the prediction of the collapse loads of thin-walled box section beams in pure bending, whereby the large deflection equations were used along with the consideration of non-linear material behaviour.

An important contribution came from Rhodes [52] and Rhodes & Harvey [58,59] on the post local buckling behaviour of thin-walled beams. Theoretical analysis and experimental work was presented for lipped channel and trapezoidal section beams subjected to pure bending conditions. Local instability was examined by using the combined strain energy stored in the component plates that made up the buckled section. Post buckling beam behaviour was studied using a semi-energy approach, whereby the stresses and deflections through the section are linked by solving the von Kàrmàn compatibility equation for the component plate, the stress and deflection magnitudes were then obtained through energy considerations. A simple plasticity theory, based upon the idealised elastic-perfectly plastic material characteristic, was incorporated in the analysis to enable the estimation of the ultimate moment capacity of the beam. The theoretical predictions were generally found to be in agreement with the experimental data. Unlike Winter who considered the compression flange of the beams as single plates, Rhodes considered the effects of the adjacent plate components on the flange by means of edge restraint coefficients. A simple expression for the critical moment to initiate local instability, together with the use of the Effective Width approach on the compression flange was also put forward for design purposes.

In two subsequent publications, Rhodes [55,56] dealt with the effects of local buckling on the behaviour of bending elements of thin-walled sections. In the first, a theoretical analysis was presented which could be used to avoid the complexities introduced by using the Effective Width approach in this kind of problem. A semi-energy method whereby a deflection form was postulated for the local buckles in the element undergoing in-plane bending. By using von Kàrmàn's compatibility equation, the corresponding stress system in the plate and the total potential energy was written in terms of the unknown deflection coefficients, the Principle of minimum potential energy was then applied to obtain the deflection magnitudes, and hence the stresses, applied loads and moment in the section. The second paper documented an

experimental investigation on the performance of unstiffened flanges of plain channel beams in bending where the flanges comprise the bending elements.

Ratliff [50] in 1975, conducted an experimental study on the combined effect of bending and web crippling on twenty six double span channel beams, with and without web reinforcements. It was found that all the specimens eventually collapsed by flange and web buckling. Empirical formulae to design against bending-crippling interaction were suggested for C-shaped beams with stiffened and unstiffened webs.

Hetrakul & Yu [21] conducted a similar study, on cold-formed steel I-beams in 1979. Interaction formulae, based on a regression analysis of the experimental results, were obtained for I-beams subjected to combined bending and web crippling.

Roberts & Azizian [64], in 1983, derived energy equations governing the geometrically non-linear behaviour of thin walled, open sectioned bars subjected to axial, flexural and torsional displacements. Assumptions of small displacements and linear elastic material behaviour were used and subsequent solutions of the governing equations were obtained using the Finite Element method. The results were combined with an approximate failure criterion to predict failure loads of I-beams with initial imperfections. The failure load predictions compared satisfactorily with experimental data.

Benson [5], studied the non-linear moment-curvature response of long, thin, open section beams which had an axis of symmetry in the cross section and bent in such a manner that a flattening of the cross section occurred symmetrically. The problem was analysed by means of a closed, convergent sequence of algebraic and integral equations solved through iterations by a micro-computer. In the paper, results of

circular and angle section beams were compared with existing literature. It was found that bifurcation of the cross sections occurred.

A number of other approaches to the problem of beams failing due to the onset of local buckling exists in current literature, one of the important methods is based on the Plastic Mechanism approach and is the subject of discussion in the next section of this review. The Finite Strip method is another important technique in the subject of thin-walled beams, this approach was used by Hancock [19], amongst other researchers, to study thin I sections in bending. The most widely used analysis method in present design codes is based on the Effective Width approach and is well reviewed in publications such as Rhodes & Walker [63] and Rhodes [57].

1.6 COLLAPSE BEHAVIOUR USING PLASTIC MECHANISM ANALYSIS

The effects of plasticity have received much attention from many researchers in the field of thin-walled structures in recent years. Much have been written on non-linear elasto-plastic buckling behaviour and most of these theories are based on numerical methods. One exception is the plastic mechanism approach, also known as spatial plastic mechanism analysis, in which relatively accurate results can be obtained in a simpler way as compared to the rigorous treatment usually employed in numerical methods. Plastic mechanism analysis produces predictions of the collapse behaviour of buckled components which can be used together with the results from a suitable elastic analysis (modelling the elastic loading up stage) to estimate ultimate load carrying capacity. In addition, this method usually produces relatively accurate load-deflection characteristics some ways after the ultimate failure has been initiated, this information can sometimes be very useful in the design of steel structural members.

Korol and Sherbourne [27] in 1972, used a plastic mechanism approach to predict the ultimate strength of plates in uniaxial compression in a theoretical investigation of plates simply supported at all four edges. The ultimate loads were estimated by the intersection of the post buckling loading path with the unloading line derived from the plastic collapse mechanism. The postulated mechanism which would later be affectionately known as the pitch-roof mechanism is shown in Fig.1.6.1 . The mechanism consists of straight hinge lines which preserves it's essential form as the deformation increased. In the collapse stage, it was assumed that the material was rigid-perfectly plastic and obeyed the Tresca yield criterion, analysis was based on the principle of virtual work and considered the model in strips, with the shear stresses between strips neglected. The geometrical proportions of the mechanism were taken as that which would correspond to the minimum end load at any given deflection.

Small initial imperfections were considered in the analysis but all strain hardening effects were ignored. The collapse model which also ignored elastic strains was kinematically admissible with the membrane strains needed to keep all edges straight while maintaining continuity taken into account in the energy terms. It was found that the ultimate load was profoundly affected by the magnitude of initial imperfections but the theoretical plastic mechanism unloading line in itself was insensitive to initial imperfections. Since the complex plastic behaviour in real plates was simulated by the simple mechanism, it was stated that the resulting strength estimates would have to be tested against experimental data to verify the validity of this method.

In a subsequent paper, Sherbourne and Korol [67] presented results from a series of tests in which six aluminium square section tubes (each simulating four plates with the unloaded edges free to rotate), made from 1.68mm thick plates with the length-to-width ratio of 3 and width-to-thickness varying from 106 to 31.8 . It was found that the very slender specimen possessed a considerable membrane strength beyond the buckling load while for the very stiff specimen, the buckling load was in excess of the theoretical ultimate load. Plots of the applied loads verses transverse deflections showed that while the initial elastic bending and membrane behaviour may have considerable variations for the four plates comprising each tubular specimen, they tend to follow the same unloading curve, particularly as the deflections became large. Good agreement between the theoretical plastic mechanism line and the experimental collapse curve was found only in the more slender specimens. It was also observed that only in early post-buckling were the upper bound requirements satisfied and for all the specimens tested the theoretical load carrying capacity underestimated that in the real plates as the deflections grew large. The authors suggested that this was due to the fact that the analysis only considered the loading of hinge lines at their "new" locations, as the deflections increased, ignoring the unbending of the hinges at the previous position. Also, the material possessed some strain hardening properties not

accounted for in the theoretical model. They concluded that the ultimate load predictions overestimated the real capacity of the plates.

The same work was also later dealt with in Sherbourne and Korol [68] and a similar approach was used in conjunction with an effective width analysis by Sherbourne and Haydl [66] to predict ultimate loads in uniaxially compressed plates.

In a study of the collapse behaviour of thin stiffened panels, subject to axial, transverse bending and combined axial-bending loads, Murray [40,41] observed two plastic failure mechanisms for the stiffened panels, which he classed as Mode I and Mode II mechanisms, shown in figure 1.6.2 . Mode I failure being caused by plate buckling and Mode II by stiffener buckling. Independent strips in the direction of the applied axial loads were considered, the load carrying capacity of each strip at any magnitude of deflection was found through considerations of beam-column interaction and integration allowed estimates for the panel as a whole. Shear effects between strips were ignored. In the rigid-plastic analysis of Mode I mechanisms, Murray used a small and a large deflection theory for the analysis. A numerical minimisation technique was employed to fix the size of the mechanism. Complimenting the theoretical study was a series of full scale tests (up to 9.5m by 2.44m) of panels stiffened by bulb flats, twelve of which were completed at the time of publication. It was found that Mode II, stiffener buckling caused rapid collapse while Mode I, plate failures were followed by gradual lost of strength. Murray emphasised the importance of the knowledge of the behaviour of structures in plastic collapse, not only to be able to predict how the structure may fail but also as a means to measure the sensitivity to imperfections, especially in thin-walled structures where very often, the ultimate load is followed by rapid failure.

Walker and Murray [79], in a paper aimed to explain and predict the manner in which rectangular plates subjected to uniform compression along two opposite edges behave

when they are compressed beyond their ultimate failure load, used a similar rigid-plastic formulation to obtain the plastic collapse curve to a pitch-roof mechanism identical in shape to the Sherbourne and Korol mechanism shown in Figure 1.6.1 . The membrane action required to render the mechanism kinematically admissible was considered in the analysis assuming that all the membrane deformation took place at the hinge lines and at a constant stress equal to the yield stress. The resulting theoretical load-deflection behaviour was compared to the experimental data from Sherbourne and Korol, and reasonable agreement was found for the maximum load and rate of plate collapse. It was shown that the elastic membrane stress in a plate can influence the final plastic mechanism developed after ultimate failure. With increasing axial load, the plate develops a regular pattern of buckles in roughly square panels, however, the irregularities of initial imperfection plays a dominant role and instead of developing a plastic mechanism observed in ref. [40,41], as shown in figure 1.6.3, only one section may become fully developed, while the buckles throughout the remainder of plate decrease in amplitude and finally disappears after failure. The pitch-roof mechanism analysis was subsequently applied to the Mode I (plate buckling) failure of the stiffened plate problem studied by Murray in ref. [40,41], again showing reasonable agreement with experimental findings. The only significant difference between Murray's mechanism and the pitch-roof mechanism is that the outer hinge lines are moved inwards, which had the affect of raising the plastic collapse line in the load-deflection plots. It was stipulated that Murray's mechanism has maximum separation of the outer hinges while the present mechanism has these hinges as close together as they can be, thus, the two collapse curves are bounds and the actual collapse curve lay somewhere between them.

In a subsequent publication, Murray [42] used the analysis and experimental findings from ref. [40,41,79] with the Perry-Robertson formula used with a newly derived expression for the imperfection coefficient and the effective width method to form an approach to the determination of collapse loads for steel plates stiffened longitudinally

with torsionally weak (open-section) stiffeners and loaded axially, in pure bending or a combination of the two. Simple design rules were also recommended in the paper for the case of axial loading, along with a slightly more complicated procedure for the cases with transverse loading.

Rawlings and Shapland [51] presented a simple theoretical analysis based on the plastic mechanism approach to accompany findings from a series of tests where very thin square box sections were axially crushed. All straight fold lines were used in an assumed geometry of fold pattern where sizes were taken off the tested specimens. Elastic deformations were neglected in the plastic analysis and the plate fully plastic moment expression was used for all hinges. Effects of kinking of the corner edges were taken into account in the analysis and it was found that these mechanisms forming at the corners contributed a significant amount of energy absorption.

Davies et.al. [15] in an investigation of the failure behaviour of stiffened and unstiffened rectangular plates under uniaxial compression, found that a consistent pattern of yield lines formed quickly after the ultimate load was reached. The idealised mechanism is again the pitch roof mechanism (figure 1.6.4(a)), and was analysed as a rigid-plastic mechanism obeying the Tresca yield criterion. The analysis included shearing forces as the authors found that shear stresses affected not only the shape of the mechanism but also the collapse behaviour of the plate. The behaviour of the mechanism was analysed by considering the plate to be made up of strips which are free to slide relative to each other. Figure 1.6.4 (b)&(c) shows two characteristic strips. The plastic hinges were assumed to be formed under the influence of a bending moment M, a compressive membrane axial force N, acting at the mid plane of the plate and a shearing force S, acting uniformly over the thickness as shown in figure 1.6.4(d). The yield criterion in terms of the moment and forces on the section is given by equation 1.6.1 and by assuming that the shearing force S is small, the

approximate yield criterion is represented by equation 1.6.2. In the equations below, σ_y is the yield strength, τ is the maximum shear stress and t is the plate thickness.

$$\frac{M}{M_o}\left\{1-\left(\frac{S}{S_o}\right)^2\right\}^{\frac{1}{2}}+\left(\frac{N}{N_o}\right)^2+\left(\frac{S}{S_o}\right)^2=1 \qquad \text{Eqn. (1.6.1)}$$

$$\frac{M}{M_o}+\left(\frac{N}{N_o}\right)^2+\left(\frac{S}{So}\right)^2=1 \qquad \text{Eqn. (1.6.2)}$$

where $M_o=\frac{\sigma_y t^2}{4}$ $\qquad N_o=\sigma_y t$ $\qquad S_o=\tau t$

The angle of the inclined hinges (relative to the unloaded edges) was fixed at 35.5° since this was the minimum angle for which the inequalities implicit in the yield criterion ($\frac{M}{M_o}\leq 1, \frac{N}{N_o}\leq 1, \frac{S}{S_o}\leq 1$) holds true. The aspect ratio of the mechanism was taken from experimental observations which indicated that a fixed value of 0.7 would be reasonable. Relatively good estimates of ultimate loads were obtained.

In 1981, Murray and Khoo [46] put forward the idea of using basic true mechanisms to construct more complicated failure mechanisms found during the collapse of thin-walled structural members. Following an experimental investigation in which various thin-walled steel sections, loaded in bending, axial compression or a combination of these loads were tested to failure, the authors developed a set of eight basic mechanisms that would form the building blocks for all the observed failure mechanisms observed in the laboratory, table 1.6.1 shows these basic mechanisms together with their corresponding characteristic equations. Further, it was suggested that three types of fully-plastic zones, namely the compression, tension and shear yield zones, could be used with the basic mechanisms to form models for quasi-mechanisms. The characteristic equations were developed using a formulation similar to that used in the first authors earlier papers, such as in ref. [41], and the analysis of

local collapse mechanisms could be done by using an assembly of the relevant basic mechanisms and yield zones such that compatibility and equilibrium are satisfied. Murray and Khoo suggested that the test results verified that the method produced fairly accurate theoretical plastic collapse behaviours although there was a tendency for the theory to underestimate the load carrying capacity during collapse, this was said to be due to two possible factors. Firstly, the local mechanisms do not always form at mid-length of a loaded member, which was assumed in the analysis presented in the paper and secondly, in quasi mechanisms, strain hardening in fully-plastic zones should be allowed for by using a higher yield stress in those zones instead of the material virgin strength that was used in their analysis.

Murray later presented the same analysis method in ref. [43,44] along with demonstrations of how to estimate energy absorption of collapsing thin-walled members through examples. More detailed analysis was also presented for some sections which were examined theoretically using combinations of the basic mechanisms.

An important contribution on the subject came from Tidbury and Kecman [72] and Kecman [25] , who was studying the bending collapse behaviour of rectangular and square section tubes, which was widely used in buses, special purpose vehicles, roll-over and falling object protective structures. Kecman used a limit analysis technique to derive a set of formulae relating the hinge moment and associated angle of rotation of the collapsing tubes. The simplified theoretical collapse mechanism based upon the hinge collapse modes observed in the laboratory, which proved to be very repeatable during numerous tests, was a true mechanism consisting of fixed and travelling yield lines, as shown in figure 1.6.5. In the analysis, the fully-plastic moment of the plate was taken as the individual hinge capacity but the usual material yield strength was replaced by an experimentally derived maximum nominal flow stress of the material in uniaxial tension. Rolling radii for the travelling yield-lines were taken

to be decreasing during global hinge rotation and was estimated using an empirical equation. The moment capacity of the collapsing beam $M(\theta)$ was found using equation 1.6.3, shown below.

$$M(\theta) = \frac{W(\theta+\Delta\theta)-W(\theta)}{\Delta\theta} \qquad \text{Eqn. (1.6.3)}$$

where W is the summation of the energy absorbed in the hinges
θ is the overall hinge rotation
and $\Delta\theta$ is a small change in hinge rotation.

The resulting theoretical moment-rotation characteristics were checked with the experimental data from 56 quasi-static tests of 27 different sections and were deemed very satisfactory.

The same plastic mechanism was observed by Seki and Sunami [65] in their investigation of the energy absorption of thin-walled box sections subjected to combined bending and axial compression.

Narayanan and Chow [47] studied biaxially compressed perforated plates and presented an approximate method of predicting the post-buckling behaviour and the ultimate load carrying capacity of approximately square thin mild steel plates with square and circular centrally located holes. The theoretical plastic unloading behaviour was obtained using a method based on plastic mechanism analysis, the mechanism used is made up of four diagonal yield lines in the square plate with rigid quadrantal segments between the yield lines, the plate edges and yield lines forming the axes of rotation for the rigid regions, as shown in figure 1.6.6 . The plastic analysis utilised a simplified form of the Von Mises yield criterion. Theoretical collapse loads were estimated from the intersection of the plastic unloading line and the elastic loading curve. A satisfactory degree of accuracy which was slightly

unconservative was found for the method in a comparison of the theoretical and experimental collapse loads.

In a study of collapse behaviour of some thin-walled sections by Sin [70], long and short uniaxially compressed flat plates, plain channels and plain trapezoidal channels in pure bending with the unstiffened elements in compression, corner crinkling and box sections loaded axially and in bending were examined. Sin used the plastic mechanism approach with a reduced hinge moment equation, shown below as equation 1.6.4, which took into account both bending moment and axially applied compressional forces in hinges inclined to the global bending axis.

$$\frac{M}{M_p} = \frac{1-\left(\frac{N}{N_o}\right)^2}{\sqrt{1-\frac{3}{4}\left(\frac{N}{N_o}\right)^2 \sin^2\gamma\left(4-3\sin^2\gamma\right)}} \qquad \text{Eqn. (1.6.4)}$$

where M = Reduced plastic moment of the inclined hinge
M_p = Fully plastic plate bending moment
γ = Hinge inclination to global bending axis
and $\frac{N}{N_o}$ = Ratio of end thrust to the section squash load.

The von Mises yield criterion was applied in the formulation. In the collapse mechanisms, membrane strain energy was considered in the quasi mechanisms, effects of initial imperfections were incorporated in some of the models and a minimisation process was adopted to fix the size and geometrical proportions of the mechanism so that the theoretical collapse load was minimum for each mechanism. Some of the plastic mechanisms analysed are shown in figure 1.6.7. In general, reasonable agreement was found with the experimental data and results from other investigators.

In an investigation into the behaviour of thin-walled channel section columns, in which slender channels fabricated from high strength steel plates by welding were the

subjects, Rasmussen [48] analysed the post-ultimate collapse behaviour of the channel section columns by employing the theory for spatial plastic mechanisms from Murray [40,41,44] and Murray and Khoo [46]. Rasmussen considered three plastic mechanism models, the true flange mechanism, the quasi flange mechanism and the web mechanism which are shown in figure 1.6.8. The mechanisms resembles those identified in the paper by Murray and Khoo [46] and the formulations follow closely to those presented in the mentioned papers, and is therefore not discussed further. Some of this work was also later published in Rasmussen and Hancock [49].

Prompted by the lack of analytical models for the design of thin-walled sections against web crippling, Bakker [3] researched into the subject with the aim of gaining understanding of web crippling behaviour in cold-formed steel members and developing a theoretical model usable in design. Bakker examined hat and deck sections with unstiffened web and flange elements subjected to the combined action of a concentrated load and a bending moment and produced a web crippling model based on the plastic mechanism analysis as shown in figure 1.6.9. The kinematically admissible plastic mechanism used the von Mises yield criterion and considered the effects of work hardening in the travelling hinges using approximate factors in the energy equations which depended primarily on the ratio of the yield and tensile strength of the basic material. From a comparison of the theoretical results generated using the mechanism with experimental data, it was found that the approach gave reasonable predictions. Much was written on the mechanics of the web crippling behaviour and it's effect on the load-deflection characteristics of the failing beams. This work was also published in ref. [2,4].

Mahendran and Murray [37] presented a paper on how imperfections in thin steel plates affected the type of plastic mechanism that forms when in-plane compression is applied. The analytical study used Galerkin's method of solving the Marguerre's equations to determine the elastic loading up behaviour of the plate with the location

of the first yield point in the imperfect plate known and subsequently the critical geometric imperfection level that would cause the "flip-disc" type mechanism to form instead of the "pitch-roof" type.

An investigation into the failure of triangular cross-section girders in pure bending was conducted by Kótelko and Królak [28] in which four possible collapse plastic mechanisms were suggested, shown in figure 1.6.10 . The fully-plastic plate bending moment was taken as the hinge moment capacities and the rolling radii of the travelling hinges were estimated using the method put forward by Kecman [25]. The authors approximated the bending moment of the collapsing beams using equation 1.6.5, below.

$$M(\theta) = \frac{W(\theta+\Delta\theta)-W(\theta-\Delta\theta)}{2\Delta\theta} \qquad \text{Eqn.(1.6.5)}$$

where M =the bending moment of the global plastic hinge
W =the sum of the energy absorbed in the yield lines
and θ =the angle of rotation of the global plastic hinge.

It was found that in the mechanism called T1, approximately 50% of the total energy absorbed during collapse was contributed by the travelling yield lines.

Zhao and Hancock [82,83] reviewed existing formulae for the reduced plastic moment capacity of an inclined yield line subjected to axial force by Murray [40,41], Davies et.al. [15], Bakker [2] and Murray [44] and found them to be statically inadmissible, since the effects of an existing twisting moment was not considered. The authors derived reduced moment formulae based on both the Tresca and the von Mises yield criterion which took the effects of the twisting moment on the reduction of the plastic moment capacity into account and verified them experimentally. It was proposed that these new formulae are statically admissible and hence lead to lower

bound solutions. The solving of these formulae requires an iterative process that makes their application rather difficult, in view of this problem, the authors also suggested simplified expressions, derived from regression studies, to permit easy application of their theory.

1.7 CONCLUDING REMARKS ON THE REVIEW OF LITERATURE

A substantial amount of literature on the buckling of structures has been published as this subject has received much attention from researchers for over two centuries. It was not the intention of this literature survey to review each contribution to the theory of buckling in structures. This chapter presented a brief discussion to highlight the contributions deemed most important and relevant to the present work, in the author's opinion. The author would like to apologise for seeming to ignore some work while mentioning other contributions which in some opinions may be of less importance.

The literature survey has highlighted some publications of historical interest and other more recent work which are typical of the active research currently being pursued. The investigations carried out in this field can be seen to have moved it's focus from the elastic buckling behaviour of plates to the study of assembled structural members, and in more recent years, into non-linear elasto-plastic and plastic behaviour where interest in ultimate strength of structures have become one of the main considerations.

A large number of investigators have studied the buckling behaviour in thin-walled structures and much has been written on the subject, but most of the theoretical analysis in current design codes dealing with thin gauge steel products are based on the elastic theory of material behaviour, which in the authors opinion, can sometimes produce very conservative estimates. There is much to gain in understanding the behaviour of the structures in the non-linear elasto-plastic and plastic region.

Researchers like Murray [40,41,45] have commented on the importance of understanding the post-failure collapse behaviour of thin-walled structures, mostly

relating to the safety aspects of a structure in the event of failure. The author agrees with that comment, adding that in the case of statically indeterminate problems, such as that found in multi-spanning beams, section failure characteristics are essential in predicting the overall collapse of the structure which experiences plastic bending moment redistribution.

Advances in the micro-computer field has made numerical methods such as Finite Elements very popular since these offer solutions to complicated problems which are otherwise insolvable, but in the authors opinion, these methods in the current stage of development requires a substantial amount of computational expenses and skilful users with experience to produce realistic results. Furthermore, setting up and fine tuning of the models can be very laborious and time consuming rendering these methods rather impractical for standardised design.

A number of researchers have used the plastic mechanism approach to approximately predict the collapse loads of various thin-walled structures by combining a suitable elastic buckling formulation with the plastic collapse characteristics derived from the rigid-perfectly plastic analysis of failure mechanisms observed in collapsing structures and it can be said that in general, rather satisfactory estimates of ultimate loads have been acquired through this technique. The analysis process is relatively simple and requires much less computing time than in the rigorous treatments used in numerical methods, rendering the method quicker and more readily applicable in design situations. These being the reasons for the adoption of this approach in the current work presented in this thesis.

The various authors have developed a number of reduced moment capacity formulae for an inclined hinge subjected to axial compression and some of these have been reviewed by Zhao and Hancock [82,83], various assumptions of stress distribution across the thickness of the plates have also been used for the formulation of the

moment capacity equations. The reduced moment equation used in the current work is developed in chapter two of this thesis, the final form is identical to that of Sin [70] but the derivation is different in some stages and is deemed by the author to be more mathematically correct. The assumed stress distributions across the plate is also detailed in section 2.4.2 of chapter two.

Walker and Murray [79] and Mahendran and Murray [37] have explored the effects of imperfections on the final form of the plastic mechanisms that develops in compressed plates. It is the author's opinion that in the failure of thin-walled beams, it is the local bending moment and in some cases the effects of concentrated loads that usually causes failure mechanisms to form at the portions of the beam that experiences the most severe loading conditions and small imperfections have a secondary role in the determination of the location and final form of the plastic mechanisms. Further, in the consideration of beams supported through cleats, which are very commonly used in purlins and cold-formed floor beams, the main subjects in this study, the presence of the cleats and bolts affects the form of the plastic mechanism in the collapsing beams.

Most of the work reviewed relating to the use of the plastic mechanism approach have studied plates, and some sections in idealised loading conditions, such as axial compression, pure bending or combinations of the two, these investigations are very useful for the understanding of general behaviours of the sections, but some allowances have to be made before such analysis can be applied to specific practical problems such as those studied in this thesis, beams with cleat supports. It is the intention of the author to investigate the problem using the plastic mechanism approach with some simplifying idealisations that permits relatively simple theoretical treatment in the analysis.

The existence of strain hardening in the materials used in forming the thin-walled structural members has the effect of increasing the local effective yield strength in parts of the member where relatively large strains are experienced. Researchers such as Sherbourne and Korol [27,67] and Murray and Khoo [46] have commented that this effect should be taken into account to produce more accurate predictions of plastic behaviour. This effect will be briefly studied in the current work and a somewhat crude but simple method of incorporating material strain hardening considerations into the plastic analysis during collapse will be discussed in chapter 8 (section 8.4).

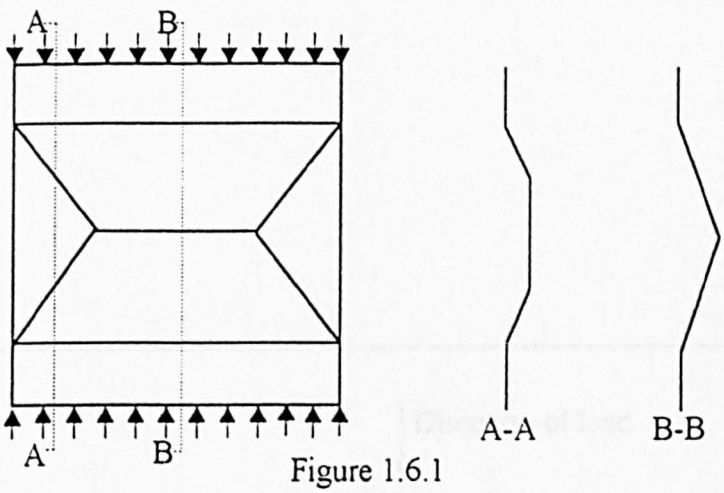

Figure 1.6.1

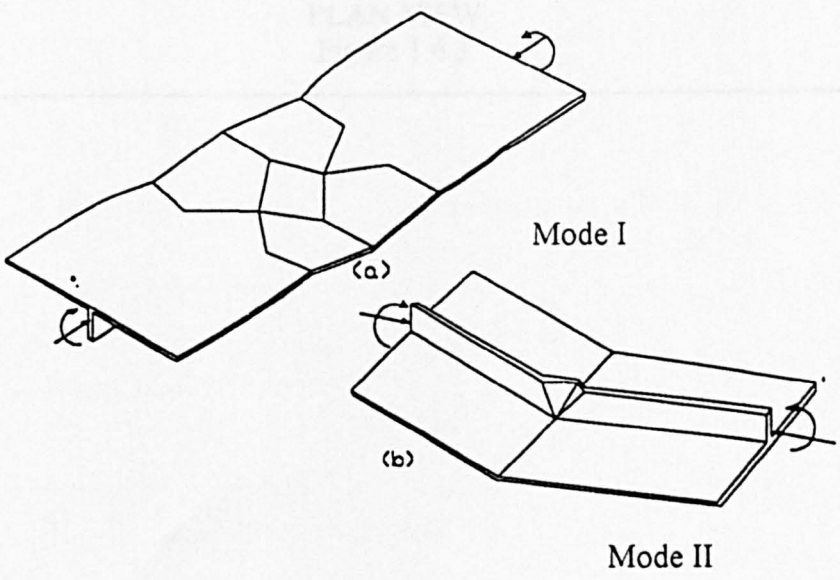

Figure 1.6.2 : Failure modes of stiffened plates

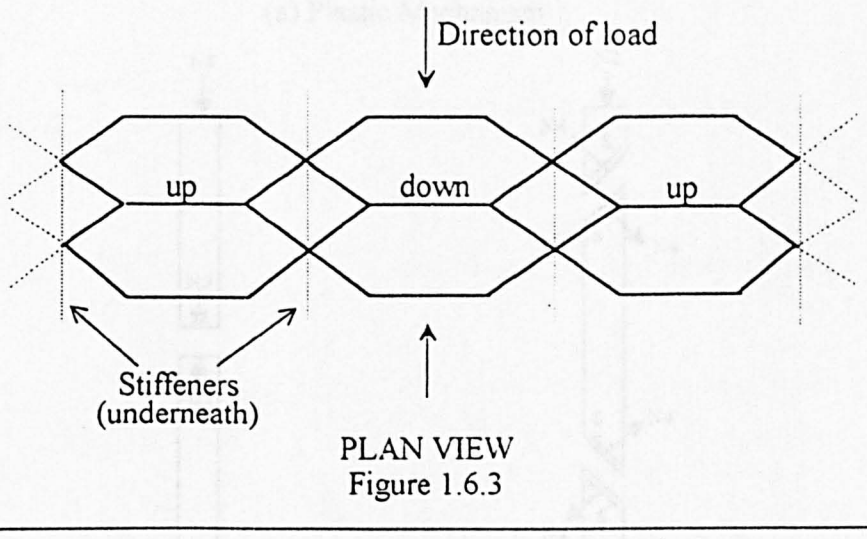

PLAN VIEW
Figure 1.6.3

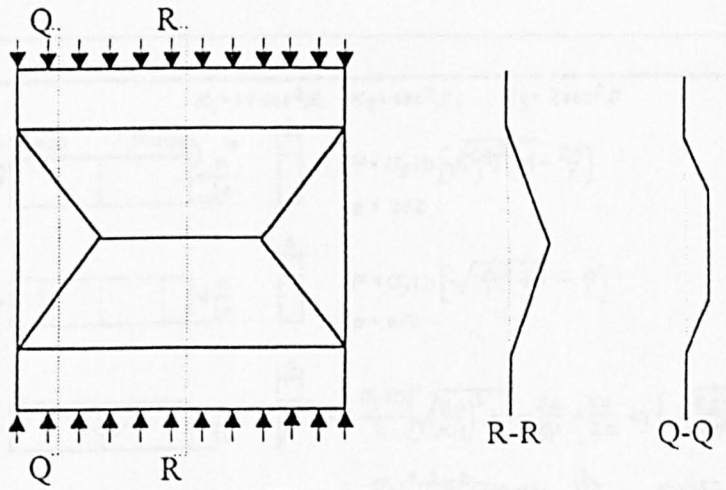

(a) Plastic Mechanism

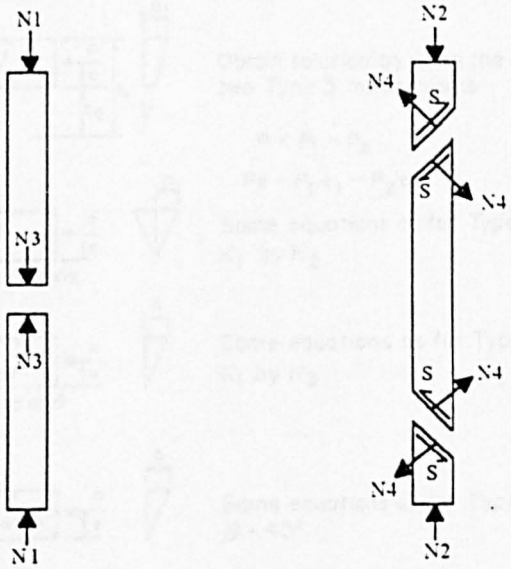

(b) Mid-zone unit strip (c) Edge zone unit strip

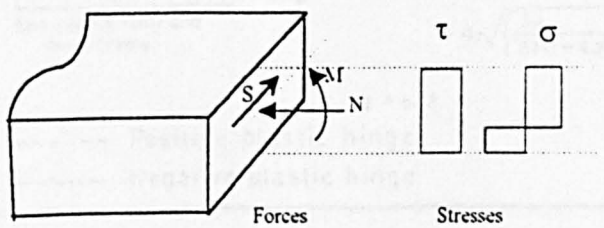

(d) Section on yield line

Figure 1.6.4

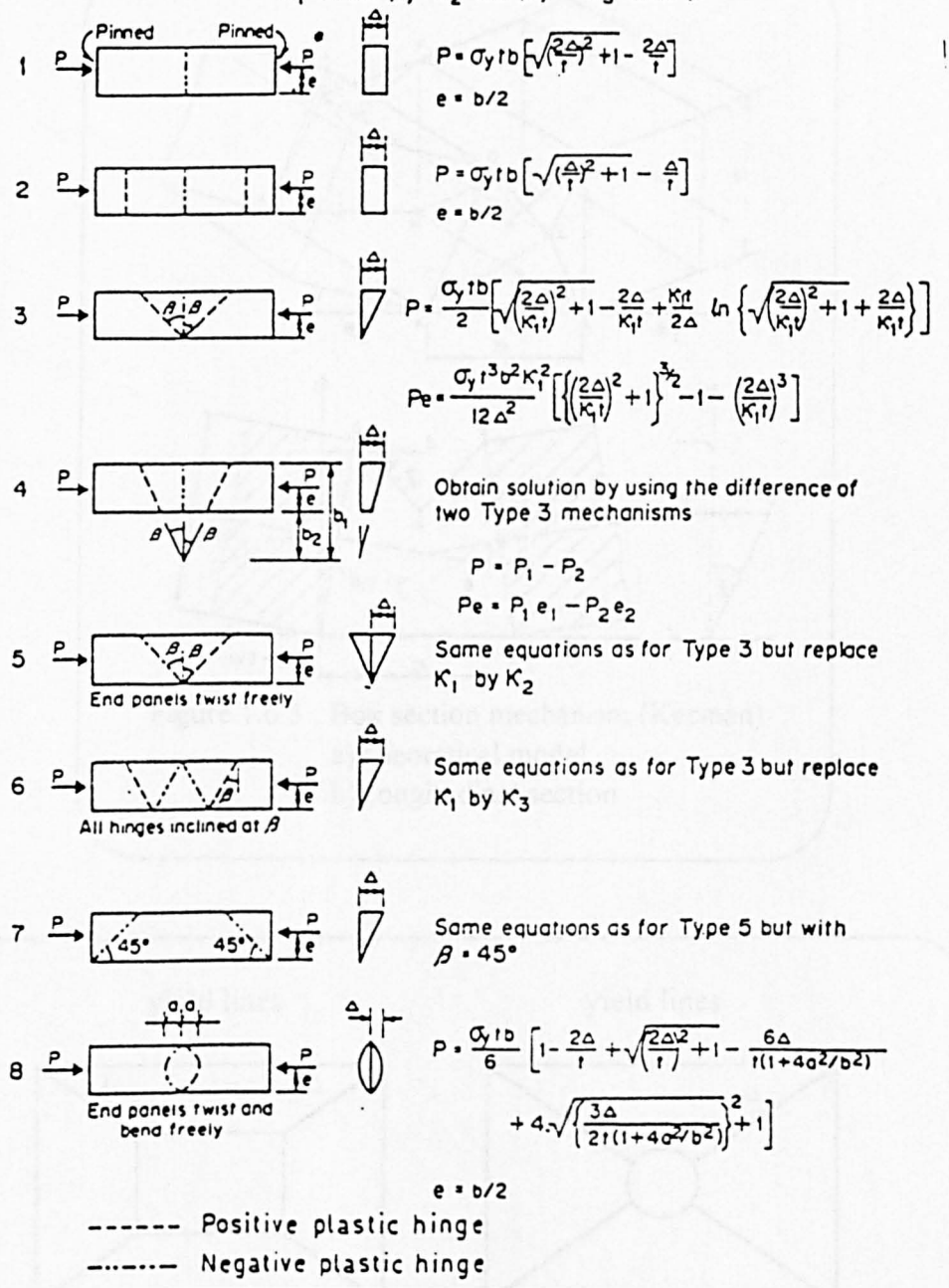

Table 1.6.1: True Basic Mechanisms

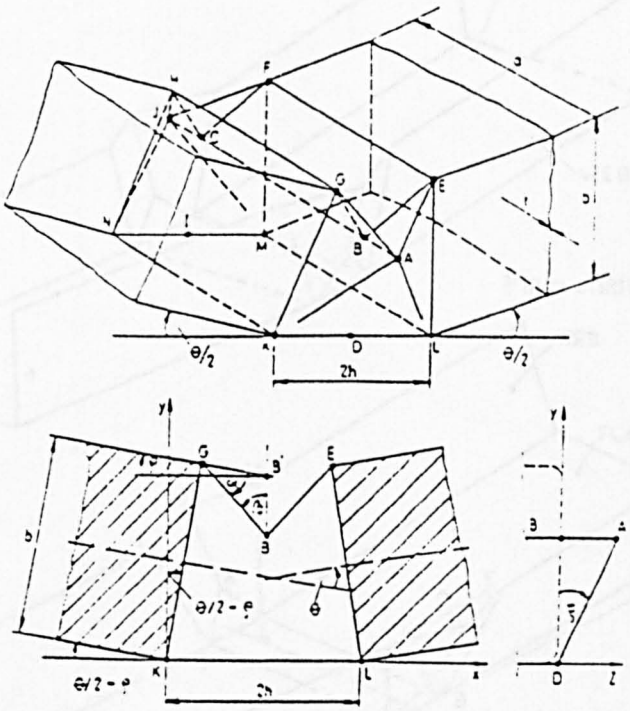

Figure 1.6.5 : Box section mechanism (Kecman)
a)Theoretical model
b)Longitudinal section

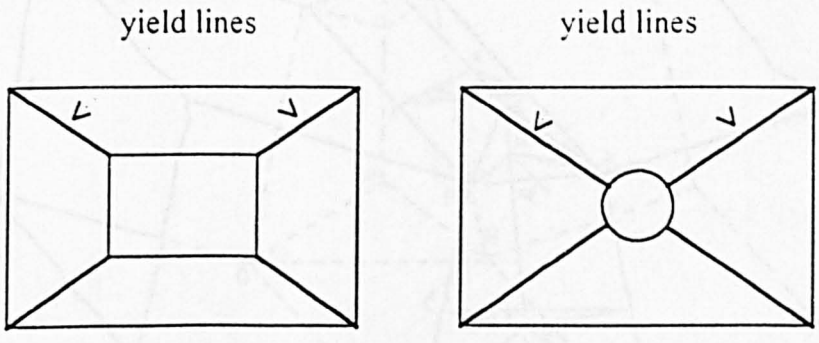

a) Plate with central rectangular hole.

b) Plate with central circular hole.

Figure 1.6.6

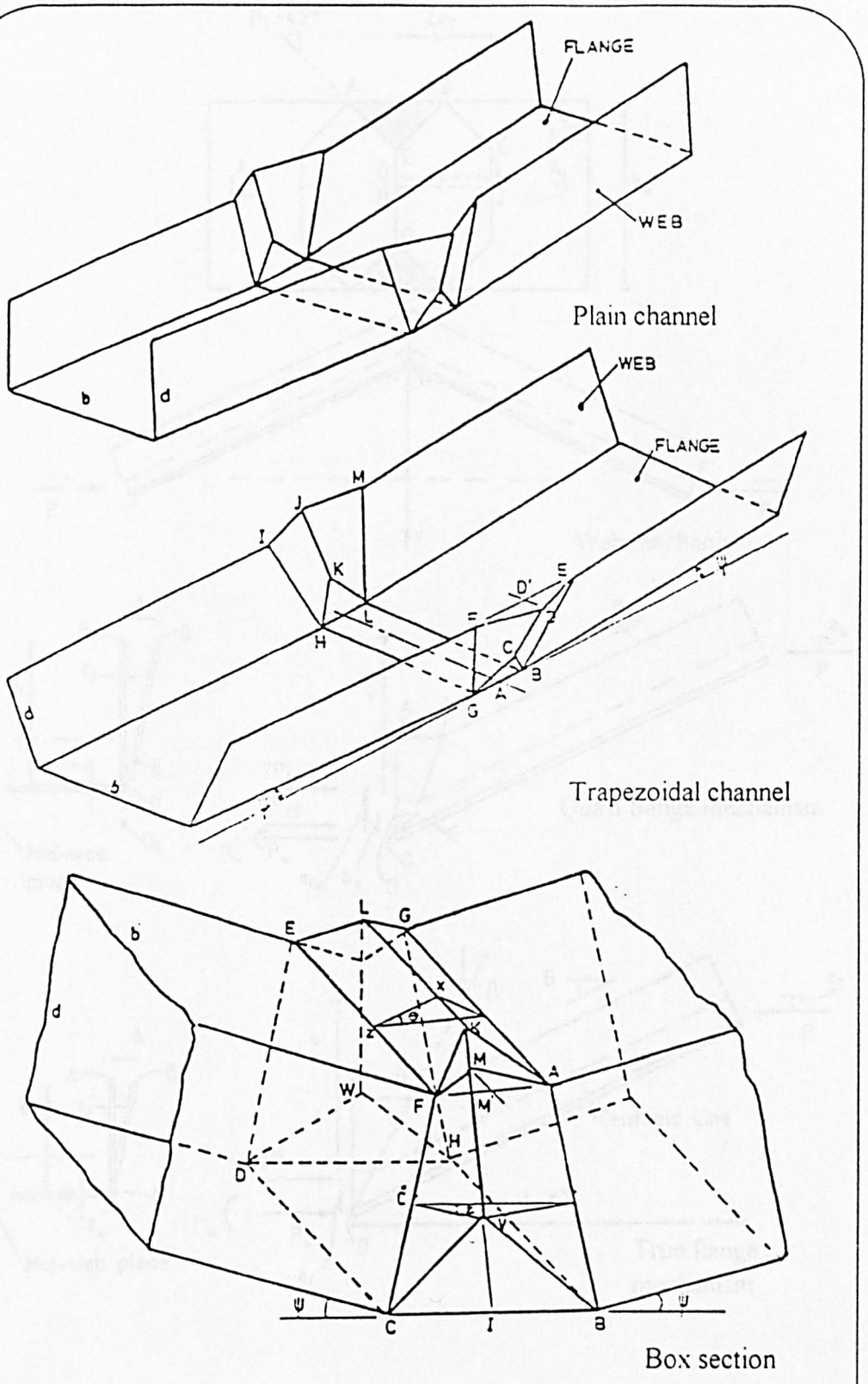

Figure1.6.7 : Some plastic mechanisms (Sin)

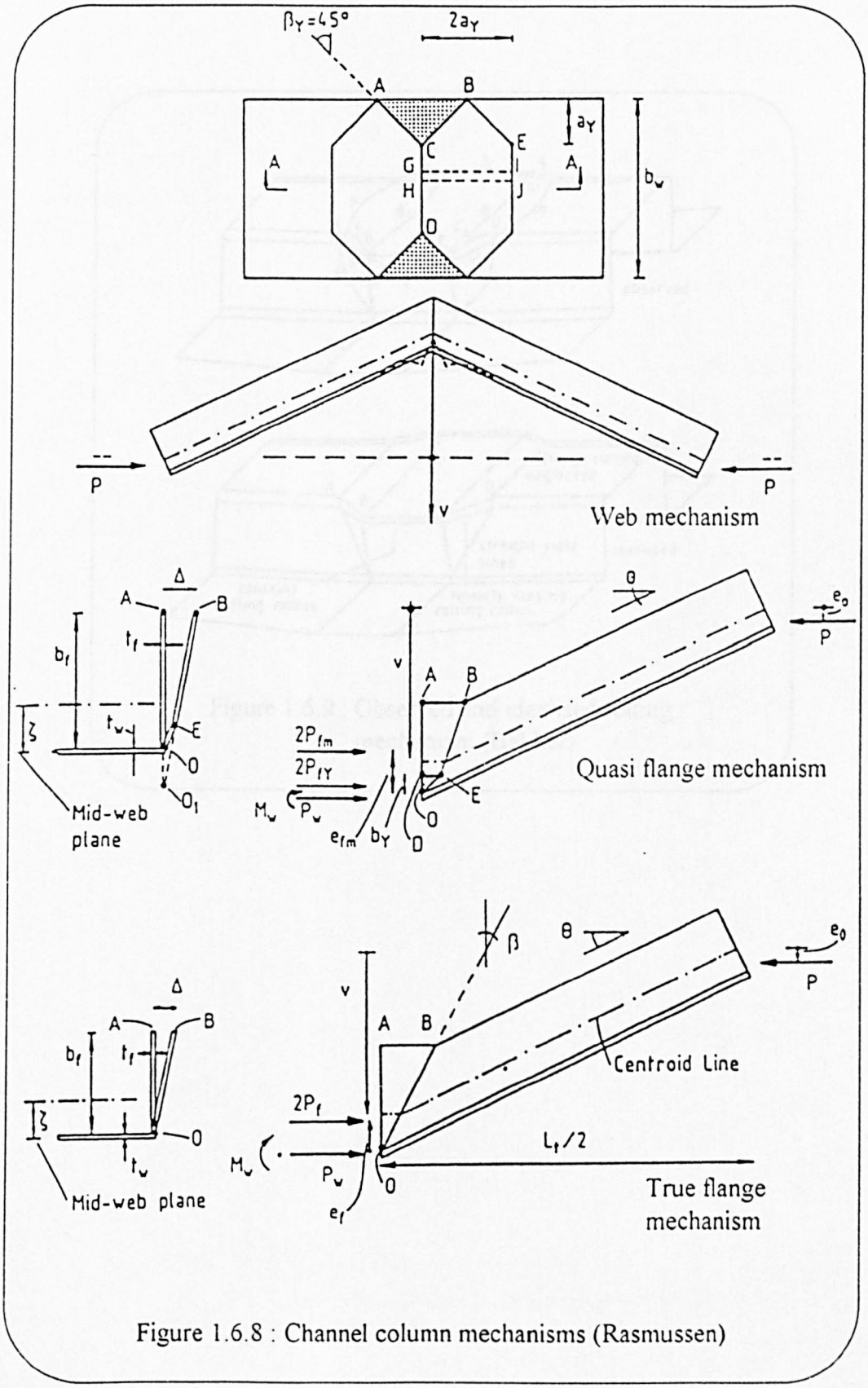

Figure 1.6.8 : Channel column mechanisms (Rasmussen)

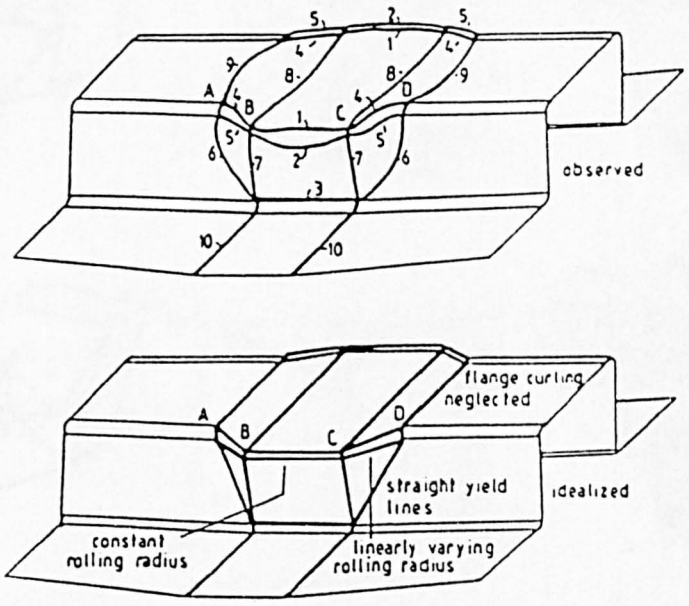

Figure 1.6.9 : Observed and idealised rolling mechanism (Bakker)

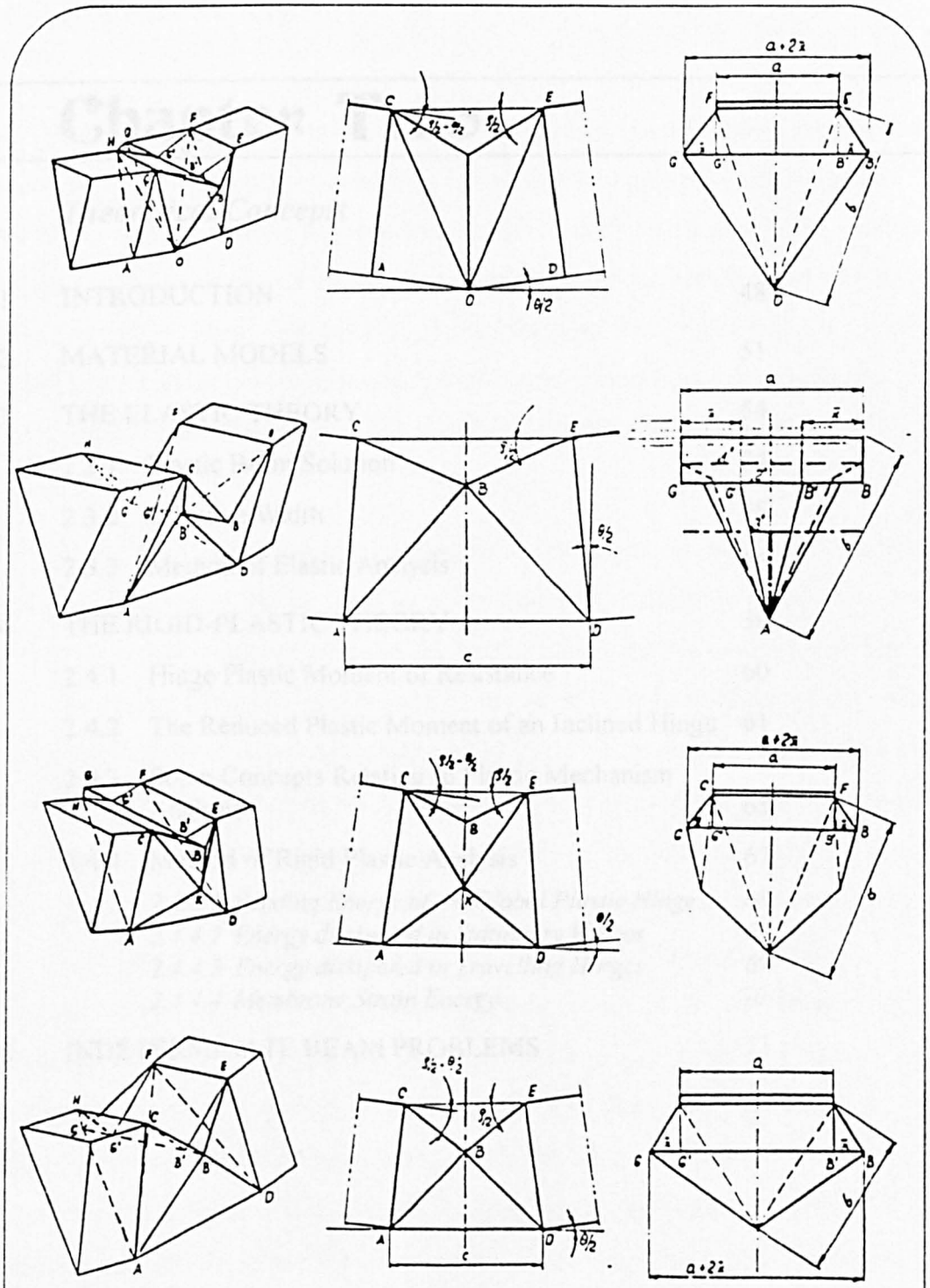

Figure 1.6.10 : Mechanisms for triangular sections
(Kotelko and Krolak)

Chapter Two

Theoretical Concepts

2.1 INTRODUCTION

The behaviour of thin-walled beams is more complicated to analyse than their thicker counterparts of more solid cross-sections for which the simple beam theories have been formulated. In addition to the infestation of plasticity, the failure of thin-walled sections could be brought about by elastic or plastic buckling, which could take the form of overall buckling, local buckling, lateral torsional buckling or a combination of the different buckling modes. In laterally stable beams, local buckling is by far the most common cause of premature failure and is the subject of the current work.

In attempting to model the problem theoretically, the effects of elastic or plastic local buckling, depending on the slenderness of the section, and plasticity must be considered. In later stages of collapse, the local plastic mechanisms that would have developed from the local buckles have to be modelled if the post-ultimate behaviour is to be predicted. In the region of the ultimate load, the beam section where failure has initiated experiences the combined effects of local buckling and perhaps the spreading of yield zones across the section, this region of the loading history is known as the elasto-plastic region of the loading characteristics, so called because the material in parts of the failure section are still elastic while other portions are plasticizing. Although this topic has been well researched, in the whole of the elasto-plastic region of behaviour, there are many gaps in the current state of knowledge and further experimentation and theoretical research is required to clarify many problems. All existing theories for the elasto-plastic region are based on deterministic techniques and attempts at analysis of this problem is indeed too complicated for practical purposes. This is unfortunate because the maximum loads tend to occur in this region, this has led to the current situation whereby there are very many theories and associated models of failure but nearly all of them seem to be based upon one or more empirical rules. However, a technique exists and has been employed by several researchers in various fields, in which a relatively simple method of arriving at an

approximation of the loading characteristics is possible without having to exactly solve the elasto-plasticity problem. This technique involves the use of a separate elastic theory with considerations for local buckling, with a rigid-plastic analysis based on the plastic mechanism approach to estimate the ultimate loads and the post-ultimate collapse behaviour of a failing member.

Figure 2.1.1 shows the load-mid span deflection plot of a typical statically determinate thin-walled beam in a three point bending configuration as it is loaded beyond the collapse load, following a linear elastic loading up stage, the beam experiences local buckling at mid span, accompanied by some plasticising at the same location causing the loading up line to become non-linear towards the ultimate load and finally curves over to unload non-linearly as the beam collapses, losing it's load carrying capacity as the deflection increases. The theoretical model consist of combining the results from an elastic analysis which incorporates an effective width approach to account for the first stages of local buckling settling in and the rigid-plastic analysis which predicts the beam behaviour in the region where collapse is well on the way and the local plastic mechanism at mid span is well developed. The intersection of the elastic loading line and the collapse curve indicates the theoretical estimation of the ultimate beam load and the elastic line before intersection is assumed to be followed immediately by the portion of the collapse curve after intersection to form the prediction for the load-deflection characteristic of the beam in the entire range of loading.

From figure 2.1.1, it can be seen that the elastic and rigid-plastic theories complement one another, the elastic theory is able to define the deflections and stresses up to a point where failure has been initiated while the position of the rigid-plastic curve determines the absolute limit of load carrying capacity, for above this region, the structure cannot carry a load and remain in a state of equilibrium, it hence intersects the elastic line preventing further increases of load at the approximate ultimate load of the theoretical load plot. Other researchers, who have been mentioned in section 1.6

of this thesis, have found this technique of using separate elastic and rigid-plastic analyses of thin-walled mild steel structures to give reliable results without excessively complicated and lengthy efforts, and it will be employed in the current study of thin-walled cold-formed beams.

In the following sections, the formulation of the equations which would be used for the analysis of the thin-walled beams in subsequent chapters will be discussed, the assumptions and simplifying idealisations required to reduce the theories to a state that would allow relatively simple computations and hence easy applicability to practical problems, will also be presented as the formulae are developed.

2.2 MATERIAL MODELS

The material properties of mild steel have made this material very popular indeed in the past century. Amongst it's wide range of applications, mild steel has been extensively used in the field of thin-walled structures, especially in the form of cold-formed steel sections. The relatively high strength and ductility of these steels permits them to be cold worked readily with little difficulties allowing the production of thin-walled sections of various shapes and sizes to be done through relatively simple cold forming processes, such as press braking, folding and cold rolling.

The cold-formed beams examined in this thesis are made from mild steels of various compositions, but material tests have shown that they generally fall into one of the two material behavioural groups described here. The typical shapes of the uni-directional tensile stress-strain characteristics, obtained through tensile testing according to BS 10 and BS EN 10 002-1 : 1990 [9], of the two groups of materials are shown in figure 2.2.1(a) & (b).

In the first, figure 2.2.1(a), more commonly found in mild steels, the stress follows a linear elastic behaviour 'oa' up to the limit of proportionality at a, after which some non-linearity occurs. The stress peaks at the upper yield point 'b' and almost immediately drops off to the lower yield point 'c' where some fluctuation usually occurs before it stabilises at the lower yield stress, the strains increase at constant stress from 'c' to 'd' and this lower yield stress is taken as the material yield strength for most design purposes. After the point 'd', the stress begins to increase with strains again, but at a rate which is only a fraction of that during the elastic loading up, this increase being brought about by strain hardening. A second peak is then reached at point 'e', known as the ultimate tensile strength of the material, after which the material breaks down causing fracture at point 'f'.

The second behaviour, illustrated in figure 2.2.1(b), is more commonly found in alloy steels and non-ferrous metals. Following the linear elastic stage of loading behaviour, non-linearity sets in as plasticizing occurs in the material to more gradually reach the plateau in the plot where the stress is constant with increasing strains, as compared to the first case. Strain hardening occurs as before to bring about the ultimate tensile load and subsequently fracture. The yield strength of the material in this case is taken as the 0.2% proof stress at point 'b', the stress corresponding to 0.2% plastic strain in the material.

In the analysis of the beams examined in the current work, two idealised material models will be employed, the first is used in the elastic theory and it is commonly referred to as the linear elastic perfectly plastic material. Figure 2.2.2 shows the characteristics of this ideal material, the linear elastic region is followed immediately by the plastic flat line where it is assumed that the plastic strain increases at a constant stress equal in value to the material yield strength until fracture occurs. This assumption has been widely used in traditional elastic failure criterion whereby failure is said to have occurred at first yield.

In the case of the current work, the elastic analysis will be used in conjunction with a plastic theory to establish the failure loads. In the plastic analysis, the rigid-plastic material assumption applies, figure 2.2.3 illustrates the stress-strain characteristics that this ideal material possesses. It neglects all elastic strains, considering all plastic strain to grow at a constant stress equal in value to the yield strength of the material.

Both the ideal material assumptions does not take into account the effects of strain hardening. This effect may become important only as the strains get large, as can be seen in figure 2.2.1, in the elastic and initial post yield regions, strain hardening effects are minute if in existence at all, hence it is perfectly acceptable to neglect it in the elastic analysis here since it is only used to model the initial loading stage where the

strains are still small. There is however the strain hardening effects left behind in the corners of the sections during fabrication, these cold-formed corners generally possess local effective yield strengths higher than that in the virgin material, which in turn has the effect of increasing the section strength. This issue will be addressed in chapter 8 and 9 of this thesis where relatively simple methods of accounting for strain hardening in the corners will be presented, together with a simple method of accounting for strain hardening in the plastic hinges.

It might also be noted that both the ideal materials do not take into consideration the Bauschinger effect, the error that this may cause is deemed to be small for the beams in this study since no full load reversals are involved.

2.3 THE ELASTIC THEORY

The elastic analysis for the current study combines the solution from the conventional elastic beam theory using the Macaulay's method with the effective width approach set out in BS 5950 : Part 5, ref. [8]. These solutions are discussed separately in the following two sections and the approach for the combined use of the two parts is explained in section 2.3.3.

2.3.1 Elastic Beam Solution

The simple elastic bending of the thin-walled beam is considered using the Macaulay's method to estimate the beam deflections for a single span beam. The beam is assumed to be simply supported at both ends and loaded by a concentrated downward force at mid span, figure 2.3.1.1 shows the beam loading configuration. From the Macaulay's solution, the deflection of the elastic beam at any point is given by Eqn.(2.3.1.1), and the mid span (also the load point) deflection is given by Eqn.(2.3.1.2).

$$v = \frac{1}{EI}\left(-\frac{P}{12}x^3 + \frac{P}{6}\left[x - \frac{L}{2}\right]^3 + \frac{PL^2}{16}x\right) \qquad \text{Eqn.(2.3.1.1)}$$

$$v_{ms} = \frac{PL^3}{48EI} \qquad \text{Eqn.(2.3.1.2)}$$

where [....] are Macaulay brackets
v is the beam deflection x mm away from the left support
v_{ms} is the mid span deflection
P is the applied mid span load
L is the beam span length
E is the Young's modulus of Elasticity
and I is the beam section second moment of area.

The elastic bending moment of the beam is given by Eqn.(2.3.1.3),

$$M = \frac{PL}{4} \qquad \text{Eqn.(2.3.1.3)}$$

where M is the maximum bending moment occuring at mid-span.

2.3.2 Effective Width

The Effective Width equations recommended in the British Standard, BS 5950 : Part 5 : 1987, ref. [8], are employed here to account for the effects of local buckling of the compression elements in the beams. Before the Effective Width can be determined, two parameters have to be worked out. The first is the local buckling critical stress, from the general solution for plate buckling, shown as Eqn.(2.3.2.1),

$$P_{cr} = K \cdot \frac{\pi^2}{b^2 t} \cdot \frac{Et^3}{12\left(1-\upsilon^2\right)} \qquad \text{Eqn.(2.3.2.1)}$$

where P_{cr} is the local buckling stress
K is the local buckling coefficient
b is the plate width
t is the plate thickness
and υ is the material Poisson's ratio.

From Eqn.(2.3.2.1), by assuming E =205 kN/mm^2 and υ =0.3, the equation can be simplified to

$$P_{cr} = 185000K\left(\frac{t}{b}\right)^2 \qquad \text{Eqn.(2.3.2.2)}$$

The local buckling coefficient for the various cases of geometry is found using the equations listed in Appendix I of this thesis.

Two Effective Width equations are then applicable, depending on the beam cross-section and plane of bending relative to the beam. These are listed below as Eqn.(2.3.2.3) and Eqn.(2.3.2.4) for the stiffened and unstiffened elements under uniform compression respectively.

$$b_{eff} = b\left[1 + 14\left\{\left(\frac{f_c}{Pcr}\right)^{\frac{1}{2}} - 0.35\right\}^4\right]^{-0.2} \qquad \text{Eqn.(2.3.2.3)}$$

$$b_{eu} = 0.89 b_{eff} + 0.11 b \qquad \text{Eqn.(2.3.2.4)}$$

where b_{eff} is the Effective Width for a stiffened element
b_{eu} is the Effective Width for an unstiffened element
and f_c is the compressional stress on the effective element.

2.3.3 Method of elastic analysis

The elastic analysis adopts the linear elastic perfectly plastic material model as illustrated in figure 2.2.2 and considers the buckling of the compression element of the beam by utilising the reduced section properties based upon the Effective Widths of the buckled elements to calculate the moment carrying capacity and deflections of the beam.

Consider the compression element of a beam section under uniaxial stress, on the onset of buckling at the critical local buckling stress, only the effective portion the element is assumed to carry any stress, therefore when the compressional stress in the element reaches or exceeds the critical buckling stress, the effective widths of the buckled element can be calculated using Eqn.(2.3.2.3) or Eqn.(2.3.2.4) and the reduced section properties of the buckled beam section can then be worked out, based on the effective widths.

With the average compressive stress on the effective element, σ_{avb} ($=f_c$ in the effective width equation), the stress distribution across the beam cross-section can be plotted, figure 2.3.3.1, and the stress on the tension edge can be found through similar triangles, in terms of the compressive stress.

$$\sigma_t = \frac{d-h}{h}\sigma_{avb} \qquad \text{Eqn.(2.3.3.1)}$$

The equivalent forces acting on the section can then be written in terms of the average compressive stress. Taking the case of the plain channel section as an example,

$$F1 = \sigma_{avb} \cdot b_{eu} \cdot t \qquad F2 = \sigma_{avb}\frac{h \cdot t}{2}$$

$$F3 = \sigma_{avb}\frac{(d-h)^2 \cdot t}{2h} \qquad F4 = \sigma_{avb}\frac{(d-h)\cdot b \cdot t}{h} \qquad \text{Eqn.(2.3.3.2)}$$

The position of the neutral axis of bending is determined by considering horizontal equilibrium,

$$F1 + F2 = F3 + F4$$

and for this case, this yields,

$$h = \frac{\left(\frac{d^2}{2}\right) + d \cdot b}{b_{eu} + b + d} \qquad \text{Eqn.(2.3.3.3)}$$

The section moment carrying capacity can now be found from the equivalent forces.

$$M_{eb} = F1 \cdot h + F2 \cdot \frac{2h}{3} + F3 \cdot \frac{2(d-h)}{3} + F4(d-h) \qquad \text{Eqn.(2.3.3.4)}$$

Considering the beam under three point bending, the mid span load is then given by

$$P = \frac{4M_{eb}}{L} \qquad \text{Eqn.(2.3.3.5)}$$

Using elastic beam theory, the mid span deflection of the beam is given by

$$v_{ms} = \frac{P \cdot L^3}{48EI_{eff}} \qquad \text{Eqn.(2.3.3.6)}$$

where I_{eff} is based on the reduced cross-section at the point along the beam where the bending moment is maximum.

In summary, before buckling initiates, deflections are worked out for the each load step from Eqn.(2.3.1.2). After buckling has started in the compression element, indicated by the local critical buckling stress, values of the longitudinal stress at the compressional elements of the buckled section are increased in steps and substituted into either Eqn.(2.3.2.3) or Eqn.(2.3.2.4) depending on the section, to find the effective width of the element. The corresponding bending moments and reduced section properties are then calculated using Eqn.(2.3.3.1) to Eqn.(2.3.3.4), after which the loads and deflections are evaluated using Eqn.(2.3.3.5) and Eqn.(2.3.3.6) respectively, for each load step. This procedure yields the data for the plotting of the theoretical elastic loading line.

2.4 THE RIGID-PLASTIC THEORY

In the behaviour of thin-walled structures after local buckling has commenced, as the local buckling deformations increase during loading, plasticity spreads in the section and the maximum plastic bending moment capacity in some portions of the component plate is eventually reached. These portions often manifest themselves in the form of yield lines in which the material has gone completely plastic. From this point onwards, the plate deformations starts to concentrate at the yield lines while the adjacent platelets flatten as they unload elastically. These yield lines will also be referred to as hinge lines or simply hinges in this thesis, so called because any attempts to increase the loading would cause the adjacent platelets to fold along these lines, which allow large rotations without significant changes in the resisting bending moment. These hinges are unlike true hinges in that they do not allow free relative rotation of the connected platelets, instead, they permit rotation with a almost constant plastic bending moment in resistance.

The system of yield lines forms plastic mechanisms, like those described in section 1.6 of this thesis, which characterises the deformation of the thin-walled member during collapse. The relatively uncomplicated geometry of these plastic mechanisms allows a simple plastic analysis of the collapse behaviour during the folding of the component plates in a buckled section. The analysis is equivalent to the plastic analysis of beams and frames of compact members presented by Horne [73], with the exception that the cross-section distortions in the locally buckled sections adds complexity to the analysis.

The theory ignores elastic deformations utilising the rigid-perfectly plastic material model, as described in section 2.2, which implies that while the rotations about the hinge lines takes place at a almost constant plastic moment, the adjacent plates

remains flat and displaces as rigid bodies, with exceptions. This assumption is difficult to justify for the initial stages for failure but it lays the foundation for a relatively simple plastic analysis of a buckled section well into collapse where the plastic mechanisms are well developed.

2.4.1 Hinge Plastic Moment of Resistance

The resisting bending moment in plastic hinges that form on buckled thin-walled structures, in the absence of significant axial, shear or torsional forces, is given by the fully plastic moment capacity of the plate,

$$m_p = Z_p \cdot \sigma_o \qquad \text{Eqn.(2.4.1.1)}$$

where m_p represents the plate fully plastic moment capacity
Z_p is the plastic section modulus
and σ_o is the material yield stress.

For a flat plate, the cross-section is essentially a simple rectangular section as shown in figure 2.4.1.1(a), and the fully plastic section modulus is given by

$$Z_p = \frac{bd^2}{4} \qquad \text{Eqn.(2.4.1.2)}$$

and the fully plastic moment capacity is

$$m_p = \sigma_o \cdot \frac{bd^2}{4} \qquad \text{Eqn.(2.4.1.3)}$$

The buckled component plates of a thin-walled beam, even when the beam is in pure bending, are subjected to axial force plus bending. The axial force has the effect of reducing the fully plastic moment capacity of the plate.

For a rectangular section subjected to a combination of axial force and bending, shown in figure 2.4.1.1(b), the fully plastic moment is reduced to

$$m_p' = m_p\left[1 - \left(\frac{P}{Po}\right)^2\right] \qquad \text{Eqn.(2.4.1.4)}$$

where P is the applied axial force
and P_o is the squash load of the section ($P_o = \sigma_o bd$).

2.4.2 The Reduced Plastic Moment of an Inclined Hinge

In the previous section, Eqn.(2.4.1.4) provides a means to calculate the plastic moment resisting hinge rotations for a plate subjected to axial compression where the hinge is perpendicular to the direction of the applied forces. In the plastic mechanisms that form during the collapse of thin-walled structures, plastic hinges can occur at various angles and this causes a further reduction in the resisting moment of the hinge.

Consider an inclined hinge AB subjected to axial compression, as shown in figure 2.4.2.1, the material within the hinge is assumed to have yielded while the adjacent platelets are rigid as bending occurs about the axis o-o. The transformed stress resultants (using two dimensional stress transformation) acting on the inclined hinge due to the end thrust are given by

$$N_y = \frac{N}{2}(1 + \cos 2\gamma) \qquad \text{Eqn.(2.4.2.1)}$$

$$N_x = \frac{N}{2}(1 - \cos 2\gamma) \qquad \text{Eqn.(2.4.2.2)}$$

$$N_{xy} = \frac{N}{2}\sin 2\gamma \qquad \text{Eqn.(2.4.2.3)}$$

where N is the applied axial stress resultant in N/mm ($= \frac{force}{b}$)
γ is the angle of hinge inclination
and N_y, N_x, N_{xy} are the resulting direct and shear stress resultants acting on the hinge.

Now consider the general case of stresses acting on the inclined hinge with the axial end compression and bending action, as shown in figure 2.4.2.2. The normal stress σ_y is produced as the combined result of N_y and the bending action, while σ_x and τ_{xy} are due purely to N_x and N_{xy} respectively.

$$\sigma_x = \frac{N_x}{t} \qquad \text{and} \qquad \tau_{xy} = \frac{N_{xy}}{t} \qquad \text{Eqn.(2.4.2.4)}$$

Assuming the yield portion follows the flow rules of the von Mises criterion in a 2-D stress system, Eqn.(2.4.2.5) relates the stresses.

$$(\sigma_1 - \sigma_2)^2 + (\sigma_2 - \sigma_3)^2 + (\sigma_3 - \sigma_1)^2 = 2\sigma_o^2 \qquad \text{Eqn.(2.4.2.5)}$$

where $\sigma_{1,2} = \left(\frac{\sigma_x + \sigma_y}{2}\right) \pm \frac{\sqrt{(\sigma_x - \sigma_y)^2 + 4\tau_{xy}^2}}{2}$.

By assuming a 2-D stress system, $\sigma_3 = 0$ and rearranging,

$$\sigma_y^2 - \sigma_x\sigma_y + \left[\sigma_x^2 + 3\tau_{xy}^2 - \sigma_o^2\right] = 0 \qquad \text{Eqn.(2.4.2.6)}$$

Solving Eqn.(2.4.2.6), which is a quadratic equation in σ_y,

$$\sigma_y = \frac{1}{2}\left[\sigma_x \pm \sqrt{\sigma_x^2 - 4\left(\sigma_x^2 + 3\tau_{xy}^2 - \sigma_o^2\right)}\right] \qquad \text{Eqn.(2.4.2.7)}$$

Across the hinge line AB, to have yield under bending action, the stress on either side of the zero stress position is given by Eqn.(2.4.2.7), which can be rewritten as

$$\sigma_y = \tfrac{1}{2}[\sigma_x \pm \alpha_o] \qquad \text{Eqn.(2.4.2.8)}$$

where $\alpha_o = \sqrt{4\sigma_o^2 - 3\sigma_x^2 - 12\tau_{xy}^2}$.

Taking o-o as the mid-thickness axis, the distribution of the normal stress, σ_y over the thickness of the hinge is shown in figure 2.4.2.3.

Considering unit width, take moments about the point O,

$$m_p'' = \tfrac{1}{2}(\sigma_x + \alpha_o)n\left(\tfrac{t}{2} - \tfrac{n}{2}\right) + \tfrac{1}{2}(\alpha_o - \sigma_x)n\left(\tfrac{t}{2} - \tfrac{n}{2}\right)$$

giving

$$m_p'' = \tfrac{n}{2}(t-n)\alpha_o \qquad \text{Eqn.(2.4.2.9)}$$

Summing the forces along axis o-o,

$$N_y = \tfrac{1}{2}(\sigma_x + \alpha_o)n - \tfrac{1}{2}(\alpha_o - \sigma_x)(t-n)$$

giving

$$n = \frac{N_y + \frac{t}{2}[\alpha_o - \sigma_x]}{\alpha_o} \qquad \text{Eqn.(2.4.2.10)}$$

Substituting Eqn.(2.4.2.10) into Eqn.(2.4.2.9) and rearranging yields

$$m_p'' = \frac{1}{2\alpha_o}\left[\frac{t^2}{4}(\alpha_o^2 - \sigma_x^2) + N_y t\sigma_x - N_y^2\right] \qquad \text{Eqn.(2.4.2.11)}$$

Taking the fully plastic plate moment capacity per unit width as

$$m_p = \frac{\sigma_o t^2}{4} \qquad \text{Eqn.(2.4.2.12)}$$

and substituting Eqn.(2.4.2.1) through to Eqn.(2.4.2.4) into Eqn.(2.4.2.11) then dividing it by Eqn.(2.4.2.12) and rearranging, we obtain the final unit width reduced moment expression for the inclined hinge under axial compression.

$$\frac{m_p''}{m_p} = \frac{\left[1-\left(\frac{N}{N_o}\right)^2\right]}{\sqrt{1-\frac{3}{4}\left(\frac{N}{N_o}\right)^2 \sin^2\gamma\left(4-3\sin^2\gamma\right)}} \qquad \text{Eqn.(2.4.2.13)}$$

where $N_o = \sigma_o t$.

A further modification to this equation has been formulated to account for material strain hardening, the plate fully plastic moment term can be replaced by one which considers the material to be rigid-linear strain hardening. The details of this modification is presented in section 8.4 of this thesis.

2.4.3 Some concepts relating to Plastic Mechanism Analysis

In the plastic mechanism analysis technique employed in the current work, it is assumed that the material follows a rigid-perfectly plastic behaviour, deformations are assumed to be concentrated at the yield lines taking the form of bending about the hinges with the platelets between the hinges remaining flat. At this point, a distinction should be made between true mechanisms and quasi mechanisms, as defined by Murray and Khoo [46]. A true mechanism is a mechanism which can develop with only rotational deformations about the yield lines alone, while quasi mechanisms cannot develop without normal or shear deformations in some of the yield lines or alternatively in-plane membrane deformations in the flat plates between the hinges. A suggested test to determine the classification of the mechanism is to construct a cardboard model of the mechanism and the true mechanism will deform with only folding of the hinges while quasi mechanisms would require some cuts to be made along some hinges before the mechanism can deform. This test can sometimes be misleading, especially when the cardboard is deteriorated. For thin plates, the energy associated with membrane strains is larger than the energy for plate bending, it then can be argued that whenever kinematically possible, a true mechanism will develop, theoretically speaking. In the collapse of real thin-walled structures however, this is rarely the case and great care has to be taken in the creation of theoretical plastic mechanisms, so that oversimplification of quasi mechanisms and neglecting of necessary membrane strains does not occur.

According to the plastic mechanism theory for beams and frameworks by Baker et.al. [1], an exact rigid-plastic solution will satisfy all three of the basic conditions listed below.

- Equilibrium - each part of the structure and the structure as a whole is in equilibrium with the applied loads and the reactions at the supports.

- Mechanism - sufficient plastic hinges are developed so that the whole or part of the structure can deflect as a mechanism.

- Yield - at no point in the structure can yield be exceeded.

Except in the simplest of structures, it is extremely difficult to satisfy all three conditions simultaneously, approximate methods that satisfies only two of the conditions are therefore very useful. The upper bound method satisfies the equilibrium and mechanism conditions and it gives estimations of the failure loads which are either equal to or more often higher than that in the actual structure. Although this method overestimates the loads, with some care, the differences can be made very small, producing very useful results. In contrast, the lower bound method gives failure predictions which are equal to or lower than the actual, this method satisfies the equilibrium and yield conditions. Since lower bound solutions are conservative, they are more readily accepted in current design situations.

The plastic mechanism analysis used in the current work adopts the upper bound approach in a limit analysis technique. The reason that overestimates are obtained in the current method is the fact that the chosen plastic mechanisms are rarely as "good" as that which the structure itself will adopt.

2.4.4 Method of Rigid Plastic Analysis

By assuming a kinematically admissible mechanism, a mechanism load can be calculated by equating the external incremental work to the total internal incremental energy dissipation in the hinges and membrane strain areas (where applicable). A series of mechanism loads are calculated, each based on a geometrical configuration differing from the previous one by a small amount corresponding to the deformation mode of the assumed mechanism. The series of mechanism load versus deformation data is used to form the rigid plastic curve that describes the collapse behaviour of the failed section.

In classical yield line theory, a mechanism is determined by defining a pattern for the overall (global) plastic mechanism which is made up of stationary hinges, different mechanisms with different yield line patterns result in different mechanism loads. The decisive mechanism is taken as the pattern which produces the smallest mechanism load. Using this method for the current work, it may be found that for increasing deformations, slightly different hinge patterns produce the smallest loads in the successive load steps. It may therefore be necessary to consider some hinges as travelling yield lines (also known as moving hinges or rolling mechanism lines), which makes it possible for the yield line pattern to change in proportion.

In practice however, it may be difficult to determine the complete yield line pattern by simply assuming any theoretical plastic mechanism and minimising the mechanism loads. It is therefore wise to base the theoretical models partly on the observations of yield patterns occurring in actual sections during tests, or on the elastic buckling behaviour of the thin-walled section. This is the approach adopted in the current work, observed plastic mechanisms are simplified to form the basic theoretical model of the plastic mechanism and the final geometrical proportions of the yield pattern is taken as that which produces the minimum failure load. The observed mechanisms for

the beams of various cross-sections examined and the simplifications are detailed in chapters 3, 4 and 5 where the theoretical plastic mechanism models for the respective sections are developed.

An energy approach based on the principle of virtual work is then applied to the theoretical yield line pattern, equating the sum of the external work from the bending about the global plastic hinge to the sum of the internal energy dissipated in the bending about the stationary yield lines, rolling of the travelling hinges and membrane straining. The energy equations used for these four actions are described in the following subsections (2.4.4.1 to 2.4.4.4). The relationships between the angular rotations of the hinges is determined by considering geometry and by writing all angles in terms of the global hinge angle and equating the energies, a governing equation describing the unloading behaviour of the failing beam may be obtained.

2.4.4.1 Bending Energy of the Global Plastic Hinge

In the collapse of the buckled beam, the rigid plastic assumption implies that all the deformations in the beam are assumed to concentrate at the plastic mechanism where failure was initiated, considering the failure section as the global plastic hinge, the external work done in the collapsing beam is simply the energy required to cause global bending about the hinge and the work done is calculated using Eqn.(2.4.4.1).

$$W_{ext} = M(\mu) \cdot \delta\mu \qquad \text{Eqn.(2.4.4.1)}$$

where $M(\mu)$ is the moment capacity of the global plastic hinge at hinge angle μ and $\delta\mu$ is a small increment in the global hinge rotation.

2.4.4.2 Energy dissipated in Stationary Hinges

The reduced moment expression derived in section 2.4.2 is used to calculate the energy dissipation at stationary hinges. The energy term for the stationary hinge is therefore given by

$$W_{sh} = m_p'' \cdot (hinge - length) \cdot \delta\alpha \qquad \text{Eqn.(2.4.4.2)}$$

where m_p'' is derived from Eqn.(2.4.2.13)
and $\delta\alpha$ is the small increment in local hinge rotation corresponding to $\delta\mu$.

2.4.4.3 Energy dissipated in Travelling Hinges

The energy dissipated in travelling hinges are calculated using a technique similar to that used by Kecman [25], and is given by

$$W_{th} = 2 \cdot m_p'' \cdot \frac{Swept-Area}{r} \qquad \text{Eqn.(2.4.4.3)}$$

where r is the rolling radius of the travelling hinge,
$Swept - Area$ is the area the hinge sweeps through corresponding to $\delta\mu$ and the factor 2 accounts for the actions of unfolding of the hinge at the original position and refolding at the new location.

It should be noted that this expression only accounts for the idealised folding and unfolding action of the travelling hinge as it is moved to the new location, it does not take into consideration the increase in hinge rotation which may have occurred during the movement.

2.4.4.4 Membrane Strain Energy

The plastic membrane strain energy is estimated by assuming that the regions experiencing membrane strain are completely plastic and that there is only uni-directional stress existing in the flat platelets, the energy dissipation is therefore calculated using

$$W_{mem} = \int_{vol}(\sigma_o \cdot \varepsilon)dvol \qquad \text{Eqn.(2.4.4.4)}$$

where ε is the unidirectional strain.

The unidirectional stress idealisation is possible for the compression flange of channel and zed sections since one of the edges is unrestrained except for the lips in the lipped sections which offers little resistance to strains in the buckled section. In cases where this assumption does not hold true, 2-D stress states would need to be used, and the total membrane strain energy would be the sum of the work in each of the principle directions.

2.5 INDETERMINATE BEAM PROBLEMS

In indeterminate beam problems, such as multi-spanning beams, collapse only occurs if sufficient failure sections develop, according to the mechanism condition of the plastic theory described previously in section 2.4.3. These failure sections would invariably occur at the locations along the beam where the bending moments are most adverse. As the deformations increase, the local buckles develop into local plastic mechanisms. The most severely stressed sections of the beam reaches their ultimate moment capacities and starts to shed some of their load. As they unload following their collapse characteristics, the load shed is taken up by other portions of the beam which were not so severely loaded. Increases of the applied loading is therefore possible up to such point where failure eventually occurs elsewhere, satisfying the mechanism condition. This phenomenon is called plastic moment redistribution and can increase the ultimate loads for multi-spanning beams by substantial amounts depending on the geometrical proportions of the beam.

In the current work, double span beams have been examined and the following paragraphs describes the technique developed to estimate the load-deflection characteristics for double spanning beams from the results obtained in the study of beams with single global plastic mechanisms.

The elastic and plastic mechanism theories described in the preceding sections enables the load-deflection characteristics of beams that fail with a single global plastic mechanism to be ascertained, this result can be converted easily to moment versus hinge rotation data, by assuming that deformations along the beam is concentrated at the global plastic hinge, which is simply another way of representing the same information.

Consider two beams with identical cross-sections in single and double span set-ups as shown in figures 2.5.1(a) and 2.5.1(b) respectively. Since the beam sections are the same, it can be assumed that the collapse mechanism that develops in both beams will be very similar, if not identical, hence it can be assumed that the moment-rotation characteristics for all the global plastic mechanisms that will develop in the beams are the same as that obtained from the modelling of single spanning beam. This is the basis of the current method.

By using an energy approach, the incremental external work done by the applied forces can be equated to the sum of the internal work by the three global plastic hinges as shown below.

$$2 \cdot P \cdot \delta v = 2 \cdot M_1(\mu_1) \cdot \delta\mu_1 + 2 \cdot M_2(\mu_3') \cdot \delta\mu_3 \qquad \text{Eqn.(2.5.1)}$$

where the moments of the failure section M_1 and M_2 are functions of half the global plastic hinge rotation angles

and $\mu_3' = \frac{\mu_3}{2}$.

The angles of rotation of the hinges can be related to the load point deflections by considering geometry and the instantaneous bending moments at any hinge angle are derived from the single span results. Eqn.(2.5.1) enables the construction of the load-deflection characteristic plot for the double spanning beams.

The simple method described above is based purely on the energy approach and is capable of producing rather good estimates in cases where the span length of the double span beam is of the same order as that of the single span beam which provides the moment-rotation data. A more generally applicable method of solution will be presented in chapter 3, section 3.5.4, in which elastic solutions are used in conjunction with the energy approach for double span beam load-deflection predictions.

Although only double span beams where investigated in the current thesis, the proposed technique can be easily extended to accommodate multi-spanning beams. Since the methods are rather simple and do not deviate too much from conventional beam analysis, it was deemed unnecessary to carry out multi-span beam experiments exclusively for the current investigation.

This chapter has briefly stated the methods used in this study of thin-walled beams in collapse, to gain fuller understanding of the approach and application of these techniques, the reader may want to proceed to chapter 3, where the models for plain channel beams are developed.

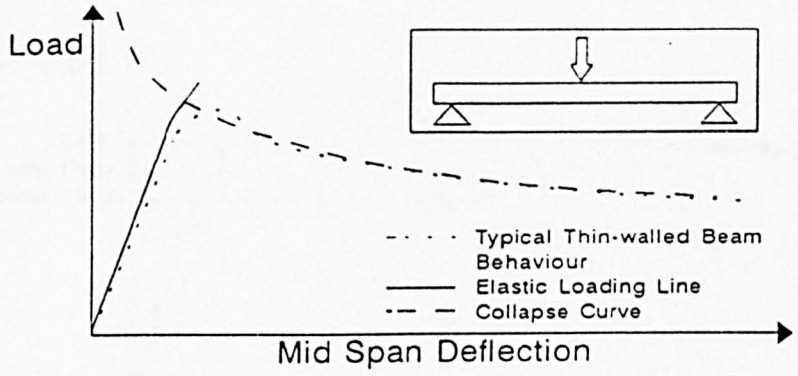

Figure 2.1.1 : Typical Thin-walled beam behaviour

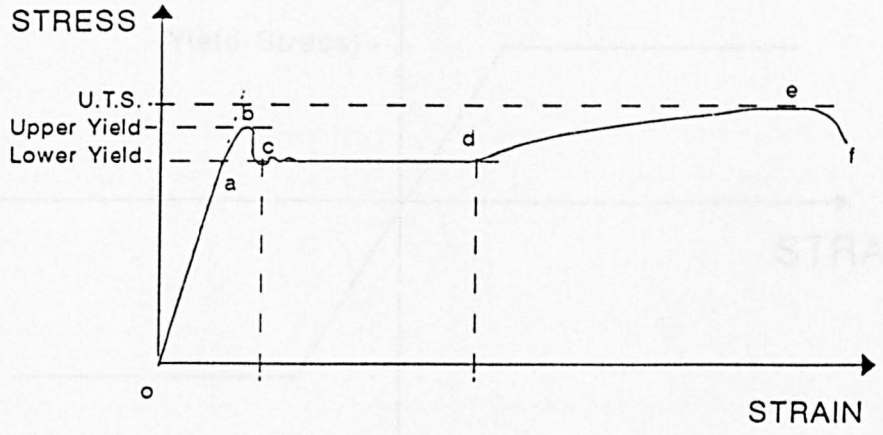

(a)

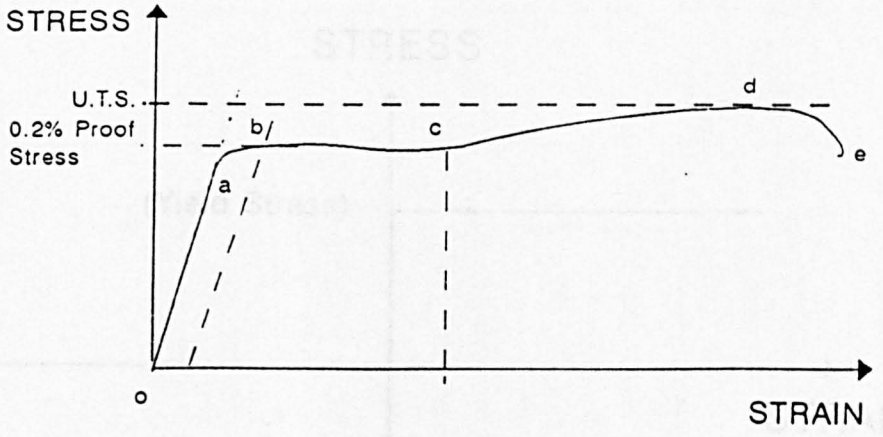

(b)

Figure 2.2.1 : Observed Material Behaviours

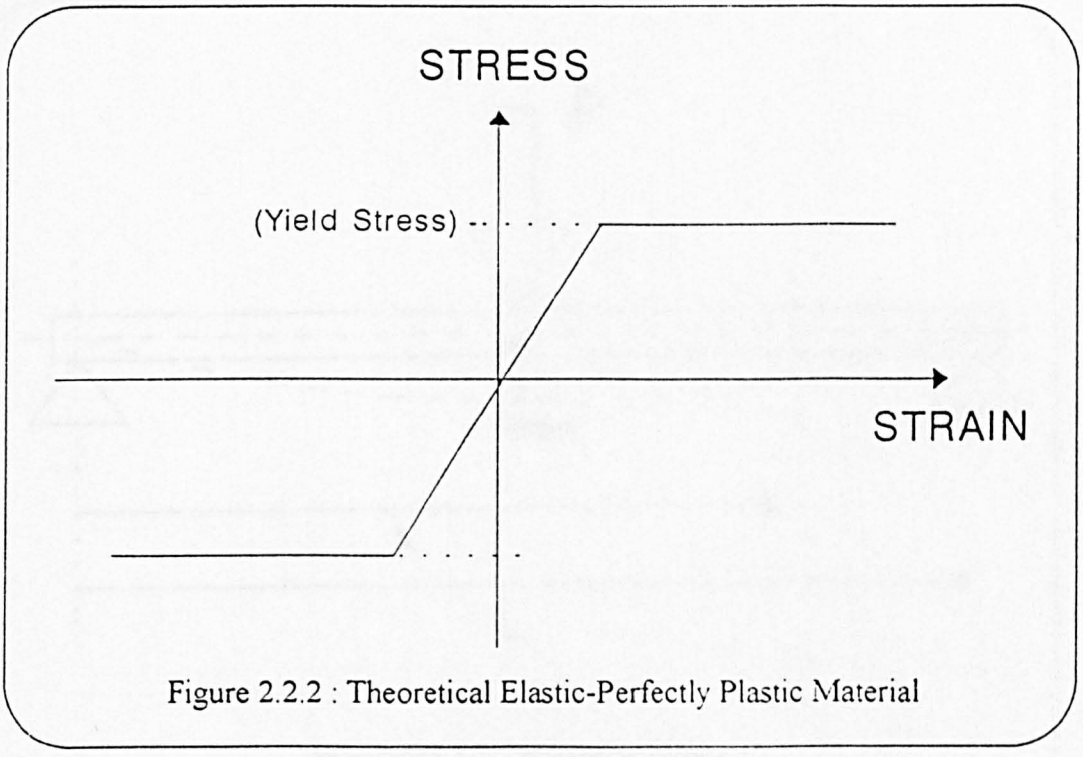

Figure 2.2.2 : Theoretical Elastic-Perfectly Plastic Material

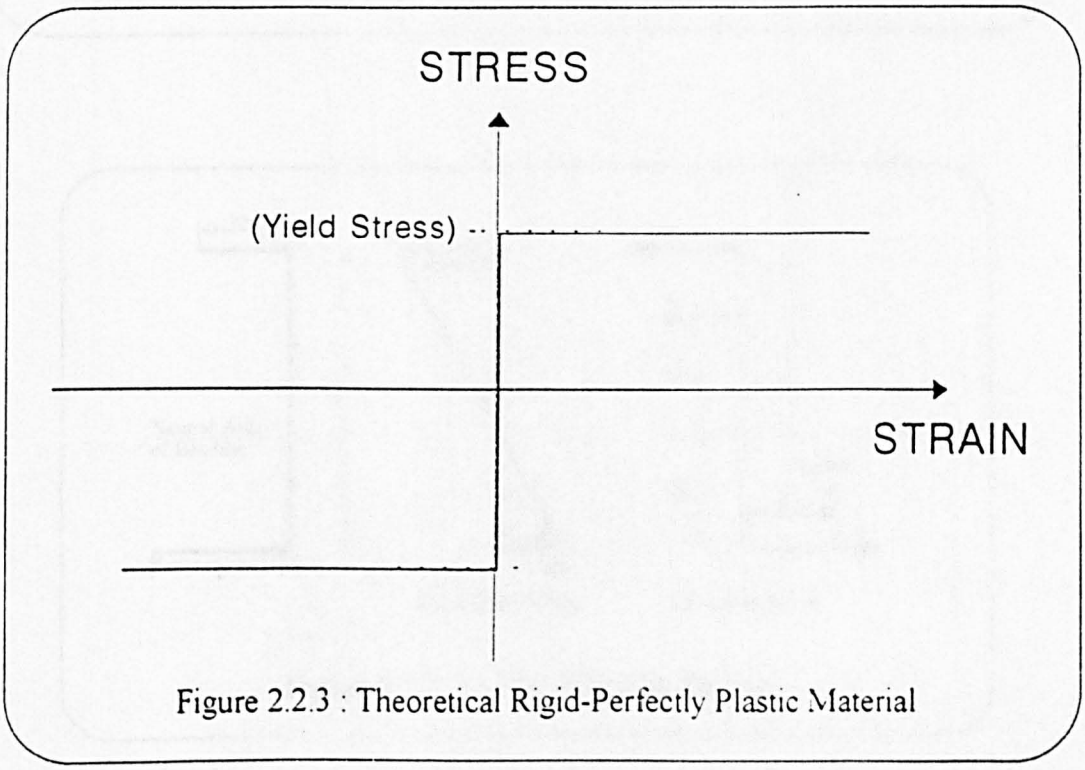

Figure 2.2.3 : Theoretical Rigid-Perfectly Plastic Material

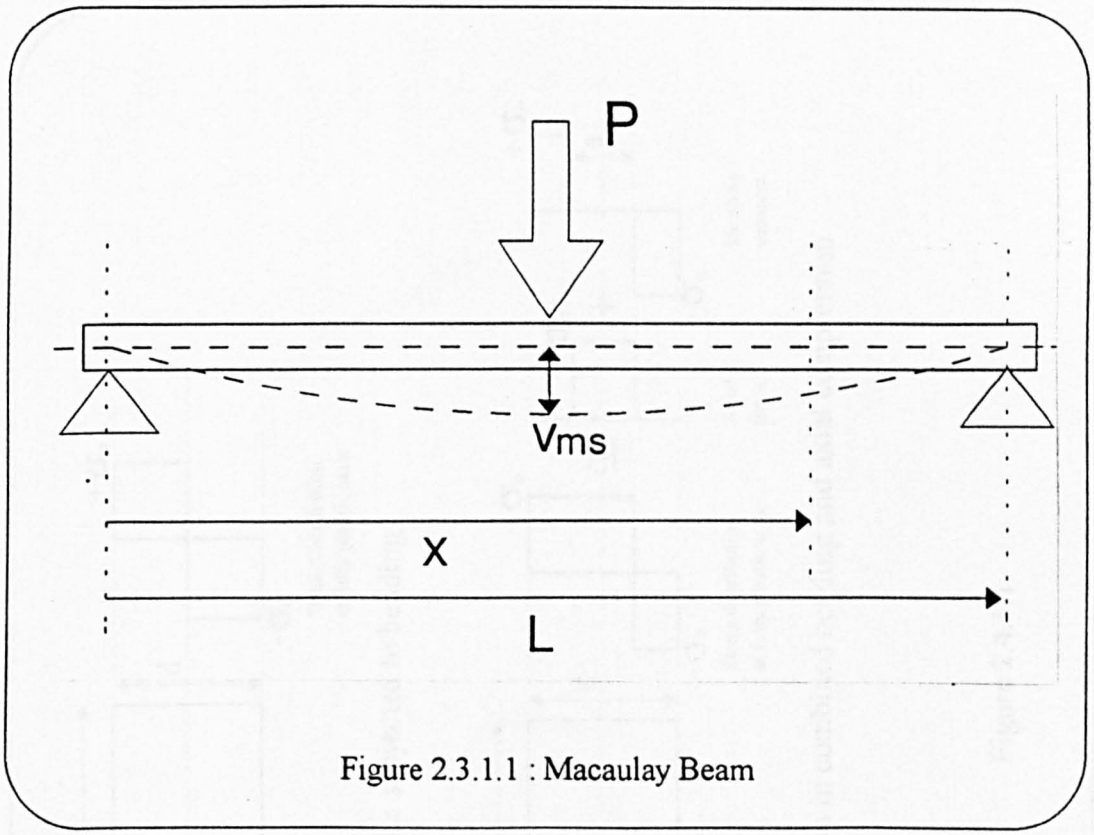

Figure 2.3.1.1 : Macaulay Beam

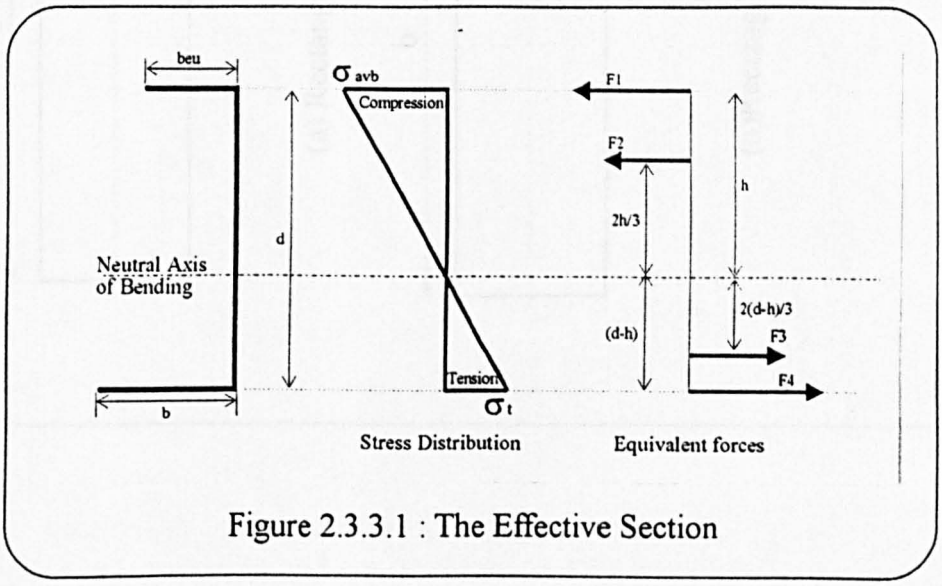

Figure 2.3.3.1 : The Effective Section

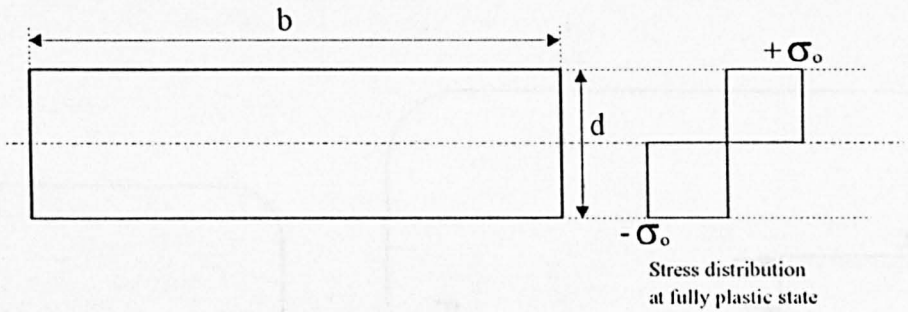

(a) Rectangular section subjected to bending

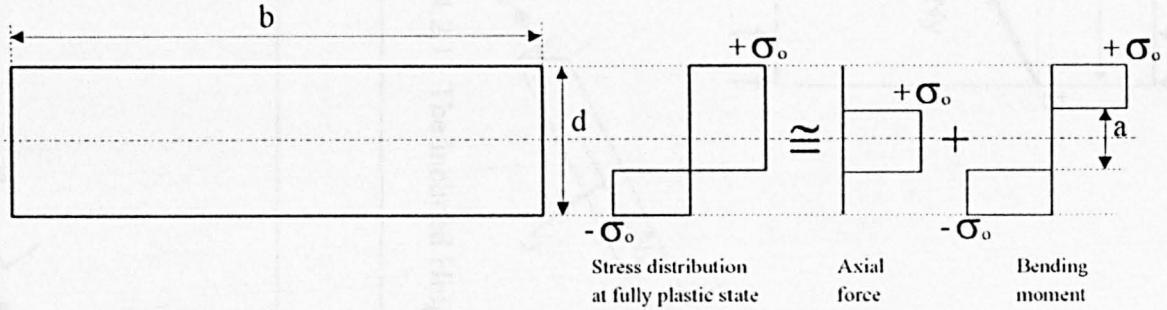

(b)Rectangular section in combined bending and axial compression

Figure 2.4.1.1

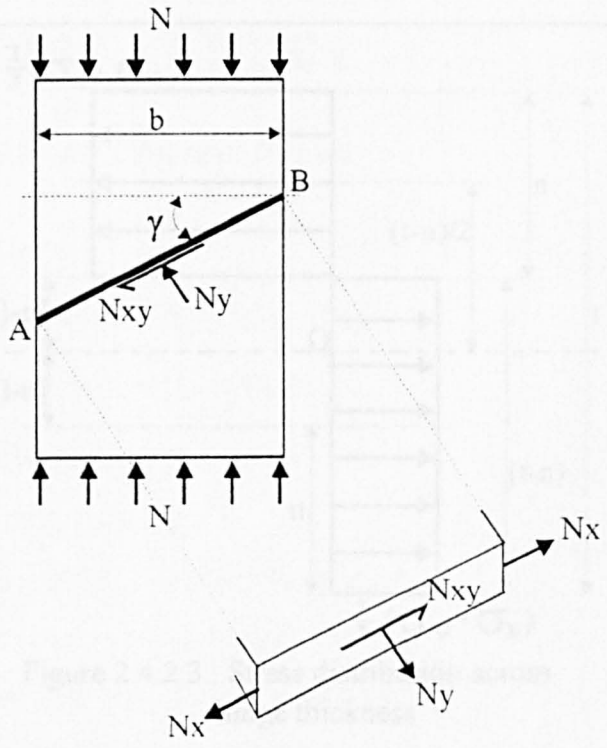

Figure 2.4.2.1 : The Inclined Hinge

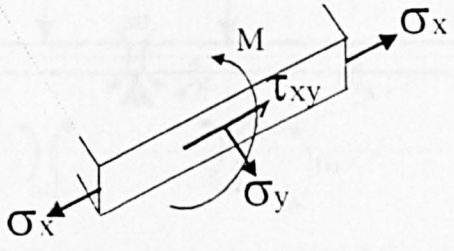

Figure 2.4.2.2 : Forces acting on the Inclined Hinge

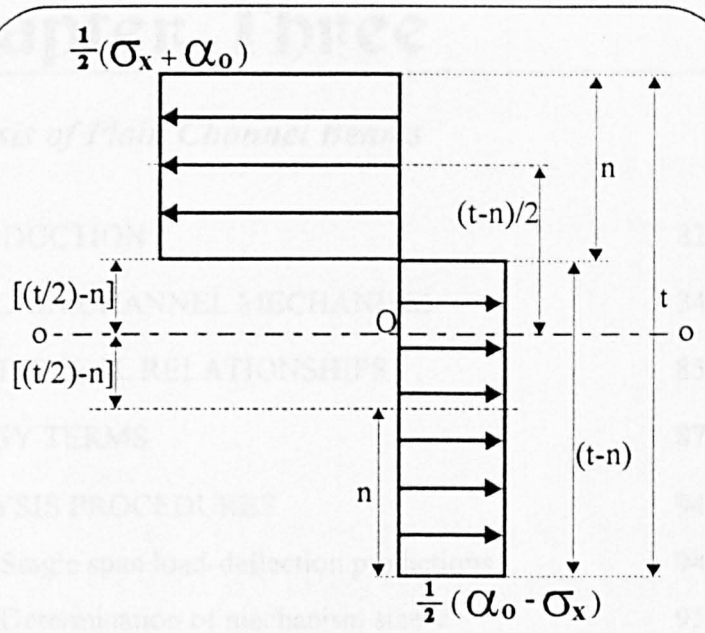

Figure 2.4.2.3 : Stress distribution across hinge thickness

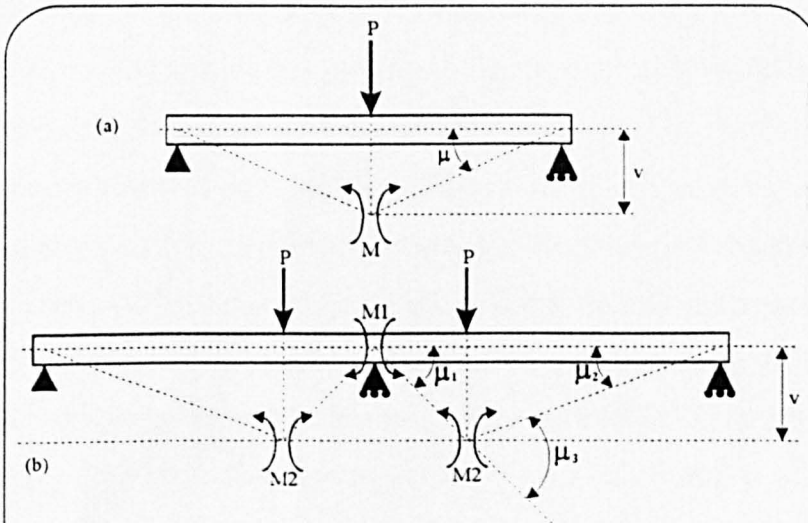

Figure 2.5.1 : Deflections in single and double span beam

Chapter Three

- *Analysis of Plain Channel Beams*

3.1 INTRODUCTION

Local buckling in thin-walled sections subjected to bending is a familiar problem which has received much attention from researchers for a number of years. Most of the work focused on the prediction of the ultimate load carrying capacity and deflection characteristics of the members which are not only prone to local buckling, but may be susceptible to torsional instability, effects of localised loading and various problems due to the support system.

Current design codes such as BS 5950 : Part 5 : 1987 [8], like most other codes from around the world which deal with thin-walled members, applies the Effective Width concept in one form or another in designing against buckling, much of the recommendations being based on empirical formulations.

Investigations carried out on plain channel sections in bending includes that by Rhodes [52] which studied channels in bending such that the unstiffened flanges comprise the bending elements, analysis involved using the effective width method. Murray and Khoo [46] and Murray [44] developed theoretical collapse analysis for plain channel columns using the plastic mechanism approach, five possible mechanisms were observed during the experimental investigation and by considering the complete mechanism as an assembly of strips of elementary mechanisms, the resulting theoretical collapse curve was in good agreement with the experimental findings. Sin [70] examined plain and trapezoidal channels in pure bending, such that the stiffened webs were in tension while the flanges were subjected to bending, failure modes similar to those found by Murray and Khoo were observed and analysis based on the plastic mechanism approach produced results which agreed well with acquired experimental data. Rasmussen [48] also studied channel section columns using the plastic mechanism approach similar to that of Murray.

The analysis of plain channel beams is the subject of this chapter, the theoretical methods discussed in chapter 2 will be applied to channels which are loaded such that the stiffened webs forms the bending elements while the thin-walled flanges could be considered to be in pure tension and compression.

An experimental investigation was performed in the laboratory, in which 48 thin-walled mild steel plain channel beams were tested. Single and double span beams are supported and loaded through cleats which are bolted to the webs of the beams. The actual yield line patterns that formed on the failed sections during the experiments were used as the basis for the simplified theoretical plastic mechanism presented later in this chapter.

The analysis presented in this chapter attempts to predict the elastic, post-buckling and post-ultimate collapse load and deflection behaviour of the beams examined. As the theories involved have already been presented in chapter 2, much of this chapter focuses on the development of the plastic collapse mechanism model which will be used to generate the collapse curves.

The general method employed to analyse the plastic mechanism is to first establish the relationship between the overall rotation of the beam portions on either side of the failure section and the rotation at each hinge line within the plastic mechanism, through geometrical considerations. The energy method is then used to equate the virtual work done due to the overall beam rotation to the sum of the internal energy dissipated during hinge rotation, travel and in any plastic membrane strain which may be required to maintain kinematic admissivity. Some sizes within the mechanism are dictated by the beam geometry and support layout but there is one independent variable in this model which would have to be found through a mechanism load minimisation process.

3.2 THE PLAIN CHANNEL MECHANISM

The experiments conducted on the plain channel specimens revealed that one failure mechanism would consistently form in the beams at the loading cleat for the case of the single span beam and at the central support and loading cleats for the double span case, which was expected as those are the regions where bending moments are most adverse. Figures 3.1.1 to 3.1.4 illustrates the typical failure mode found on the tested plain channels. The observed pattern of yield lines were simplified to form the postulated theoretical plastic mechanism shown in figure 3.2.1 and 3.2.2.

The simplified mechanism consists of 6 fixed hinges, 4 stationary hinges with variable length and 3 travelling hinge lines, all of which were assumed to be straight. There are also two triangular regions in plastic membrane strain in the tension flange. The independent mechanism size 'c', see figure 3.3.1, would later have to found through load minimisation. In comparing the theoretical mechanism with the observed failure section, the most prominent difference is found in the compression flange, hinges 'AE' and 'DH' were assumed to be perpendicular to the flange edge while the corresponding lines in the actual failure section are almost invariably inclined. The reason for not using an inclination on hinges 'AE' and 'DH' is that this would introduce an independent angle which would be reduced to zero in a load minimisation process. Twisting occurs as the mechanism matures, however, most of the effects are considered elastic and therefore neglected in this analysis.

It should also be noted that the presence of the bolts on the web has two significant effects, firstly in determining the length of hinge 'FG' and secondly in limiting its' travel down the web as the mechanism develops.

3.3 GEOMETRICAL RELATIONSHIPS

The angle μ is taken as the primary independent variable in this model and all varying sizes and hinge angles are written directly or indirectly in terms of it. The following equations defines the important sizes and angles required for the analysis of the plastic mechanism.

From figure 3.3.1,

$$\tan\xi_2 = \frac{c}{d} \qquad \text{Eqn.(3.3.1)}$$

Due to the travel of hinge 'FG', from figure 3.3.2(a) and (b),

$$\tan\theta_2 = \frac{a}{d} \qquad \text{Eqn.(3.3.2)}$$

where a is the distance that hinge 'FG' has travelled.

From figures 3.3.1 and 3.3.3, taking the origin of the co-ordinate axis at the node 'I',

$$y_{F'} = d - a(1 + \sin\theta_2) \qquad \text{Eqn.(3.3.3)}$$

$$y_E = c \cdot \sin\mu + d \cdot \cos\theta_2 \cdot \cos\mu \qquad \text{Eqn.(3.3.4)}$$

$$x_E = c \cdot \cos\mu - d \cdot \cos\theta_2 \cdot \sin\mu \qquad \text{Eqn.(3.3.5)}$$

$$\tan\xi_2' = \frac{x_E}{y_E} \qquad \text{Eqn.(3.3.6)}$$

and $$\mu = \xi_2 - \xi_2' \qquad \text{Eqn.(3.3.7)}$$

Referring to figure 3.3.3, it can be shown that,

$$\sin(\theta_3 + \mu) = \left[\frac{y_E - y_{F'}}{c}\right] \qquad \text{Eqn.(3.3.8)}$$

Also $\cos(\theta_3 + \mu) = \frac{x_E}{c}$ Eqn.(3.3.9)

Hence, using Eqn.(3.3.8) and (3.3.9) and substituting into the expression Eqn.(3.3.3), (3.3.4) and (3.3.5), we obtain,

$$d \cdot \cos\mu \cdot \cos\theta_2 + a(1 + \sin\theta_2) - c \cdot \sin\left(\cos^{-1}\left[\frac{c\cdot\cos\mu - d\cdot\cos\theta_2\cdot\sin\mu}{c}\right]\right) = d - c \cdot \sin\mu \qquad \text{Eqn.(3.3.10)}$$

where $\theta_2 = \tan^{-1}\left(\frac{a}{d}\right)$

Eqn.(3.3.10) may used to find the distance of travel for hinge 'FG', a at any angle μ.

3.4 ENERGY TERMS

Hinges AE and DH

The angle θ_3 is defined by Eqn.(3.3.8), referring to figure 3.3.2(b) and figure 3.3.3, it can be shown that

$$\theta_3' = \tan^{-1}(\tan\theta_3 \cdot \cos\theta_2)$$
$$= \tan^{-1}\left(\tan\left[\sin^{-1}\left\{\frac{c\cdot\sin\mu+d\cdot\cos\theta_2\cdot\cos\mu-d+a(1+\sin\theta_2)}{c}\right\}-\mu\right]\cdot\cos\theta_2\right)$$

Eqn.(3.4.1)

The energy dissipated in hinges 'AE' and 'DH' is then given by

$$W_1 = 2\cdot m_p\left[1-\left(\frac{M}{M_u}\right)^2\right]\cdot b\cdot\theta_3'$$

$$W_1 = 2\cdot m_p\left[1-\left(\frac{M}{M_u}\right)^2\right]\cdot b\cdot$$
$$\tan^{-1}\left(\tan\left[\sin^{-1}\left\{\frac{c\cdot\sin\mu+d\cdot\cos\theta_2\cdot\cos\mu-d+a(1+\sin\theta_2)}{c}\right\}-\mu\right]\cdot\cos\theta_2\right)$$

Eqn.(3.4.2)

Hinges BF and CG

It can be shown that, (where $(\theta_3+\mu)'$ is viewed in line with 'BF')

$$(\theta_3+\mu)' = \tan^{-1}(\tan[\theta_3+\mu]\cdot\cos\theta_2) \qquad \text{Eqn.(3.4.3)}$$

Hence, the energy dissipated in hinges 'BF' and 'CG' is given by

$$W_2 = 2 \cdot m_p \left[1 - \left(\frac{M}{M_u} \right)^2 \right] \cdot (b + a) \cdot (\theta_3 + \mu)' \qquad \text{Eqn.(3.4.4)}$$

$$W_2 = 2 \cdot m_p \left[1 - \left(\frac{M}{M_u} \right)^2 \right] \cdot (b + a) \cdot \tan^{-1}\left(\tan\left[\sin^{-1}\left\{ \frac{c \cdot \sin\mu + d \cdot \cos\theta_2 \cdot \cos\mu - d + a(1+\sin\theta_2)}{c} \right\} \right] \cdot \cos\theta_2 \right) \qquad \text{Eqn.(3.4.5)}$$

Hinges KI and JL

The energy dissipated in hinges 'KI' and 'JL' is

$$W_3 = 2 \cdot m_p \left[1 - \left(\frac{M}{M_u} \right)^2 \right] \cdot b \cdot \mu \qquad \text{Eqn.(3.4.6)}$$

Hinges FI and GJ

Referring to figure 3.4.1(a), the coordinates of P4 is given by

$$x_{P4} = f \cdot \cos\mu - g \cdot \sin\mu \qquad \text{Eqn.(3.4.7)}$$

$$y_{P4} = f \cdot \sin\mu + g \cdot \cos\mu \qquad \text{Eqn.(3.4.8)}$$

and $$z_{P4} = g \cdot \tan\theta_2 \qquad \text{Eqn.(3.4.9)}$$

Also $y_{P4} = d - a$ Eqn.(3.4.10)

Therefore, from Eqn.(3.4.8) and Eqn.(3.4.10),

$$f \cdot \sin\mu + g \cdot \cos\mu = d - a \qquad \text{Eqn.(3.4.11)}$$

Now, from figure 3.4.1(a) and (b),

$$\tan\xi_2 = \frac{f \cdot \cos\theta_2}{g}$$

and substituting Eqn.(3.3.1) into the above expression,

$$g = \frac{f \cdot d \cdot \cos\theta_2}{c} \qquad \text{Eqn.(3.4.12)}$$

then substituting Eqn.(3.4.12) into Eqn.(3.4.11) yields,

$$f = \frac{d - a}{\sin\mu + \frac{d \cdot \cos\theta_2 \cdot \cos\mu}{c}} \qquad \text{Eqn.(3.4.13)}$$

So that

$$\theta_4 = \tan^{-1}\frac{z_{P4}}{x_{P4}} = \tan^{-1}\left(\frac{g \cdot \left[\frac{a}{d}\right]}{f \cdot \cos\mu - g \cdot \sin\mu}\right) \qquad \text{Eqn.(3.4.14)}$$

The energy dissipated by hinges 'FI' and 'GJ' is given by

$$W_4 = 2 \cdot m_p \left[1 - \left(\frac{M}{M_u} \right)^2 \right] \cdot (d-a) \cdot \theta_4$$

$$W_4 = 2 \cdot m_p \left[1 - \left(\frac{M}{M_u} \right)^2 \right] \cdot (d-a) \cdot \tan^{-1} \left(\frac{g \cdot \left[\frac{a}{d} \right]}{f \cdot \cos\mu - g \cdot \sin\mu} \right) \qquad \text{Eqn.(3.4.15)}$$

Hinges EI and HJ

Consider the point P5' originally perpendicular to 'EI' and intersecting 'FI' at F in the undeformed state, as shown in figure 3.4.2, the length from P5' to F is given by

$$(P5'F) = (d-a) \cdot \sin\xi_2 \qquad \text{Eqn.(3.4.16)}$$

In any deformed state, where the new position of P5' is indicated by P5, since the elemental plates are assumed inextensible, this length remains the same.

Now $h' = (d-a) - (P5'F)\sin\xi_2$

$= (d-a) \cdot \cos^2\xi_2$ Eqn.(3.4.17)

and $h = h' \cdot \cos\theta_2$

Substituting Eqn.(3.4.17) into the above equation,

$$h = (d-a) \cdot \cos^2\xi_2 \cdot \cos\theta_2 \qquad \text{Eqn.(3.4.18)}$$

The z co-ordinate of point P5 is given by

$$z_{P5} = h' \cdot \sin\theta_2$$
$$= (d-a) \cdot \cos^2\xi_2 \cdot \sin\theta_2 \qquad \text{Eqn.(3.4.19)}$$

The angle of rotation of hinge 'EI' is then given by

$$\theta_5 = \sin^{-1}\left(\frac{\left[\frac{z_{P5}}{\cos\theta_2}\right]}{(P5'F)}\right)$$
$$= \sin^{-1}([\tfrac{a}{c}] \cdot \cos\xi_2) \qquad \text{Eqn.(3.4.20)}$$

And the energy dissipated in hinges 'EI' and 'HJ' is given by

$$W_5 = 2 \cdot \frac{m_p\left[1-\left(\frac{M}{Mu}\right)^2\right]}{\sqrt{1-\frac{3}{4}\left(\frac{M}{Mu}\right)^2 \sin^2\xi_2 \cdot \left(4-3\cdot\sin^2\xi_2\right)}} \cdot \left(\sqrt{c^2+d^2}\right) \cdot \sin^{-1}([\tfrac{a}{c}] \cdot \cos\xi_2)$$

Eqn.(3.4.21)

Hinge FG

The total energy dissipated in hinge 'FG' is given by two components, the first from the hinge travel and the second from the increment in hinge rotation angle and can be expressed as

$$W_6 = 2 \cdot \frac{m_p\left[1-\left(\frac{M}{Mu}\right)^2\right]}{\sqrt{1-\frac{3}{4}\left(\frac{M}{Mu}\right)^2}} \cdot \frac{(a \cdot l_b)}{r} + \frac{m_p\left[1-\left(\frac{M}{Mu}\right)^2\right]}{\sqrt{1-\frac{3}{4}\left(\frac{M}{Mu}\right)^2}} \cdot l_b \cdot \theta_2 \qquad \text{Eqn.(3.4.22)}$$

where l_b is dictated by the position of the bolts that is tightened to the cleat and r is the rolling radius for the travelling hinge.

Hinges EF and HG

Assuming that since the hinge lengths and change in hinge angles are small, the energy due to the change in hinge rotation angle is also small and hence can be neglected, the energy dissipated in hinges 'EF' and 'HG' due to hinge travel is

$$W_7 = 2\frac{m_p\left[1-\left(\frac{M}{M_u}\right)^2\right]}{\sqrt{1-\frac{3}{4}\left(\frac{M}{M_u}\right)^2}} \cdot \frac{c \cdot a}{r}$$

Eqn.(3.4.23)

Membrane strain in tension flange

Referring to figure 3.2.1, 3.3.2(b) and figure 3.4.3, due to the rotation of section b-b, the point P6' at the edge of the tension flange on section b-b moves to a new location P6 causing the strain (in the x-direction) on the edge of the flange between P6 and K. This strain is assumed to occur within the triangular area K-P6-I and can be calculated from the expression below,

$$\varepsilon_x = \sqrt{1-\frac{b^2\sin^2\theta_2}{c^2}} - 1$$

Eqn.(3.4.24)

Assuming this is a plastic strain, the membrane energy is given by

$$\begin{aligned} W_{mem} &= 2 \cdot \sigma_o \cdot t \int_0^b \varepsilon_x \cdot \frac{z \cdot c}{b} \cdot dz \\ &= \sigma_o \cdot t \cdot \varepsilon_x \cdot b \cdot c \end{aligned}$$

Eqn.(3.4.25)

Hence, the total internal energy dissipation is given by

$$W_{int}(\mu) = W_1 + W_2 + W_3 + W_4 + W_5 + W_6 + W_7 + 2 \cdot W_{mem}$$

$$= 2 \cdot m_p \left[1 - \left(\frac{M}{M_u}\right)^2 \right] \cdot b \cdot \tan^{-1}\left(\tan\left[\sin^{-1}\left\{ \frac{c \cdot \sin\mu + d \cdot \cos\theta_2 \cdot \cos\mu - d + a(1+\sin\theta_2)}{c} \right\} - \mu \right] \cdot \cos\theta_2 \right)$$

$$+ 2 \cdot m_p \left[1 - \left(\frac{M}{M_u}\right)^2 \right] \cdot (b+a) \cdot \tan^{-1}\left(\tan\left[\sin^{-1}\left\{ \frac{c \cdot \sin\mu + d \cdot \cos\theta_2 \cdot \cos\mu - d + a(1+\sin\theta_2)}{c} \right\} \right] \cdot \cos\theta_2 \right)$$

$$+ 2 \cdot m_p \left[1 - \left(\frac{M}{M_u}\right)^2 \right] \cdot b \cdot \mu$$

$$+ 2 \cdot m_p \left[1 - \left(\frac{M}{M_u}\right)^2 \right] \cdot (d-a) \cdot \tan^{-1}\left(\frac{g \cdot \left[\frac{a}{d}\right]}{f \cdot \cos\mu - g \cdot \sin\mu} \right)$$

$$+ 2 \cdot \frac{m_p \left[1 - \left(\frac{M}{M_u}\right)^2 \right]}{\sqrt{1 - \frac{3}{4}\left(\frac{M}{M_u}\right)^2 \sin^2\xi_2 \cdot \left(4 - 3 \cdot \sin^2\xi_2\right)}} \cdot \left(\sqrt{c^2 + d^2} \right) \cdot \sin^{-1}\left(\left[\frac{a}{c}\right] \cdot \cos\xi_2 \right)$$

$$+ 2 \cdot \frac{m_p \left[1 - \left(\frac{M}{M_u}\right)^2 \right]}{\sqrt{1 - \frac{3}{4}\left(\frac{M}{M_u}\right)^2}} \cdot \frac{(a \cdot l_b)}{r} + \frac{m_p \left[1 - \left(\frac{M}{M_u}\right)^2 \right]}{\sqrt{1 - \frac{3}{4}\left(\frac{M}{M_u}\right)^2}} \cdot l_b \cdot \theta_2$$

$$+ 2 \cdot \frac{m_p \left[1 - \left(\frac{M}{M_u}\right)^2 \right]}{\sqrt{1 - \frac{3}{4}\left(\frac{M}{M_u}\right)^2}} \cdot \frac{c \cdot a}{r}$$

$$+ \sigma_o \cdot t \cdot \left(\sqrt{1 - \frac{b^2 \sin^2\theta_2}{c^2}} - 1 \right) \cdot b \cdot c$$

Eqn.(3.4.26)

3.5 ANALYSIS PROCEDURES

The following sections details the procedures adopted for obtaining the theoretical results for the plain channel beams.

3.5.1 Single span load-deflection predictions

The total internal energy can be equated to the external virtue work done derived in the previous section as follows

$$2 \cdot M \cdot (2 \cdot \delta\mu) = W_{int}(\mu + \delta\mu) - W_{int}(\mu - \delta\mu) \qquad \text{Eqn.(3.5.1)}$$

Eqn.(3.5.1) was then used to calculate the plastic mechanism moment capacity M at any angle μ.

The equation had to be solved by trial and error for every step increment of the overall hinge angle, the program PC8.bas, written in BASIC, was created to deal with the evaluation of the data points, this program is listed in Appendix II. The output from this calculation program includes the load versus deflection data for the entire range of overall hinge angle, up to the limiting lock-up condition, and the results were then used to construct the theoretical collapse curves.

The evaluation of the elastic loading line follows the procedure discussed in chapter 2. Another BASIC program was written to perform the calculations, listed in Appendix II as ELASTIC5.bas, it was created to generate the elastic line data. The elastic line can then be plotted together with the collapse curve to form the theoretical load- deflection prediction for the single span beams.

3.5.2 Determination of mechanism size 'c'

The theoretical plain channel mechanism described in sections 3.2 to 3.4 has two lock-up conditions, when these occur, the characteristics of the mechanism drastically changes and no additional rotation is possible without a new set of equations, and since parts of the mechanism have come into contact, the mechanism loads would tend to increase again with further increases in overall hinge rotation after a lock-up condition has been reached.

The first lock-up condition occurs when the size 'a', travel distance for the hinge 'FG', reaches the maximum as dictated by the location of the bolts that secures the beams to the cleats. This lock-up condition is delayed when the size 'c' is reduced.

The second lock-up condition occurs when

$$c \cdot \cos\mu - d \cdot \cos\theta_2 \cdot \sin\mu \leq 0 \qquad \text{Eqn.(3.5.1)}$$

This lock-up condition is hastened by reductions in the mechanism size 'c'.

Reducing the size 'c' is generally accompanied by reductions in mechanism loads for all rotation angles that can be evaluated using the equations stated in sections 3.3 and 3.4. This is illustrated in figure 3.5.1, where the collapse curves using a number of different c to d ratios are plotted. It can be observed that the change in mechanism loads are very small for ratios between 0.127 to 0.164, with the longest possible collapse curve corresponding to (c/d)=0.145.

Based on these findings, the size of 'c' was taken as 0.145 d for the plain channel mechanism model, the size that would minimise the theoretical mechanism loads without causing premature lock-up.

The chosen size for 'c' agreed well with the observed corresponding sizes in the tested beams which varied between 0.14d to 0.18d. Hence all the theoretical results for the plain channels were analysed using c=0.145d.

3.5.3 Double span load-deflection predictions

The theoretical double span beam load-deflection predictions are derived from the single span load-deflection characteristics assuming that all the three portions in the beams where bending moments are the most adverse will collapse with the same characteristics as that in the single span beams. The first failure section to develop will be found at the central support, this being followed by similar failure modes at the load points.

The theoretical double span predictions can be based on the experimental single span results or from the theoretical single span data. The first stage of the process is to convert the load-deflection data to moment versus (deflection / half span length) or simply called moment-hinge rotation data, for the single failure section. The double span loads can then be found from using the energy method to equate the virtual work done by the applied loads and the energy dissipated due to the rotation of the 'global hinges', of which the characteristic are known from the single span analysis.

From section 2.5 of this thesis, referring to figure 2.5.1, the energy equation is

$$P \cdot \delta v = M(\mu_1) \cdot \delta\mu_1 + M(\mu_3') \cdot \delta\mu_3$$

where $\mu_3' = \frac{\mu_3}{2}$.

Since $\mu_1 = \sin^{-1}(\frac{v}{L_1})$ Eqn.(3.5.2)

$\mu_2 = \sin^{-1}(\frac{v}{L_2})$ Eqn.(3.5.3)

and $\mu_3 = \mu_1 + \mu_2$ Eqn.(3.5.4)

Differentiating Eqn.(3.5.2) and (3.5.3), gives

$$\delta\mu_1 = \frac{1}{\sqrt{1-\left(\frac{v}{L_1}\right)^2}\cdot L_1}\cdot \delta v \qquad \text{Eqn.(3.5.5)}$$

and $$\delta\mu_3 = \left[\frac{1}{\sqrt{1-\left(\frac{v}{L_1}\right)^2}\cdot L_1}\right] + \left[\frac{1}{\sqrt{1-\left(\frac{v}{L_2}\right)^2}\cdot L_2}\right]\cdot \delta v \qquad \text{Eqn.(3.5.6)}$$

Putting Eqn.(3.5.5) and (3.5.6) into the energy expression gives

$$P = M(\mu_1)\cdot\frac{1}{\sqrt{1-\left(\frac{v}{L_1}\right)^2}\cdot L_1} + M(\mu_3')\cdot\left[\frac{1}{\sqrt{1-\left(\frac{v}{L_1}\right)^2}\cdot L_1} + \frac{1}{\sqrt{1-\left(\frac{v}{L_2}\right)^2}\cdot L_2}\right] \qquad \text{Eqn.(3.5.7)}$$

where $M(\mu_1)$ and $M(\mu_3')$ are derived from the single span results
and $\mu_3' = \frac{\mu_3}{2}$.

The analysis method described above was written into a BASIC program which was then used to evaluate theoretical double span beam results using both theoretical and experimental single span load-deflection data. The program is listed in Appendix II as DSB3.bas.

3.5.4 Alternative Double span analysis

The procedure described in the previous section considers the double spanning beams collapsing by means of a single overall beam mechanism which consists of three similar failure points along the beam. It is therefore essentially a mechanism approach which is inherently rather sensitive to errors in any part of the single span moment-hinge rotation characteristics. The span lengths of the double spanning beams and the single span beam analyses which provide the moment-rotation data must also be of the same order to facilitate good predictions. An alternative method for multi-span beam analysis will be presented in this section. This analytical procedure is based on the elastic beam analysis technique employing the Macaulays' method and uses only the collapse portion of the moment-rotation characteristics found in the study of the single span beams.

Two separate Macaulay solutions are formulated for the beam, the first models the initial linear elastic loading of the complete double spanning beam as shown in figure 3.5.2, this solution is applied up to the point where the ultimate moment of the beam portion over the central support is reached. As the beam fails at the support, the second Macaulays' solution is invoked, as shown in figure 3.5.3, the double span beam is now considered as two simply supported beams with a moment applied at the location of the central support, this resisting moment simulates the effects of the collapse mechanism which has formed at the support. The magnitude of the resisting moment varies with the slope of the beam over the support and can be determined from the collapse portion of the moment-rotation characteristics as found from the single span analysis.

From the Macaulays' solution for the first stage, the load point deflection is given by

$$v = \frac{1}{EI_{eff}}\left(c \cdot [L - L_1] - \frac{R_A}{6} \cdot [L - L_1]^3\right) \qquad \text{Eqn.(3.5.8)}$$

where $R_A = \frac{P}{2} \cdot \left(3\left(\frac{L_1}{L}\right)^2 - \left(\frac{L_1}{L}\right)^3\right)$

and $c = \frac{R_A \cdot L^2}{6} - \frac{P \cdot L_1^3}{L}$

On the onset of collapse over the central support, the second Macaulays' solution provides the deflection expression shown below as Eqn.(3.5.9).

$$v = \frac{P}{3EI_{eff}} \cdot \frac{L_1^2 \cdot (L - L_1)^2}{L} + \frac{M(\mu) \cdot L^2}{6EI_{eff}} \cdot \left(3\left(\frac{L_1}{L}\right)^2 - \left(\frac{L_1}{L}\right)^3 - 2 \cdot \left(\frac{L_1}{L}\right)\right) \qquad \text{Eqn.(3.5.9)}$$

where $M(\mu)$ is the resisting moment of the collapsing section over the support.

As the failed section over the centre sheds it's load, the resisting moment decreases as the load point deflections increase, and the corresponding load at any angle of rotation of the beam over the support is found from Eqn.(3.5.10).

$$P = \frac{6EI_{eff} \cdot \mu \cdot L + 2 \cdot M(\mu) \cdot L^2}{L_1 \cdot (L - L_1) \cdot (2L - L_1)} \qquad \text{Eqn.(3.5.10)}$$

where μ represents the slope of the deflected beam over the support.

The loading on the beam sections at the load points increases until their ultimate moment capacities are eventually reached, at which point the entire beam collapses as

a mechanism with three hinges along it's length and Eqn.(3.5.7) is employed to relate the applied loads to the deflections, as described in section 3.5.3.

The elastic buckling effects can be taken into account in this analysis by using the effective cross-sectional properties as found according to the equations set out in the BS5950 ; Part 5 ; 1987, used in the same manner as in the elastic solution for the single span beams discussed previously. The minimum effective cross-sectional properties which is found from considering the most adverse bending moments at the central support are assumed for the entire length of the beam.

The Basic program written for this double span analysis is listed in Appendix II as MSBPC.bas.

The comparison between the theoretical single and double span results evaluated using the methods described in this chapter and the experimental findings is presented in chapter 7 of this thesis. The theoretical loads tend to be underestimates when the deflections become large, especially in the double span beams but the ultimate load predictions agreed rather well with the experimental findings in most cases. Further discussion of the results and the plain channel mechanism model will be carried out in chapter 9.

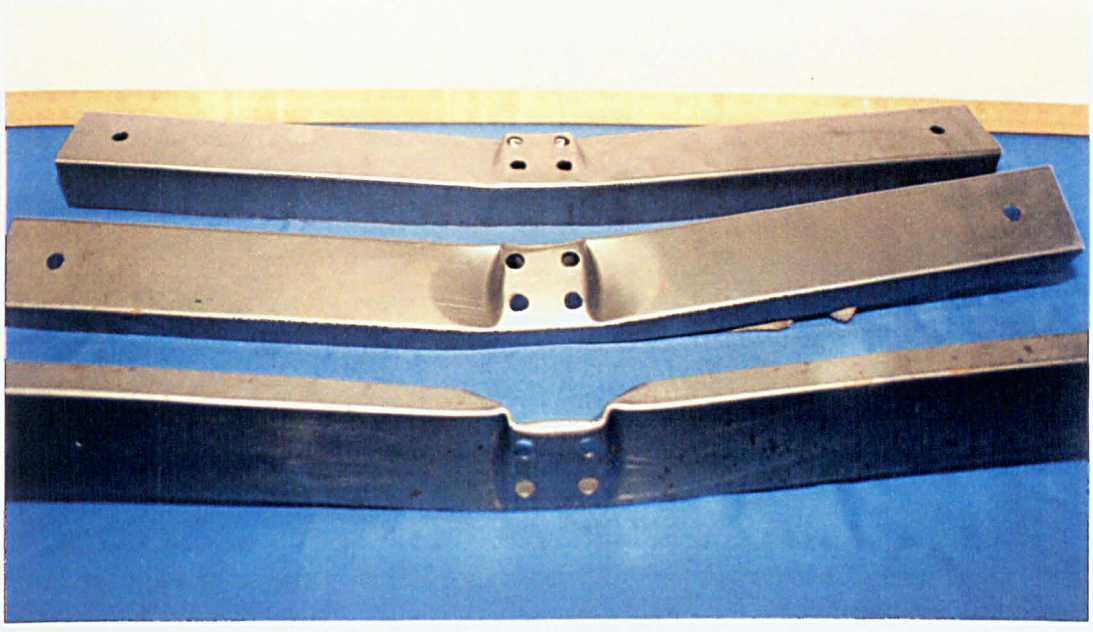

Figure 3.1.1 : Observed Plain Channel mechanism

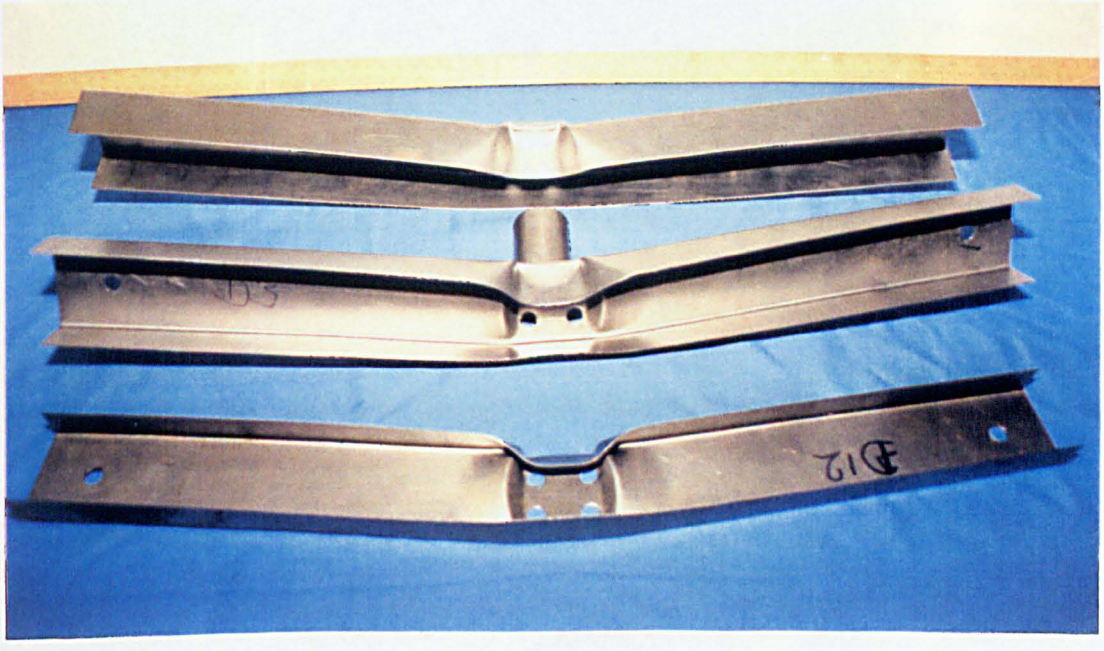

Figure 3.1.2 : Observed Plain Channel mechanism

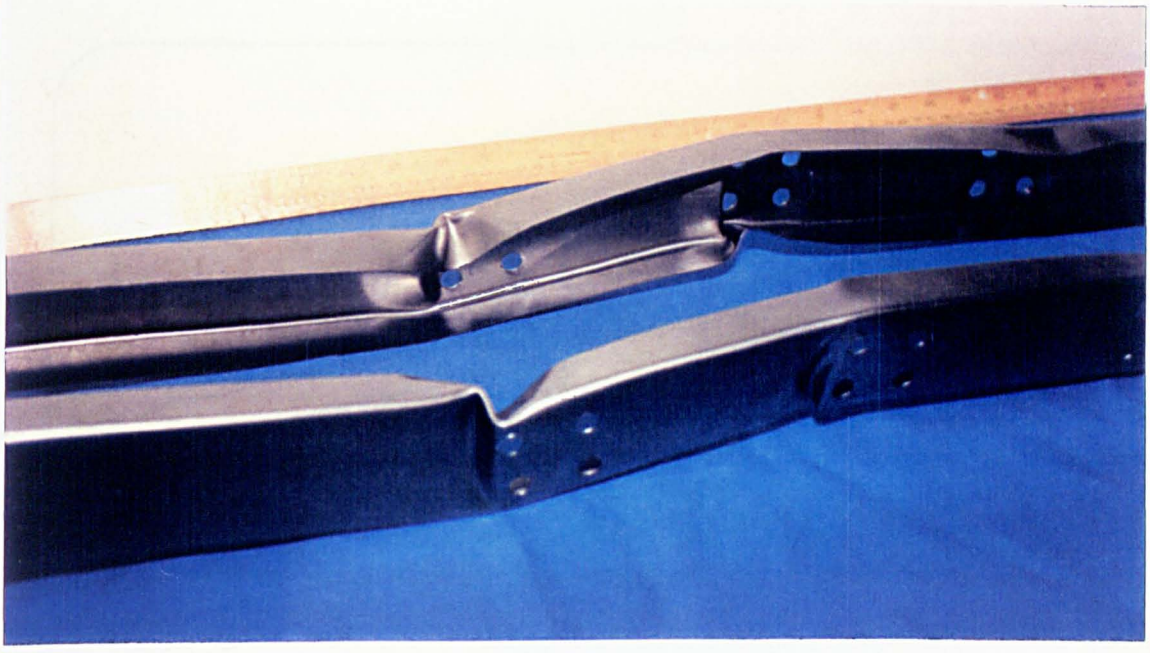

Figure 3.1.3 : Observed Plain Channel mechanism

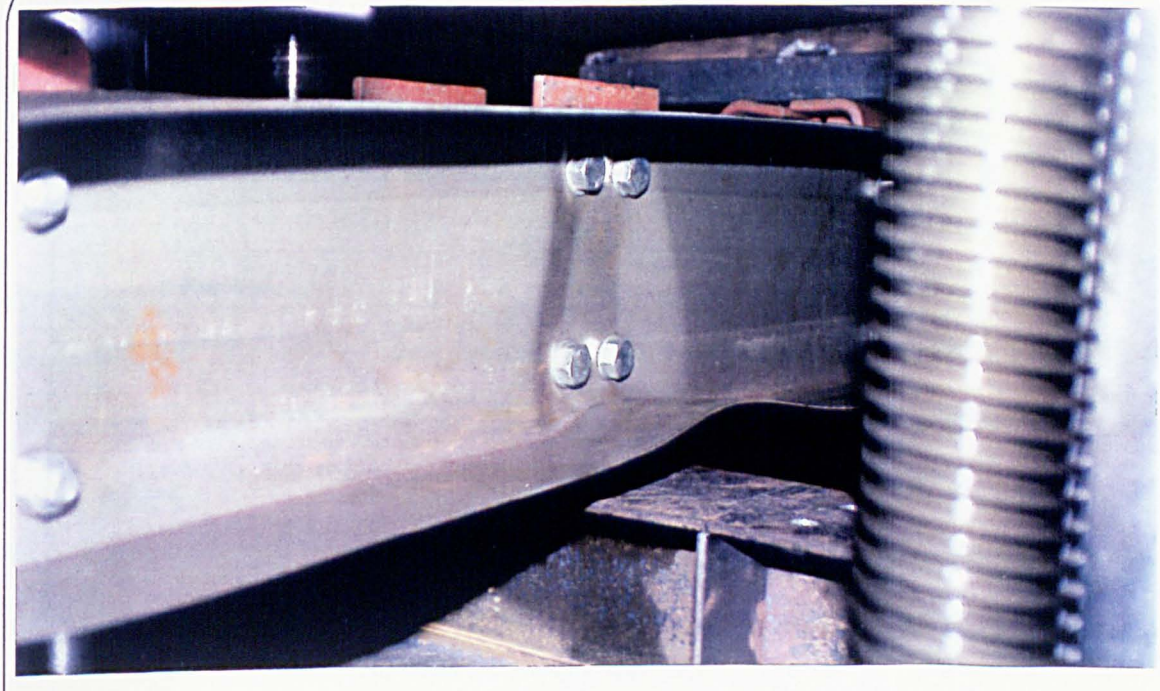

Figure 3.1.4 : Observed Plain Channel mechanism

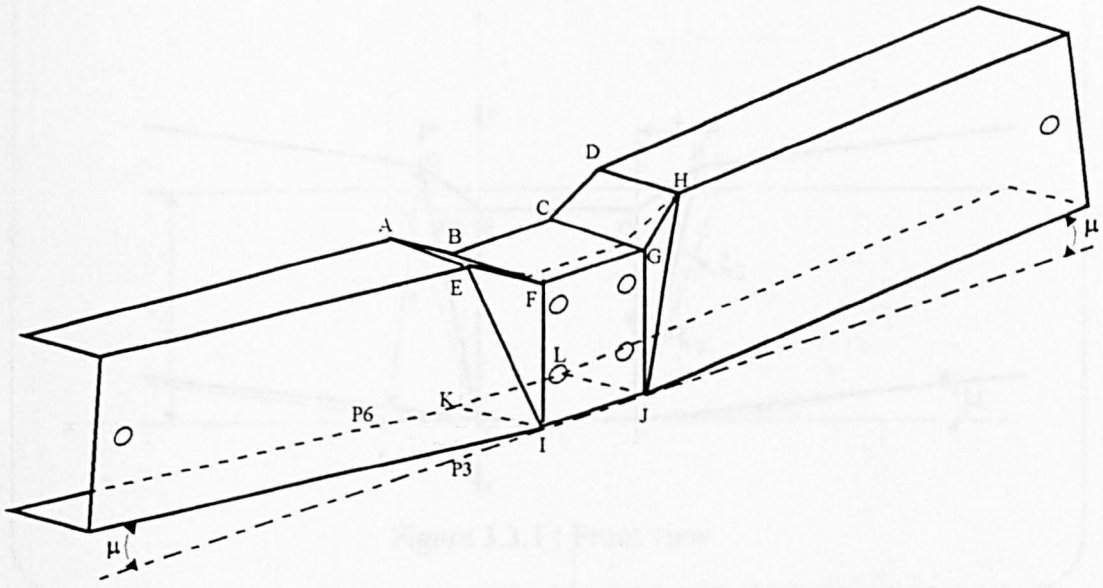

Figure 3.2.1 : Theoretical Plain Channel mechanism

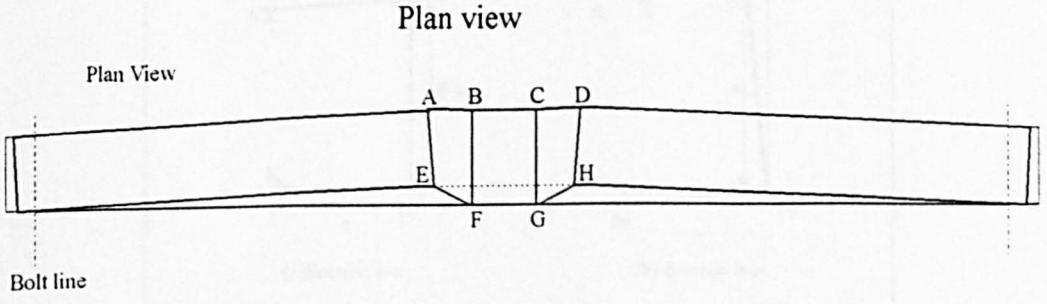

Figure 3.2.2 : Theoretical Plain Channel mechanism

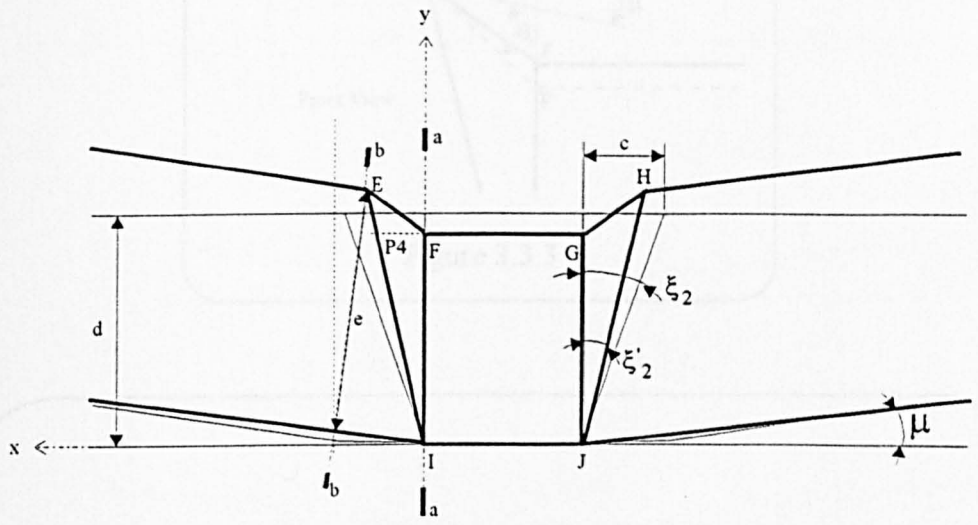

Figure 3.3.1 : Front view

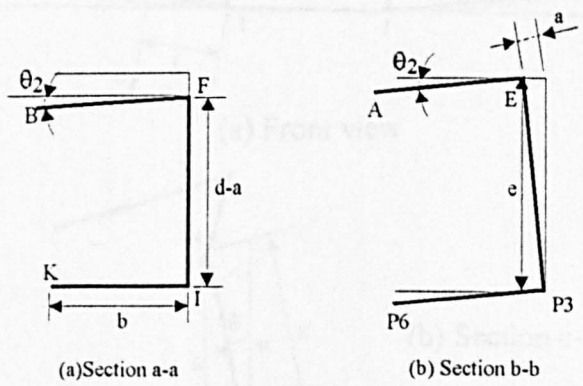

Figure 3.3.2

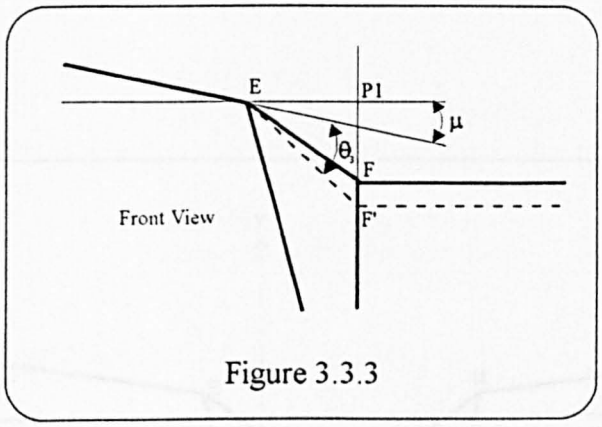

Figure 3.3.3

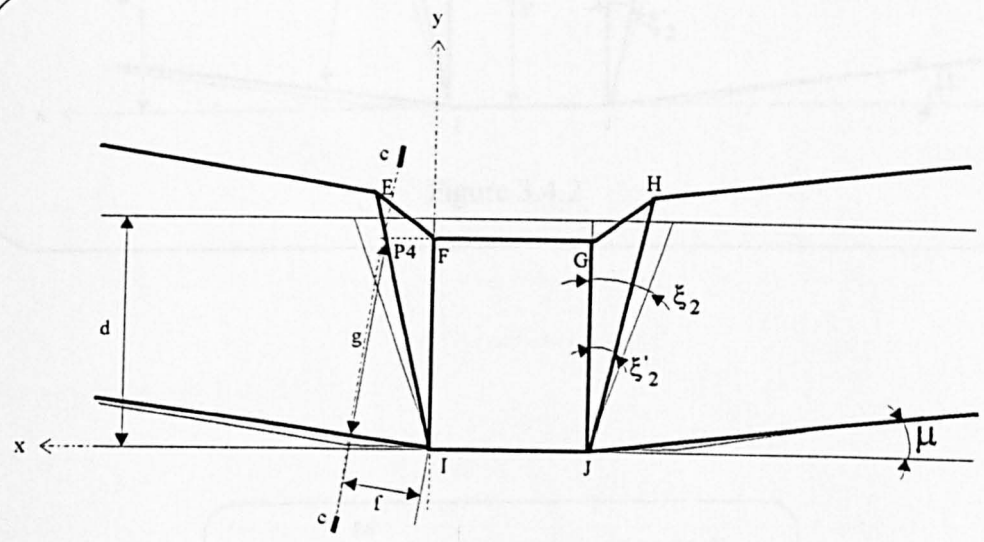

(a) Front view

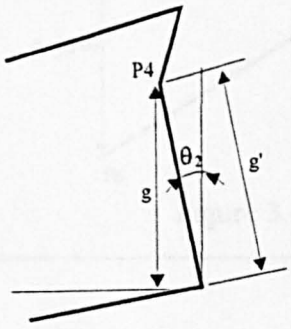

(b) Section c-c

Figure 3.4.1

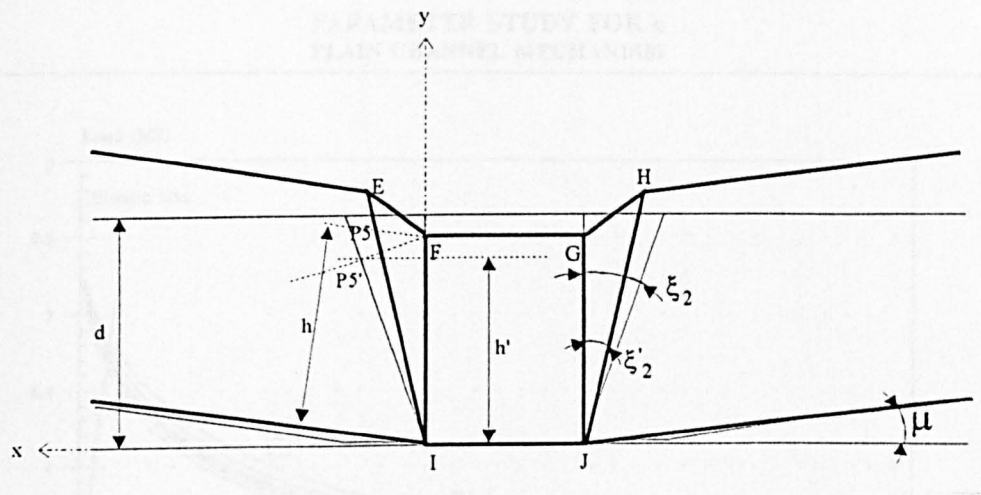

Figure 3.4.2

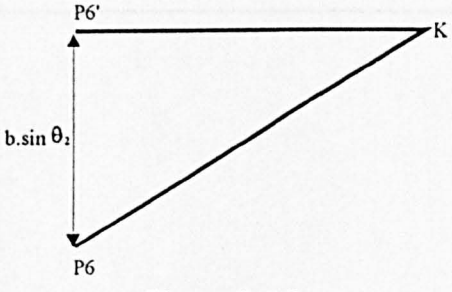

Figure 3.4.3

PARAMETER STUDY FOR c
PLAIN CHANNEL MECHANISM

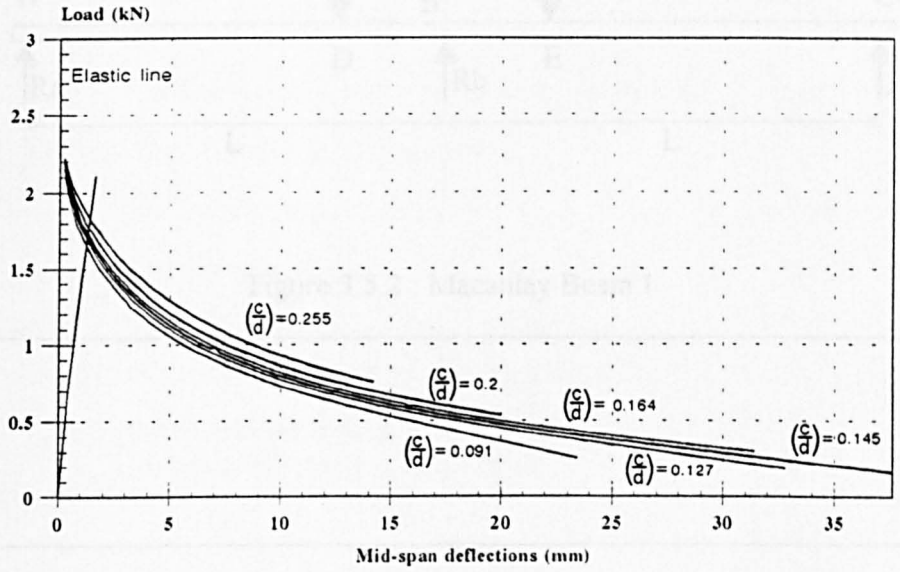

Using the 22.5x55 Section, t=.6 Span=550

Figure 3.5.1

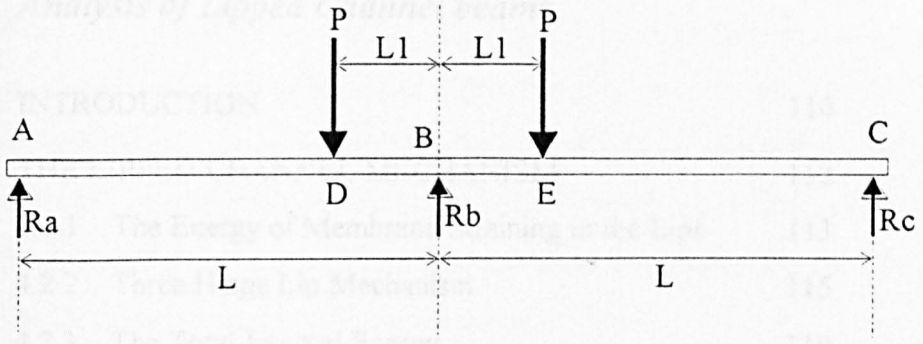

Figure 3.5.2 : Macaulay Beam I

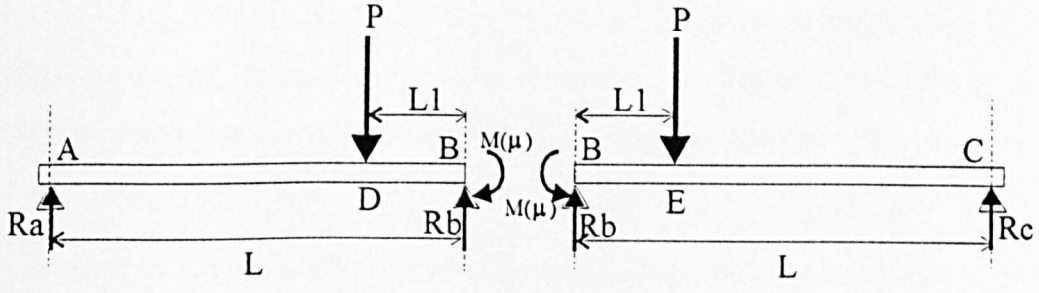

Figure 3.5.3 : Macaulay Beam II

Chapter Four

- *Analysis of Lipped Channel beams*

4.1 INTRODUCTION

This chapter presents the study conducted on lipped channel sections loaded as beams in the same manner as the plain channels of chapter 3. The addition of lips to the channel not only increases the modulus of the section through the addition of material, but in cases where the lip is of adequate width, it also serves as a stiffener for the flange, thus increasing the critical buckling stress of the compressed flange and preventing early buckling. Lipped channel sections are more widely used as structural members than their plain channel counterparts, common examples are the C-section beams for Mezzanine floors and beams for suspended ceilings.

The analysis techniques for the lipped channels examined in this chapter is essentially the same as that for the plain channels described previously. The formulation would look very similar to those found in the previous chapter with the addition of some terms to account for the effects of the presence of the lips. In the elastic analysis, the compressive flanges are considered to be stiffened elements if the size of the lip is at least 20% of the flange width, according to BS5950 ; Part 5 ; 1987, ref. [8]. The corresponding buckling coefficients and critical buckling stresses are then worked out for the compression flange using the equations stated in chapter 2 of this thesis. The effective section properties used in the analysis also takes account of the lips.

As in the plain channel study, this investigation commenced with the testing of a set of 72 lipped channel beams in the laboratory. These beams were produced from mild steel sheets of three different thicknesses and consisted of sections with four different lip sizes for each thickness. As before, the theoretical collapse plastic mechanism was modelled to closely resemble those observed in the experimental investigation. It may be useful to state again that these single and double span beams examined were supported and loaded through cleats which are fastened to the webs of the beams by

means of bolts. The effects of this method of support have been discussed in chapter 3 and are also relevant for the lipped sections.

In addition, the results from a set of 6 full scale cleat supported lipped channel floor beam experiments, tested in double span configuration in a vacuum box which subjects the beams to uniformly distributed loading were analysed. The layout and conditions of these experiments are described in detail in chapter 6 of this thesis. These C-section floor beams were supplied by Metal Sections Limited of West Midlands, United Kingdom and are marketed as standard components for mezzanine flooring systems.

The following sections details the analytical study of the beams under the different conditions of loading. Since the theoretical concepts applied in the analysis has already been discussed in chapter 2, the following work presented will mainly focus on the development of the plastic mechanism for the lipped channel beams.

In the analysis of the double spanning beams under uniformly distributed loading, an additional theoretical plastic collapse mechanism for failure at a location along the span (not affected by the presence of cleat supports) will be developed and presented in chapter 5 of this thesis. In view of the similarities between these analyses and those for the zed sections examined in chapter 5, the theoretical work for these beams will not be detailed in this chapter.

4.2 THE LIPPED CHANNEL MECHANISM

The observed pattern of yield lines found on the tested lipped channels are very similar to those found in the plain channels, figures 4.2.1 and 4.2.2 illustrates the typical failure form. Since the yield lines in the web and flanges were so similar to those in the plain channel specimens, the postulated plastic failure mechanism for the lipped channels is merely an extension of the plain channel mechanism. The governing energy equation would be taken as that stated in the previous chapter as Eqn.(3.4.26) with the addition of three terms to account for the energy dissipated in the lips of the current subjects. Figure 4.2.3 shows the theoretical plastic mechanism for the lipped channels.

On close examination of the lips on the test specimens, when the overall plastic mechanism was well developed, two types of idealised lip behaviour can be used to summarise the failure modes in the lips. Referring to figure 4.2.3, the lips are in compression at locations 'A', 'D', 'K' and 'L', with the compressive strain minimum at the flange edge and maximum at the lip edge. The second mode of lip failure occurs at locations 'B' and 'C' where the lip seems to experience in-plane bending. With considerations to these observations, it was decided that the three hinge lip mechanism which will be detailed in section 4.2.2, would be most appropriate for the sections of the lips that were in compression and that the second mode of failure would be modelled as membrane bending of the lips. The following subsections details the formulation of the energy terms that would be used to account for these two effects.

4.2.1 The Energy of Membrane Straining in the Lips

The behaviour of the lip at the locations 'B' and 'C' (figure 4.2.3), is theoretically modelled as elements subjected to in-plane bending. The rigid-perfectly plastic material behaviour is assumed to be governing in the plastic mechanism analysis and as such, the portions of the lip that experiences membrane strains are assumed to be completely plastic and under unidirectional stress with the magnitude equal to the material yield strength.

Figure 4.2.4 shows the geometry of the lip section in in-plane bending. Noting that the lip size is a mid-thickness dimension, the radii of curvatures for the membrane lip can be determined from the radius of bend of the hinges 'BF' and 'CG' to maintain compatibility between the flange edge and the lip material. The mean radius of curvature and radii at the extreme fibres of the lip is therefore given by,

$$R_o = r + \frac{w}{2} \qquad \text{Eqn.(4.2.1)}$$

$$R_t = R_o + \frac{w}{2} \qquad \text{Eqn.(4.2.2)}$$

$$R_c = R_o - \frac{w}{2} = r \qquad \text{Eqn.(4.2.3)}$$

where R_o is the mean radius of curvature
R_t and R_c are the radii of curvature of the extreme fibre on the tension and compression sides respectively
r is the local hinge radius of bend
and w is the lip size.

From the geometry (figure 4.2.4), the extreme fibre strain can be derived,

$$\varepsilon = \frac{R}{R_o} - 1 \qquad \text{Eqn.(4.2.4)}$$

Referring to figure 4.2.4, the original area (undeformed state) affected by the membrane strain can be written as

$$A = R_o \cdot \theta_6 \cdot dR \qquad \text{Eqn.(4.2.5)}$$

where $\theta_6 = (\theta_3 + \mu)'$, the angle of rotation of hinges 'BF' and 'CG', see figure 3.3.3.

The plastic membrane strain energy in the tension side is given by

$$\begin{aligned} W_{lmt} &= t \cdot \int_{Ro}^{Rt} \sigma_o \cdot \varepsilon \cdot R_o \cdot \theta_6 \cdot dR \\ &= t \cdot \int_{Ro}^{Rt} \sigma_o \cdot \left(\frac{R}{R_o} - 1\right) \cdot R_o \cdot \theta_6 \cdot dR \\ &= t \cdot \sigma_o \cdot \theta_6 \cdot \frac{w^2}{8} \end{aligned} \qquad \text{Eqn.(4.2.6)}$$

Similarly, on the compression side, the membrane energy is

$$\begin{aligned} W_{lmc} &= t \cdot \int_{Rc}^{Ro} (-\sigma_o) \cdot \left(\frac{R}{R_o} - 1\right) \cdot R_o \cdot \theta_6 \cdot dR \\ &= t \cdot \sigma_o \cdot \theta_6 \cdot \frac{w^2}{8} \end{aligned} \qquad \text{Eqn.(4.2.7)}$$

The total membrane energy of lip bending at locations B and C is therefore

$$W_{lm} = t \cdot \sigma_o \cdot \theta_6 \cdot \frac{w^2}{2} \qquad \text{Eqn.(4.2.8)}$$

4.2.2 Three Hinge Lip Mechanism

The postulated plastic mechanism for the lip at the flange locations 'A', 'D', 'K' and 'L' is shown in figures 4.2.5. It consists of three straight stationary hinge lines and has one independent variable, β, which describes the angle that separates the hinges.

Hinge AN

Referring to figure 4.2.5(b) and (c), length MN is given by

$$MN = w \cdot \tan\beta \qquad \text{Eqn.(4.2.9)}$$

and lengths j and k are given by

$$j = MN \cdot \cos\theta_7 \qquad \text{Eqn.(4.2.10)}$$

$$\begin{aligned} k &= MN \cdot \cos\left(\frac{\theta_3'}{2}\right) - j \\ &= w \cdot \tan\beta \cdot \left[\cos\left(\frac{\theta_3'}{2}\right) - \cos\theta_7\right] \end{aligned} \qquad \text{Eqn.(4.2.11)}$$

Also

$$k = w \cdot \sin\left(\frac{\theta_3'}{2}\right) \qquad \text{Eqn.(4.2.12)}$$

From Eqn.(4.2.11) and Eqn.(4.2.12),

$$\theta_7 = \cos^{-1}\left[\cos\left(\frac{\theta_3'}{2}\right) - \frac{\sin\left(\frac{\theta_3'}{2}\right)}{\tan\beta}\right] \qquad \text{Eqn.(4.2.13)}$$

Hence, the energy dissipated in hinge 'AN' is given by

$$W_{l1} = 2 \cdot m_p \left[1 - \left(\frac{M}{M_u} \right)^2 \right] \cdot w \cdot \theta_7$$

$$= 2 \cdot m_p \left[1 - \left(\frac{M}{M_u} \right)^2 \right] \cdot w \cdot \left\{ \cos^{-1} \left[\cos\left(\frac{\theta_3'}{2} \right) - \frac{\sin\left(\frac{\theta_3'}{2} \right)}{\tan\beta} \right] \right\} \quad \text{Eqn.(4.2.14)}$$

Hinges AM and AO

Referring to figure 4.2.5(d) and (e), it can shown that

$$\theta_7' = \tan^{-1}[\tan\theta_7 \cdot \cos\varphi] \quad \text{Eqn.(4.2.15)}$$

and

$$\sin\varphi = \frac{m}{w} \quad \text{Eqn.(4.2.16)}$$

From figure 4.2.5(b), the length n is given by

$$n = w \cdot \tan\beta \cdot \sin\left(\frac{\theta_3'}{2} \right) + w \cdot \cos\left(\frac{\theta_3'}{2} \right) \quad \text{Eqn.(4.2.17)}$$

And from figure 4.2.5(e)

$$\cos\varphi = \frac{w}{n}$$

$$= \frac{1}{\tan\beta \cdot \sin\left(\frac{\theta_3'}{2} \right) + \cos\left(\frac{\theta_3'}{2} \right)} \quad \text{Eqn.(4.2.18)}$$

Rearranging Eqn.(4.2.18) and substituting it into Eqn.(4.2.16) yields

$$m = w \cdot \sin\left[\cos^{-1}\left(\frac{1}{\tan\beta \cdot \sin\left(\frac{\theta_3'}{2}\right) + \cos\left(\frac{\theta_3'}{2}\right)}\right)\right] \qquad \text{Eqn.(4.2.19)}$$

Consider a point P7 perpendicular to 'AO' and intersecting 'AN' at 'N', as shown in figure 4.2.5(b), assuming that the platelets between the hinges are inextensible, the length P7-N remains constant and is given by

$$(P7 - N) = w \cdot \sin\beta \qquad \text{Eqn.(4.2.20)}$$

Hence, from figure 4.2.5(f)

$$\sin\theta_8 = \frac{m}{(P7-N)}$$

giving

$$\theta_8 = \sin^{-1}\left[\frac{\sin\varphi}{\sin\beta}\right] \qquad \text{Eqn.(4.2.21)}$$

The energy dissipated at hinges 'AM' and 'AO' is therefore

$$W_{l2} = 2 \cdot \frac{m_p\left[1-\left(\frac{M}{M_u}\right)^2\right]}{\sqrt{1-\frac{3}{4}\left(\frac{M}{M_u}\right)^2 \sin^2\beta \cdot \left(4-3\cdot\sin^2\beta\right)}} \cdot \frac{w}{\cos\beta} \cdot \theta_8$$

$$= 2 \cdot \frac{m_p\left[1-\left(\frac{M}{M_u}\right)^2\right]}{\sqrt{1-\frac{3}{4}\left(\frac{M}{M_u}\right)^2 \sin^2\beta \cdot \left(4-3\cdot\sin^2\beta\right)}} \cdot \frac{w}{\cos\beta} \cdot \left\{\sin^{-1}\left[\frac{\sin\varphi}{\sin\beta}\right]\right\} \qquad \text{Eqn.(4.2.22)}$$

$$\text{where } \varphi = \cos^{-1}\left(\frac{1}{\tan\beta\cdot\sin\left(\frac{\theta_3'}{2}\right)+\cos\left(\frac{\theta_3'}{2}\right)}\right)$$

Therefore, the total energy dissipated in the lip mechanisms at 'A' and 'D' is given by

$$W_{lA} = 2(W_{l1} + W_{l2}) \qquad \text{Eqn.(4.2.23)}$$

The three hinge mechanisms at 'K' and 'L' are identical to those at 'A' and 'D' except that they depend on the angle μ instead of θ_3'. The energy terms are therefore

$$W_{l3} = 2 \cdot m_p\left[1-\left(\frac{M}{M_u}\right)^2\right] \cdot w \cdot \left\{\cos^{-1}\left[\cos\left(\frac{\mu}{2}\right) - \frac{\sin\left(\frac{\mu}{2}\right)}{\tan\beta}\right]\right\} \qquad \text{Eqn.(4.2.24)}$$

and

$$W_{l4} = 2 \cdot \frac{m_p\left[1-\left(\frac{M}{M_u}\right)^2\right]}{\sqrt{1-\frac{3}{4}\left(\frac{M}{M_u}\right)^2 \sin^2\beta \cdot \left(4-3\cdot\sin^2\beta\right)}} \cdot \frac{w}{\cos\beta} \cdot \left\{\sin^{-1}\left[\frac{\sin\varphi'}{\sin\beta}\right]\right\} \qquad \text{Eqn.(4.2.25)}$$

$$\text{where} \quad \varphi' = \cos^{-1}\left(\frac{1}{\tan\beta\cdot\sin\left(\frac{\mu}{2}\right)+\cos\left(\frac{\mu}{2}\right)}\right)$$

The total energy dissipation of the lip mechanisms at 'K' and 'L' is

$$W_{lK} = 2(W_{l3} + W_{l4}) \qquad \text{Eqn(4.2.26)}$$

4.2.3 The Total Internal Energy

The total internal energy dissipated in the lipped channel mechanism is given by the eight terms of Eqn.(3.4.26) and Eqn.(4.2.8), (4.2.23) and (4.2.26) derived previously, shown as the following Eqn.(4.2.17).

$$
\begin{aligned}
W_{int}(\mu) = W_1 + W_2 + W_3 + W_4 + W_5 + W_6 + W_7 + 2\cdot W_{mem} + W_{lm} + W_{l4} + W_{lK} \\
= \quad & 2\cdot m_p\left[1-\left(\frac{M}{M_u}\right)^2\right]\cdot b\cdot \\
& \tan^{-1}\left(\tan\left[\sin^{-1}\left\{\frac{c\cdot\sin\mu+d\cdot\cos\theta_2\cdot\cos\mu-d+a(1+\sin\theta_2)}{c}\right\}-\mu\right]\cdot\cos\theta_2\right) \\
+ \quad & 2\cdot m_p\left[1-\left(\frac{M}{M_u}\right)^2\right]\cdot(b+a)\cdot \\
& \tan^{-1}\left(\tan\left[\sin^{-1}\left\{\frac{c\cdot\sin\mu+d\cdot\cos\theta_2\cdot\cos\mu-d+a(1+\sin\theta_2)}{c}\right\}\right]\cdot\cos\theta_2\right) \\
+ \quad & 2\cdot m_p\left[1-\left(\frac{M}{M_u}\right)^2\right]\cdot b\cdot\mu \\
+ \quad & 2\cdot m_p\left[1-\left(\frac{M}{M_u}\right)^2\right]\cdot(d-a)\cdot\tan^{-1}\left(\frac{g\cdot\left[\frac{a}{d}\right]}{f\cdot\cos\mu-g\cdot\sin\mu}\right) \\
+ \quad & 2\cdot\frac{m_p\left[1-\left(\frac{M}{M_u}\right)^2\right]}{\sqrt{1-\frac{3}{4}\left(\frac{M}{M_u}\right)^2\sin^2\xi_2\cdot\left(4-3\cdot\sin^2\xi_2\right)}}\cdot\left(\sqrt{c^2+d^2}\right)\cdot\sin^{-1}\left(\left[\frac{a}{c}\right]\cdot\cos\xi_2\right) \\
+ \quad & 2\cdot\frac{m_p\left[1-\left(\frac{M}{M_u}\right)^2\right]}{\sqrt{1-\frac{3}{4}\left(\frac{M}{M_u}\right)^2}}\cdot\frac{(a\cdot l_b)}{r}+\frac{m_p\left[1-\left(\frac{M}{M_u}\right)^2\right]}{\sqrt{1-\frac{3}{4}\left(\frac{M}{M_u}\right)^2}}\cdot l_b\cdot\theta_2 \\
+ \quad & 2\cdot\frac{m_p\left[1-\left(\frac{M}{M_u}\right)^2\right]}{\sqrt{1-\frac{3}{4}\left(\frac{M}{M_u}\right)^2}}\cdot\frac{c\cdot a}{r} \\
+ \quad & \sigma_o\cdot t\cdot\left(\sqrt{1-\frac{b^2\sin^2\theta_2}{c^2}}-1\right)\cdot b\cdot c \\
+ \quad & \sigma_o\cdot t\cdot(\theta_3+\mu)'\cdot\frac{w^2}{2} \\
+ \quad & 4\cdot m_p\left[1-\left(\frac{M}{M_u}\right)^2\right]\cdot w\cdot\left\{\cos^{-1}\left[\cos\left(\frac{\theta_3'}{2}\right)-\frac{\sin\left(\frac{\theta_3'}{2}\right)}{\tan\beta}\right]\right\} \\
+ \quad & 4\cdot\frac{m_p\left[1-\left(\frac{M}{M_u}\right)^2\right]}{\sqrt{1-\frac{3}{4}\left(\frac{M}{M_u}\right)^2\sin^2\beta\cdot\left(4-3\cdot\sin^2\beta\right)}}\cdot\frac{w}{\cos\beta}\cdot\left\{\sin^{-1}\left[\frac{\sin\varphi}{\sin\beta}\right]\right\} \\
+ \quad & 4\cdot m_p\left[1-\left(\frac{M}{M_u}\right)^2\right]\cdot w\cdot\left\{\cos^{-1}\left[\cos\left(\frac{\mu}{2}\right)-\frac{\sin\left(\frac{\mu}{2}\right)}{\tan\beta}\right]\right\} \\
+ \quad & 4\cdot\frac{m_p\left[1-\left(\frac{M}{M_u}\right)^2\right]}{\sqrt{1-\frac{3}{4}\left(\frac{M}{M_u}\right)^2\sin^2\beta\cdot\left(4-3\cdot\sin^2\beta\right)}}\cdot\frac{w}{\cos\beta}\cdot\left\{\sin^{-1}\left[\frac{\sin\varphi'}{\sin\beta}\right]\right\}
\end{aligned}
$$

Eqn.(4.2.17)

4.3 ANALYSIS PROCEDURE

The analysis of the lipped channel beams follows the procedures discussed in section 3.5 of this thesis. Relevant changes were made in the formulations for the elastic analysis to consider the compression flange as stiffened elements where the lips were of an adequate size (b/5) and to include the effects of the lips in the determination of the second moment of area of the sections.

The following BASIC programs written for the calculations are listed in Appendix II.

- ELASTIC8.bas - For the elastic loading line.
- LC8.bas - For the plastic collapse curve.
- MSBLC.bas - For the construction of the double span load-deflection characteristics using the alternative method discussed in section 3.5.4 of the thesis.
- DSB3.bas - For the double span load-deflection characteristics using the energy approach detailed in section 3.5.3 of this thesis.

4.3.1 Determination of the hinge inclination angle for the three hinge lip mechanism

The three hinge lip mechanism described in section 4.2.2 has an independent variable, β which dictates the inclination of the two outer hinge lines. The angle that was used for the final analyses was determined by a mechanism load minimisation process. The parameter study on β found that the minimum energy dissipation in the three hinge mechanism of the lip occurred when $\beta = 50°$.

Figure 4.3.1 shows the moment contribution of the three hinge mechanisms with β set to 30°, 35°, 40°, 45°, 50° and 60°. Little difference was found between the 45° and 50° lines, the 55° line almost coincides with the 45° line and is therefore not shown.

4.3.2 Analysis of the beams subjected to Uniformly Distributed Loading

The analysis method used to examine the double spanning lipped channel beams subjected to Uniformly Distributed Loading is almost identical to the analysis of the zed sections tested under similar conditions, which is presented in the following chapter. The only difference between the two formulations is in the sizes of the flanges and lips of the sections, the lipped channels have an axis of symmetry while the zed sections studied have flanges and lips of unequal sizes on either sides of the web. Keeping this point in view, the reader may want to proceed to chapter 5 for the details of the theoretical analysis of these beams.

The results from the experiments conducted on the lipped channel beams and the theoretical predictions are presented in chapter 7 of this thesis and discussed in chapter 9. By considering the lips of the channels in the manner described, the interaction between the stresses at the edge of the flange and lip is neglected but the postulated theoretical plastic mechanism predicted the collapse behaviour of the beams rather well in most of the cases examined.

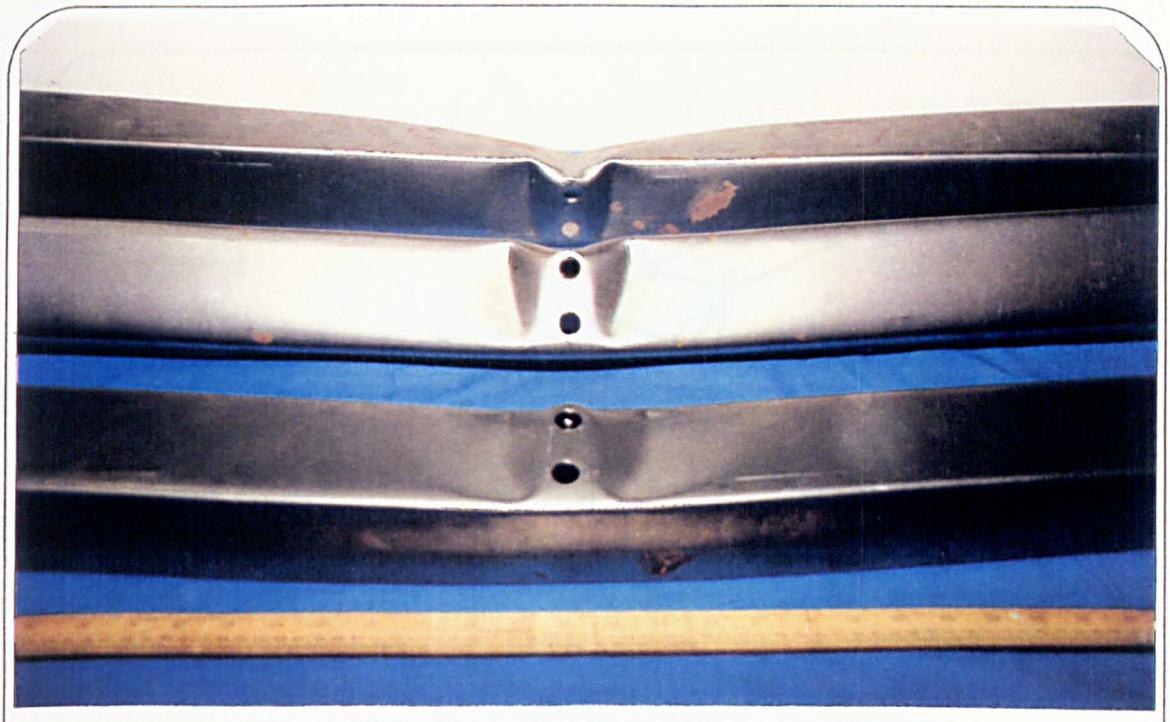

Figure 4.2.1 : Observed Lipped Channel mechanism

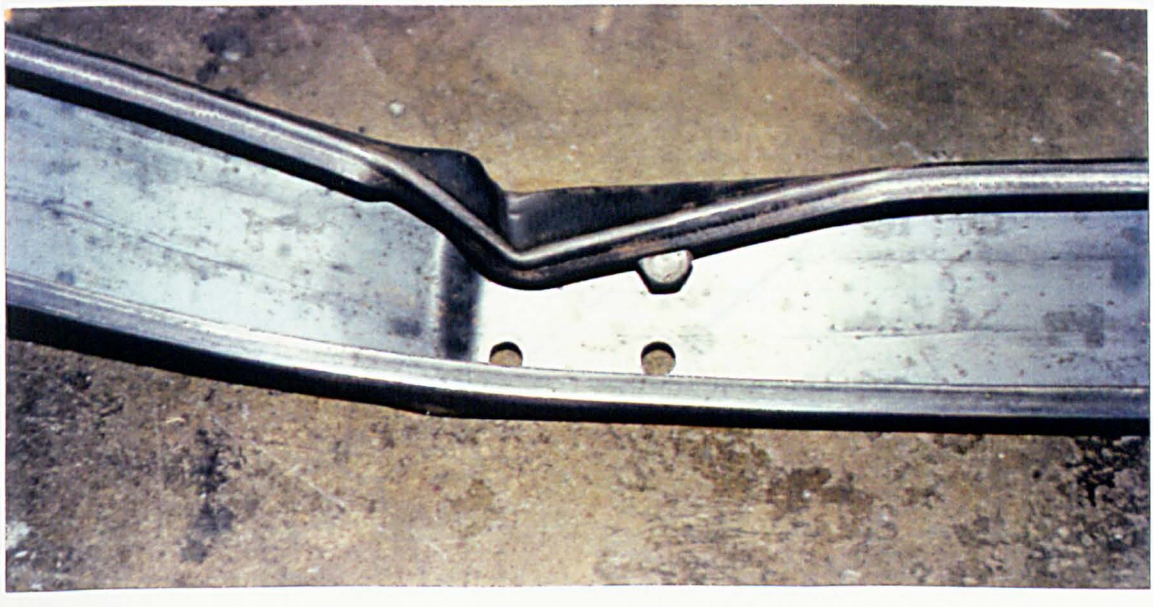

Figure 4.2.2 : Observed Lipped Channel mechanism

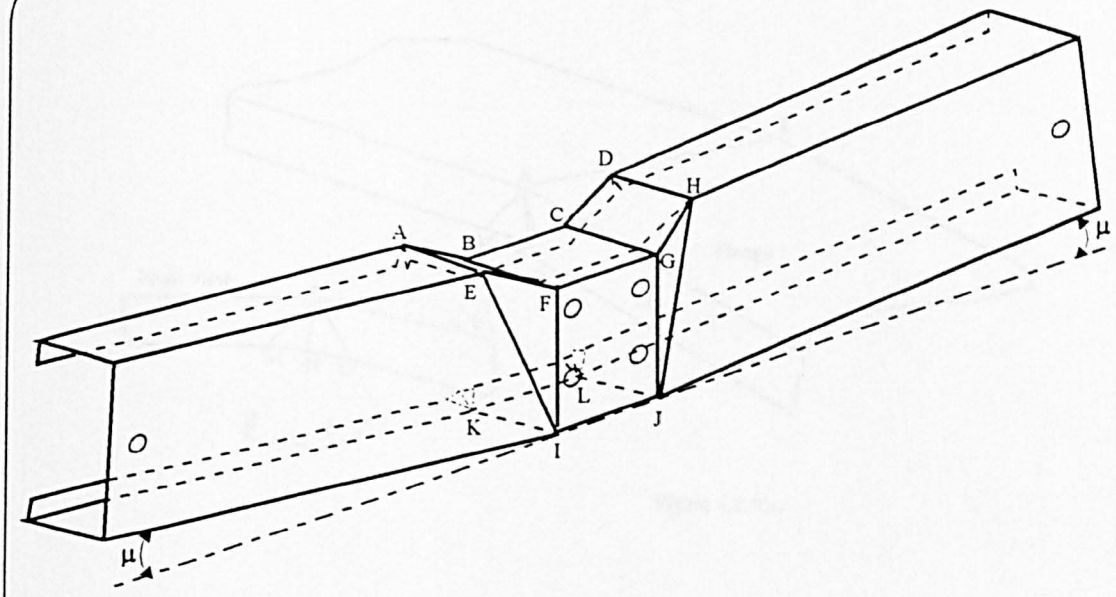

Figure 4.2.3 : Theoretical Lipped Channel mechanism

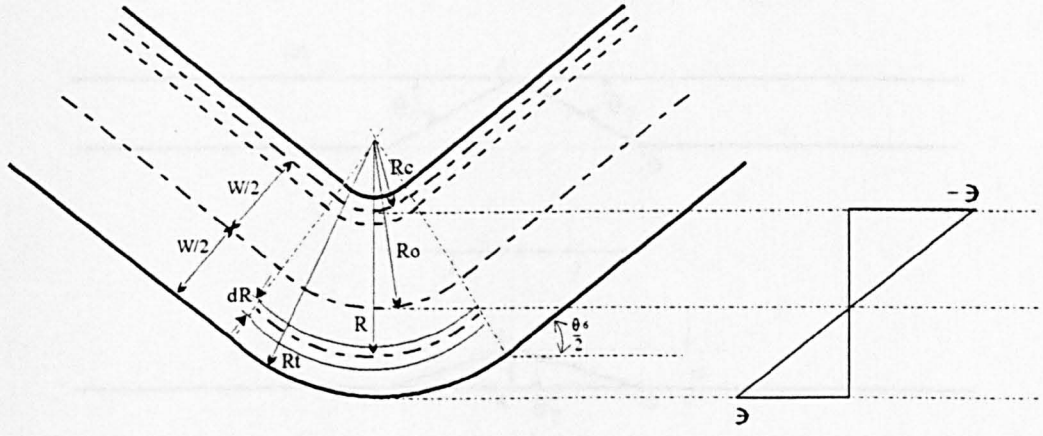

Figure 4.2.4 : Membrane Bending of the Lip

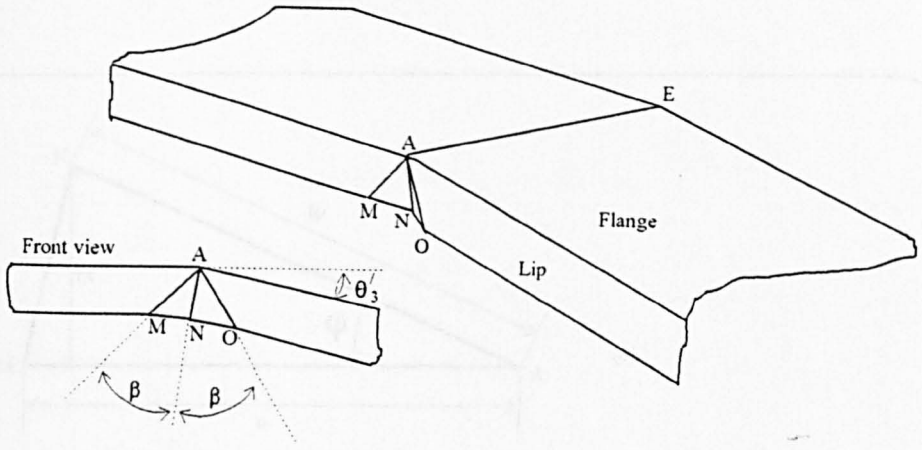

Figure 4.2.5(a)

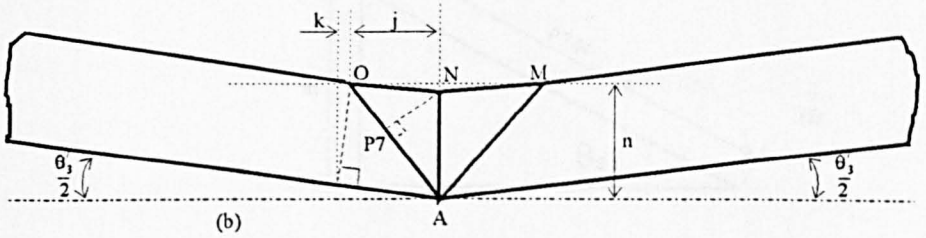

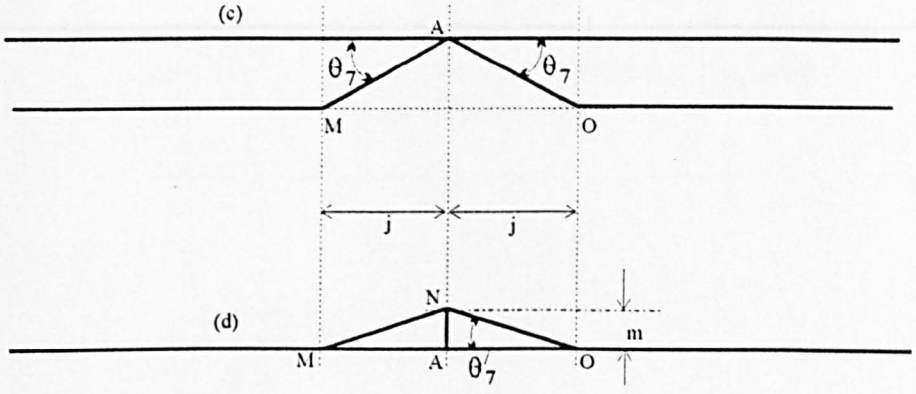

Figure 4.2.5 : The Three Hinge Lip Mechanism

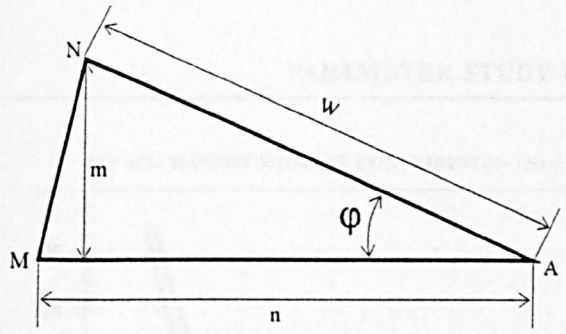

(e)

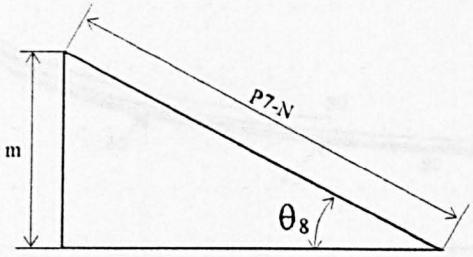

(f)

Figure 4.2.5 : The Three Hinge Lip Mechanism

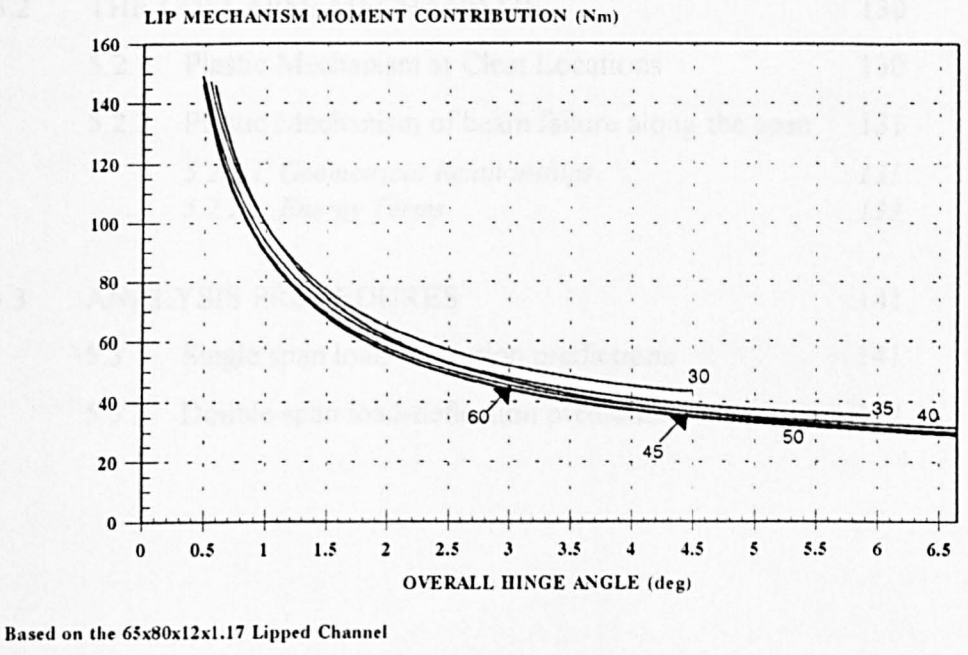

Figure 4.3.1 : Parameter Study of Inclination Angle for the Three Hinge Lip Mechanism

Chapter Five

- ***Analysis of Zed Section beams***

5.1 INTRODUCTION

The work presented in this chapter deals with thin-walled cold formed lipped zed section beams which are commonly used as purlins in roof systems. The specimens examined in this investigation were standard sections as components of roofing systems as supplied by Metal Sections Limited of West Midlands, United Kingdom. These sections differ from the lipped channels in geometry since the flanges on opposing faces of the web are of unequal widths, the nesting flange where the roof sheetings are mounted being wider. The lip stiffeners on the flanges of any zed section are also of different sizes.

As with the plain and lipped channel studies, beam specimens of various sizes were examined in the laboratory. A set of 28 single span zed section beams were tested in the three point bending configuration, pinned on either end and centrally loaded through cleats which were bolted to the webs of the beams. The cleats and bolts used in the experiments were also of standard dimensions which were designed for the beam sections and supplied by Metal Sections Limited. A further set of 8 double span beams were tested in a vacuum box, these beams being supported at either end and centrally by cleats and subjected to uniformly distributed loading. The test details of both sets of experiments, along with a description of the working principles of the vacuum box will be presented in chapter 6 of this thesis.

Theoretical analysis of the zed section beams follows the procedures already discussed in chapters 2, 3 and 4. The remainder of this chapter presents the modifications and additional formulations used in this theoretical investigation of zed section beams studied.

5.2 THE COLLAPSE MECHANISMS

The use of uniformly distributed loading in the double span beam tests brought about an additional degree of realism to these studies as the beams are rarely point loaded through cleats in practice. The theoretical analysis of these beams requires the examination of failure modes at the cleat supports and at the portion of the beam along the span where bending moments are most adverse after the section over the supports have started to fail. Two plastic collapse mechanisms are therefore needed for the analysis. The following sections detail the mechanisms used in the current work.

5.2.1 Plastic Mechanism at Cleat Locations

The experimental investigations revealed that the plastic mechanisms which brought about collapse in the beam sections at the location of the cleat supports were consistent with those found in the lipped channels. Figure 5.2.1 and 5.2.2 shows the typical failure form observed during the testing of the single span zed section beams. The pattern of yield lines appearing on the web, flanges and lips of the collapsing beams are the same as those discussed in chapter 4, as such, the postulated theoretical lipped channel mechanism can be applied to the zed sections. Figure 5.2.3 illustrates the theoretical plastic mechanism assumed in the current investigation. The energy equation stated in the previous chapter as Eqn.(4.2.17) was adapted for the analysis of the zed section beams, the modifications to the energy terms were merely to account for the non-symmetrical flange and lip sizes. The modified equation will not be shown in this chapter as the changes only involve the flange and lip sizes, b and w respectively.

5.2.2 Plastic Mechanism of beam failure along the span

The observations made during the experimental examination of double span lipped channel and zed section beams with uniformly distributed loads applied along the entire span were used to construct the theoretical plastic mechanism for failures along the beam span presented in this section. The failure form is illustrated in figures 5.2.4 and 5.2.5, with the simplified theoretical model shown in figure 5.2.6. The theoretical mechanism is similar in form to the plain and lipped channel mechanism presented previously, however, since there is no cleat to hold the web in position or control the horizontal size of the mechanism, it is simpler and has no twisting effects. This mechanism can be considered a simplified version of the lipped channel mechanism.

The independent parameters, mechanism size 'c' and angle of the inclined hinges in the lips are taken as those used in the plain and lipped channel mechanism analyses in chapters 3 and 4. The following paragraphs develops the geometrical relationships and energy terms for the mechanism.

5.2.2.1 Geometrical Relationships

Referring to figure 5.2.7(a), taking the reference co-ordinate axis at the node 'I' as shown in figure 5.2.6, let the position of point 'F' in the z-direction be represented by a, from continuity considerations,

$$FI = d - a \qquad \text{Eqn.(5.2.1)}$$

where d is the web depth of the section.

The height of 'F' is then given by

$$y_F = \sqrt{FI^2 - a^2}$$
$$= \sqrt{d^2 - 2 \cdot a \cdot d} \qquad \text{Eqn.(5.2.2)}$$

From figure 5.2.7(c), with the mechanism size 'c' as defined in figure 5.2.7(b),

$$y_E = c \cdot \sin\mu + d \cdot \cos\mu$$

and $$x_E = c \cdot \cos\mu - d \cdot \sin\mu \qquad \text{Eqn.(5.2.3)}$$

Also from figure 5.2.7(c),

$$c^2 = x_E^2 + (y_E - y_F)^2$$

Substituting Eqn.(5.2.2) and (5.2.3) into the above expression and rearranging yields

$$a = \frac{d^2 - \left(c \cdot \sin\mu + d \cdot \cos\mu - \sqrt{c^2 - (c \cdot \cos\mu - d \cdot \sin\mu)^2}\right)^2}{2 \cdot d} \qquad \text{Eqn.(5.2.4)}$$

which describes the size 'a' in terms of the overall hinge rotation μ.

5.2.2.2 Energy Terms

Hinges AE and DH

From figure 5.2.7(c),

$$\sin(\mu+\theta_3) = \frac{y_E - y_F}{c}$$

substituting Eqn.(5.2.2) and (5.2.3) into the expression and rearranging,

$$\theta_3 = \sin^{-1}\left(\frac{c\cdot\sin\mu + d\cdot\cos\mu - \sqrt{d^2 - 2\cdot a\cdot d}}{c}\right) - \mu \qquad \text{Eqn.(5.2.5)}$$

Hence, the energy dissipated in hinges AE and DH is given by

$$\begin{aligned} W_1 &= 2\cdot m_p\left[1-\left(\frac{M}{M_u}\right)^2\right]\cdot b2\cdot\theta_3 \\ &= 2\cdot m_p\left[1-\left(\frac{M}{M_u}\right)^2\right]\cdot b2\cdot\left(\sin^{-1}\left(\frac{c\cdot\sin\mu + d\cdot\cos\mu - \sqrt{d^2-2\cdot a\cdot d}}{c}\right) - \mu\right) \end{aligned} \qquad \text{Eqn.(5.2.6)}$$

Hinge BF

Using Eqn.(5.2.5), the energy dissipated in hinge BF is

$$W_2 = 2 \cdot m_p \left[1 - \left(\frac{M}{M_u} \right)^2 \right] \cdot (b2 + a) \cdot (\theta_3 + \mu)$$
$$= 2 \cdot m_p \left[1 - \left(\frac{M}{M_u} \right)^2 \right] \cdot (b2 + a) \cdot \sin^{-1} \left(\frac{c \cdot \sin \mu + d \cdot \cos \mu - \sqrt{d^2 - 2 \cdot a \cdot d}}{c} \right)$$

Eqn.(5.2.7)

Hinge KI

The energy dissipated in KI is given by

$$W_3 = 2 \cdot m_p \left[1 - \left(\frac{M}{M_u} \right)^2 \right] \cdot b1 \cdot \mu$$ Eqn.(5.2.8)

Hinge FI

Referring to figure 5.2.7(d),

$$\theta_2 = \sin^{-1} \left(\frac{a}{d - a} \right)$$ Eqn.(5.2.9)

and $f = a \cdot \cos\theta_2$ Eqn.(5.2.10)

From figure 5.2.7(e),

$$\xi_2 = \tan^{-1}\left(\frac{c}{d}\right) \quad \text{Eqn.(5.2.11)}$$

and $\xi_2' = \xi_2 - \mu$ Eqn.(5.2.12)

Also from figure 5.2.7(e), consider the point P2, which lies on the hinge 'EF' and at the same height as the point 'F', using the co-ordinate axis with the origin at I,

$$x_{P2} = y_F \cdot \tan\xi_2' \quad \text{Eqn.(5.2.13)}$$

Looking in the line of 'FI', as shown in figure 5.2.7(f),

$$\tan\theta_4 = \frac{f}{x_{P2}}$$

substituting Eqn.(5.2.2) and Eqn.'s (5.2.9) to (5.2.13) into the above expression, and rearranging, yields

$$\theta_4 = \tan^{-1}\left(\frac{a\cdot\cos\left[\sin^{-1}\left(\frac{a}{d-a}\right)\right]}{\sqrt{d^2-2\cdot a\cdot d}\cdot\tan\left[\tan^{-1}\left(\frac{c}{d}\right)-\mu\right]}\right) \quad \text{Eqn.(5.2.14)}$$

Therefore, the energy dissipated by the hinge FI is

$$W_4 = 2 \cdot m_p \left[1 - \left(\frac{M}{M_u} \right)^2 \right] \cdot (d-a) \cdot \theta_4$$
$$= 2 \cdot m_p \left[1 - \left(\frac{M}{M_u} \right)^2 \right] \cdot (d-a) \cdot \tan^{-1} \left(\frac{a \cdot \cos\left[\sin^{-1}\left(\frac{a}{d-a} \right) \right]}{\sqrt{d^2 - 2 \cdot a \cdot d} \cdot \tan\left[\tan^{-1}\left(\frac{c}{d} \right) - \mu \right]} \right)$$

Eqn.(5.2.15)

Hinges EI and HI

Referring to figure 5.2.7(g), consider the point P3 on 'EI' such that the line 'P3-F' is perpendicular to 'EI' and passes through the point 'F'. The length 'P3-F' can be estimated as

$$(P3F) = FI \cdot \sin \xi_2$$
$$= (d-a) \cdot \sin \xi_2$$

Eqn.(5.2.16)

From figure 5.2.7(h), looking in the line of 'EI',

$$\theta_5 = \sin^{-1}\left(\frac{a}{P3F} \right)$$
$$= \sin^{-1}\left(\frac{a}{(d-a) \cdot \sin \xi_2} \right)$$

Eqn.(5.2.17)

Hence, the energy dissipated in hinges EI and HI is given by

$$W_5 = 2 \cdot \frac{m_p\left[1-\left(\frac{M}{M_u}\right)^2\right]}{\sqrt{1-\frac{3}{4}\left(\frac{M}{M_u}\right)^2 \sin^2\xi_2\left(4-3\cdot\sin^2\xi_2\right)}} \cdot \sqrt{c^2+d^2} \cdot \theta_5$$

$$= 2 \cdot \frac{m_p\left[1-\left(\frac{M}{M_u}\right)^2\right]}{\sqrt{1-\frac{3}{4}\left(\frac{M}{M_u}\right)^2 \sin^2\xi_2\left(4-3\cdot\sin^2\xi_2\right)}} \cdot \sqrt{c^2+d^2} \cdot \sin^{-1}\left(\frac{a}{(d-a)\cdot\sin\xi_2}\right)$$

Eqn.(5.2.18)

Hinges EF and FH

Neglecting the small changes of angle of the hinges, the energy dissipated in the travelling hinges EF and FH is

$$W_6 = 2 \cdot \frac{m_p\left[1-\left(\frac{M}{M_u}\right)^2\right]}{\sqrt{1-\frac{3}{4}\left(\frac{M}{M_u}\right)^2}} \cdot \frac{a\cdot c}{r}$$

Eqn.(5.2.19)

where r is the mean hinge rolling radius.

Lip Membrane Energy

Adopting the formulation developed in chapter 4, Eqn.(4.2.8), the lip membrane energy is given by

$$W_{lm} = \sigma_o \cdot t \cdot \theta_6 \cdot \frac{w2^2}{2} \qquad \text{Eqn.(5.2.20)}$$

where $\theta_6 = \theta_3 + \mu$
σ_o is the material yield strength
and t is the material thickness.

Lip Three Hinge Mechanism at A and D

The lip mechanism energy dissipation at A and D is given by Eqn.(4.2.14) and Eqn.(4.2.22) developed in the previous chapter, these equations are adapted as shown below

$$W_{Li} = 4 \cdot m_p \left[1 - \left(\frac{M}{M_u}\right)^2 \right] \cdot w2 \cdot \left\{ \cos^{-1} \left[\cos\left(\frac{\theta_3}{2}\right) - \frac{\sin\left(\frac{\theta_3}{2}\right)}{\tan\beta} \right] \right\}$$
$$+4 \cdot \frac{m_p \left[1-\left(\frac{M}{M_u}\right)^2 \right]}{\sqrt{1-\frac{3}{4}\left(\frac{M}{M_u}\right)^2 \sin^2\beta \cdot \left(4-3\cdot\sin^2\beta\right)}} \cdot \frac{w2}{\cos\beta} \cdot \left\{ \sin^{-1} \left[\frac{\sin\varphi}{\sin\beta} \right] \right\} \qquad \text{Eqn.(5.2.21)}$$

where $\varphi = \cos^{-1}\left(\frac{1}{\tan\beta \cdot \sin\left(\frac{\theta_3}{2}\right) + \cos\left(\frac{\theta_3}{2}\right)} \right)$

Lip Three Hinge Mechanism at K

The equations developed in chapter 4, stated as Eqn.(4.2.24) and (4.2.25) are again adapted for the current mechanism. The energy dissipated in the lip mechanism at the location K is given by

$$W_{lK} = 4 \cdot m_p \left[1 - \left(\frac{M}{M_u} \right)^2 \right] \cdot w1 \cdot \left\{ \cos^{-1} \left[\cos\left(\frac{\mu}{2} \right) - \frac{\sin\left(\frac{\mu}{2} \right)}{\tan\beta} \right] \right\}$$

$$+4 \cdot \frac{m_p \left[1 - \left(\frac{M}{M_u} \right)^2 \right]}{\sqrt{1 - \frac{3}{4}\left(\frac{M}{M_u} \right)^2 \sin^2\beta \cdot \left(4 - 3 \cdot \sin^2\beta \right)}} \cdot \frac{w1}{\cos\beta} \cdot \left\{ \sin^{-1} \left[\frac{\sin\varphi'}{\sin\beta} \right] \right\} \qquad \text{Eqn.(5.2.22)}$$

where $\varphi' = \cos^{-1}\left(\frac{1}{\tan\beta \cdot \sin\left(\frac{\mu}{2} \right) + \cos\left(\frac{\mu}{2} \right)} \right)$

The total internal energy dissipation is therefore given by

$$
\begin{aligned}
W_{int} &= W_1 + W_2 + W_3 + W_4 + W_5 + W_6 + W_{lm} + W_{LA} + W_{LK} \\
&= 2 \cdot m_p \left[1 - \left(\frac{M}{M_u} \right)^2 \right] \cdot b2 \cdot \left(\sin^{-1} \left(\frac{c \cdot \sin\mu + d \cdot \cos\mu - \sqrt{d^2 - 2 \cdot a \cdot d}}{c} \right) - \mu \right) \\
&+ 2 \cdot m_p \left[1 - \left(\frac{M}{M_u} \right)^2 \right] \cdot (b2 + a) \cdot \sin^{-1} \left(\frac{c \cdot \sin\mu + d \cdot \cos\mu - \sqrt{d^2 - 2 \cdot a \cdot d}}{c} \right) \\
&+ 2 \cdot m_p \left[1 - \left(\frac{M}{M_u} \right)^2 \right] \cdot b1 \cdot \mu \\
&+ 2 \cdot m_p \left[1 - \left(\frac{M}{M_u} \right)^2 \right] \cdot (d - a) \cdot \tan^{-1} \left(\frac{a \cdot \cos\left[\sin^{-1} \left(\frac{a}{d-a} \right) \right]}{\sqrt{d^2 - 2 \cdot a \cdot d} \cdot \tan\left[\tan^{-1} \left(\frac{c}{d} \right) - \mu \right]} \right) \\
&+ 2 \cdot \frac{m_p \left[1 - \left(\frac{M}{M_u} \right)^2 \right]}{\sqrt{1 - \frac{3}{4} \left(\frac{M}{M_u} \right)^2 \sin^2\xi_2 \left(4 - 3 \cdot \sin^2\xi_2 \right)}} \cdot \sqrt{c^2 + d^2} \cdot \sin^{-1} \left(\frac{a}{(d-a) \cdot \sin\xi_2} \right) \\
&+ 2 \cdot \frac{m_p \left[1 - \left(\frac{M}{M_u} \right)^2 \right]}{\sqrt{1 - \frac{3}{4} \left(\frac{M}{M_u} \right)^2}} \cdot \frac{a \cdot c}{r} \\
&+ \sigma_o \cdot t \cdot (\theta_3 + \mu) \cdot \frac{w2^2}{2} \\
&+ 4 \cdot m_p \left[1 - \left(\frac{M}{M_u} \right)^2 \right] \cdot w2 \cdot \left\{ \cos^{-1} \left[\cos\left(\frac{\theta_3}{2} \right) - \frac{\sin\left(\frac{\theta_3}{2} \right)}{\tan\beta} \right] \right\} \\
&+ 4 \cdot \frac{m_p \left[1 - \left(\frac{M}{M_u} \right)^2 \right]}{\sqrt{1 - \frac{3}{4} \left(\frac{M}{M_u} \right)^2 \sin^2\beta \cdot \left(4 - 3 \cdot \sin^2\beta \right)}} \cdot \frac{w2}{\cos\beta} \cdot \left\{ \sin^{-1} \left[\frac{\sin\varphi}{\sin\beta} \right] \right\} \\
&+ 4 \cdot m_p \left[1 - \left(\frac{M}{M_u} \right)^2 \right] \cdot w1 \cdot \left\{ \cos^{-1} \left[\cos\left(\frac{\mu}{2} \right) - \frac{\sin\left(\frac{\mu}{2} \right)}{\tan\beta} \right] \right\} \\
&+ 4 \cdot \frac{m_p \left[1 - \left(\frac{M}{M_u} \right)^2 \right]}{\sqrt{1 - \frac{3}{4} \left(\frac{M}{M_u} \right)^2 \sin^2\beta \cdot \left(4 - 3 \cdot \sin^2\beta \right)}} \cdot \frac{w1}{\cos\beta} \cdot \left\{ \sin^{-1} \left[\frac{\sin\varphi'}{\sin\beta} \right] \right\}
\end{aligned}
$$

Eqn.(5.2.23)

5.3 ANALYSIS PROCEDURES

The analysis methods used in the theoretical treatment of the zed section beams are essentially the same as in the previous two chapters where plain and lipped channels were studied. The following sections are intended to highlight the modifications which have been made to the formulations in order to cope with the zed sections, most important is the section on double span beam analysis since the loading conditions are quite different from that discussed in the previous two chapters.

5.3.1 Single span load-deflection predictions

All the single span zed section beams were tested in the same manner as the channel sections, theoretically, they were considered to be simply supported at both ends and loaded centrally through a cleat bolted to the web. Essentially, this is a study of the beam behaviour at the point of support.

The theoretical collapse analysis of these beams was done using the lipped channel mechanism described by Eqn.(4.2.17) in chapter 4 with relevant changes to the flange and lip sizes in the equations. The total internal energy was equated to the external work done using Eqn.(3.5.1) as before and the elastic solution was obtained from a modified version of ELASTIC8.bas, which considered the unsymmetrical geometry of the zed cross-section. Since this work is so similar to that for the lipped channels, the reader may refer to chapter 4 for the details of the analysis.

5.3.2 Double span load-deflection predictions

The theoretical methods detailed in this section were applied in the study of the double spanning zed section beams and some of the lipped channel beams first introduced in chapter 4. These beams were subjected to uniformly distributed loading in a vacuum box and supported by cleats at mid-length and each end. The reader may want to refer to chapter 6 for the detailed test descriptions.

As in the point loaded double span beams, with initial loading, maximum bending moments would be found at the central support and it is at this point along the beam that buckling and subsequently plastic mechanisms will first appear. On further loading, the beam section over the support would eventually proceed into the collapse mode, shedding some of it's moment carrying capacity as the deflections increased. At this point, the distributed loads carried by the beam can still be increased since the portions of the beam between the supports have yet to reach their full load carrying potential. Hence, the loads continue to rise until such time that the ultimate bending moment is reached at a location somewhere along the beam span, after which the loads drop off as the beam collapses.

The ultimate moment and collapse characteristics of the beam section over the central support can be obtained from the single span beam studies described in section 5.3.1. Similar analyses were carried out for the ultimate moment and collapse behaviour of the beam sections along the span, away from the supports. Using the mechanism developed in section 5.2.2, described by Eqn.(5.2.23) and the same elastic analysis used for the single span beams, moment-rotation information was obtained for beam failure along the span.

The following paragraphs detail the method used to construct the theoretical double span load-deflection predictions from the two types of beam collapse behaviour characteristics in terms of moment-rotation data of the failure section.

The technique applied in this section was first introduced in chapter 3, section 3.5.4 of this thesis. The analysis essentially consist of three parts, the initial elastic loading stage, the subsequent loading stage where the beams over the central support has started to fail and the final collapse stage.

In the initial loading stage, the complete double span beam is analysed as an elastic beam using the Macaulay's beam method. Figure 5.3.1 shows the forces acting on the elastic beam in this first stage. The second moment of area used for the Macaulay solution is based on the minimum effective section as calculated according to BS5950 ; Part 5 ; 1985, ref. [8], as detailed in chapter 2 of this thesis. This minimum effective section was calculated using the maximum bending moment along the beam which occurs over the central support. The elastic mid-span deflection from the Macaulay's solution is given by

$$v_{ms} = \frac{U \cdot L^4}{192 \cdot EI_{eff}} \qquad \text{Eqn.(5.3.1)}$$

where v_{ms} is the mid-span deflection
U is the applied uniformly distributed load
L is the span length between supports
E is the material Young's modulus of elasticity
and I_{eff} is the second moment of area of the minimum effective cross-section.

The bending moment at the central support, M_B, is calculated from

$$M_B = \frac{U \cdot L^2}{8} \qquad \text{Eqn.(5.3.2)}$$

As the loads are increased, the bending moment at the central support eventually reaches the ultimate value as found from the single span analysis, the moment capacity of the beam over the support starts to decrease according to the collapse characteristics and the analysis moves onto the second stage. The double spanning beam is then considered as two simply supported single span beams with a resisting moment at the location of the former central support, as shown in figure 5.3.2. The magnitude of this resisting moment is a function of the angle of rotation which in this part of the analysis is the slope of the beam at point 'B'. Therefore, by increasing this slope in steps, the resisting moment can be found from the single span moment-rotation data for beam collapse at cleat supports. The applied distributed load can be evaluated from the slope equation of the Macaulay's solution at x=0,

$$EI_{eff} \cdot \mu = \frac{U \cdot L^3}{24} - \frac{M_B(\mu) \cdot L}{3}$$

Rearranging gives

$$U = \frac{24\left(EI_{eff} \cdot \mu + \frac{M_B(\mu) \cdot L}{3}\right)}{L^3} \qquad \text{Eqn.(5.3.3)}$$

where $M_B(\mu)$ is the resisting moment of the failing beam portion at the support and μ is the slope of the beam at x=0.

The mid-span deflection can then be determined from the Macaulay's solution as

$$v_{ms} = \frac{1}{EI_{eff}}\left(\frac{5U \cdot L^4}{384} - \frac{M_B(\mu) \cdot L^2}{16}\right) \qquad \text{Eqn.(5.3.4)}$$

The second stage solution is applicable up to the point where the maximum bending moment along the beam span reaches the ultimate value. The Macaulay moment equation for the second stage analysis is

$$M_x = -M_B(\mu) + \left[\frac{M_B(\mu)}{L} + \frac{U \cdot L}{2}\right] \cdot x - \frac{U \cdot x^2}{2} \qquad \text{Eqn.(5.3.5)}$$

where [....] are Macaulay brackets.

For the position along the span where maximum bending moment occurs at any instance, $\frac{dM_x}{dx} = 0$, therefore

$$\left(\frac{M_B(\mu)}{L} + \frac{U \cdot L}{2}\right) - U \cdot x_m = 0$$

giving

$$x_m = \frac{M_B(\mu)}{U \cdot L} + \frac{L}{2} \qquad \text{Eqn.(5.3.6)}$$

Substituting Eqn.(5.3.6) into Eqn.(5.3.5) yields the expression for the maximum bending moment along the beam

$$M_m = \frac{M_B(\mu)^2}{2U \cdot L^2} + \frac{U \cdot L^2}{8} - \frac{M_B(\mu)}{2} \qquad \text{Eqn.(5.3.7)}$$

The collapse point along the beam is given by the value of x_m when M_m reaches the ultimate moment capacity and the collapse plastic mechanism will form at this position along the beam span.

The final collapse stage is theoretically treated using the energy method in the same manner as in chapter 3. Eqn.(3.5.7) states the governing equation for the point loaded double span beams. With a similar procedure, it can be shown that the governing equation for the beam subjected to uniform distributed loading is

$$U = \frac{M_B(\mu_1)\cdot\dfrac{1}{\sqrt{1-\left(\frac{v}{L_1}\right)^2}}\cdot L_1 + M_D(\mu_3')\cdot\left[\dfrac{1}{\sqrt{1-\left(\frac{v}{L_1}\right)^2}}\cdot L_1 + \dfrac{1}{\sqrt{1-\left(\frac{v}{L_2}\right)^2}}\cdot L_2\right]}{\left(\frac{L}{2}\right)} \qquad \text{Eqn.(5.3.8)}$$

where $M_B(\mu_1)$ is the instantaneous value of resisting moment over the central support from the single span moment-rotation data

$M_D(\mu_3')$ is the instantaneous moment capacity of the beam section along the span that has begun to fail

and $\mu_3' = \frac{\mu_3}{2}$.

The entire procedure was coded into a program written in BASIC named MSBZ2.bas which is listed in Appendix II of this thesis.

With slight modifications, the program was adapted for the double span lipped channel beams under uniformly distributed loading. Since the changes only affected the calculations for evaluating the effective second moment of area, the modified program is not listed.

The results of both the experimental and analytical investigations will be presented in chapter 7 of the thesis and they will be further discussed in chapter 9. Generally, the theoretical predictions agreed well with the experimental findings, especially for the double spanning zed sections.

Figure 5.2.1 : Observed Zed Mechanism at Cleat Location

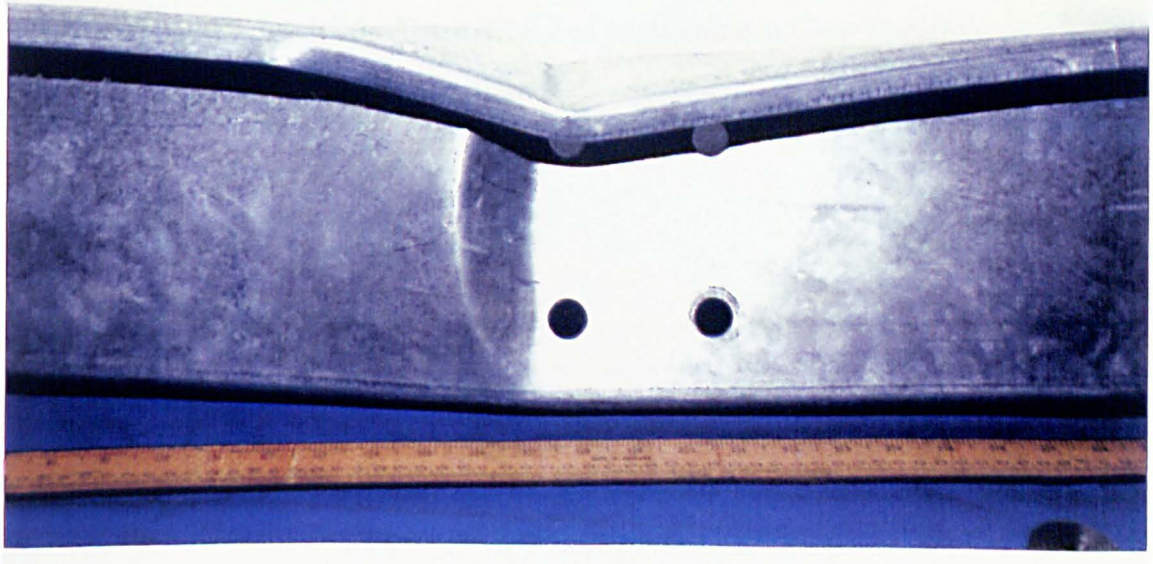

Figure 5.2.2 : Observed Zed Mechanism at Cleat Location

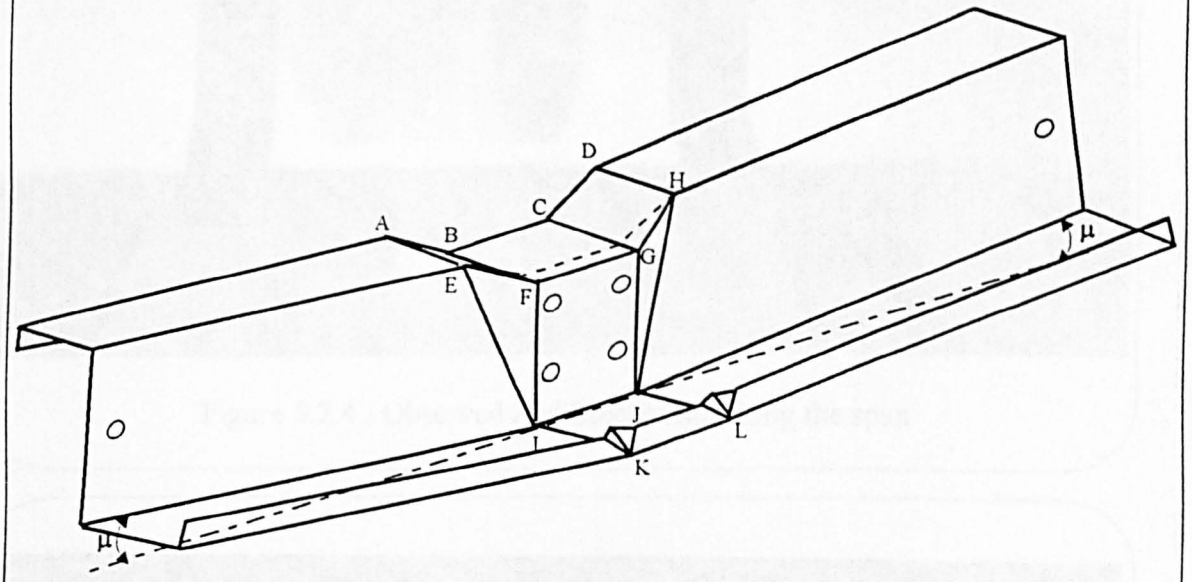

Figure 5.2.3 : Theoretical Zed Mechanism at Cleat Location

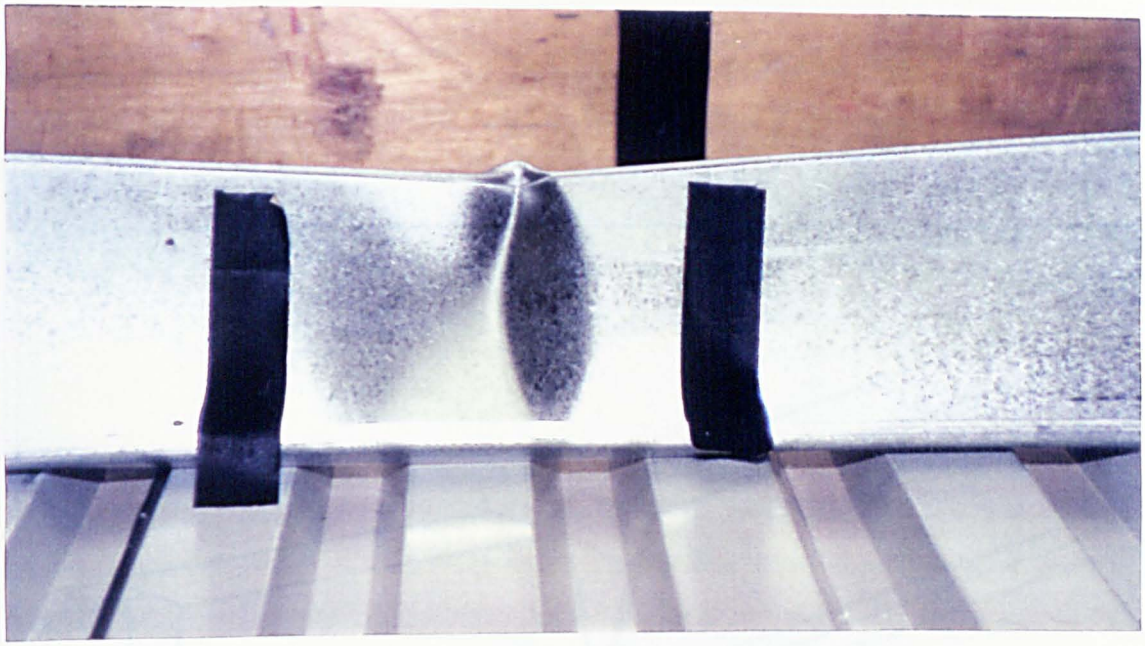

Figure 5.2.4 : Observed Zed Mechanism along the span

Figure 5.2.5 : Observed Zed Mechanism along the span

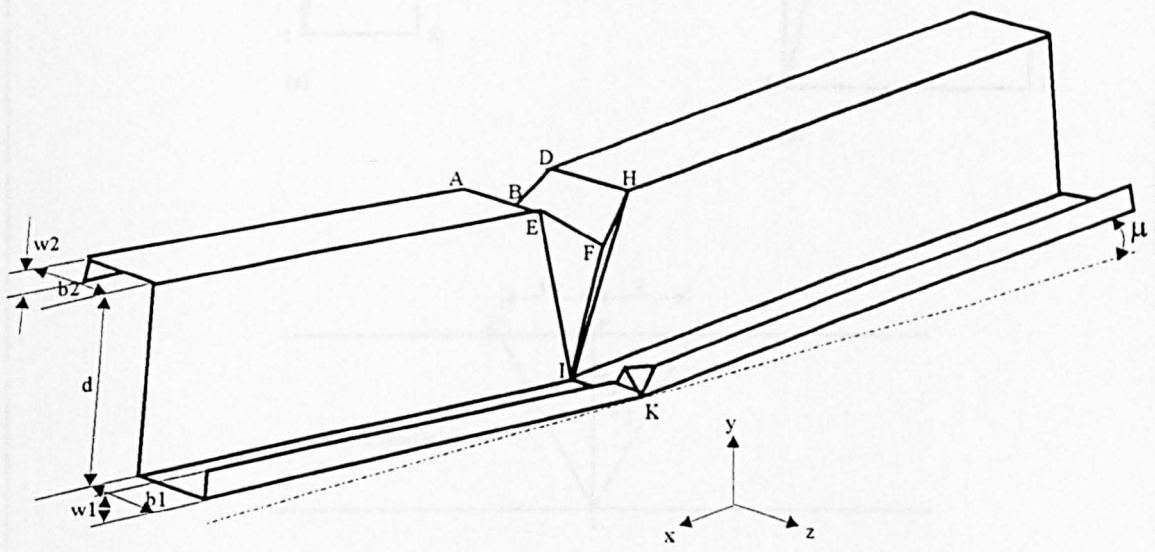

Figure 5.2.6 : Theoretical Zed Mechanism along Span

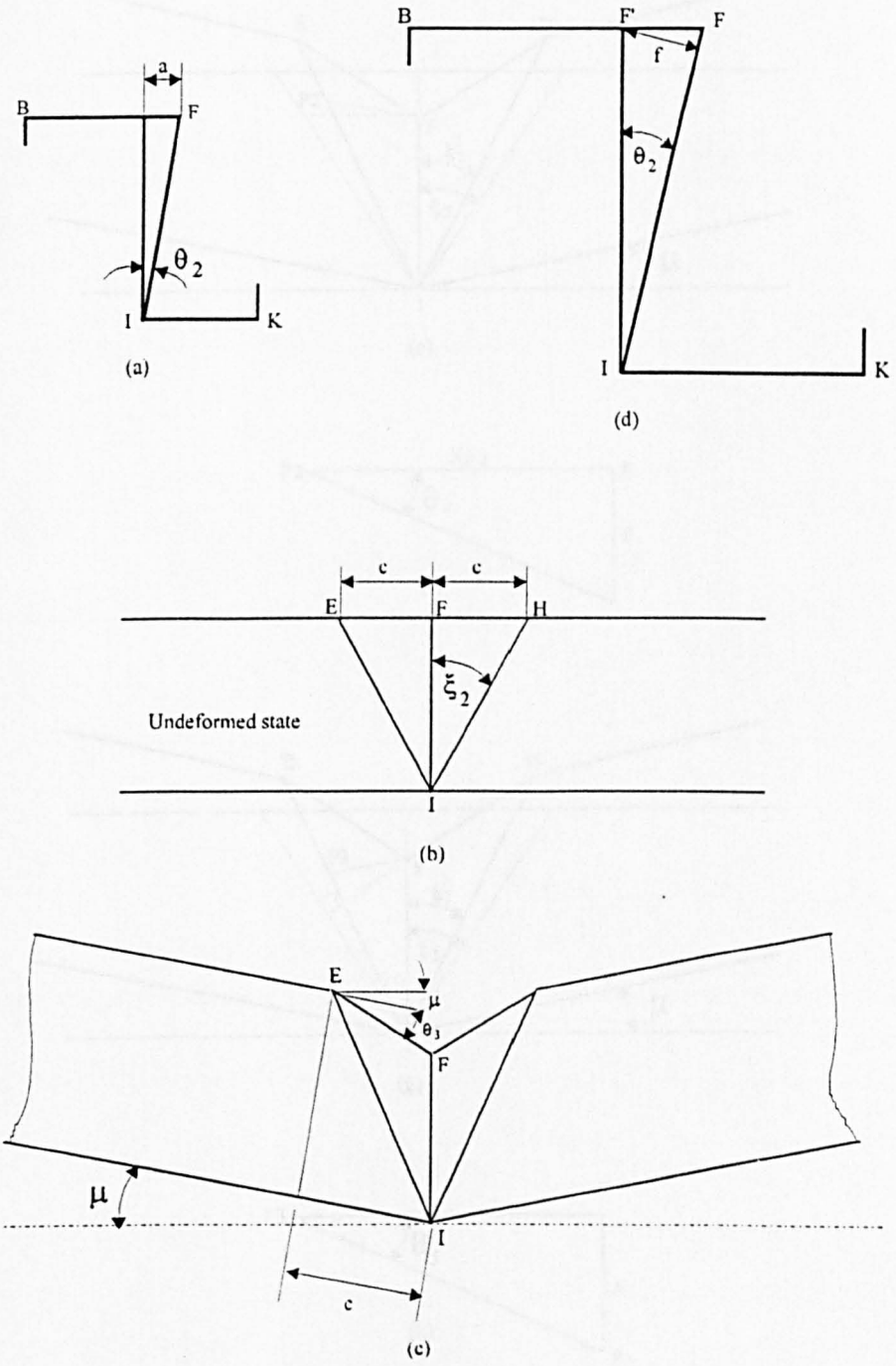

Figure 5.2.7 : The Zed Mechanism (Along the span)

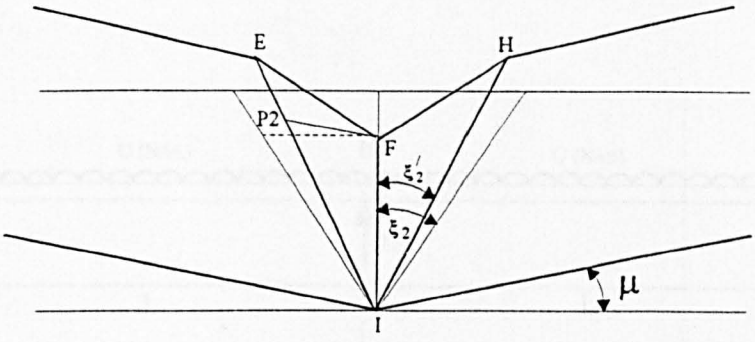

(e)

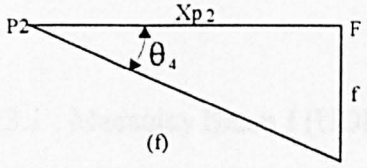

(f)

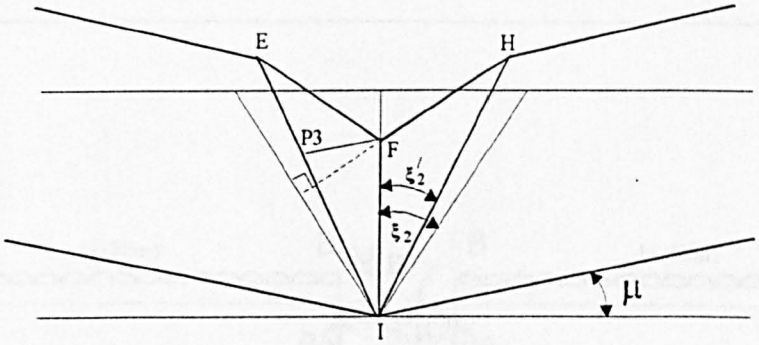

(g)

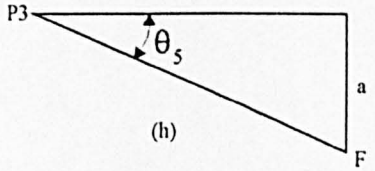

(h)

Figure 5.2.7 : The Zed Mechanism (Along the span)

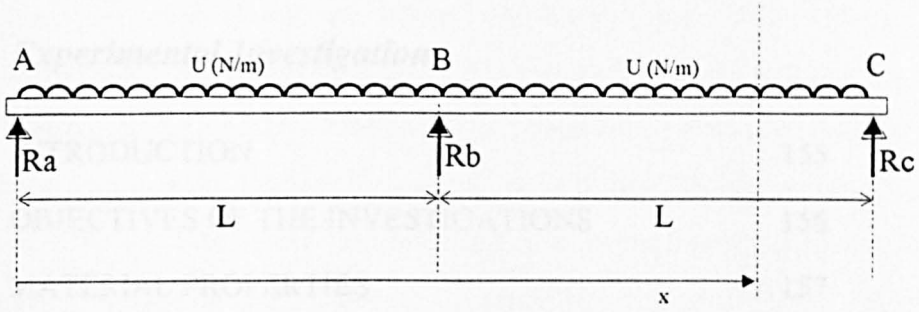

Figure 5.3.1 : Macaulay Beam I (UDL)

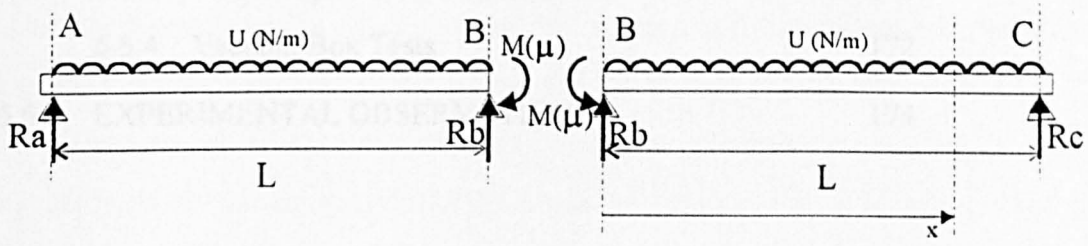

Figure 5.3.2 : Macaulay Beam II (UDL)

Chapter Six

- *Experimental Investigations*

6.1 INTRODUCTION

Researchers in the fields of the applied sciences and engineering are often plagued by the danger of becoming totally preoccupied with the idealised world of theoretical interpretation and mathematical simulation which may lead to the loss of sight of the realities of the material world. Proof testing has been a long standing tradition in engineering development and it is the author's opinion that this practice is not only important in the creation of new 'hardware' but in theoretical work as well. Experimental verification is crucial in any research program which aims to form new theory and the collected experimental data should become the target for theoretical predictions. It is with this spirit that the current studies were carried out.

This chapter details the test program which was carried out with the aim of providing ideas and experimental verification data for the development of the theories presented in the preceding chapters. The experiments were designed to suit the primary objectives of the current study and closely conform with the assumed conditions for the theoretical models while maintaining a high degree of practicality, as far as possible. Generally, the test beams were designed to fail in bending with local buckling effects being the major cause of the initiation of failure. In order to facilitate the study of the effects of plastic moment redistribution on the ultimate loads of multi-spanning beams, the study of the single spanning beam sections under investigation had to extend beyond the ultimate failure load region of loading history, some ways into the collapse behaviour. With these objectives in view, extensive experimental investigations were carried out on plain channel, lipped channel and zed section beams which were supported through cleats and loaded either through similar cleats or subjected to simulated uniformly distributed loading conditions. The particular interests for the study were in the pattern of yield lines that form during collapse and the load-deflection behaviour through the entire range of loading.

6.2 OBJECTIVES OF THE INVESTIGATIONS

The basic objective of the experimental investigations detailed in this chapter is to study the most common failure modes that bring about ultimate failure in the selected beam sections and the subsequent collapse behaviour associated with those failure modes. The aims of the experiments are as follows :

(i) To study the general behaviour of thin-walled beams which are supported through cleats as they are loaded beyond ultimate failure and into collapse.

(ii) To obtain information on the failure modes associated with the collapse of plain channel, lipped channel and zed section beams in order to facilitate the construction of theoretical plastic collapse mechanisms for the rigid-plastic analysis of the beams.

(iii) To examine the load-deflection behaviour of the selected beam sections in the entire range of loading.

(iv) To provides the means to verify and assess the results of the theoretical models developed in chapters 3, 4 and 5 of this thesis.

6.3 MATERIAL PROPERTIES

The beam specimens tested in the experimental investigations came from various sources, some of the sections were prefabricated (cold rolled) while others were produced from mild steel sheets by cold folding. In all cases, samples of the beam material were tested for the mechanical properties of the steels in accordance with BS 18 ; Part 3 ; 1987, for thin steel specimens and BS EN 10 002-1 ; Part 1 ; 1990, for the tensile testing of metallic materials.

A total of 35 tensile tests were conducted to ascertain the relevant material properties of the beam materials examined in the current study. All tensile test specimens were machined to the shape and sizes as detailed in figure 6.3.1 and tested in a Mayse Testing Machine which has a closed-loop hydraulic system with computer control and extensometer feedback ensuring a constant strain rate. During the tests, a Denison electronic extensometer with a 50 mm gauge length was affixed onto the specimen to give instantaneous output of the specimen strain. The machine was set to test at 6.4 mm/min which introduced a strain rate of 0.08 mm/min to the tensile specimens, which is well within the BS 18 specification of 0.15 mm/min. Voltage signals proportional to the applied load were derived from a specially fitted transducer which was calibrated by certified personnel. The signals from the extensometer and load transducer were fed into an A3-size X-Y plotter which automatically recorded the load/extension behaviour of the specimens onto graph paper.

Typical stress-strain behaviour found in the beam materials have been discussed in chapter 2 of this thesis. Table 6.3.1 summarises the relevant results of these tensile tests.

Source	Thickness (mm)	Yield Stress (N/mm^2)	Ultimate Stress (N/mm^2)
203mm deep Plain Channel	2	261.5	314
55mm deep Plain Channel	0.6	260.5	342
80mm deep Lipped Channel	0.78	174.14	303
80mm deep Lipped Channel	1.17	181.63	317.44
80mm deep Lipped Channel	1.97	201.1	320.56
165mm deep Lipped Channel	1.6	410	533
220mm deep Lipped Channel	1.79	412	535.6
127mm deep Lipped Channel	2	358	465.4
122mm deep Zed Section	1.48	324	465
142mm deep Zed Section	1.49	345	446
172mm deep Zed Section	1.52	308	393.4
122mm deep Zed Section	1.56	362	458
232mm deep Zed Section	1.73	326	464.7
262mm deep Zed Section	1.74	350	451
142mm deep Zed Section	1.96	306	387
172mm deep Zed Section	2.35	352	450
262mm deep Zed Section	2.99	320	443.82

Table 6.3.1 : Mechanical Properties of Beam Materials

6.4 APPARATUS

In the 9 sets of experiments which make up the test program for the current study of thin-walled beams, two test apparatus were used. The first being the Tinius Olsen electro-mechanical testing machine which was used for all the single span beam tests and the double span beams which were loaded through cleats. The second apparatus is a vacuum box which was used for the two sets of double span tests in which the beams were subjected to simulated uniformly distributed loads. The following two sections describes these two test machines along with the supporting instrumentation which was used in the beam experiments.

6.4.1 Tinius Olsen Electro-Mechanical Testing Machine

The Tinius Olsen testing machine is a 200,000 lb universal screw driven machine installed in a laboratory of the Mechanical Engineering department of the University of Strathclyde. It is calibrated annually by Namas Test House (Bayliss Brown Limited) according to the specifications of BS 1610:11:85, and the built-in load transducer was certified to be within 0.5% accuracy for the entire period in which the test program was carried out.

The test machine applies loads by means of a moving crosshead which is raised or lowered by the action of four electrically controlled power screws. The screws rotate in synchronicity and in different directions so as to avoid applying torsional stresses to test specimens. Loads are measured by means of a torsion bar system installed in the machine base and indicated on an analogue meter on the control panel of the machine, a voltage signal output proportional to the load is also available for additional instrumentation.

The speed of the crosshead movement during test is electronically controlled by setting the control unit to either displace the crosshead at a constant speed or automatically adjust the movement to apply loads at a constant rate. The former mode was used for all the beam experiments of the study.

The following additional instruments were used with the Tinius Olsen for the beam experiments :

(a) Displacement Transducers

In all the beam experiments, electrical resistive displacement transducers were employed to monitor the beam deflections at selected points. These transducers have a maximum range of approximately 70 mm and were powered using signal amplifiers which provided a stable DC voltage. Output voltage signals were linearly proportional to the detected displacements throughout the transducer range.

(b) X-Y Graph Plotters

Gould series 2000 X-Y plotters manufactured by Bryans Recorders Ltd, were used to record the continuous signals from the Tinius load transducer and the displacement transducers as the beams were loaded to failure. These plotters were regularly calibrated to the transducers to ensure accurate load and deflection readings of the optimum range for each test. The instantaneous output from these plotters also served to provide a means to monitor the progress of each beam test during the loading process.

Figure 6.4.1 shows the Tinius Olsen testing machine with a typical beam test set-up.

6.4.2 Vacuum Box

The vacuum box in which 2 sets of the double span beam experiments (subjected to uniformly distributed loading) were conducted, is situated in the main laboratory of the Mechanical Engineering department of the University of Strathclyde. Figure 6.4.2 shows the vacuum box. The apparatus was constructed for the purpose of testing cold-formed roof purlins and is essentially an airtight box of wooden construction, 12.01 m in length, 2.438 m wide and 1 m high. It was designed to accommodate thin-walled beams of up to 12 m lengths and is equipped with a vacuum system capable of producing partial vacuums within the box of up to approximately 10% of the atmospheric pressure, which converts to approximately 8.83 kN/m^2 of effective pressure. The applied vacuum within the box effectively induces an applied pressure (atmospheric pressure) onto the outside walls of the box and the top surface which is usually covered by thin-walled steel roof sheeting which is supported by the beams under test. Atmospheric pressure is therefore used to simulate the uniformly distributed loading condition on the test subjects within the airtight test environment.

The typical test set-up is illustrated in figure 6.4.3. Longitudinal beams securely bolted to the strong-floor of the laboratory provides the rigid base for the test structure to be installed on. In a typical beam test, cross beams are fastened to these longitudinal beams and the cleats which support the thin-walled test beams are bolted onto the top of the relatively rigid cross beams. Corrugated steel roof sheeting are installed onto the test beams providing the surface area for atmospheric pressure to act upon. The assembly is subsequently covered by a strong continuous polythene sheet which is sealed against the walls of the vacuum box to provide the airtight environment necessary for the pressure test.

During the tests, air removal by the suction pump is regulated by a butterfly valve which controls the rate of pressure change within the vacuum box, which effectively controls the rate of load application. The relative pressure of the partial vacuum within the box is monitored by a calibrated manometer, a diaphragm type electronic pressure transducer and a hand-held digital electronic pressure gauge for quick readings of pressure. The pressure transducer provides an output voltage linearly proportional to the applied vacuum and this signal was channelled to a calibrated X-Y graph plotter. Displacement transducers were used for the measurement of mid-span beam deflections and together with the continuous pressure signals, were recorded by the X-Y plotter onto A3 size graph paper. The displacement transducers and X-Y graph plotters used in these experiments were the same as those used in the Tinius Olsen beam tests.

The partial vacuum created within the airtight box during the tests were measured and recorded in terms of barometric column height of water (cm [H_2O]). These readings can be converted to pressure acting on the covering which is supported by the test beams using Eqn.(6.4.1) below.

$$Q = \rho \cdot g \cdot \frac{H}{100} \qquad \text{Eqn.(6.4.1)}$$

where Q is the effective applied pressure in (N/m^2)
ρ is the density of water (= 1000 kg/m^3)
g is the gravitational acceleration (= 9.81 m/sec^2)
and H is the measured head in (cm [H_2O]).

This pressure can then be converted to applied effective uniformly distributed load on each of the two test beams using :

$$U_p = \frac{Q \cdot B}{2 \cdot 1000}$$
$$= \frac{\left(1000 \cdot 9.81 \cdot \frac{H}{100}\right) \cdot B}{2 \cdot 1000}$$
$$= 0.0981 \cdot H \cdot \frac{B}{2} \qquad \text{Eqn.(6.4.2)}$$

where U_p is the applied effective load due to the applied vacuum in (kN/m)
B is the internal width of the vacuum box = 2.438 m
and the factor 2 is to account for the two test beams installed.

and $U = U_p + U_s + U_b$ Eqn.(6.4.3)

where U is the overall load carried by each beam in (kN/m)
U_s is the loading due to the weight of the covering
and U_b is the self-weight of the beam under test.

6.5 TEST PROGRAM

The test program for the current study of thin-walled beams consists of 9 sets of experiments on 3 different beam cross-sections of various thicknesses and proportions. All of the experiments reported in this chapter were conducted by the author except the set of lipped channel double span beam tests which were performed by J.Rhodes, C.B.Chan and S.H.Tan in April of 1990 for Metal Sections Limited, who graciously consented to the use of the findings in the current investigation. All Zed section tests and a number of the Lipped Channel tests were commissioned by Metal Sections Limited and the details are reproduced here with the permission of that company.

The important details of the experiments will be presented in the following subsections.

6.5.1 Some Important Considerations and Aspects of Test Design

This section highlights the important aspects and constraints related to the design of the beam tests. It also details the criteria which governed the selection of some of the important dimensions of the test beam specimens. Much of the constraints discussed in the following paragraphs are due to limiting factors of available machinery in the laboratories.

6.5.1.1 Beam Dimensions

The current investigation is intended to study the bending effects in the selected thin-walled beam sections, as such, it is of interest to avoid the situation where failure is brought about mainly by shear force effects. The span of the beam specimens had to

be of sufficient length for this reason. Based loosely on the BS 5950 ; Part 5 ; 1987 recommendations (Section 10.3) on the testing of members in bending, which limits the minimum length of test specimen to 8 times the greatest cross-sectional dimension. It was adopted as a general rule that beams for the current study would have spans of at least 8 times the greatest cross-sectional dimension (which in all cases for the sections studied, is the depth of the beams).

It was the intention of the author to study beam sections with a small range of flange width to web depth ratios and flange width to thickness ratios. This was not completely possible for the lipped channels which were fabricated in the laboratories since the minimum flange width was limited by the size of the clamping blades of the folding machine. The depth of the beams could not be increased since this would require the beam span to be made longer, according to the rule discussed in the previous paragraph, which could not be achieved in the laboratory since the length of the fabricated beams were limited by the 2 m length capacity of the folding machine and guillotine used to produce the specimens.

The thickness of the fabricated beam specimens was also limited to 2 mm, since this was the thickest mild steel material that the folding machine could take.

In an attempt to maintain consistency with the cold-formed steel manufacturers, the radii of cold-formed corners were kept to the minimum. The ideal mean radius of bend to thickness ratio of 1 was never achieved in any of the fabricated sections due to the rigidity and design of the folding machines available in the laboratories. The typical radius to thickness ratio found in the cold-folded sections ranged from 2 to over 3.

6.5.1.2 Sizing of Bolted Connections

Hexagonal bolt and nuts were used to secure the beam specimens through their webs onto the supporting cleats. In keeping with the standard tolerance that cold-formed steel manufacturers use for their cleat supported systems, all the bolt holes used in the experiments were sized 2 mm larger than the nominal bolt sizes.

In the zed section and some of the lipped channel beams which were supplied by Metal Sections Limited, the M16 and M12 bolts used were part of a set of the standard accessories that were designed for the beam sections.

For the remainder of the beam tests, bolt sizes were selected in accordance to the recommendations outlined in section 8.2 of BS 5950 ; Part 5 ; 1987, for bolted connections. In the design of the beam tests, the shear capacity of the bolts were checked against the estimated maximum possible shear loads the bolts may be exposed to. These maximum loads were based on the fully plastic beam section modulus which provided crude overestimates of the maximum loading conditions. The bearing capacity of the connected elements were also considered in the bolt selection process and the estimated fully plastic loads were again used to design against bearing failure at the connections.

6.5.1.3 Double Beam Double Span system

In view of the fact that the beam sections studied in the current investigation are open sections which are not symmetrical about the plane of the webs, all the double span beam tests were conducted in the double beam configuration in which two identical sections were loaded in each double span beam test, such that the webs of the beams faced one another. This was done to minimise the torsional effects such as cleat

rotation about the beam longitudinal axis, which may be induced during the loading process. This problem did not exist in the single span tests since the loading cleats were firmly bolted to the testing machine crosshead which prevented cleat rotation. In the double span tests however, loads were applied through a lever system which was designed to maintain equal magnitudes of applied forces on each of the loading points located in each span, torsional effects were therefore designed against using the double beam system which provided an additional axis of symmetry for the beam assembly. The layout of the assembly will be detailed in section 6.5.3.

With the double beam system, spacers were used to separate the two beams so that at no time are the beams in contact with each other, this prevented the buckles that formed on the webs of each beam from interfering with each other.

6.5.2 Single Span Beam Tests

In the current study of thin-walled beams, 4 sets of beam specimens were experimentally examined in the single span configuration. These specimens were pinned by means of a single bolt at each end, which were hand tightened to allow free end rotation during the loading process, simulating the simply supported end conditions. Loads were applied using a single cleat securely bolted to the beam at the web and firmly attached to the crosshead of the Tinius Olsen testing machine. Figure 6.5.1 shows the general test layout.

Load point beam deflections were measured by a displacement transducer positioned to monitor displacements of the lower web/flange junction as indicated in figure 6.5.2, this being the area of the beam section where local deformations are least likely to affect the deflection readings.

In order to minimise the end shortening effects on the applied loads, the bolt holes in the support cleats were flattened at the base to allow horizontal movement of the end bolts towards beam centre. This modification to the bolt holes is illustrated in figure 6.5.3.

Test Procedure

The procedure followed for the performance of the single span beam tests is briefly summarised in this section. These practices were adopted to reduce experimental errors, which may affect the test results, to a minimum.

All on-line X-Y graph plotters were carefully calibrated to the load and displacement transducers prior to the tests. The axes for the A3 sized graphs were set to appropriate ranges to maximise the data resolution for each test.

The Tinius Olsen testing machine and signal amplifier which powered the displacement transducers were switched on at least 15 mins before the commencement of each test to allow the equipment to "warm up" so that stabilised voltages are supplied to the transducers during the recorded experiments. This practice however, does not result in stabilised voltage supplies during the beginning and end of normal office hours when the 240 volt main power supply experiences fluctuations.

The following is a step by step listing of the procedure taken during the tests which also served as a checklist when the tests were being conducted.

(1) With the supports and displacement transducer (with mounting) on the test bed of the Tinius Olsen testing machine, set the load readings on the Tinius load indicator and graph plotter to zero, ensuring that the machine is set to the appropriate loading range.

(2) Fit the test beam to the loading cleat, hand tightening the bolts.

(3) Adjust the machine crosshead position and assemble the end supports, leaving the bolts hand tightened, ensuring alignment of the loading and supporting cleats.

(4) Tighten all bolts, except the ones that pin the beam ends, and secure the support beams to the machine test bed using G-clamps.

(5) Position the displacement transducer and set deflection reading on the graph plotter to zero.

(6) Apply a pre-test loading of approximately 75% of the first yield load to remove any possible slippage in the assembly and to allow supports to "settle into place". Check that the load and defection transducers are on-line, then remove the pre-test load.

(7) Re-zero the deflection reading on the graph plotter and commence the actual beam test.

Steps (1) to (7) were then repeated for the next beam specimen.

6.5.3 Double Span Cleat Loaded Beam Tests

The experimental investigations included 3 sets of double beam, double span tests conducted on the Tinius Olsen test machine, applying equal loads via a roller and lever system at 2 locations along each beam through loading cleats. The beams were supported by cleats at mid-length and the ends. Figure 6.5.4 shows the general layout of the these tests.

Deflections of the beam at both the load points along the beam were monitored and the measured machine load was later divided equally into 4 for the applied load at each loading point of each beam.

Three methods of separating the beams during the tests were used. The first method was used for the 55 mm deep plain channels in which washers were used to separate the loading cleats as shown in figure 6.5.5. The second method was applied to the 203 mm deep plain channels, in which tubes and long bolts were used to separate the beams at 4 locations along the beams, see figure 6.5.6. The lipped channel beams tested with cleat loading used a method similar to the first. Instead of using washers between the loading cleats, a rigid steel plate was employed to hold the loading cleats apart. This method is illustrated in figure 6.5.7.

The end support cleats were prepared in the same manner as in the single span tests to allow end shortening of the beams.

Test Procedure

The pre-test procedures for these double span beam tests were the same as that described in section 6.5.2. The following lists the step by step procedure which is slightly different from that for the single span tests.

(1) Assemble the beam specimens onto the supports with all the bolts firmly tightened (except for the end bolts) and the end support beams secured to the machine test bed by means of G-clamps.

(2) With the displacement transducers (with mountings) on the test bed, set the load readings on the Tinius load indicator and the graph plotter to zero.

(3) Fit the loading cleats onto the beams and place the loading beam along with the rollers in position as shown in figure 6.5.4.

(4) Position the displacement transducers under the loading points and set the deflection readings on the graph plotters to zero.

(5) A pre-test load of 0.75 times the first yield load is then applied to take out the slippage within the assembly and then removed.

(6) The deflections on the plotters are reset to zero and the actual beam test is performed.

The above steps (1) to (6) are repeated for the next pair of double span beams.

6.5.4 Vacuum Box Tests

Of the 5 sets of double spanning beam tests, 2 were performed using the vacuum box. The working principles of the box have been briefly described in section 6.4.2. This section details the important information regarding test procedures used to carry out the beam tests.

The layout of the test set-up is shown in figure 6.4.3, the test beams were mounted onto the supporting cleats using 4 bolts at the central support and 2 bolts at each of the ends. In the set of double span zed section beam tests, galvanised steel roof sheeting were secured onto the beams using self-drilling, self tapping screws, approximately 200mm apart. In the case of the lipped channel double spans, 38 mm clipboard floor boards were used instead of the roof sheeting.

Displacement transducers were used to measure mid-span deflections. The transducers were positioned mid way across the roof sheeting and connected to a X-Y graph plotter which also received signals from the pressure transducer.

The procedure followed during the tests are as follows :

(1) Set up the test assembly as shown in figure 6.4.3 ensuring that all cross beams are secured to the longitudinal beams and all bolts are tightened.

(2) Cover up the assembly with an appropriately sized polythene sheet which is free from leakage and seal the sheet against the walls of the vacuum box (using strong waterproof duct tape) ensuring that the box is completely air tight and there is sufficient loose polythene to wrap around all corners without having to break the seal.

(3) Position the displacement transducer and set the deflection and pressure readings of the graph plotter to zero.

(4) Open up the suction control valve to apply an appropriate pre-test load, unload and begin the actual test.

Steps (1) through (4) is repeated for subsequent beam tests.

In the set of double span zed section beams tested, two of the beam experiments were conducted with the beams set up with the nesting flange facing downwards and the roof sheeting mounted onto the underside of the beams. This effectively simulated the up-lifting of the roof and enabled the current study to examine the effectiveness of the theoretical beam models in such situations.

All important dimensions of the test set-ups are summarised at the end of this chapter in table 6.5.1 referring to figures 6.5.8, 6.5.9 and 6.5.10 for the layouts. Individual beam specimen dimensions will be presented in chapter 7 of this thesis along with the relevant results from the experiments.

6.6 EXPERIMENTAL OBSERVATIONS

This section presents the general observations made during the laboratory testing of the beam sections. These observations and their implications with regard to the experimental results and the theoretical assumptions are considered in detail in chapter 9 although some of the points are briefly discussed as they are presented in this section.

The failure mechanisms observed on the plain channels, lipped channels and zed sections were almost identical in shape, as expected. In almost all of the tests, buckling initiated first in areas of the flanges under compression at the loading point along the single span beams and the central support for the doubles. Although these buckles were the first to develop, they did not seem to bring about ultimate failure which only occurred after local buckles in the web had formed. This observation is true for all the beams except in the case of the double span lipped channels tested on the Tinius Olsen testing machine which seem to failure by a different mode, this will be discussed further later in this section. The typical web and flange mechanisms observed have been previously presented in chapters 3, 4 and 5 of the thesis. The dimension that characterises the mechanism size, described by 'c' in the theoretical mechanisms were found to range between 0.145 to 0.2 times the web depth of the tested beam sections.

Yield "zones" that form the observed failure mechanisms tended to be curved and had definite radii of bending as opposed to the theoretical assumption of straight hinges of concentrated yield lines.

Elastic buckles were seen to form in the flanges of the plain channel beams, these local buckles were observed as wavelike formations along the free edge of the compression flange which disappeared when the loads were removed following the end of the pre-test loading procedure. During the actual test, the amplitude of these "waves" which initially seem to growth proportionally with increases in overall beam deformations eventually reduced as the plastic mechanisms developed, but they did not completely disappear until the applied loads were completely removed. It would appear that as the plastic mechanisms matured, additional deformations tended to concentrate at the yield regions but the elastic buckles were not completely absorbed as assumed in the theory.

In the double span tests, collapse usually occurred only in one of the spans. For the beams tested in the Tinius Olsen testing machine, as the ultimate load is reached in one of the spans, further increases in load are impossible since the failed span of the beam is experiencing a reduction of load carrying capacity and would simply deform as the crosshead moved down, the beam assembly would therefore be unable to sustain loads high enough to fail the second span.

Symmetry was not always achieved in the mechanisms forming in the single span beams, this is especially evident in the zed sections. Due to misalignments in the drilled bolt holes which accommodated the loading cleats and slippage occurring at some bolts and not others, half mechanisms sometimes developed, in which plastic hinges only formed on one side of the loading cleat.

Almost all the outer hinges forming in the flanges of the beams of all three cross-sections were inclined, instead of being perpendicular to the edge of the flange as assumed in the theoretical models. The observed inclination angles measured relative to the beam longitudinal axis ranges from 30° to 60°. This was accompanied by some flange curling which was relatively more severe for the compression flanges.

Due to the cross-sectional shape of the zed sections, the beam section would be expected to tend to deflect horizontally (sideways as seen from the end of the beam) as well as vertically when loads are applied. In the single span experiments conducted on these sections, any horizontal beam movement was prevented by the loading cleat which was firmly secured to the machine crosshead and the end supports which were clamped to the machine test bed. Due to the restraining of the horizontal movements, the zeds tended to experience some twisting which caused the beams to exhibit a little more flange curling than the channels.

The phenomenon of flange curling was extreme in many of the double spanning lipped channels which were tested in the Tinius Olsen machine, in which typical mechanisms did not form. Figures 6.6.1 and 6.6.2 illustrates this behaviour where the failure mode is very different from that found in the other sections. This was assessed to occur in beams where the depth of the beam cross-section was close to the width of the flanges, especially as the lip size increased. The loads measured in the tests where this behaviour was observed tended to be lower than those for the beams that failed with the typical plastic mechanisms forming in the web and flanges.

In order to ensure repeatability of the experiments, at least two tests were conducted in each of the beam experiments. Except for the case of the fabricated double span lipped channels tested in the Tinius Olsen machine, all observed plastic mechanisms were consistent and the beam tests were repeatable within normal experimental tolerances.

From the testing of the plain channels, it can be seen that variations in the flange width did not affect the web mechanisms or the general pattern of the complete web and flange collapse mechanism. However, such variations can affect the loads since increasing the flange width lowers the critical buckling stress of the flange promoting early initiation of local buckling.

The abruptness of the collapse of the beams tested in the Tinius Olsen test machine was not identified although local buckles did develop rather suddenly, especially in the thinner specimens, which was evident from the noise the beams made during some of the tests. The test beams did not collapse suddenly as the testing machine applied loads by means of crosshead movement which was set to a constant rate of displacement. This method of load application constitutes static testing which is appropriate for the single span experiments since the collapse behaviour was of importance, for later application in multi span analysis. The double span beam tests conducted in the vacuum box were more realistic in terms of practical collapse speed characteristics. The beams were seen to collapse very suddenly after attaining peak loading levels. This was observed as rapid beam deflections accompanied by loud "bangs" during the tests, typically two in which failure sequence, the first when the beam section above the central support failed and the second when failure along one of the spans occurred.

Some bearing problems were observed in the end bolt holes of the beam specimens tested in the Tinius Olsen machine. This became apparent as some of the bolt holes were found to have been elongated by the end bolts. The effect was rather small, approximately 1 mm of elongation in the case of the 55 mm deep plain channels and up to approximately 2.5 mm in the 203 mm deep sections.

Although attempts were made to remove all possible slippage in the beam assemblies using the pre-test loading procedure, the applied loads (0.75 times the first yield load) were sometimes insufficient to ensure "contact" in all the bolt connections. As a result, small amounts of slippage occurred during some of the tests.

In general, the experimental results obtained indicate that the theoretical analysis adequately simulates the behaviour of the beams under investigation within reasonable accuracy and the primary objectives of the experimental study was achieved.

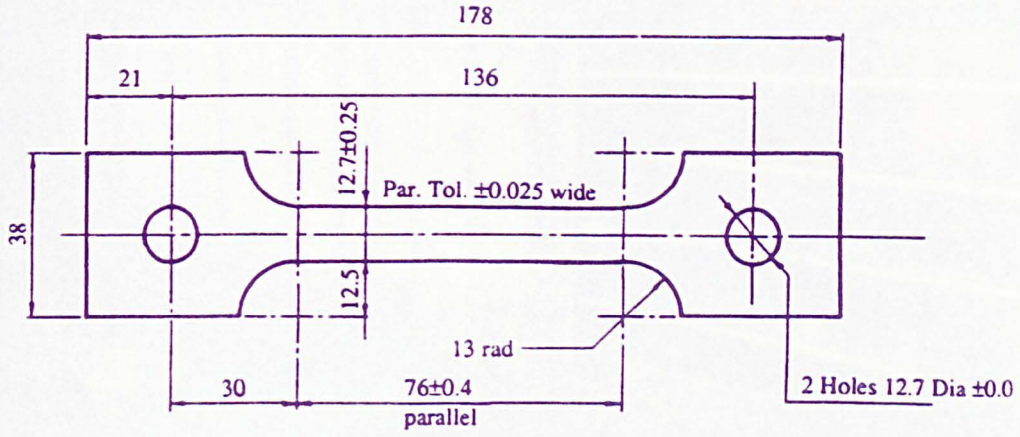

Figure 6.3.1 : Tensile Test Specimen

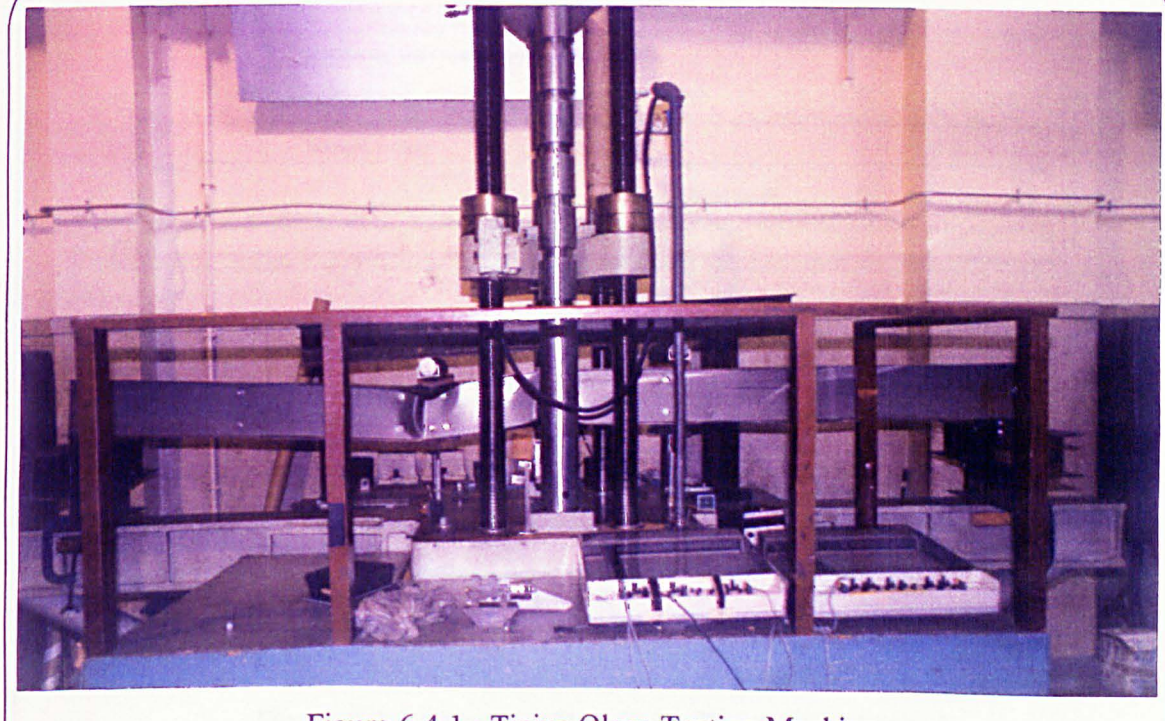

Figure 6.4.1 : Tinius Olsen Testing Machine

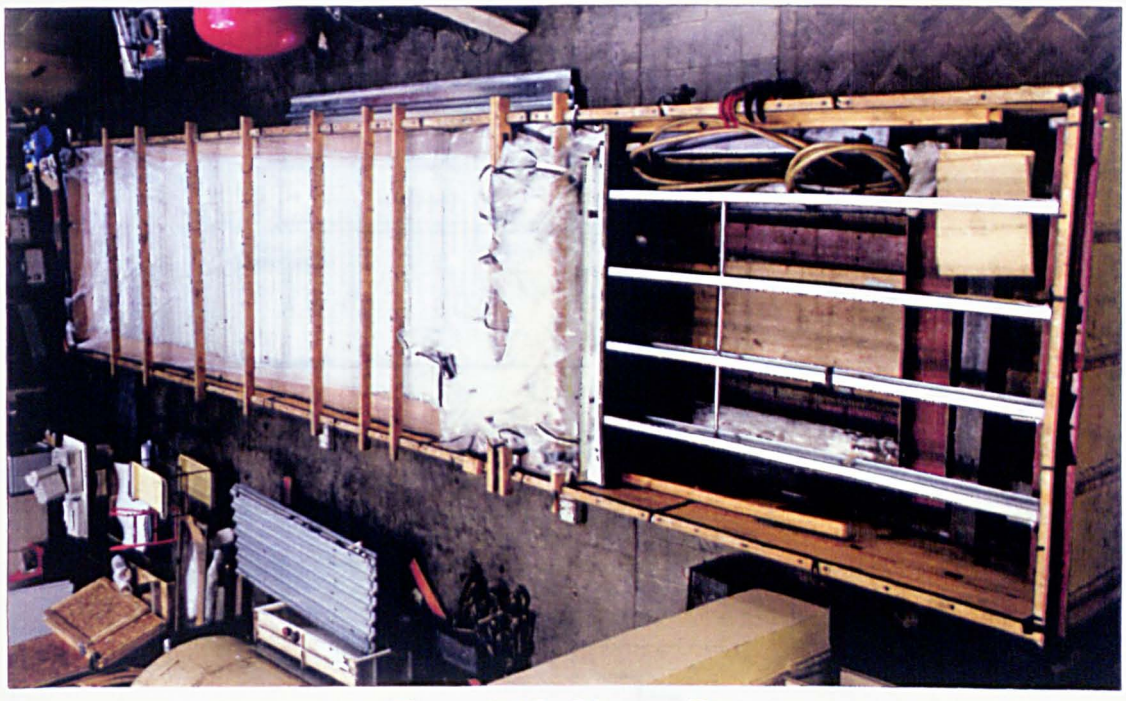

Figure 6.4.2 : Vacuum Box

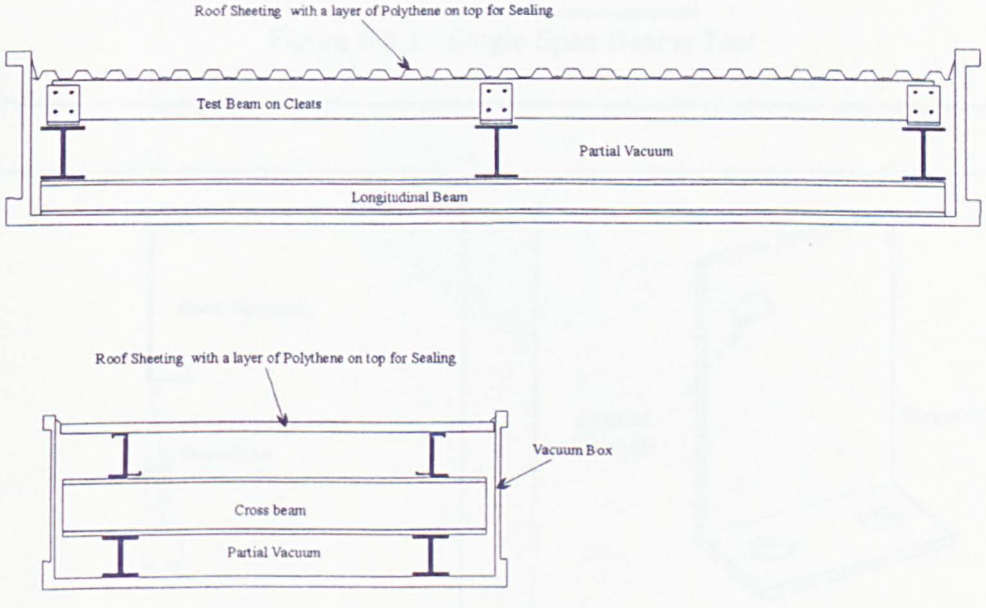

Figure 6.4.3 : Vacuum Box (with Zed section Beams)

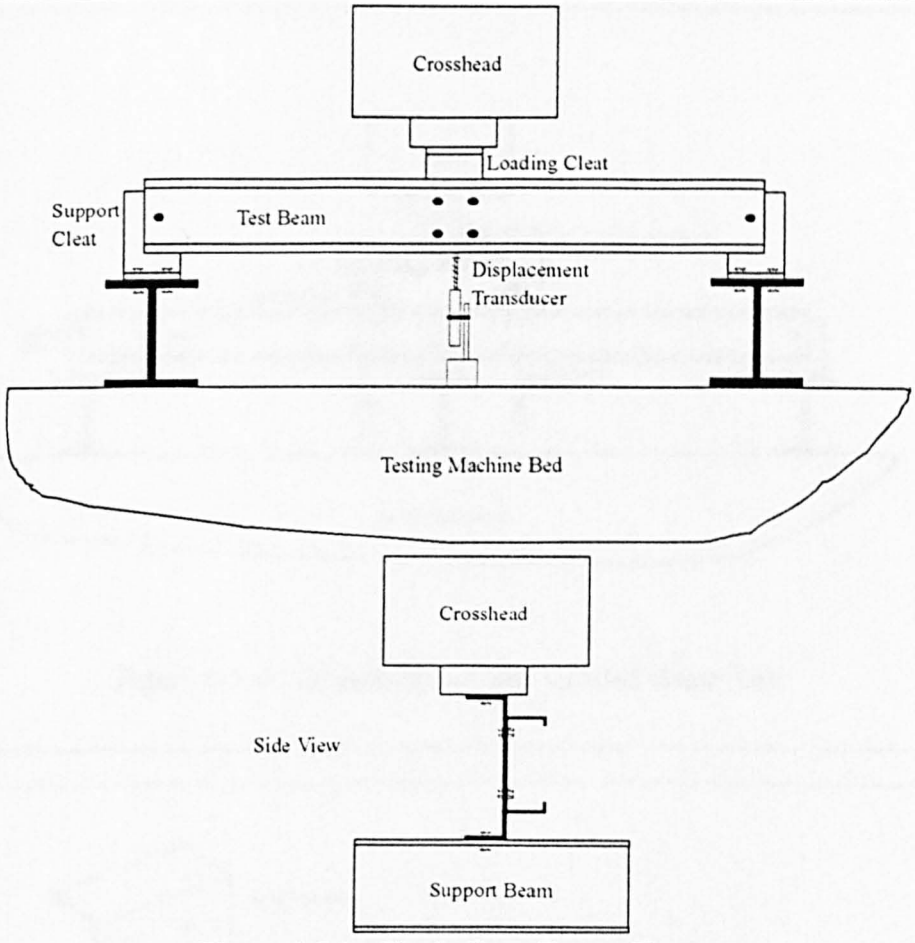

Figure 6.5.1 : Single Span Beams Test

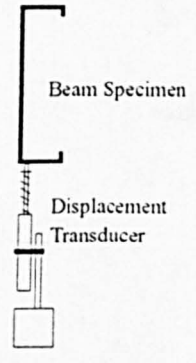

Figure 6.5.2 : Displacement Transducer

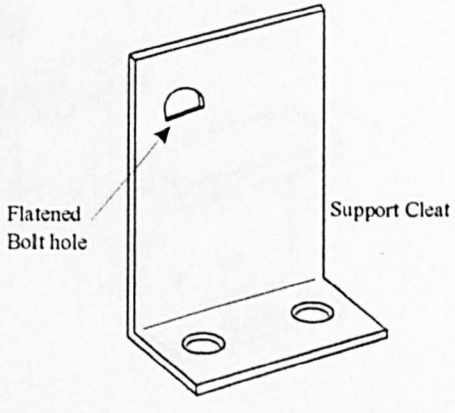

Figure 6.5.3 : End Support Cleat

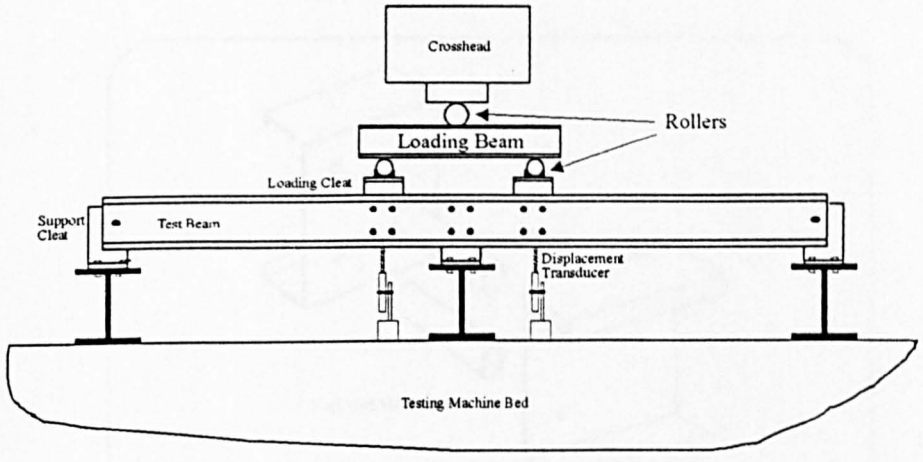

Figure 6.5.4 : Double Span Cleat Loaded Beam Test

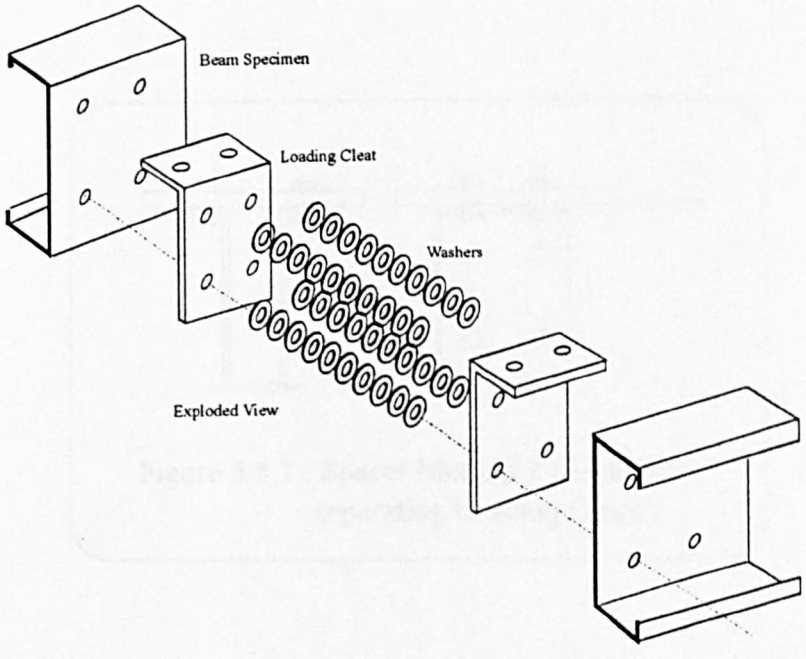

Figure 6.5.5 : Spacer Method 1 (Washers to separate loading cleats)

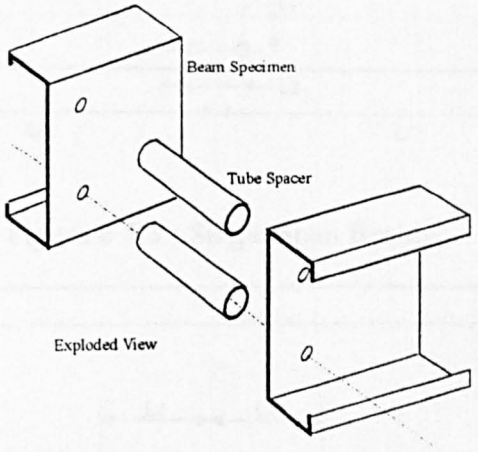

Figure 6.5.6 : Spacer Method 2 (Tube Beam Spacers)

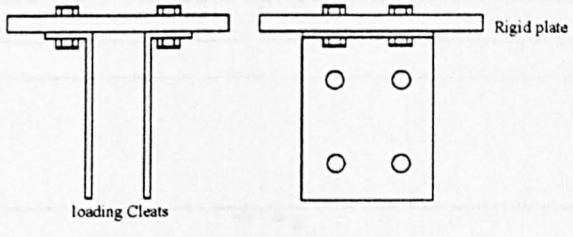

Figure 6.5.7 : Spacer Method 3 (Rigid Plate separating Loading Cleats)

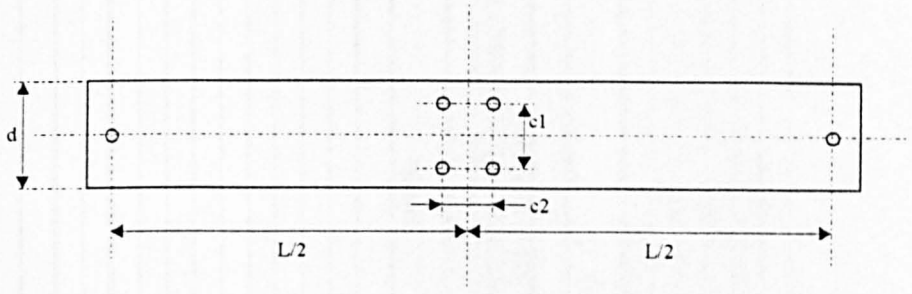

Figure 6.5.8 : Single Span Beam

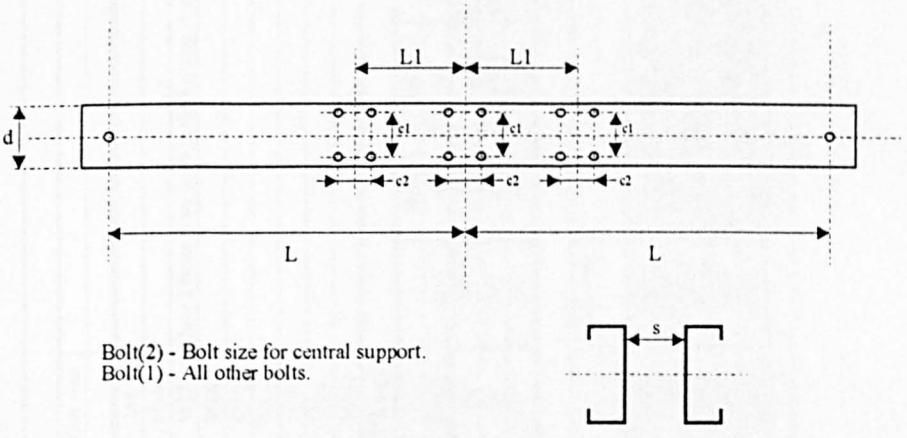

Figure 6.5.9 : Double Span Beam (Cleat Loaded)

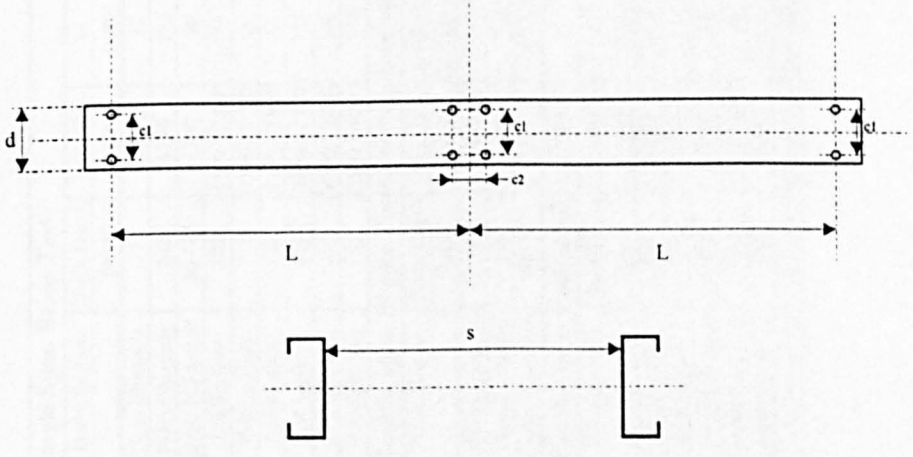

Figure 6.5.10 : Double Span Beam (Vacuum box Test)

Single Span Beam Tests

Beam Section	Beam Depth (mm)	Span [L] (mm)	c1 (mm)	c2 (mm)	Bolt size	Remarks
Plain Channels	55	550	25	30	M8	
Plain Channels	203	1750	135	62	M16	
Lipped Channels	80 / 85	1200	30	0	M12	Only 2 bolts were used in the loading cleat.
Zed Sections	122	1500 / 2250	56	70	M16	
Zed Sections	142	1750 / 3000	56	70	M16	
Zed Sections	172	2250 / 3500	86	70	M16	
Zed Sections	202	2250 / 3750	116	70	M16	
Zed Sections	232	2500 / 4000	146	70	M16	
Zed Sections	262	2500 / 4000	176	70	M16	

Double Span Beams Tested with Loads applied through Cleats

Beam Section	Beam Depth (mm)	Span [L] (mm)	Load point [L1] (mm)	c1 (mm)	c2 (mm)	s (mm)	Bolt(1) size	Bolt(2) size	Remarks
Plain Channels	55	550	150	25	30	50	M8	M8	Spacer method 1. *
Plain Channels	203	1800	450	120	50	140	M16	M22	Spacer method 2, 4 pairs of tubes equally spaced along beams. *
Lipped Channels	80 / 85	975	292.5	30	0	50	M12	M12	2 bolts on each loading cleat, spacer method 3. *

Double Span Vacuum Box Tests

Beam Section	Beam Depth (mm)	Span [L] (mm)	c1 (mm)	c2 (mm)	s (mm)	Bolt size	Remarks
Zed Sections	172	6000	86	70	1220	M16	Covered with corrugated steel roof sheeting.
Zed Sections	202	6000	116	70	1220	M16	Covered with corrugated steel roof sheeting.
Lipped Channels	127	5000	50	66	1260	M12	Covered with 38mm floor boards.
Lipped Channels	165	4000 / 5500	80	66	1260	M12	Covered with 38mm floor boards.
Lipped Channels	220	6000	100	66	1260	M12	Covered with 38mm floor boards.

* Refer to section 6.5.3 for the descriptions of the spacer methods

Table 6.5.1 : Beam Test Set-up Dimensions

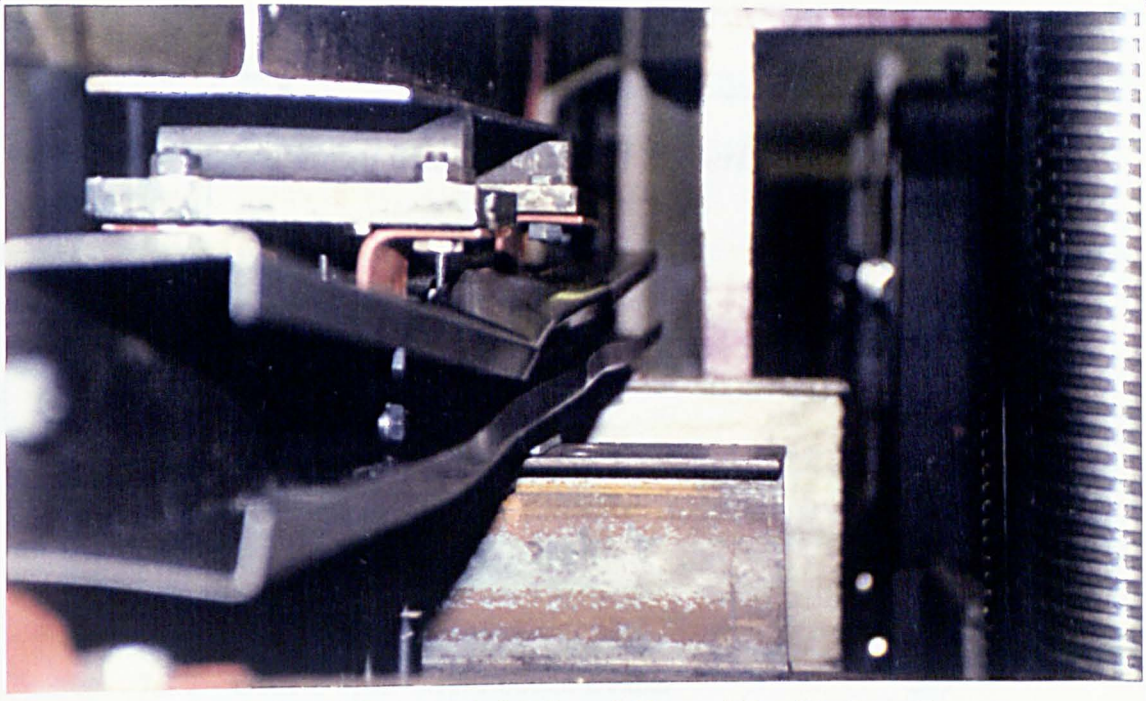

Figure 6.6.1 : Failure mode in Lipped Channel Double Span Beams

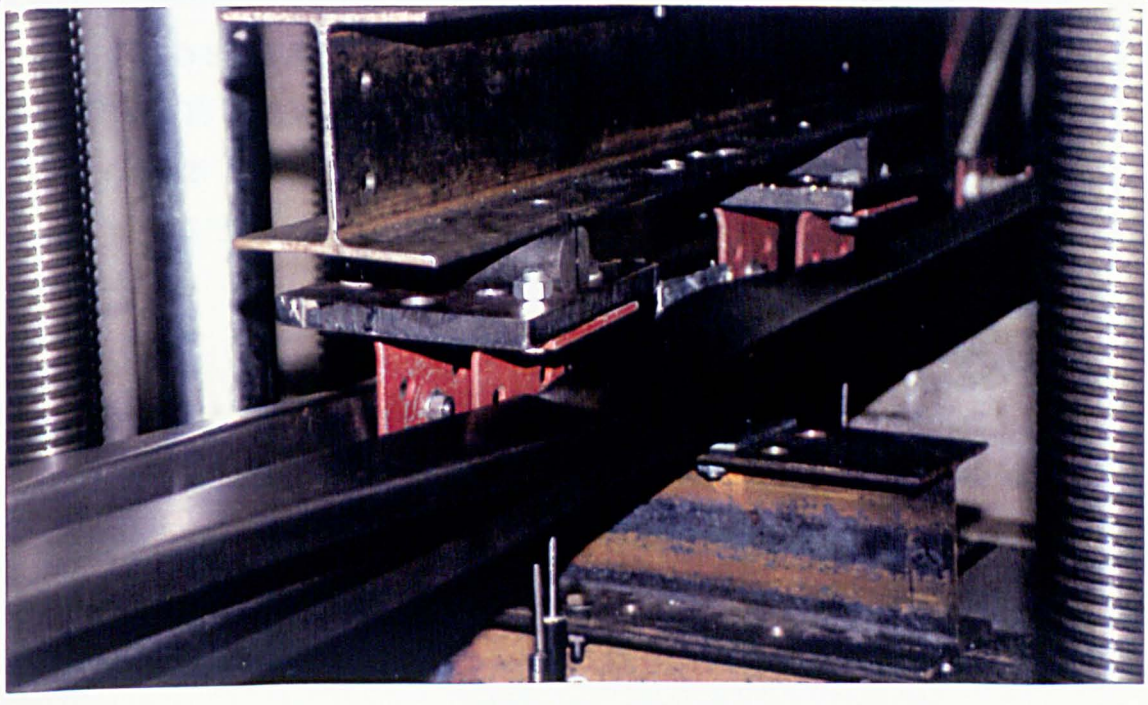

Figure 6.6.2 : Failure mode in Lipped Channel Double Span Beams

Chapter Seven

- *Examination of Theoretical and Experimental Results*

7.1 INTRODUCTION

Theoretical models for the analysis of plain channel, lipped channel and zed section beams supported by means of cleats and fail in bending mainly due to the infestation of local buckling have been presented in chapters 3, 4 and 5 respectively. The testing of beam specimens of these cross-sections in simple and rather extensive experimental investigations of the subject have been described in chapter 6. The results from the theoretical and experimental studies will be examined in this chapter which aims to present the acquired beam load-deflection behavioural characteristics in a comparative manner. The adequacy of the analysis methods used to generate the theoretical results will be assessed in this chapter with particular attention directed towards the accuracy of the ultimate load predictions. The ultimate moment capacity results from the single span beam studies will also be compared to predictions based on the design methods suggested in BS 5950 : Part 5 : 1987, ref. [8], for the design of cold-formed sections.

This chapter only serves to present the consolidated results from the investigations of the previous four chapters and to highlight the findings from the comparison of the theoretical results and the experimental data. Discussions of the findings from this examination will be presented in detail in chapter 9, although some brief initial remarks may be included in the following sections.

The results will be presented in three separate sections, categorised by the beam cross-sections. Due to the volume of results obtained from the studies, only selected plots of beam load versus deflection behaviour will be shown, with all ultimate moment capacity findings summarised in data tables for the single span beams at the end of each section. Tables for the double span beams are presented to compare the ultimate load results from the experiments and some design criterions.

7.2 PLAIN CHANNEL BEAMS

The study of plain channel beams examined two sets of slender sections in the single and double span configuration, which included 4 sets of beam experiments carried out in the Tinius Olsen testing machine. The two sets of sections are grouped according to the depth of the beam webs, these being 203 mm and 55 mm. Three flange widths were examined in the first group (50 mm, 75 mm and 100 mm) and four in the second group (15 mm, 22.5 mm, 27.5 mm and 32.5 mm). The sections were made from 2 mm and 0.6 mm thick mild steel respectively. The plain channel sections will be referred to in this thesis by the flange width followed by the web depth in mm.

7.2.1 Single Span Beams

The experimental load-deflection behaviour of the plain channel single span beams are plotted together with the corresponding theoretical elastic loading lines and collapse curves in figures 7.2.1, 7.2.2, 7.2.3 and 7.2.4 which shows the results for the 50-203, 15-55, 22.5-55, and 27.5-55 sections respectively. Theoretical ultimate loads calculated using the first yield and fully plastic section bending moment capacities based on the full cross-sectional dimensions and the bending moment capacity of the beam sections according to the recommendations of BS 5950 : Part 5 : 1987, are also indicated in the figures. The BS 5950 moment capacity of the sections are essentially the first yield bending moments based on the effective cross-sectional dimensions as found from the consideration of local buckling in the compression flange of the beams, the method of estimation is outlined in Appendix III of this thesis.

The collapse curves for the 203 mm deep channels were constructed using the mean corner radius to thickness ratio of 2.5 while the 55 mm deep sections utilised the ratio of 2. These being the average values found on the experimental beam sections.

50-203-2-PLAIN CHANNEL
SINGLE SPAN (1750 mm)

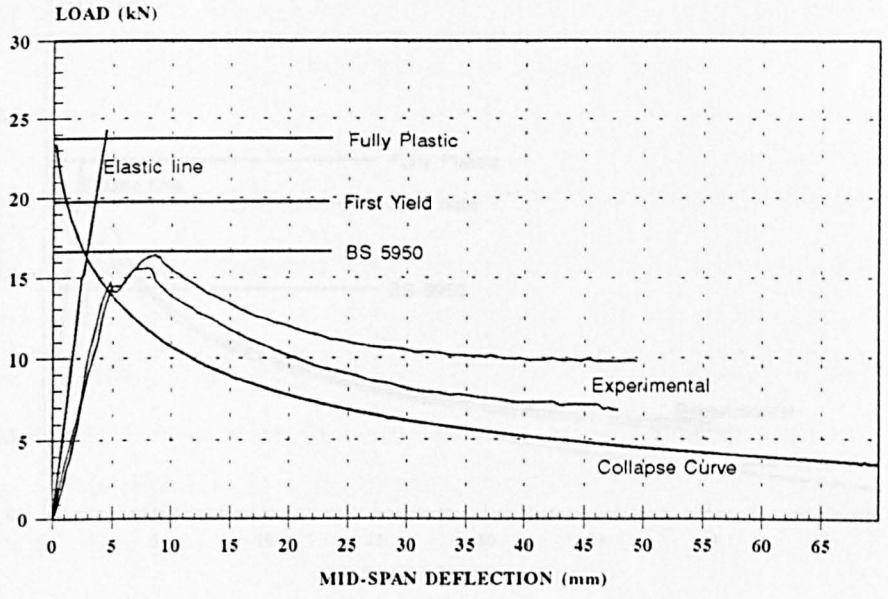

Figure 7.2.1

15-55-0.6-PLAIN CHANNEL
SINGLE SPAN (550 mm)

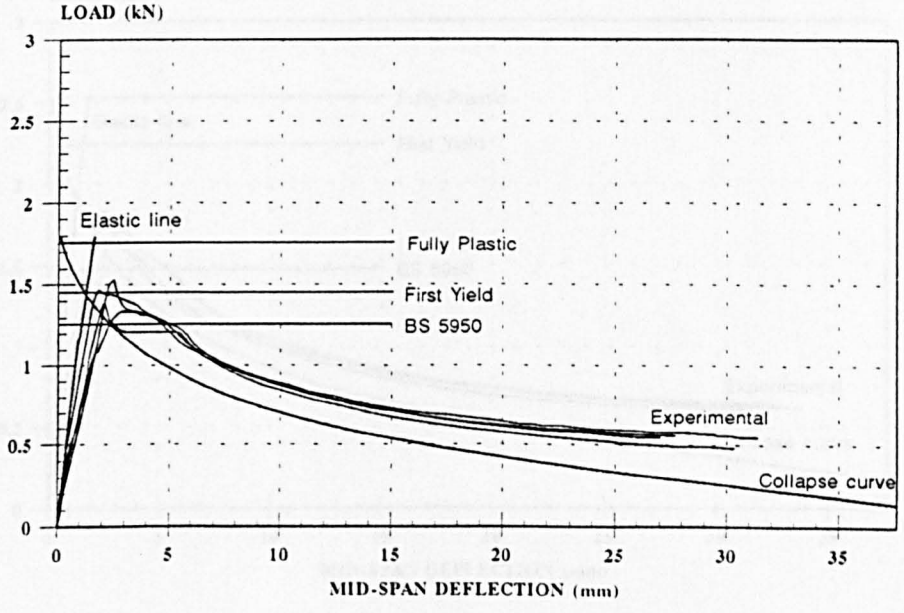

Figure 7.2.2

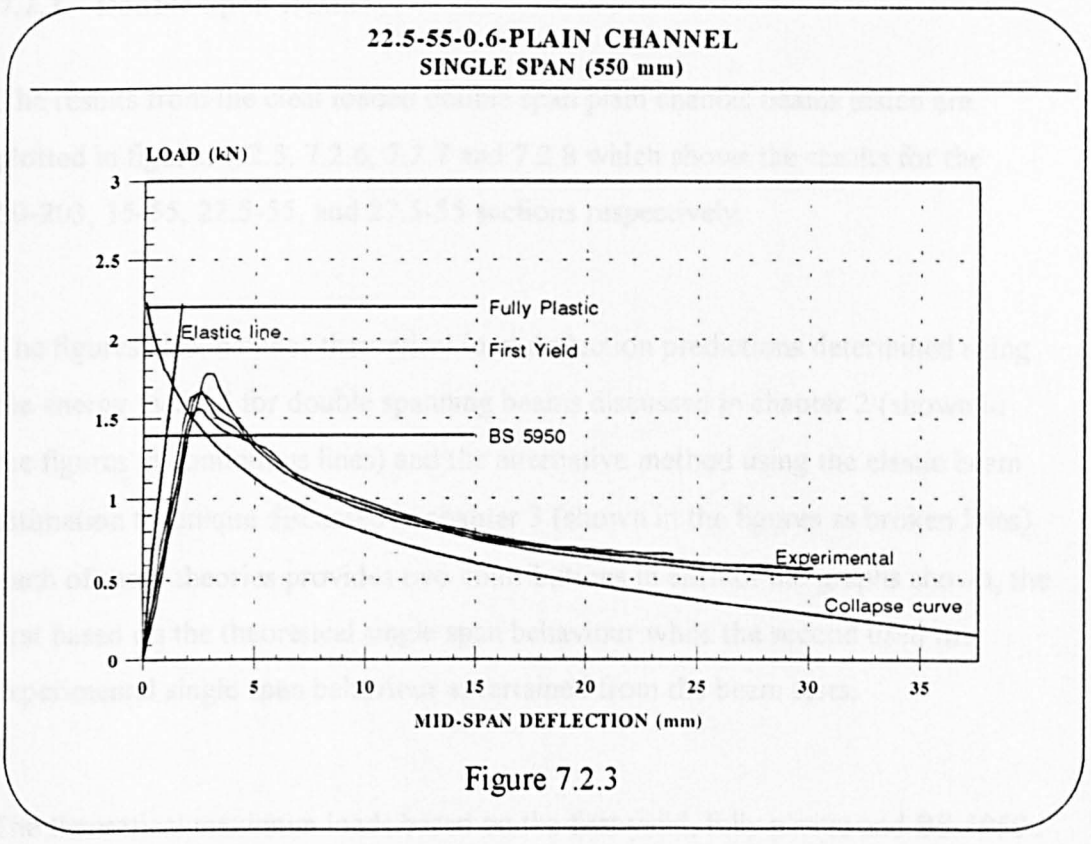

Figure 7.2.3

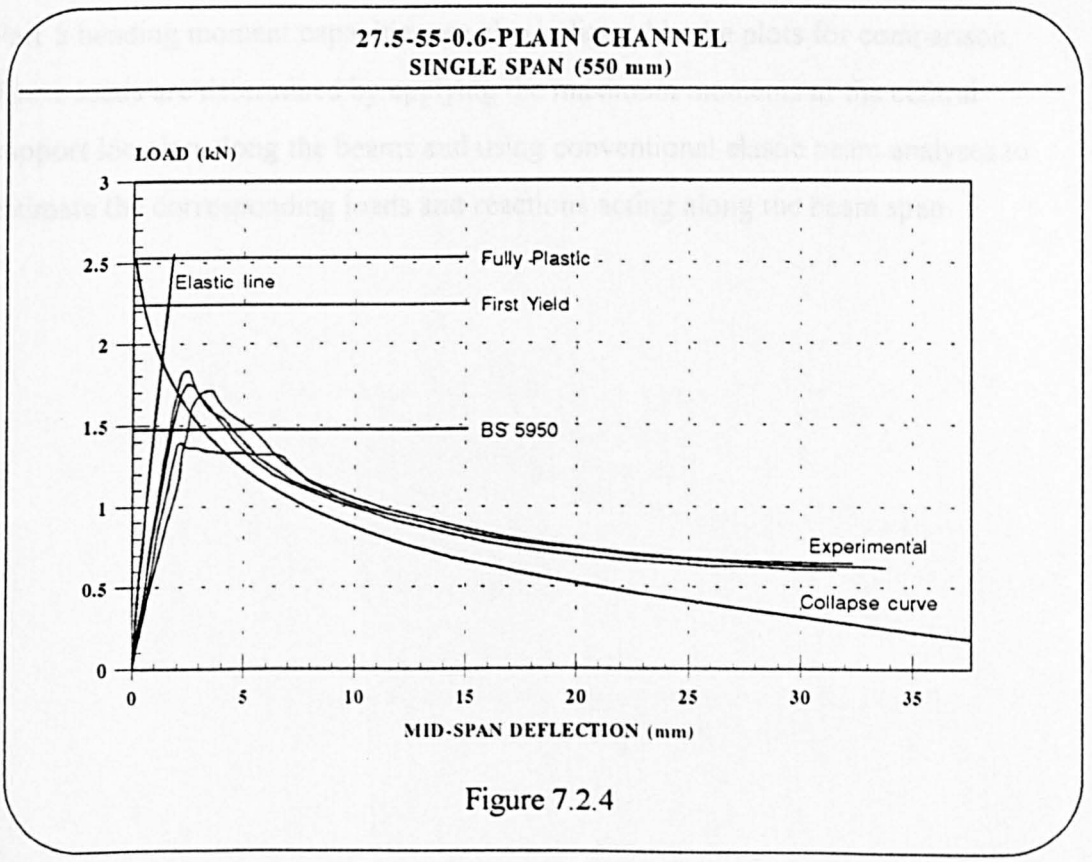

Figure 7.2.4

7.2.2 Double Span Beams

The results from the cleat loaded double span plain channel beams tested are plotted in figures 7.2.5, 7.2.6, 7.2.7 and 7.2.8 which shows the results for the 50-203, 15-55, 22.5-55, and 27.5-55 sections respectively.

The figures also includes theoretical load-deflection predictions determined using the energy method for double spanning beams discussed in chapter 2 (shown in the figures in continuous lines) and the alternative method using the elastic beam estimation technique discussed in chapter 3 (shown in the figures as broken lines). Each of these theories provides two contributions in each of the graphs shown, the first based on the theoretical single span behaviour while the second used the experimental single span behaviour ascertained from the beam tests.

The theoretical maximum loads based on the first yield, fully plastic and BS 5950 : Part 5 bending moment capacities are also indicated in the plots for comparison. These loads are determined by applying the maximum moments at the central support location along the beams and using conventional elastic beam analyses to estimate the corresponding loads and reactions acting along the beam span.

50-203-2-PLAIN CHANNEL
DOUBLE SPAN (1800 mm)

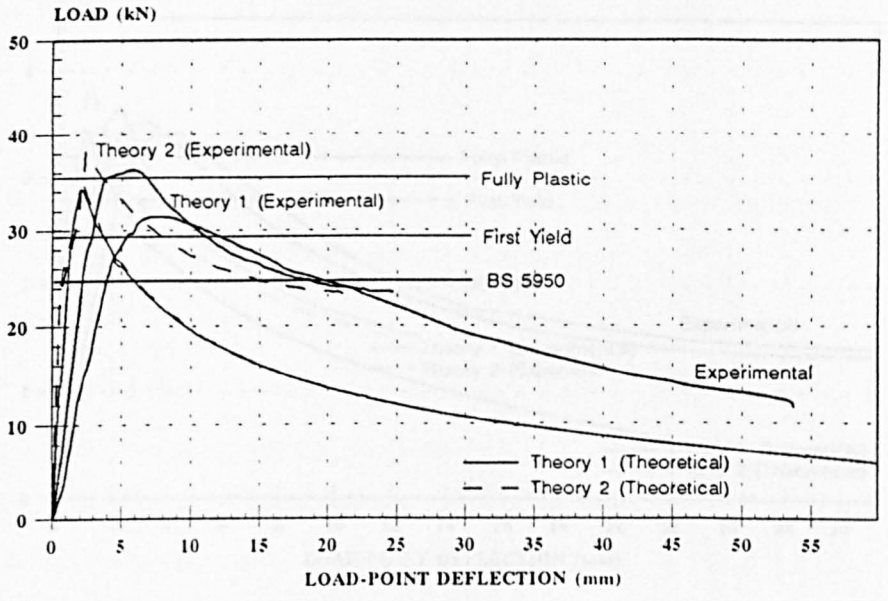

Figure 7.2.5

15-55-0.6-PLAIN CHANNEL
DOUBLE SPAN (550 mm)

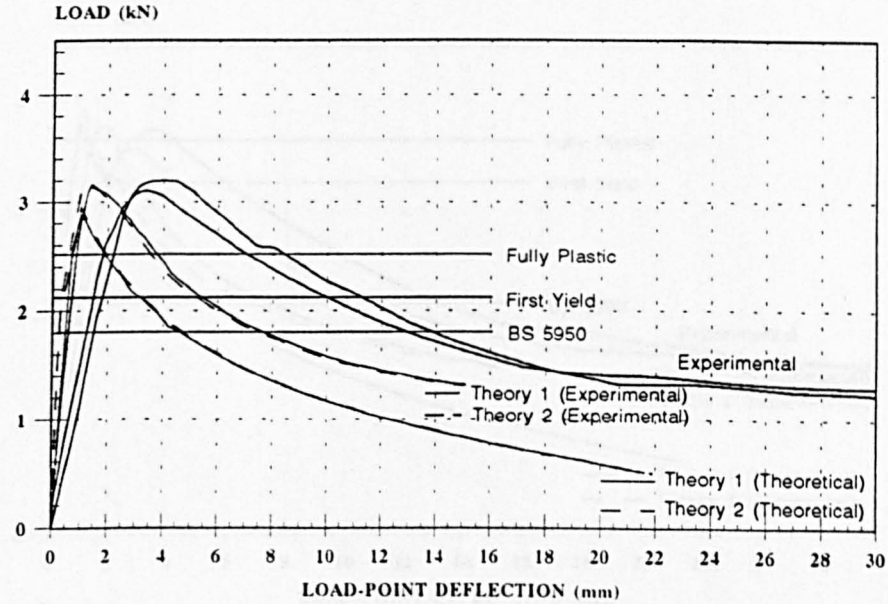

Figure 7.2.6

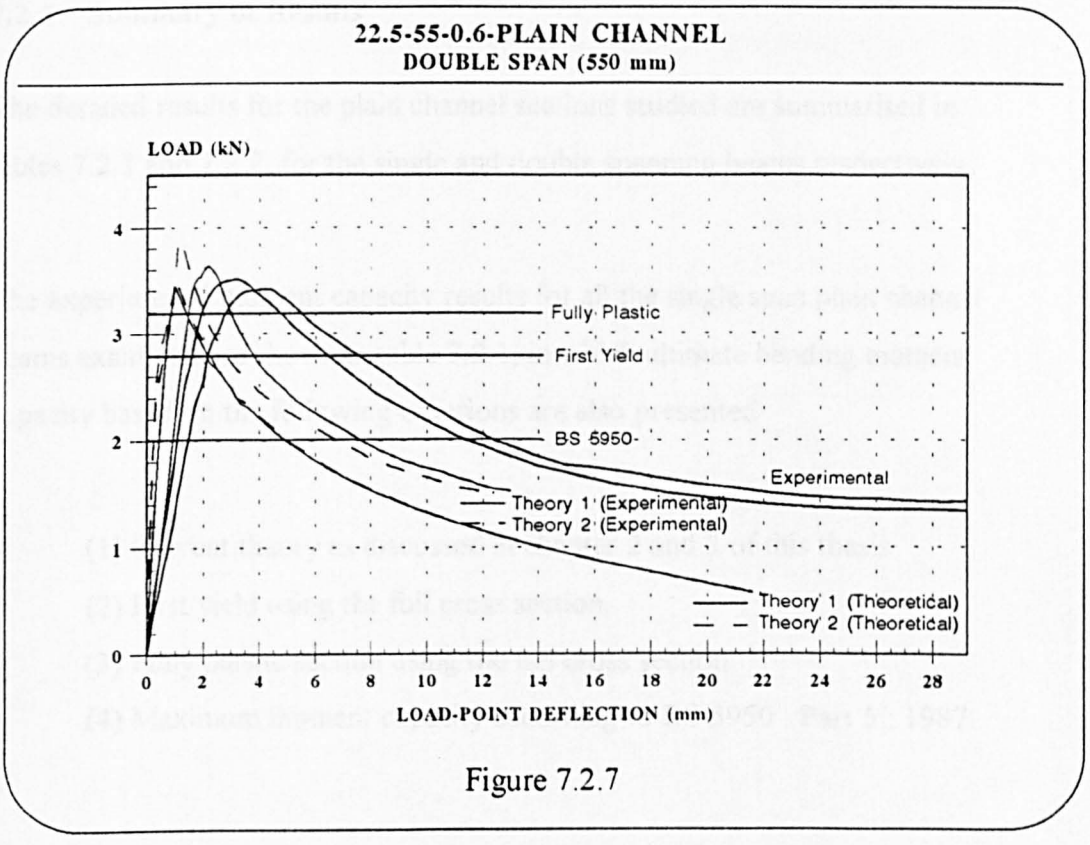

Figure 7.2.7

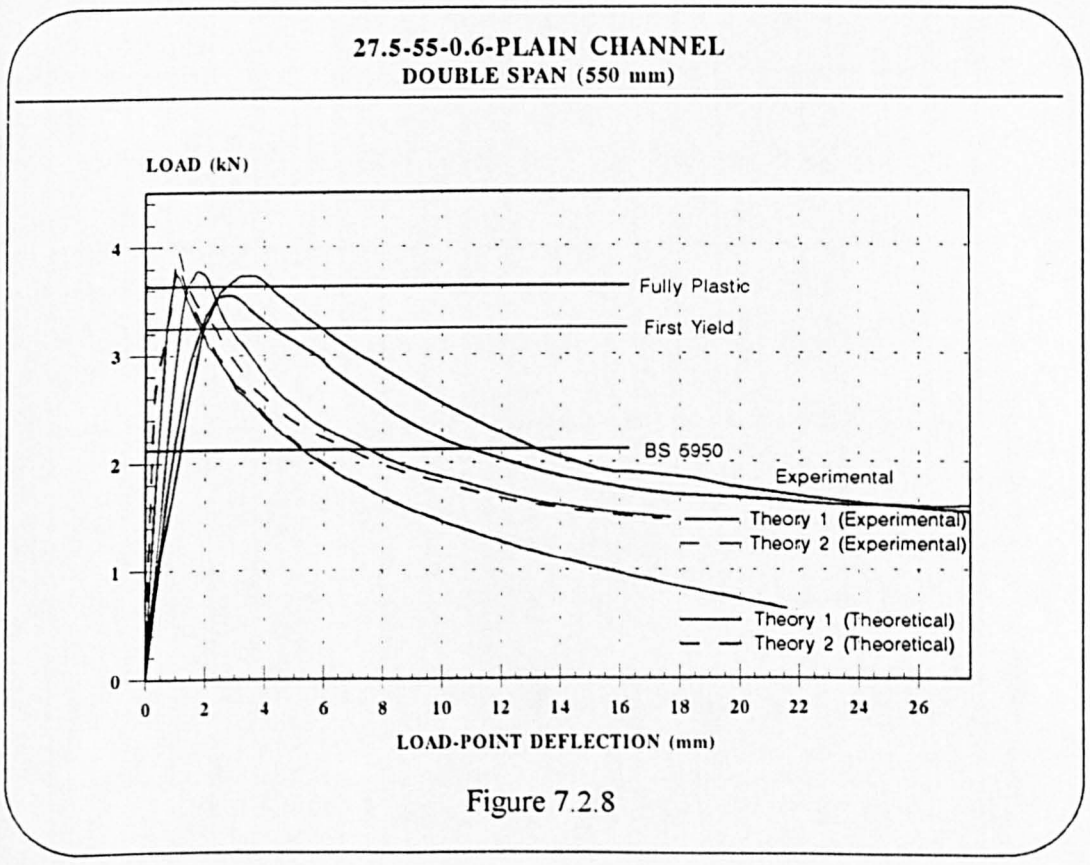

Figure 7.2.8

7.2.3 Summary of Results

The detailed results for the plain channel sections studied are summarised in tables 7.2.1 and 7.2.2, for the single and double spanning beams respectively.

The experimental moment capacity results for all the single span plain channel beams examined are shown in table 7.2.1, in which ultimate bending moment capacity based on the following criterions are also presented :

(1) Current theory as discussed in chapter 2 and 3 of this thesis.
(2) First yield using the full cross section.
(3) Fully plastic section using the full cross section.
(4) Maximum moment capacity according to BS 5950 : Part 5 : 1987.

Beam Section					Ultimate Moment Capacity (Nmm)				
S/No	Flange Width (mm)	Web Depth (mm)	Thickness (mm)	Beam Span (mm)	Experimental	Current Theory	First Yield	Fully Plastic	BS 5950 Part 5
1	50	203	2	1,750	7,218,750	7,109,375	8,672,819.23	10,433,457.75	7,256,056.53
2	50	203	2	1,750	6,825,000	7,109,375	8,672,819.23	10,433,457.75	7,256,056.53
3	75	203	2	1,750	7,000,000	8,312,500	11,300,980.96	13,061,532.75	8,108,952.18
4	75	203	2	1,750	6,912,500	8,312,500	11,300,980.96	13,061,532.75	8,108,952.18
5	15	55	0.6	550	209,687.5	197,656.25	202,086.43	240,626.98	171,825.24
6	15	55	0.6	550	202,812.5	197,656.25	202,086.43	240,626.98	171,825.24
7	15	55	0.6	550	190,781.25	197,656.25	202,086.43	240,626.98	171,825.24
8	15	55	0.6	550	184,250	197,656.25	202,086.43	240,626.98	171,825.24
9	22.5	55	0.6	550	244,750	235,468.75	265,859.42	304,397.38	192,350.54
10	22.5	55	0.6	550	226,875	235,468.75	265,859.42	304,397.38	192,350.54
11	22.5	55	0.6	550	230,312.5	235,468.75	265,859.42	304,397.38	192,350.54
12	22.5	55	0.6	550	214,500	235,468.75	265,859.42	304,397.38	192,350.54
13	27.5	55	0.6	550	251,625	259,531.25	308,374.74	346,910.98	203,783.95
14	27.5	55	0.6	550	240,625	259,531.25	308,374.74	346,910.98	203,783.95
15	27.5	55	0.6	550	235,125	259,531.25	308,374.74	346,910.98	203,783.95
16	27.5	55	0.6	550	191,812.5 *	259,531.25	308,374.74	346,910.98	203,783.95
17	32.5	55	0.6	550	258,500	283,250	350,890.07	389,424.58	214,290.4
18	32.5	55	0.6	550	247,500	283,250	350,890.07	389,424.58	214,290.4
19	32.5	55	0.6	550	240,625	283,250	350,890.07	389,424.58	214,290.4
20	32.5	55	0.6	550	220,000	283,250	350,890.07	389,424.58	214,290.4

* Beam test affected by support misalignment.

Table 7.2.1 : Single Span Plain Channel Beams.

The double span ultimate load experimental results are presented in table 7.2.2, along with the maximum theoretical loads based on the following criterions :

(1) Current theory using the energy method for double span predictions (as presented in section 3.5.3) using the theoretical single span beam behaviour. [Shown in table 7.2.2 as Theory 1 (Theoretical).]

(2) Current theory using the energy method for double span predictions (as presented in section 3.5.3) using the experimental single span beam behaviour.[Shown in table 7.2.2 as Theory 1 (Experimental).]

(3) Alternative theory based on the elastic beam solutions for double spanning beams (as presented in section 3.5.4) using the theoretical collapse curves obtained from single span beam analyses.
[Theory 2 (Theoretical) in table 7.2.2.]

(4) Alternative theory based on the elastic beam solutions for double spanning beams (as presented in section 3.5.4) using experimental collapse curves obtained from the single span beam tests.
[Theory 2 (Experimental) in table 7.2.2.]

(5) First yield occurring over the central support.

(6) Beam section over the central support becoming fully plastic.

(7) Bending moment over the central support reaches the maximum moment capacity as determined according to BS 5950 : Part 5 : 1987.

Beam Section			Ultimate Beam Load (kN)							
S/no	Flange Width - Web Depth - Thickness (mm)	Beam Span - L1* (mm)	Experimental	Theory 1 (Theoretical)	Theory 1 (Experimental)	Theory 2 (Theoretical)	Theory 2 (Experimental)	First Yield	Fully Plastic	BS 5950 Part 5
21	50-203-2	1800-450	31.4	34.4	36.4	35.4	38.4	29.37	35.33	24.57
22	75-203-2	1800-450	34	39.9	35.6	41	37	38.27	44.23	27.46
23	75-203-2	1800-450	32	39.9	35.6	41	37	38.27	44.23	27.46
24	100-203-2	1800-450	35.5	45	-	47.2	-	47.17	53.13	29.83
25	100-203-2	1800-450	34.6	45	-	47.2	-	47.17	53.13	29.83
26	15-55-0.6	550-150	3.2	2.9	3.15	2.95	3.19	2.12	2.52	1.8
27	15-55-0.6	550-150	3.1	2.9	3.15	2.95	3.19	2.12	2.52	1.8
28	22.5-55-0.6	550-150	3.5	3.41	3.64	3.5	3.88	2.79	3.19	2.02
29	22.5-55-0.6	550-150	3.4	3.41	3.64	3.5	3.88	2.79	3.19	2.02
30	27.5-55-0.6	550-150	3.74	3.76	3.78	3.86	3.96	3.23	3.64	2.14
31	27.5-55-0.6	550-150	3.56	3.76	3.78	3.86	3.96	3.23	3.64	2.14
32	32.5-55-0.6	550-150	3.76	4.1	3.92	4.2	4.05	3.68	4.08	2.25

* L1 is the position of the loading points from the central support.

Table 7.2.2 : Double Span Plain Channel Beams

On close examination of the results from the single span plain channel beams, it may be observed that the current theory, using the combination of an elastic analysis and collapse plastic mechanism analysis to estimate the ultimate loads, has proven to give rather good approximations that agrees well with the experimental findings.

Although the BS 5950 : Part 5 recommendations on the bending moment capacity of the beams seem to work well for the extremely slender sections, the method tends to underestimate the ultimate loads in most practical cases. This is to be expected since it considers first yield for the maximum moment capacity.

The theoretical double span ultimate load predictions from both the theories presented in chapters 2 and 3 provides reasonable estimates for the plain channel beams examined. All the other design criterions considered for the double spanning beams underestimates the ultimate loads since they do not take plastic moment redistribution into account at all. This finding proves that the effects of moment redistribution is very important in double and multi-spanning beams such as those examined in the current study.

In general, the current theory and the plain channel collapse mechanism for failure at cleat locations have proven to be reasonably adequate for the plain channel sections. The theoretical results compares well with the experimental findings in most cases.

7.3 LIPPED CHANNEL BEAMS

The study of lipped channel beams in the current work attempted to examine 2 sets of thin-walled cold-formed lipped channel sections of various proportions and thicknesses. Single and double span beams were loaded through cleats on the Tinius Olsen test machine and an additional set of double span beams were subjected to uniformly distributed loading in the vacuum box, described in chapter 6 of this thesis. Similar to the plain channels of the previous section, the lipped channels in this section will be identified by their flange width, web depth, lip size and thickness (in mm) separated by hyphens.

7.3.1 Single Span Beams

The experimental load-deflection behaviour of some of the single span beams are plotted together with the theoretical predictions in figures 7.3.1, 7.3.2, 7.3.3 and 7.3.4, which shows the results for the 67-80-9-1.17, 65-80-12-1.17, 70-80-25-1.17 and 75-85-20-1.965 sections respectively. As in the previous section, theoretical loads based on the first yield, fully plastic and the BS 5950 : Part 5 for each of the sections are indicated in the graphs.

The mean corner radius to thickness ratio for the specimens made from the two different materials was found to be 2. This being the average value measured on the fabricated sections and this was used in the theoretical plastic mechanism analyses.

67-80-9-1.17-LIPPED CHANNEL
SINGLE SPAN (1200 mm)

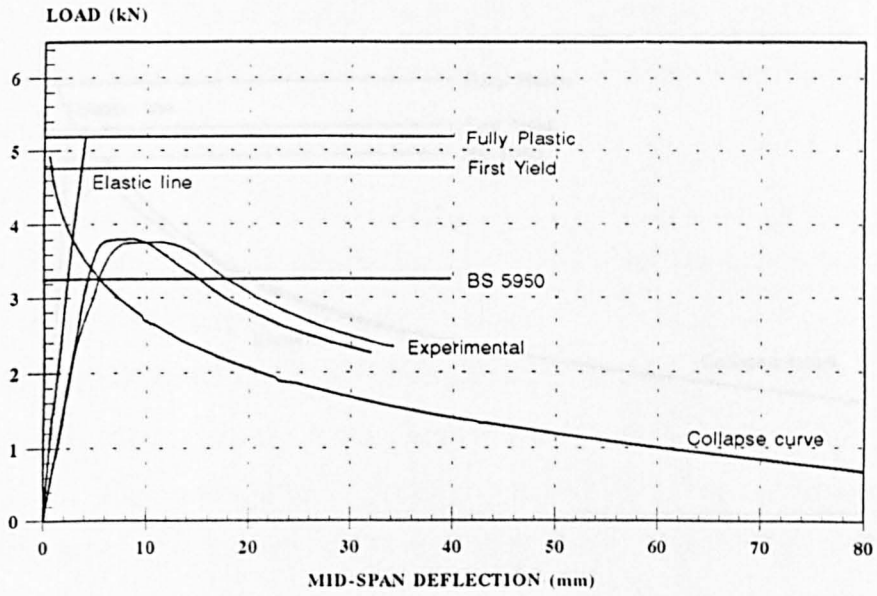

Figure 7.3.1

65-80-12-1.17-LIPPED CHANNEL
SINGLE SPAN (1200 mm)

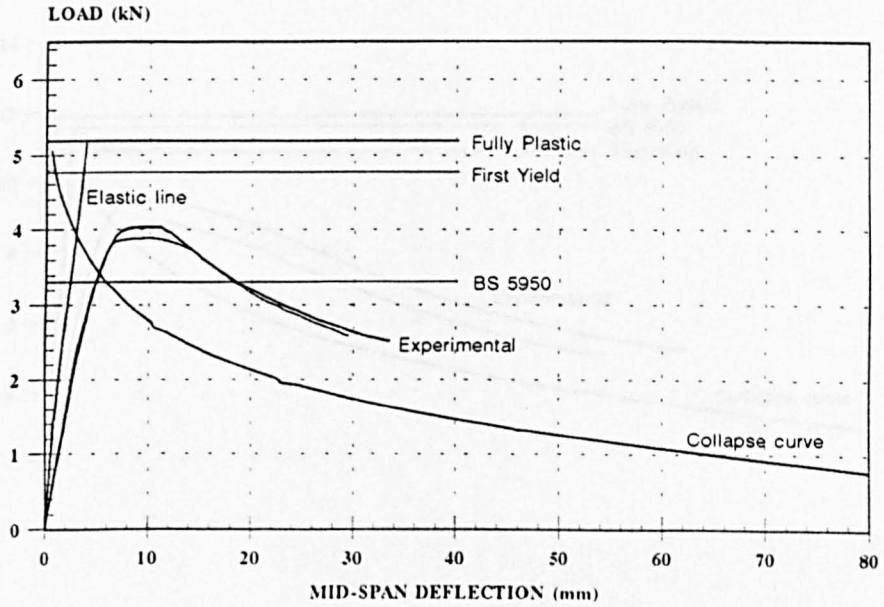

Figure 7.3.2

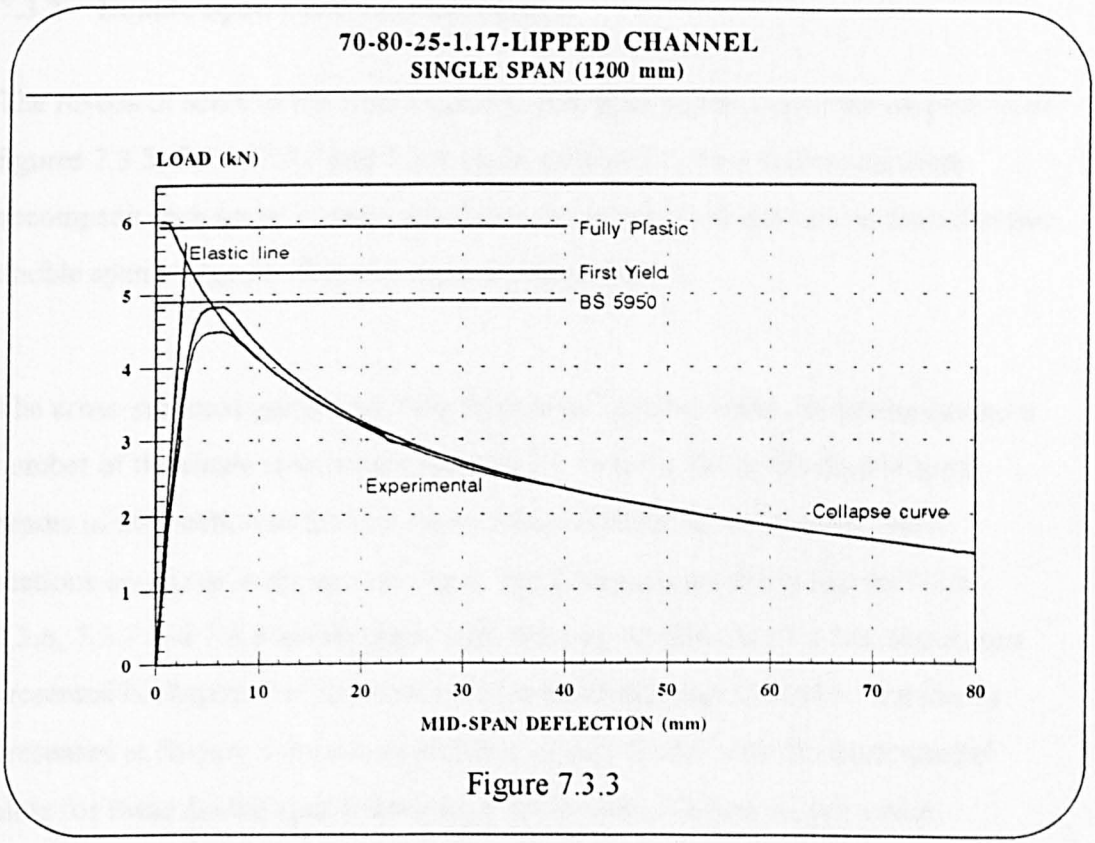

Figure 7.3.3

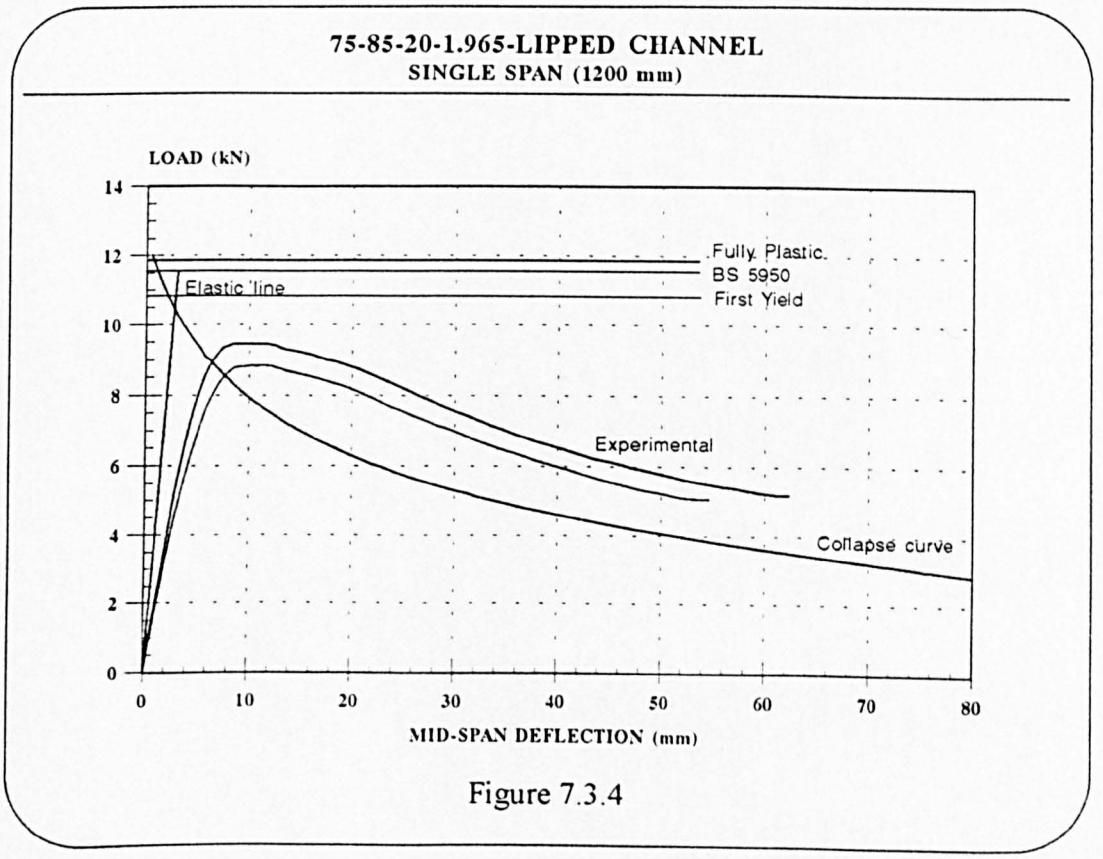

Figure 7.3.4

7.3.2 Double Span Cleat Loaded Beams

The results of some of the cleat loaded double span beams examined are plotted in figures 7.3.5, 7.3.6, 7.3.7 and 7.3.8. As in section 7.2, four theoretical plots accompany each set of experimental lines, these being the predictions from the two double span analysis techniques discussed in chapter 4.

The cross-sectional geometry of the fabricated lipped channel specimens caused a number of the single span beams (section 7.3.1) and most of the double span beams of this section to fail in a mode rather different from the other beam sections examined in the current work. The presented graphs in figures 7.3.5, 7.3.6, 7.3.7 and 7.3.8 are therefore included only as reference for the discussions presented in chapter 9 of this thesis. The theoretical results based on the theory presented in chapter 4 are not expected to compare well with the experimental plots for these double span beams since the modes of failure do not match.

65-80-12-1.17-LIPPED CHANNEL
DOUBLE SPAN (CLEAT LOADED) (975 mm)

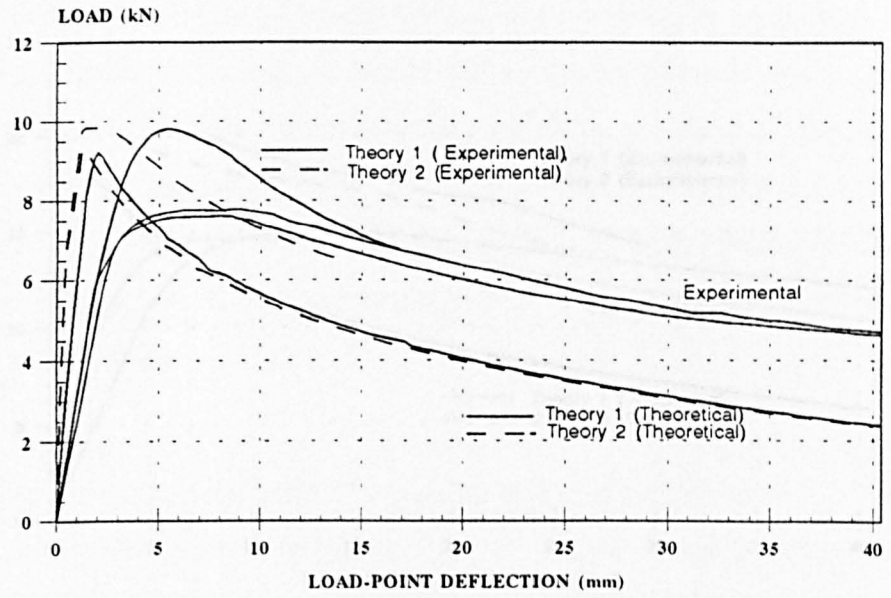

Figure 7.3.5

67-80-9-1.965-LIPPED CHANNEL
DOUBLE SPAN (CLEAT LOADED) (975 mm)

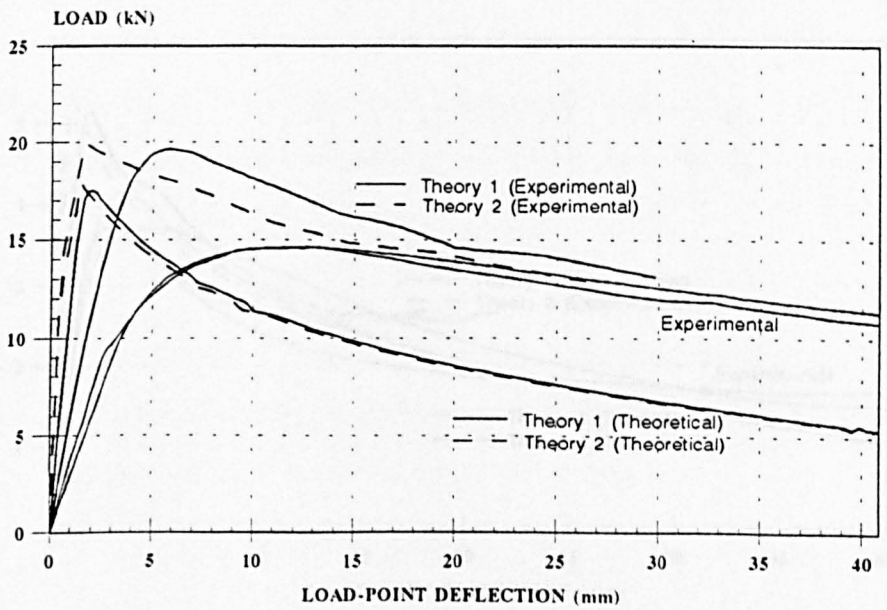

Figure 7.3.6

65-80-12-1.965-LIPPED CHANNEL
DOUBLE SPAN (CLEAT LOADED) (975 mm)

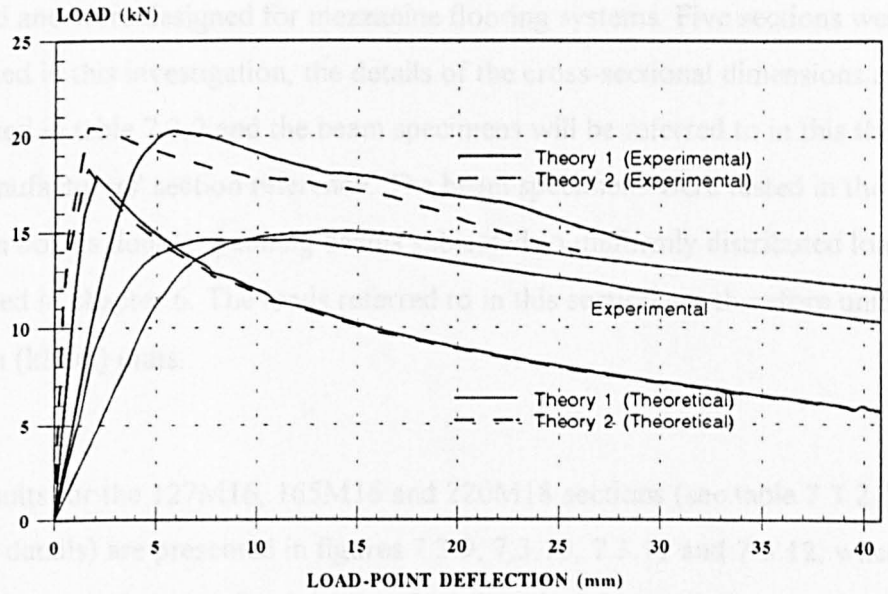

Figure 7.3.7

67-80-9-0.775-LIPPED CHANNEL
DOUBLE SPAN (CLEAT LOADED) (975 mm)

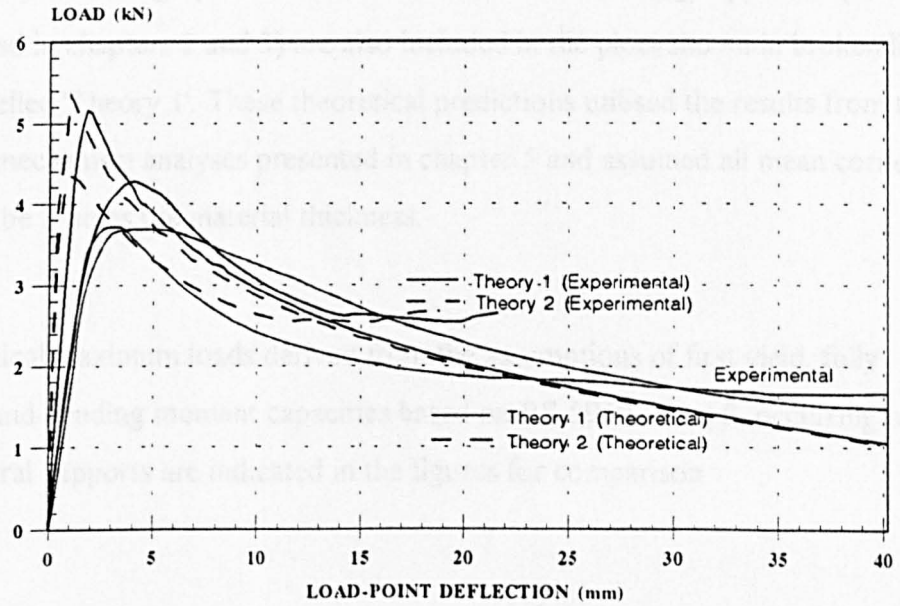

Figure 7.3.8

7.3.3 Double Span Beams Subjected to Uniformly Distributed Loads

The beam sections examined in this section were supplied by Metal Sections Limited and were designed for mezzanine flooring systems. Five sections were examined in this investigation, the details of the cross-sectional dimensions are presented in table 7.3.2 and the beam specimens will be referred to in this thesis by the manufacturers' section reference. The beam specimens were tested in the vacuum box as double spanning beams subjected to uniformly distributed loads as described in chapter 6. The loads referred to in this section are therefore uniform loads in (kN/m) units.

The results for the 127M16, 165M16 and 220M18 sections (see table 7.3.2 for section details) are presented in figures 7.3.9, 7.3.10, 7.3.11 and 7.3.12, where the experimental mid-span deflections are plotted against the applied loads. Theoretical load-deflection predictions based on the elastic beam approximation method for double span beam analysis (detailed in section 5.3.2 of chapter 5) are also plotted over the experimental results and shown in continuous lines labelled as 'Theory 2' in the graphs. Theoretical results from the energy approach (as discussed in chapters 2 and 3) are also included in the plots shown in broken lines and labelled 'Theory 1'. These theoretical predictions utilised the results from the plastic mechanism analyses presented in chapter 5 and assumed all mean corner radii to be 2 times the material thickness.

Theoretical maximum loads derived from the assumptions of first yield, fully plastic and bending moment capacities based on BS 5950 : Part 5, occurring over the central supports are indicated in the figures for comparison.

127M16-LIPPED CHANNEL
DOUBLE SPAN (U.D.L.) [5000 mm]

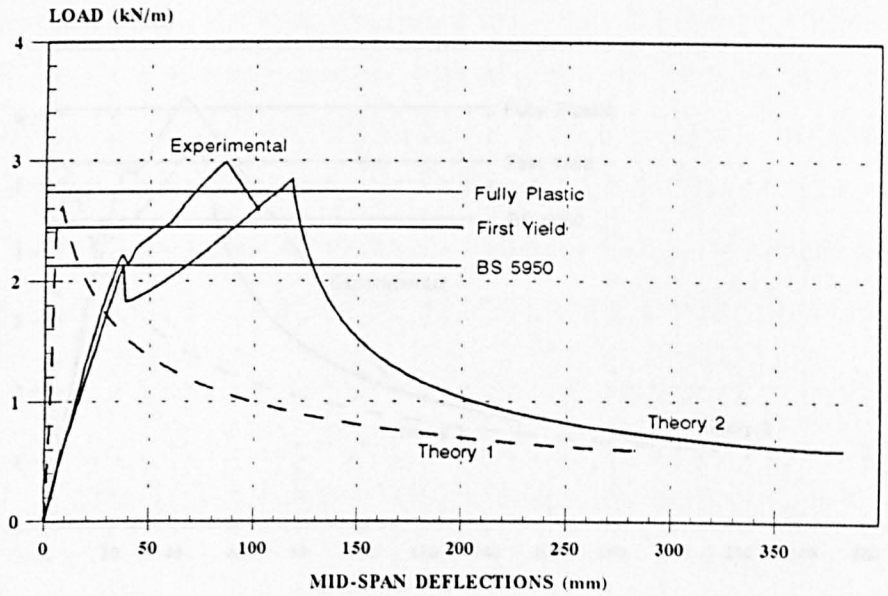

Figure 7.3.9

165M16-LIPPED CHANNEL
DOUBLE SPAN (U.D.L.) [5500 mm]

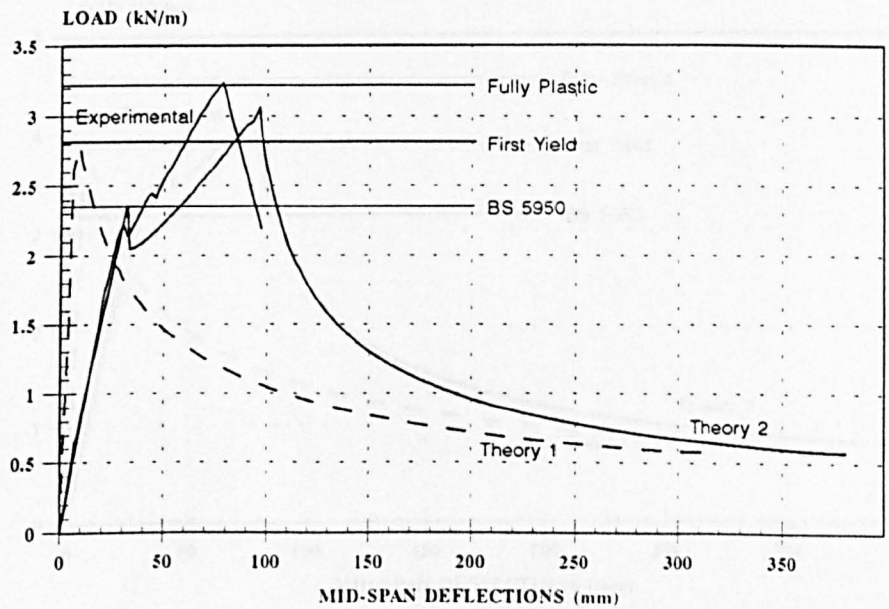

Figure 7.3.10

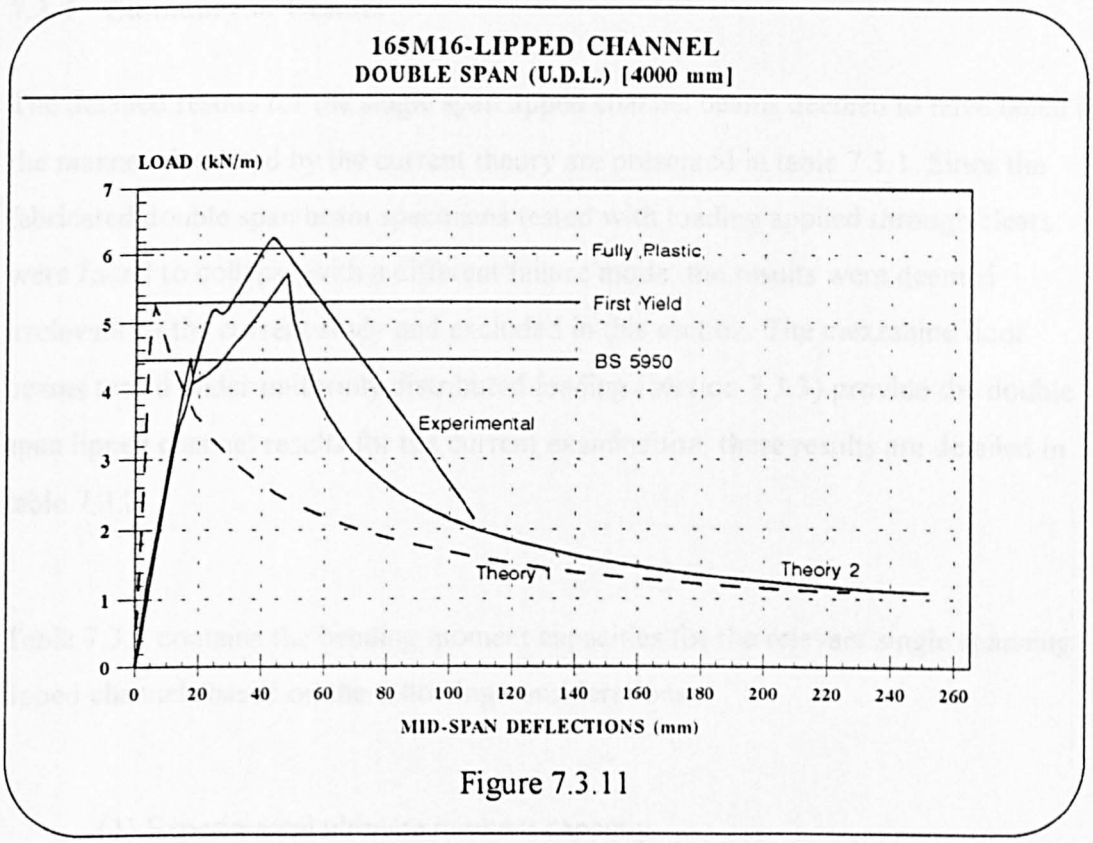

Figure 7.3.11

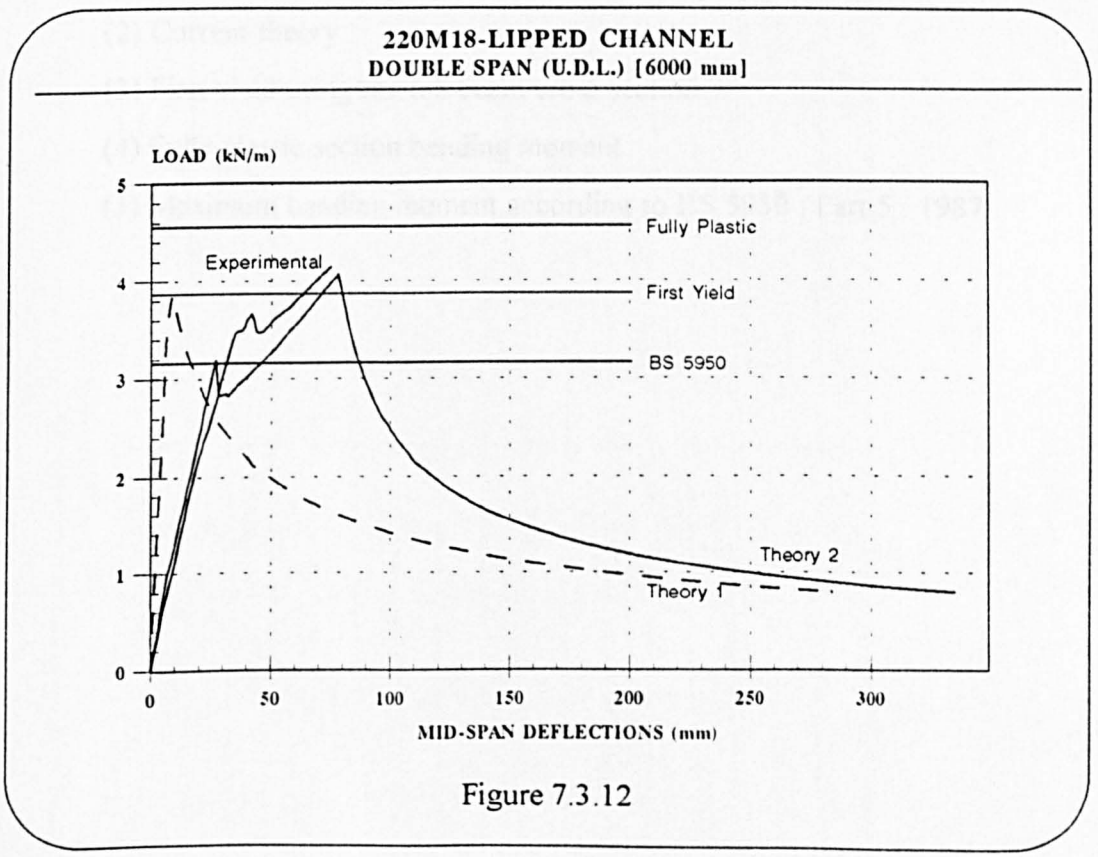

Figure 7.3.12

7.3.4 Summary of Results

The detailed results for the single span lipped channel beams deemed to have failed in the manner simulated by the current theory are presented in table 7.3.1. Since the fabricated double span beam specimens tested with loading applied through cleats were found to collapse with a different failure mode, the results were deemed irrelevant to the current study and excluded in this section. The mezzanine floor beams tested under uniformly distributed loading (section 7.3.3) provide the double span lipped channel results for the current examination, these results are detailed in table 7.3.2.

Table 7.3.1 contains the bending moment capacities for the relevant single spanning lipped channels based on the following considerations :

(1) Experimental ultimate moment capacity.
(2) Current theory.
(3) First yield using the full beam cross section.
(4) Fully plastic section bending moment.
(5) Maximum bending moment according to BS 5950 : Part 5 : 1987.

Beam Section						Ultimate Moment Capacity (Nmm)				
S/No	Flange Width (mm)	Web Depth (mm)	Lip Size (mm)	Thickness (mm)	Beam Span (mm)	Experimental	Current Theory	First Yield	Fully Plastic	BS 5950 Part 5
33	67	80	9	1.17	1,200	1,140,000	1,132,500	1,435,966.488	1,558,838.044	969,581.668
34	67	80	9	1.17	1,200	1,125,000	1,132,500	1,435,966.488	1,558,838.044	969,581.668
35	65	80	12	1.17	1,200	1,212,000	1,182,000	1,430,636.287	1,562,947.931	991,884.104
36	65	80	12	1.17	1,200	1,170,000	1,182,000	1,430,636.287	1,562,947.931	991,884.104
37	75	85	20	1.17	1,200	1,350,000	1,665,000	1,774,623.454	1,954,354.133	1,586,319.263
38	75	85	20	1.17	1,200	1,320,000	1,665,000	1,774,623.454	1,954,354.133	1,586,319.263
39	70	80	25	1.17	1,200	1,455,000	1,635,000	1,581,174.396	1,765,499.073	1,471,208.671
40	70	80	25	1.17	1,200	1,350,000	1,635,000	1,581,174.396	1,765,499.073	1,471,208.671
41	67	80	9	1.965	1,200	2,453,076.9	2,225,000	2,606,832.931	2,828,857.187	2,707,218.075
42	67	80	9	1.965	1,200	2,225,000	2,225,000	2,606,832.931	2,828,857.187	2,707,218.075
43	65	80	12	1.965	1,200	2,515,384.6	2,296,153.8	2,598,074.932	2,837,127.917	2,754,451.81
44	65	80	12	1.965	1,200	2,400,000	2,296,153.8	2,598,074.932	2,837,127.917	2,754,451.81
45	75	85	20	1.965	1,200	2,850,000	3,112,500	3,232,799.992	3,558,673.056	3,490,138.66
46	75	85	20	1.965	1,200	2,662,500	3,112,500	3,232,799.992	3,558,673.056	3,490,138.66
47	70	80	25	1.965	1,200	2,475,000	3,000,000	2,877,719.105	3,212,205.334	3,165,431.031
48	70	80	25	1.965	1,200	2,025,000	3,000,000	2,877,719.105	3,212,205.334	3,165,431.031

Table 7.3.1 : Single Span Lipped Channel Beams

The experimental results found from the testing of the lipped channel floor beams in the vacuum box are represented in table 7.3.2, with the theoretical beam loads based on the following criterions :

(1) Current double span theory based on the energy approach and using theoretical loading characteristics.
[Shown in table 7.3.2 as Theory 1]

(2) Alternative double span beam theory based on the elastic beam approach and using theoretical collapse characteristics.
[Shown in table 7.3.2 as Theory 2]

(3) First yield occurring over the central support.

(4) Fully plastic section over the central support.

(5) Bending moment of the beam over the central support attains the moment capacity as determined according to BS 5950 : Part 5 : 1987.

Section Details				
Section reference No.	Flange Width (mm)	Web Depth (mm)	Lip Size (mm)	Thickness (mm)
127M16	63	127	13	1.6
127M20	63	127	13	2
165M16	63	165	13	1.6
165M20	63	165	13	2
220M18	63	220	13	1.79

Beam Section			Ultimate Beam Load (kN/m)					
S/No.	Section Reference	Beam Length per Span (mm)	Experimental	Theory 1 (Theoretical)	Theory 2 (Theoretical)	First Yield	Fully Plastic	BS 5950 Part 5
49	127M16	5,000	2.95	2.615	2.854	2.429	2.731	2.124
50	127M20	5,000	3.94	3	3.24	2.626	2.953	2.568
51	165M16	5,500	3.229	2.8	3.057	2.809	3.219	2.34
52	165M16	4,000	6.257	5.257	5.714	5.312	6.085	4.425
53	165M20	5,500	4.48	3.24	3.48	3.04	3.484	2.855
54	220M18	6,000	4.14	3.88	4.08	3.876	4.549	3.187

Table 7.3.2 : Double Span Lipped Channel Beams (U.D.L.)

On examination of the results for the fabricated lipped channel beams tested in the single span configuration, is may be observed that in a number of the experiments, comparatively larger gaps separates the experimental and theoretical collapse curves as compared to the plain channel results. This is thought to be due to the effects of flange curling in these lipped sections which had rather large flange widths relative to the web depths. The amount of flange curling varied from section to section, in some cases, the effects were so substantial that the current theory was completely unsuitable for the mode in which the beams failed. This occurred for almost all of the 0.775 mm thick single spans and the double span beams.

The results for the double span floor lipped channel beams tested in the vacuum box seems to show that the current theory for double span predictions using the elastic beam method [Theory 2] (detailed in section 5.3.2 of chapter 5) produces results that agree well with the experimental findings while the energy approach [Theory 1] does not. This shows that the energy method only works well when the deflections at the region of the ultimate load are small. In the case of the relatively long floor beams examined, where there is quite a large amount of elastic beam deflections between the failure at the central support and the ultimate failure, the energy method is rather unreliable, since it does not adequately consider the elastic deformations of the beam between supports.

The theoretical ultimate load predictions for the double span floor beams (based on the current 'theory 2') tend to be underestimates when compared to the experimental findings of the beam loads, this may be due to the use of 38 mm thick floor boards during the beam tests. The rather thick floor boards that were screwed onto the beams would be likely to increase the bending moment capacity of the portions of the beam experiencing failure where the deformations are large.

Further discussion of the results will be presented in chapter 9 of this thesis.

7.4 ZED SECTION BEAMS

The study of zed section beams examined a set of sections supplied by Metal Sections limited which were designed to serve as purlins for roof systems. Single span specimens were tested in the Tinius Olsen Test machine and pairs of double span beams were tested in the vacuum box which applied uniformly distributed loading as described in chapter 6. As in section 7.3.3, the zed sections will be referred to in this thesis by the manufacturers' section reference, the section details will be listed with the tabulated results in section 7.4.3. It should be noted that these zed sections have a nesting flange, onto which roof sheeting are attached, which is wider than the other flange, the lips of each section are also of unequal sizes.

7.4.1 Single Span Beams

The selected experimental load-deflection behaviour for the single span zed sections are plotted in figures 7.4.1 to 7.4.8 with the corresponding theoretical elastic lines and collapse curves derived from the analysis presented in chapter 5. The theoretical loads based on the first yield, fully plastic section and maximum moment capacity according to BS 5950 : Part 5 : 1987 are also indicated in the graphs for comparison. It should be noted that these Zed sections were designed to be used with roof sheeting which are screwed onto the beams. The absence of the sheeting in these beam tests coupled with the fact that the Zed cross-section is not doubly symmetrical (which gives rise to bi-axial bending tendencies) caused premature collapse of the specimens tested. The maximum moment capacity calculated according to BS 5950 : Part 5 which does not consider these factors therefore tends to overestimate the ultimate loads.

All the theoretical collapse curves for the zed sections were calculated using the mean corner radius to thickness ratio of 2, this being the average value found on the specimens examined in the experimental investigation.

122Z15 ZED SECTION
SINGLE SPAN (2250 mm)

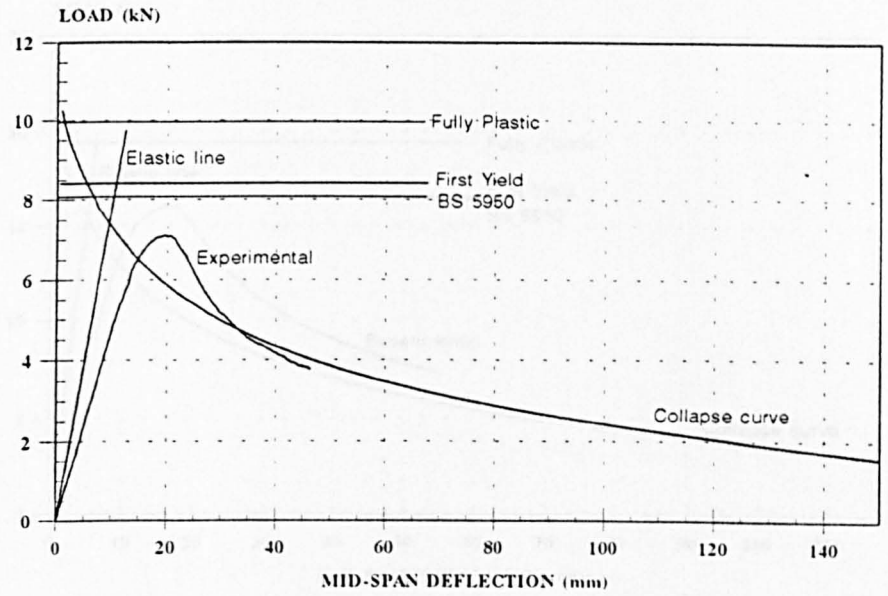

Figure 7.4.1

142Z15 ZED SECTION
SINGLE SPAN (1750 mm)

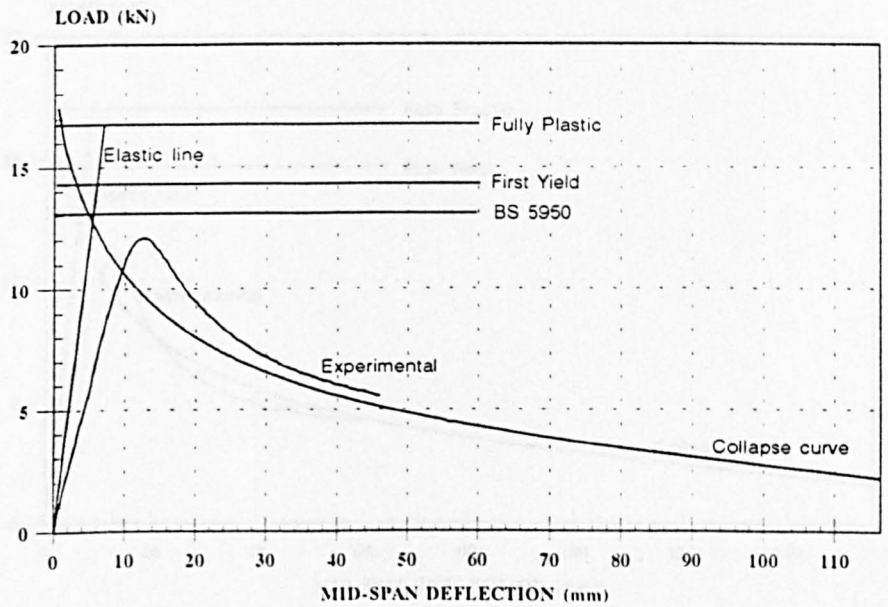

Figure 7.4.2

142Z20 ZED SECTION
SINGLE SPAN (1750 mm)

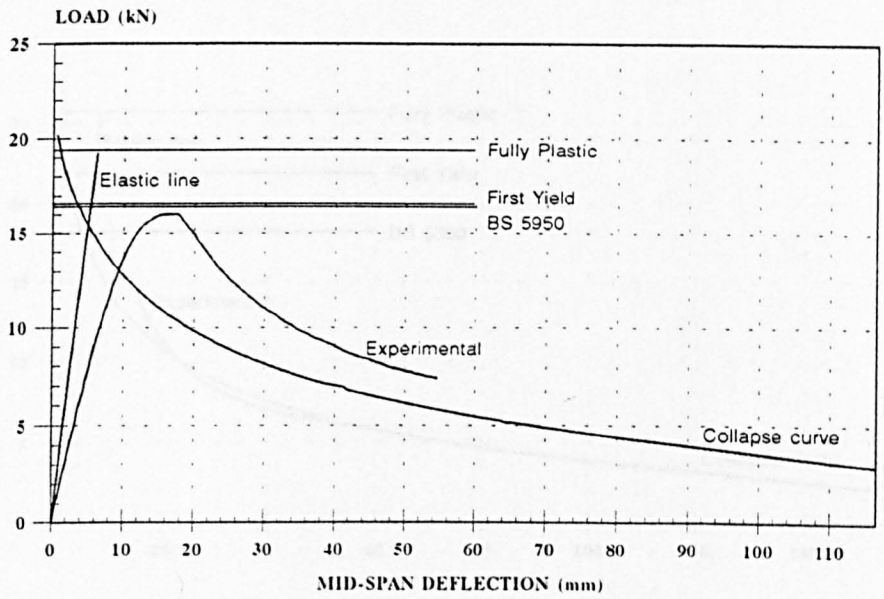

Figure 7.4.3

172Z15 ZED SECTION
SINGLE SPAN (2250 mm)

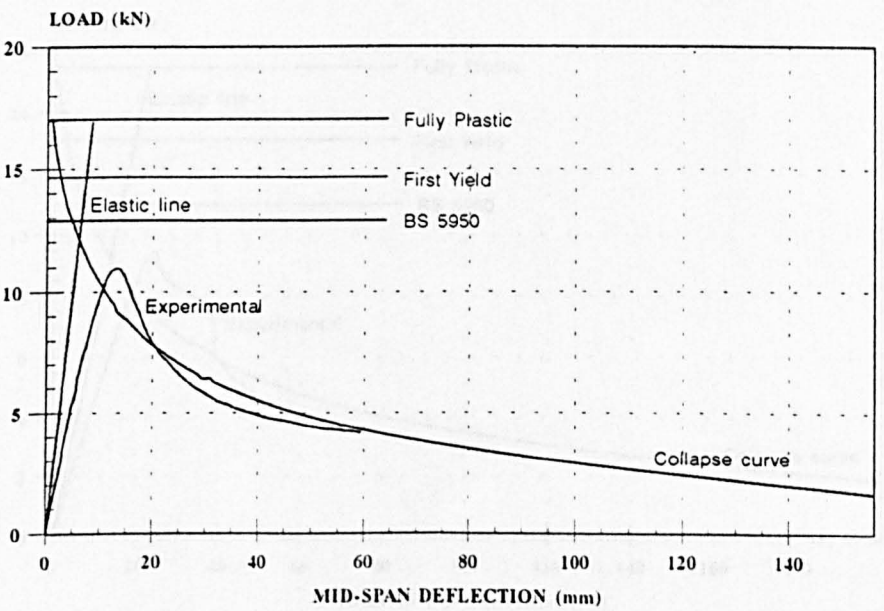

Figure 7.4.4

202Z16 ZED SECTION
SINGLE SPAN (2250 mm)

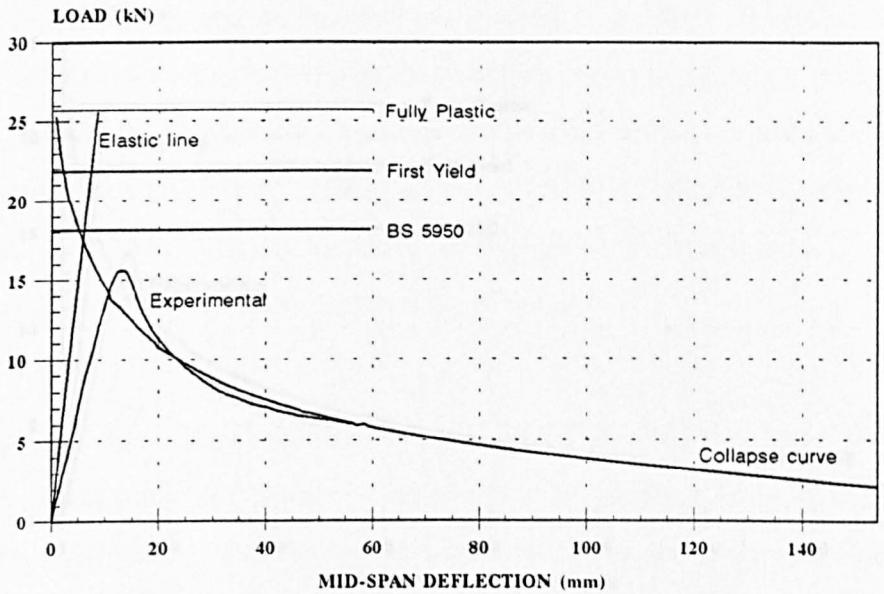

Figure 7.4.5

202Z16 ZED SECTION
SINGLE SPAN (3750 mm)

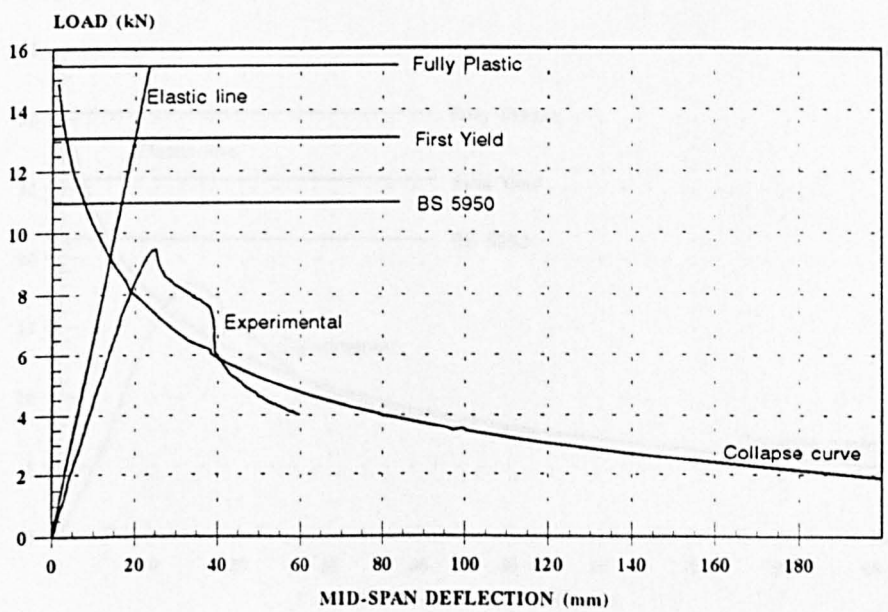

Figure 7.4.6

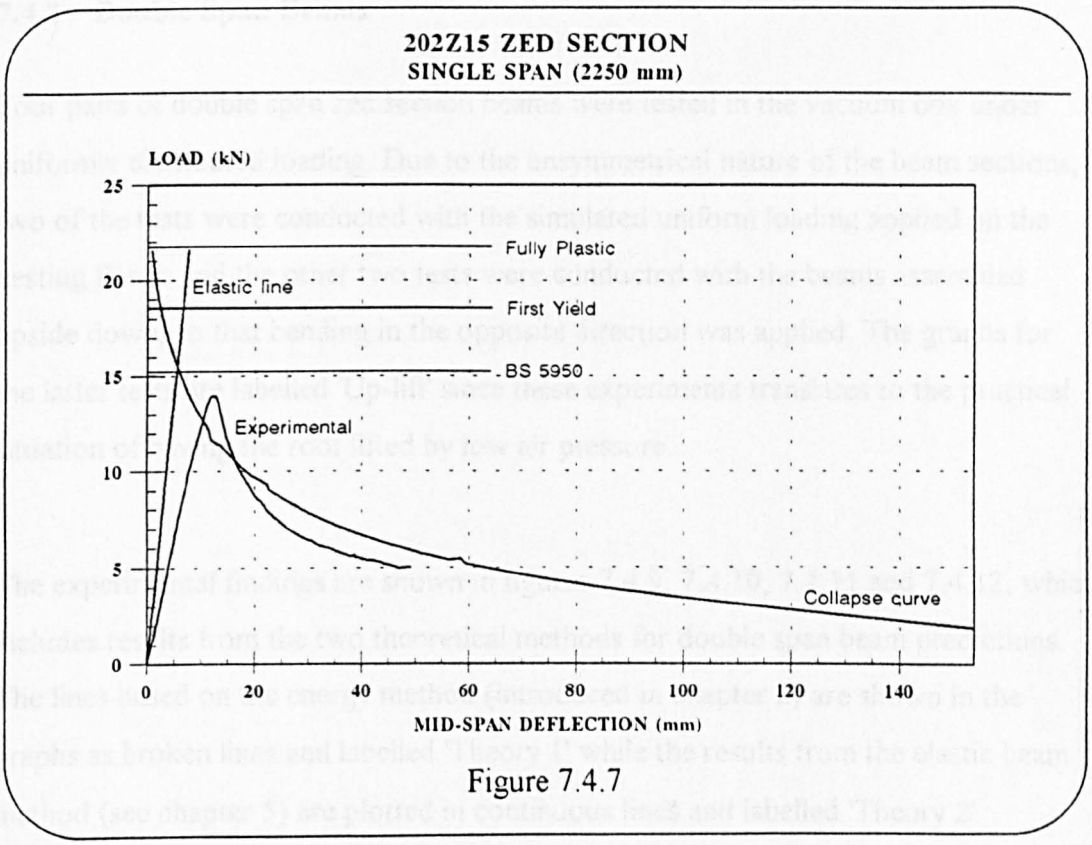

Figure 7.4.7

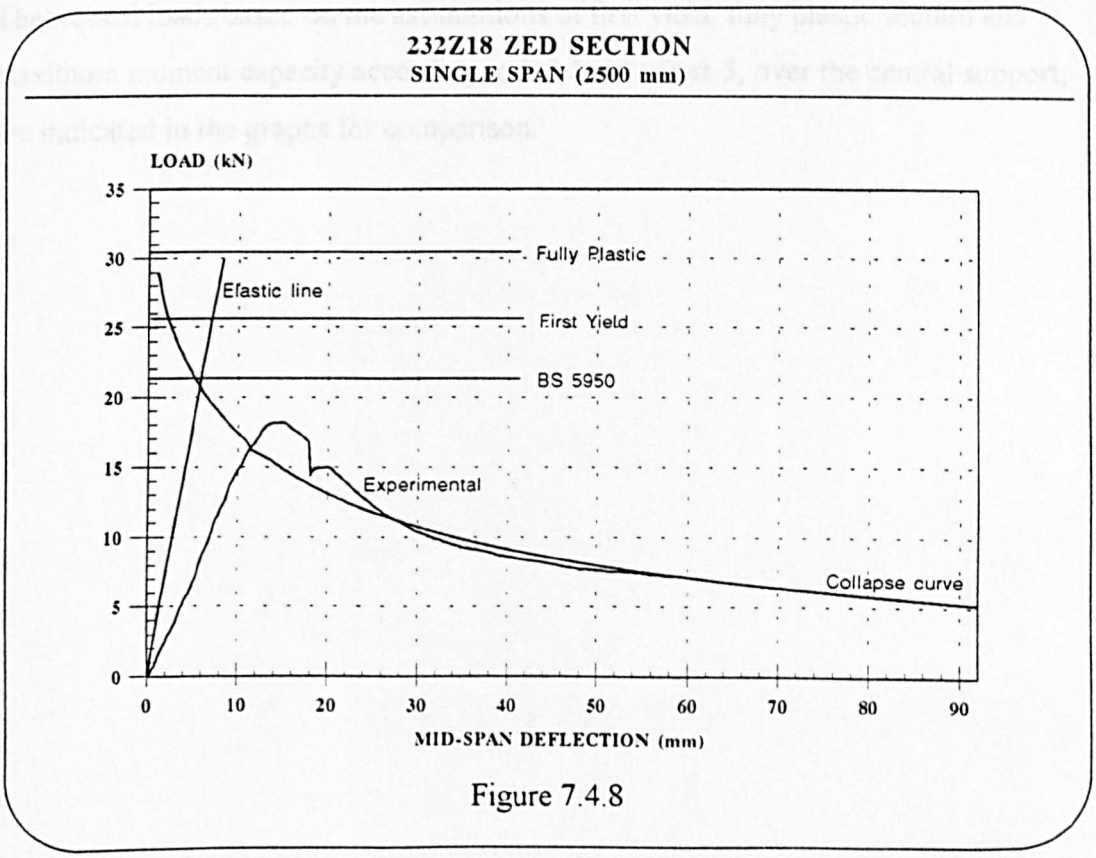

Figure 7.4.8

7.4.2 Double Span Beams

Four pairs of double span zed section beams were tested in the vacuum box under uniformly distributed loading. Due to the unsymmetrical nature of the beam sections, two of the tests were conducted with the simulated uniform loading applied on the nesting flange and the other two tests were conducted with the beams assembled upside down, so that bending in the opposite direction was applied. The graphs for the latter tests are labelled 'Up-lift' since these experiments translates to the practical situation of having the roof lifted by low air pressure.

The experimental findings are shown in figures 7.4.9, 7.4.10, 7.4.11 and 7.4.12, which includes results from the two theoretical methods for double span beam predictions. The lines based on the energy method (introduced in chapter 2) are shown in the graphs as broken lines and labelled 'Theory 1' while the results from the elastic beam method (see chapter 5) are plotted in continuous lines and labelled 'Theory 2'. Theoretical loads based on the assumptions of first yield, fully plastic section and maximum moment capacity according to BS 5950 : Part 5, over the central support, are indicated in the graphs for comparison.

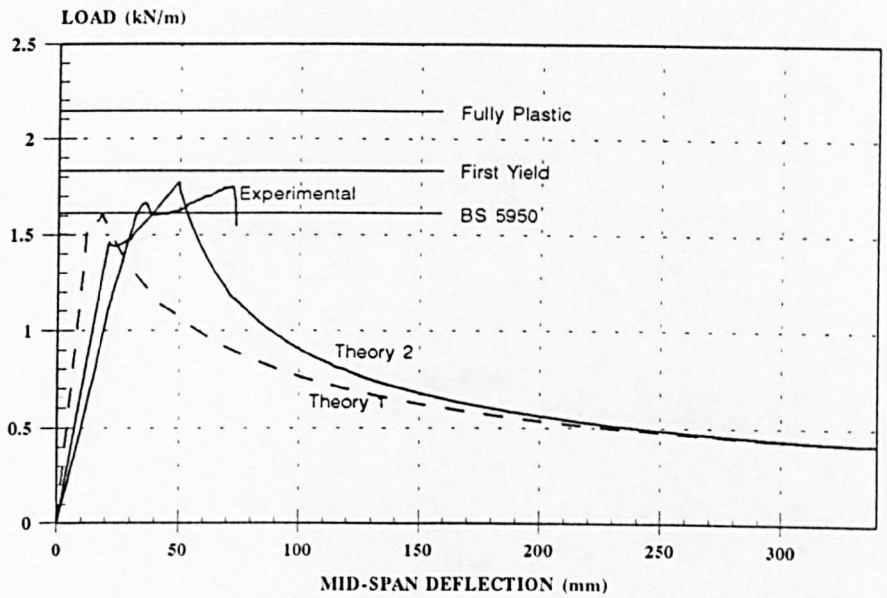

Figure 7.4.9

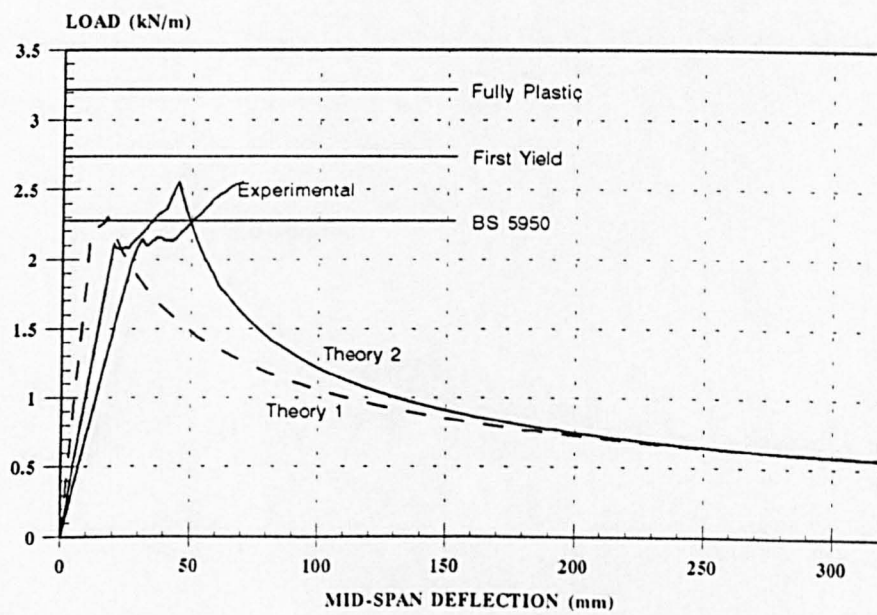

Figure 7.4.10

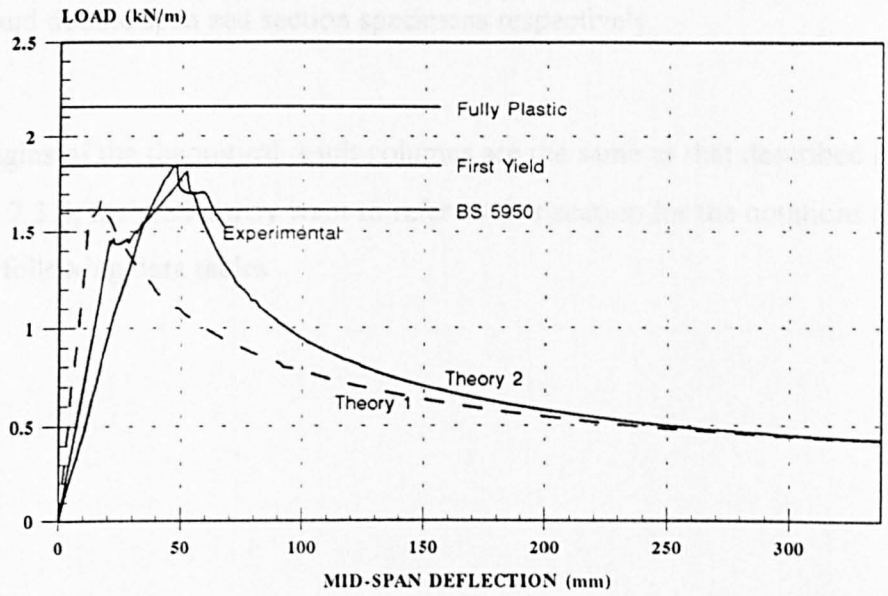

Figure 7.4.11

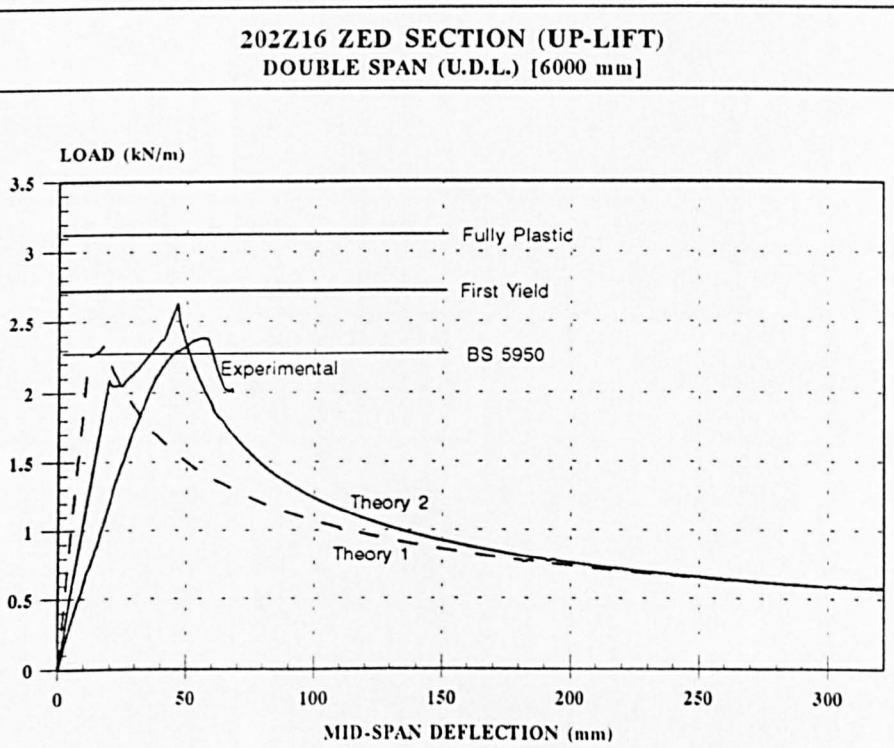

Figure 7.4.12

7.4.3 Summary of Results

The experimental and theoretical results are presented in tables 7.4.1 and 7.4.2 for the single and double span zed section specimens respectively.

The origins of the theoretical result columns are the same as that described in section 7.3.4, the reader may want to refer to that section for the notations adopted for the following data tables.

Beam Section							Ultimate Moment Capacity (Nmm)				
S/No	Section Reference No.	Flange Widths (mm)	Web Depth (mm)	Lip Sizes (mm)	Thickness (mm)	Beam Span (mm)	Experimental	Current Theory	First Yield	Fully Plastic	BS 5950 Part 5
55	122Z15	54 / 49	122	19 / 21	1.48	1,500	3,750,000	4,537,500	4,777,708.32	5,565,642.674	4,531,095.641
56	122Z15	54 / 49	122	19 / 21	1.48	2,250	3,993,750	4,162,500	4,777,708.32	5,565,642.674	4,531,095.641
57	122Z16	54 / 49	122	19 / 21	1.56	1,500	4,672,500	5,105,625	5,615,086.773	6,541,389.168	5,321,206.547
58	122Z16	54 / 49	122	19 / 21	1.56	2,250	5,062,500	4,687,312.5	5,615,086.773	6,541,389.168	5,321,206.547
59	142Z15	54 / 49	142	19 / 21	1.49	1,750	5,317,375	5,519,062.5	6,266,171.59	7,347,925.876	5,741,976.498
60	142Z15	54 / 49	142	19 / 21	1.49	3,000	5,587,500	4,912,500	6,266,171.59	7,347,925.876	5,741,976.498
61	142Z20	54 / 49	142	19 / 21	1.96	1,750	7,000,000	6,737,500	7,229,146.017	8,479,966.096	7,123,908.104
62	142Z20	54 / 49	142	19 / 21	1.96	3,000	7,237,500	6,000,000	7,229,146.017	8,479,966.096	7,123,908.104
63	172Z15	65 / 60	172	19 / 21	1.52	2,250	6,187,500	6,750,000	8,261,509.429	9,629,271.995	7,246,970.08
64	172Z15	65 / 60	172	19 / 21	1.52	3,500	6,825,000	6,125,000	8,261,509.429	9,629,271.995	7,246,970.08
65	172Z25	65 / 60	172	19 / 21	2.35	2,250	13,218,750	12,093,750	14,353,776.816	16,739,019.64	13,955,135.19
66	172Z25	65 / 60	172	19 / 21	2.35	3,500	13,562,500	10,850,000	14,353,776.816	16,739,019.64	13,955,135.19
67	202Z16	65 / 60	202	19 / 21	1.58	2,250	8,789,062.5	9,703,125	12,292,390.73	14,472,286.75	10,214,918.35
68	202Z16	65 / 60	202	19 / 21	1.58	3,750	8,554,687.5	8,906,250	12,292,390.73	14,472,286.75	10,214,918.35
69	202Z25	65 / 60	202	19 / 21	2.35	2,250	18,562,500	15,058,125	17,816,928.46	20,990,000.44	16,844,934.28
70	202Z25	65 / 60	202	19 / 21	2.35	3,750	17,812,500	13,312,500	17,816,928.46	20,990,000.44	16,844,934.28
71	202Z15	65 / 60	202	19 / 21	1.47	2,250	7,875,000	8,606,250	10,430,082.97	12,278,610.97	8,562,806.85
72	232Z18	76 / 69	232	19 / 21	1.73	2,500	11,428,750	12,946,250	16,055,690.41	18,941,321.51	13,308,364.51
73	232Z18	76 / 69	232	19 / 21	1.73	4,000	12,154,000	11,615,000	16,055,690.41	18,941,321.51	13,308,364.51

Table 7.4.1 : Single Span Zed Section Beams (Continued on the next page)

Beam Section							Ultimate Moment Capacity (Nmm)				
S/No	Section Reference No.	Flange Widths (mm)	Web Depth (mm)	Lip Sizes (mm)	Thickness (mm)	Beam Span (mm)	Experimental	Current Theory	First Yield	Fully Plastic	BS 5950 Part 5
74	232Z25	76 / 69	232	19 / 21	2.35	2,500	20,187,500	18,750,000	23,306,802.17	27,509,577.24	21,317,870.03
75	232Z25	76 / 69	232	19 / 21	2.35	4,000	24,900,000	16,750,000	23,306,802.17	27,509,577.24	21,317,870.03
76	232Z16	76 / 69	232	19 / 21	1.58	2,500	10,687,500	12,125,000	16,052,948.81	18,935,790.54	12,371,059.29
77	262Z20	80 / 72	262	19 / 21	1.96	2,500	15,562,500	16,375,000	20,562,643.3	24,429,881.58	17,518,858.93
78	262Z20	80 / 72	262	19 / 21	1.96	4,000	17,100,000	14,800,000	20,562,643.3	24,429,881.58	17,518,858.93
79	262Z29	80 / 72	262	19 / 21	2.99	2,500	25,000,000	27,856,250	32,282,290.58	38,389,122.03	30,720,858.37
80	262Z29	80 / 72	262	19 / 21	2.99	4,000	27,000,000	25,000,000	32,282,290.58	38,389,122.03	30,720,858.37
81	262Z16	80 / 72	262	19 / 21	1.58	2,500	11,153,750	14,711,250	19,397,989.65	23,038,474.66	14,163,772.56
82	262Z18	80 / 72	262	19 / 21	1.74	2,500	12,875,000	16,250,000	20,950,540.8	24,885,896.71	16,321,097.21

Table 7.4.1 : Single Span Zed Section Beams (Continued)

Section Details								
Section reference No.		Flange Widths (mm)	Web Depth (mm)	Lip Sizes (mm)	Thickness (mm)			
172Z15		65 / 60	172	19 / 21	1.52			
202Z16		65 / 60	202	19 / 21	1.58			
Beam Section			**Ultimate Beam Load (kN/m)**					
S/No.	Section Reference	Beam Length per Span (mm)	Experimental	Theory 1 (Theoretical)	Theory 2 (Theoretical)	First Yield	Fully Plastic	BS 5950 Part 5
83	172Z15	6,000	1.7575	1.6125	1.775	1.8359	2.14	1.61
84	202Z16	6,000	2.5625	2.3	2.5625	2.7316	3.216	2.27
85	172Z15 (Up-lift)	6,000	1.85	1.675	1.825	1.8359	2.14	1.61
86	202Z16 (Up-lift)	6,000	2.3875	2.33	2.625	2.7316	3.216	2.27

Table 7.4.2 : Double Span Zed Section Beams (U.D.L.)

The theoretical results for the zed section specimens examined suggested that these sections have relatively narrow flanges and according to the BS 5950 : Part 5 : 1987 recommendations, the compression flanges do not experience elastic buckling before the ultimate bending moment, determined by the plastic mechanism theory, is reached. On examination of the single span experimental results, it may be observed that the maximum loads calculated using the moment capacity based on the BS 5950 : Part 5 recommendations tends to overestimate the ultimate loads for a number of the sections. This is due to the bi-axial bending effects in these beam sections which are not doubly symmetrical that were not accounted for in the BS 5950 : Part 5 calculations. In most cases, the current theory produces ultimate load predictions which agree better with the experimental findings.

On examination of the theoretical and experimental load-deflection behaviour plots for the single span specimens, it can be seen that the experimental deflections at which the ultimate loads occur tend to be larger than the theoretical predictions and that the difference is more pronounced in these zed sections than in the plain channel sections and some of the lipped channel specimens examined. This is thought to be due to the tendency of the flanges to curl as the beams are loaded. With the presence of the lips, this tendency is higher than that for the plain channels and the effect is further encouraged by the cross-sectional asymmetry of the zed sections. However, the current theory does produce good estimates of the ultimate section bending moment capacities and the experimental results shows that the theory is generally applicable for the zed sections investigated.

From the double span beam results, two observations may be immediately obvious. The first concerns the adequacy of the two theoretical methods for the analysis of the double span beams. The plots indicate that the energy method (Theory 1), first introduced in chapter 2 of this thesis, produces results which are inferior to the elastic beam approach presented in chapter 5. This is again attributed to the fact that these

relatively long beams tends to exhibit rather large elastic deformations before the ultimate failure occurs, just as in the lipped channel floor beams examined in the previous section. This further supports the conclusion that the latter method for analysis of multi-spanning beams is more reliable for beams which ultimately collapses after a relatively large amount of elastic beam deformation along the spans following the development of plastic mechanisms at the supports between the spans.

The second observation for the double span specimens relates to the difference between the shapes of the theoretical and experimental load-deflection plots for the beams tested for up-lift. The match in the shape of the theoretical plots with the experimental are not as good as in the first two tests where the beams are loaded on the nesting flange. This is thought to be due to the fact that the compression flanges along the span of the beams in the up-lift experiments are unrestrained against side way movement whereas the roof sheeting screwed onto the compression flanges of the first two beam tests prevents any such side way movements. The beams in the up-lift tests hence failed with some torsional buckling effects, however, the current theory was still able to produce rather good ultimate load predictions.

Further discussion of all the findings will be carried out in chapter 9 of this thesis, the reader may want to proceed to that chapter for a fuller understanding of the discoveries made during these beam investigations.

Chapter Eight

• *Effects of Strain Hardening in Cold Formed Sections*

8.1 INTRODUCTION

It has long been known that the processes of cold forming in the fabrication of many thin-walled steel structural members causes profound changes in the material properties of the metal in the finished sections. Three most commonly used production methods for cold-formed steel are press braking, cold rolling and folding, all of which generally have the effect of increasing the yield and ultimate strengths of the material in the region of the cold formed corners, which is accompanied by a reduction in ductility. In the case of cold rolling, the normal pressure applied to the flat portions during fabrication can cause marked changes in the local material properties in regions away from the corners.

In the design of cold-formed steel sections, it seems only just to consider any such effects as the heightened strength levels which can contribute substantially to the effective load carrying capacity of the structural sections, can lead to more economical designs. This prompted the author to dedicate a chapter of the current thesis to study the positive effects that can be gained from considering strain hardening in the material of the cold-formed sections. Experimental investigations were conducted with the aim of understanding the strength characteristics and the distribution and extent of the cold forming effects, with particular interest in the yield strength of cold-formed corners. Experimental results are compared with available theories to determine the improved section properties of thin-walled mild steel sections that were produced by imposing large plastic strains during a cold forming process.

Researchers such as Walker [76] had discovered that the material properties were not uniform over the entire cross section of cold-formed sections, the yield as well as the ultimate material strengths were higher in the region of the corners as compared to

the flats, tensile tests on strips cut from channels revealed the strength distributions as shown in figure 8.1.1.

In the first of a series of three papers, Chajes et.al. [11] studied the effects of cold work in cold forming on the mechanical properties of light-gauge steel, by investigating simple unidirectional tensile straining of flat sheet steel. This initial study, although not directly relevant to the current work, lead to an important contribution to the subject by Karren [23], that dealt with more complex types of cold straining associated with the forming of corners in the manufacturing of structural steels. Karren assumed that the plastic strain hardening region of the stress-strain trace of the steels he investigated could be represented by a power law, as described in Eqn.(8.1.1).

$$\bar{\sigma} = k \cdot (\bar{\varepsilon})^n \qquad \text{Eqn.(8.1.1)}$$

where k is the strength coefficient
n is the strain hardening exponent
and $\bar{\sigma}$ & $\bar{\varepsilon}$ are the generalised stress and strain respectively.

Deriving the material constants empirically, the concepts of effective stress and effective strain from plasticity theory were employed to develop equations to predict tensile yield strength of corners. Two analytical corner models were used, the first considered wide flat sheets subjected to pure flexure while the second included the effect of radial pressure during plastic forming. The resulting formulae are shown here as Eqn.(8.1.2) and Eqn.(8.1.3) respectively.

For wide flat plates subjected to pure flexure, the corner yield stress is

$$\sigma_{yc} = \frac{kb}{\left(\frac{a}{t}\right)^m} \qquad \text{Eqn.(8.1.2)}$$

where $b = 0.945 - 1.315n$ and $m = 0.803n$ these being empirical variables and $\left(\frac{a}{t}\right)$ is the ratio of the inside corner radius to the sheet thickness.

Considering the effect of radial pressure during forming, the corner yield stress is

$$\sigma_{yc} = kb\left(\frac{a}{t}\right)^m \qquad \text{Eqn.(8.1.3)}$$

where $b = 1.0 - 1.3n$ and $m = 0.855n + 0.035$.

The theoretical predictions compared well with experimental findings and it was found that the yield strength after cold working may be considerably higher than the original ultimate tensile strength of the material. Also, the increase in ultimate strength due to strain hardening in corners was smaller than the increase in yield strength, causing marked reductions in the spread between yield and ultimate strengths.

In a subsequent paper, Karren and Winter [24], conducted an extensive experimental investigation to study the mechanical properties of full cold formed sections in relation to the virgin materials from which the sections were fabricated and presented a method by which the full section tensile yield strength of members may be predicted from the results of simple tensile coupon tests. This was accomplished by using the equations developed in Karren [23], to estimate the strength of the corners and a weighted averaging technique, which took into account the areas of the flats and the corners, for the overall average section strength. Yield strength found in corners were considerably higher than those in the flat portions, as illustrated in figure 8.1.2. The effects of the increased yield strength on the inelastic buckling of thin-walled columns

were also dealt with experimentally and theoretically. Theoretical predictions of the buckling behaviour using the weighted average yield strength and a generalised tangent modulus equation for the columns was in good agreement with experimental results. It was observed during the stub column tests that buckling always began in the flat elements, spreading to the corners after additional loading, evidently, the flats having a lower yield point, started to buckle locally at an average cross-sectional stress at or slightly above their own lower yield point, thus preventing the higher yield strength of the corners to be fully effective. It was also found that the changes in yield and ultimate strengths in the flats were small if not negligible in the sections produced by press braking but these changes may be much larger in cold rolled sections.

Lind and Schroff [30] presented a similar theory, based on fewer assumptions, the theory produced an analysis which was considerably simplified and specialised for a simple linear strain hardening law. The idea of the theory was that whether a corner had a large or small radius, the cold work, equal to the integral of the applied moment with respect to the angle of bend, should be about equal if the strain hardening is linear. The work is therefore independent of the corner radius, neglecting the elastic effects. Further, if the increase in yield strength is a linear function of the work of forming, the increase in yield strength of the corner will also be a linear function of the work of forming. The increase in yield force is given by Eqn.(8.1.4).

$$\Delta P = (5t) \cdot t \cdot (f_u - f_y) \cdot \left(\frac{\theta^o}{90^o}\right) \qquad \text{Eqn.(8.1.4)}$$

where t is the material thickness
and f_u & f_y are the ultimate and yield strength of the material respectively.

The results obtain from using Eqn.(8.1.4) compared well with experimental data and Karren's findings.

The formulation developed by Lind and Schroff formed the basis of the clauses for section yield strength in the BS 5950 : Part 5 : 1987 [8] for calculating the increased average yield strength in cold-formed sections, Eqn.(8.1.5) shows the expression as written in the code.

$$Y_{sa} = Y_s + \frac{5Nt^2}{A}(U_s - Y_s) \qquad \text{Eqn.(8.1.5)}$$

where Y_{sa} and Y_s are the increased average and virgin yield stresses
U_s is the virgin material ultimate strength
N is the number of full 90° bends
and A is the gross area of the cross-section.

According to the code, the average section yield stress is limited to 1.25 times virgin strength or the ultimate strength, whichever is smaller for the case. Modifications would have to be made for the compressional yield strength if the increased strength is to be applied to elements in compression.

The formulation developed by Lind and Schroff [30] and is essentially the same as that in the BS 5950 : Part 5 : 1987 [8], which is based on a linear strain hardening model and takes the increase in strength due to cold work into account by replacing the yield strength by the ultimate strength at each 90° bend over an arc length of five times the material thickness. This arc length is modified in proportion to the angle of bending for angles other than 90°. The method was adopted in BS 5950 : Part 5 because of it's simplicity and the ease of application which made it readily applicable in the design of cold formed sections. This method of estimating the work hardened strength does not consider the radius of bend as a parameter, the theory assumes that the increase in strength is a linear function of the cold work involved in forming the bend which is independent of the bend radius, a smaller radius simply concentrates the same amount of work into a smaller area, the net average increase in strength remaining the same. It is also assumed that the yield strength in compression is the

same magnitude as the yield in tension, this does not cause too much inaccuracies as found by Karren [23] and Lind and Schroff [30].

The changes in mechanical properties of the cold formed steels are mainly caused by strain hardening and strain ageing, these effects are illustrated in figure 8.1.3. Curve A represents the stress-strain behaviour of the virgin material, curves B and C shows unloading in the strain hardening range and subsequent reloading, while curve D demonstrates the reloading behaviour after strain ageing. Both strain hardening and ageing causes increases in the apparent yield strength on subsequent reloading with reductions in ductility. The degree and extent of these effects seem to be dependent on a number of factors, which are listed below :-

- Type of steel.
- Magnitude of the stresses involved.
- Direction of stress with respect to the direction of cold work.
- Material stress-strain index.
- Ratio of ultimate-to-yield strength.
- Radius of bend to thickness ratio.

and

- The extent of cold work.

Amongst the items listed, the ratio of ultimate-to-yield strengths in the virgin material and radius-to-thickness ratio of the formed corners are the most important factors, higher strength ratio generally means more potential in the increase of corner strengths and tighter radii of bends causes greater degrees of straining and hence higher local yield strengths.

The increase in yield strength due to strain hardening occurs when cold working of the material in the sections causes sufficiently large strains which drives the material

behaviour into the work hardening range. The physical problem dealt with is the subsequent uniaxial tension and compression of the formed corners in the direction perpendicular to the initial cold work applied to the steel plates during fabrication.

In relation to the current investigation, the effects of strain hardening can alter the effective section strength in elastic bending. In addition, the relatively large strains that exists at the hinges of the plastic collapse mechanisms can also cause increases in the plastic moment of the hinged plate, this increase can be accounted for by a simple means, which will be discussed in section 8.4 of this chapter. This simple method was applied in the plastic mechanism analyses presented in chapters 3, 4 and 5 of this thesis.

The following two sections present the experimental investigations conducted by the author to study the effects of strain hardening on the yield strength of cold formed corners. Due to the complexity of the theoretical aspects of the problem and time constraints, the analytical study has not been completed and may be the subject of further research. The experimental studies undertaken were aimed to increase the understanding of the characteristics of the work hardened corners. Two types of experiments were carried out, the first (section 8.2), consisted of tensile testing of cold formed mild steel specimens which included corners, this enabled the consolidation of a set of data which describes the strengths of the corners in uniaxial tension for a range of thicknesses and radii of bend. The second type of experiments (section 8.3), involved the use of hardness testing to estimate the relative strength of the material distributed within the corner regions, this also enabled the determination of the spread of the effects of cold work in the region of the bends.

8.2 TENSILE TESTING OF COLD FORMED CORNERS

In order to quantify the average strength of cold formed corners, tension tests on specimens consisting of flat and corner elements were the subjects of this first type of strain hardening experiments. The specimens were fabricated from mild steel sheets similar to those used to produce the plain and lipped channel beams examined in earlier chapters. Two series of experiments were conducted on such tensile test specimens made in a small range of thicknesses and ratios of corner radius to thickness. In the first series, the specimens were bolted at the ends as the specimens were subjected to tension and in the second series, similar specimens were held at the ends by way of pins and clamping blocks. These experiments are detailed in the following subsections.

8.2.1 Corner Tensile Experiments (Series One)

In this first series of corner tensile experiments, specimens were manufactured from mild steel sheet material in which the thickness ranged from 1.6 mm to 3 mm with 45° and 90° bends and corner radius to thickness ratios ranged from 1 to 3. A total of 20 corner specimens were successfully tested along with 8 flat specimens which provided the virgin material properties.

The specimens were tested in the Tinius Olsen Testing machine where tensile forces were applied onto the specimens through purpose designed end pieces which will be detailed in section 8.2.1.2.

8.2.1.1 Fabrication of the Test Specimens

The corners were formed in a roller bending rig designed and constructed for the purpose of fabricating these specimens, figures 8.2.1.1 and 8.2.1.2 illustrates the rig construction and the corner forming process respectively. This rig was designed to form corners with controlled radii of bend on thin gauge mild steel, this being achieved by means of the lower forming roller of the bending rig which is ideally of the same radius as the inside radius to be formed on the specimens. A number of lower rollers were prepared for the various corner sizes. The bending process is summarised in the following procedure list :

1) Referring to figure 8.2.1.2(i), the flat plate which had been cut to the appropriate width is clamped onto the base plate of the bending rig by means of a clamping plate. The forming rollers are then adjusted for position such that they are in contact with the specimen plate.

2) The upper roller that is pinned onto the roller arm which is pivoted about an axis coinciding with that of the lower roller, is then brought around to form the corner on the specimen. See figures 8.2.1.2 (ii) and (iii).

3) The angle of the formed corner is checked with a template and further bending is performed if necessary. The specimen is only released from the bending rig when the required angle of bend is achieved.

The specimens are then trimmed and milled to the final shape as shown in figure 8.2.1.3, in which mid section containing the gauge length of 50 mm is approximately one third the width of the end portions. Figures 8.2.1.4 and 8.2.1.5 shows the final dimensions of each of the tested specimens.

Standard flat tensile specimens according to BS EN 10002-1 : 1990 were also prepared from each material, the shape and dimensions of these flat specimens is shown in figure 6.3.1 of chapter 6. The specimens containing the corners were dimensioned similar to the standard pieces as far as possible, with a similar "bone-shaped" outline to ensure that failure would not occur at the held ends during the tension test.

8.2.1.2 Tension Tests

Both types of tensile specimens were tested on the 200,000 lbs Tinius Olsen universal testing machine, figures 8.2.1.6 and 8.2.1.7 shows the test set-up, in which a Denison 50 mm extensometer was used to monitor the strains within the gauge length of the test pieces. All specimens were tensioned to fracture with the gauge length strains and applied tensile loads continuously monitored and recorded by an X-Y plotter (described in chapter 6) in the form of load-extension graphs. The test conditions are the same as that for the tension tests described in section 6.3 of this thesis for material properties. A more detailed description of this series of experiments along with a full set of the recorded graphs can be found in Chua [76].

8.2.1.3 Results (Corner Tensile Tests, Series One)

Some selected plots of the stress-percentage elongation behaviour of the tensile tests specimens are shown at the end of this chapter. Figures 8.2.1.8 and 8.2.1.9 illustrates the typical results observed for the flat specimens which indicate the virgin material characteristics. Figures 8.2.1.10 to 8.2.1.12 shows the typical findings for specimens with 45° corners while the figures 8.2.1.13 to 8.2.1.15 were plotted for specimens with 90° corners.

Table 8.2.1 summarises the consolidated results from these series of experiments, along with theoretical predictions of average corner strength calculated using the methods by Karren [23] and Lind and Schroff [30]. In the table, corner areas are calculated for the portion of the cross section within the gauge length of the specimens that is within the 90° or 45° arc. With the corner and overall cross sectional areas known, the average yield strength of the corners can be calculated since the resisting force contribution by the flat portions of the cross-section can be estimated from the virgin yield strength of the material. This inherently assumes that the cold forming effects only affect the portion of the cross section within the corner region, an assumption which will be supported by findings presented in section 8.3 of this thesis. The use of various permanent set values of yield approximations will be discussed in section 8.2.1.4.

Test No.	Inside Radius (mm)	Thickness (mm)	Angle (Deg)	Corner Area (mm^2)	Virgin(2%) Yield Stress	Ultimate Tensile Stress	P.S.	Virgin(PS) Yield Stress	Expt.(PS) Yield Stress	Expt.% Increase	Karren % Increase	Lind % Increase
2A	4	2	90	15.7079	230.57	327.37	0.6	232.33	416.45	79.25	56.16	53.45
2B	4	2	90	21.544	230.57	327.37	0.6	232.33	430.13	85.14	56.16	38.97
2C	6	2	90	28.51	230.57	327.37	0.6	232.33	429.63	84.92	43.85	29.45
2D	6	2	90	29.748	230.57	327.37	0.6	232.33	397.63	71.15	43.85	28.23
2E	2.5	2	90	10.9955	230.57	327.37	0.6	232.33	682.91	193.94	71.76	76.36
3C	7	3	90	40.6553	300.531	466.3	1	341.08	447.12	31.09	65.93	61.05
3D	7	3	90	40.0553	300.531	466.3	1	341.08	458.47	34.42	65.93	61.97
M6	4	1.6	90	12.0637	444.43	548.76	0.4	465.07	456.26	-1.89	28.84	24.91
M7	6	2.5	90	28.4707	486.02	546.26	0.2	486.02	607.3	24.95	16.22	13.60
M8	6	2.5	90	28.0747	486.02	546.26	0.2	486.02	570.28	17.34	16.22	13.80
2H	10	2	45	17.2787	230.57	327.37	0.6	232.33	423.12	82.12	29.71	24.30
2I	10	2	45	17.2787	230.57	327.37	0.6	232.33	424.98	82.92	29.71	24.30
2J	10	2	45	17.2787	230.57	327.37	0.6	232.33	398.87	71.68	29.71	24.30
2K	10	2	45	17.2787	230.57	327.37	0.6	232.33	386.78	66.48	29.71	24.30
2L	12	2	45	20.4203	230.57	327.37	0.6	232.33	427.11	83.84	25.01	20.56
2M	12	2	45	20.4203	230.57	327.37	0.6	232.33	380.65	63.84	25.01	20.56
3G	12	3	45	31.8086	300.531	466.3	1	341.08	497.33	45.81	49.42	39.02
3H	12	3	45	31.8086	300.531	466.3	1	341.08	502.56	47.34	49.42	39.02
3I	15	3	45	38.8772	300.531	466.3	1	341.08	471.45	38.22	43.07	31.92
3J	15	3	45	38.8772	300.531	466.3	1	341.08	486.13	42.53	43.07	31.92

Note : - All Stresses in N/mm^2.
- P.S. is the Permanent Set % Plastic Strain at which the Experimental Stresses are compared.
- % Increases are the improvements in Corner Yield Stresses over the Virgin Yield Strength.

Table 8.2.1 : Corner Tensile Experiments (Series One)

8.2.1.4 Observations and Comments (Corner Tensile Tests, Series One)

Average corner strengths found in this set of experiments generally ranged from 17% to 85% over the yield strength of the virgin material, these values being calculated based on corner areas in the 90° or 45° arc. This implies that all the effects of the cold work were assumed to occur within the bent portions of the plates.

The bending rig was design for forming the corners of the corner specimens with a tight control of the inside corner radius. The use of this rig however, required the shaping of the specimens to be done after the corners were formed, since a rather large clamping area was necessary during the bending process. This presented some difficulties in the machining process, leading to a compromise of having the edges angled rather than perpendicular to the flat elements. Figure 8.2.1.16 illustrates the milling process for the corner specimens.

The rigidity of the bending rig was also found to be inadequate for the 3 mm thick plates, especially for the smaller bend radii. The adjustable parts of the rig which was implemented to allow various sizes of specimens to be fabricated in the same rig proved to be problematic, as a result, many intended specimens had to be temporarily abandoned.

The use of bolts to fasten the specimens between the cross-heads of the Tinius Olsen testing machine allowed ill effects of bending of the specimens containing the corners as the loads were applied, figure 8.2.1.17 illustrates this problem whereby some bearing of the bolt holes occurred. This lead to non-uniform yielding over the cross-section of some of the tensile specimens which showed up in the load-extension plots as rather irregular shaped traces before the curve stabilised when yielding had spread over the entire cross-section.

On close examination of the experimental results, it may be realised that the elasto-plastic region of load-extension plots for the corner specimens are rather different from those found in the virgin materials. The corner specimens tended to exhibit relatively more gradual transition from elastic to plastic behaviour with a longer elasto-plastic curve as compared to the flat specimens which had not been cold worked. For this reason, the conventional method of estimating the yield stress of material (with a relative smooth transition between elastic and plastic behaviour) in which the 0.2% permanent set value of stress is taken as the yield was deemed to be unsuitable for the corner specimens, since the material in the gauge length of the specimens are still in the early stages of the elasto-plastic transition at strains of 0.2%. For the purpose of the current work, larger permanent set values of stress were used to assess the yield strength of the corner specimens. A permanent set value was chosen for each of the material thicknesses such that the stress at these chosen strains were in the plastic region of the load-extension behaviour that was 'linear'. By taking the virgin strength of the material at the same permanent set as for the corner specimens, the increase in yield strength could be estimated and it is on the basis of this increase that the experimental results were compared to the theoretical results presented in table 8.2.1.

From the data presented in table 8.2.1, it can be seen that rather large differences exists between theoretical predictions using the methods by Karren [23] and Lind and Schroff [30] and the experimental findings for some of the specimens, with most of the theoretical estimates on the conservative side.

Further discussion of the experimental findings will be presented in chapter 9 of this thesis.

8.2.2 Corner Tensile Experiments (Series Two)

In this series of corner tensile experiments, specimens similar to those of the first series were fabricated for testing. Specimens containing 90° corners were made from mild steel sheet material of 5 different thicknesses, with the ratio of inside bend radius to thickness ranging from 0.917 to 3.16. A total of 42 corner specimens along with 10 standard flat tensile specimens were successfully tested in this series.

8.2.2.1 Fabrication of the Test Specimens

An air-braking rig was designed and constructed for the purpose of cold forming the corners of the specimens, this rig is shown in figure 8.2.2.1 and is used with the Tinius Olsen Testing machine which provides the driving force for the bending operation. The rig essentially consists of two main parts, the lower roller assembly which sits on the test bed of the Tinius Olsen and rigidly holds the two lower rollers in position during the bending operation and the upper roller which is attached through a ram to the moving crosshead of the Tinius Olsen machine. The size of the upper roller controls the inside radius of the cold formed corners, for the current set of specimens, 5 sets of upper roller/ram were manufactured to enable the fabrication of the test specimens. A pair of guide pins were welded to each of the upper rollers, these pins serves to hold the test specimens in place as the upper roller is brought down to form the corners.

In the forming operation, specimens which had been milled to the final 'bone' shape and size, and with the pin holes drilled, are positioned onto the lower rollers and aligned using the guide pins of the upper roller. Figure 8.2.2.2 illustrates this

operation. The upper roller is then brought down by lowering the crosshead of the Tinius Olsen to form the required 90° corner on the test specimen. By monitoring the displacement of the upper roller and the applied bending force, the energy applied in the cold working process of forming the corners could later be estimated.

Packing plates on the sides of the lower rollers allowed minor adjustments and the lower roller mountings could be positioned to suit each thickness of specimen. The final position of the lower rollers and final depth of the upper roller movement was found by trial and error operations on sample specimens. Figure 8.2.2.3 details the specimen dimensions.

8.2.2.2 Tension Tests

The fabricated corner specimens were clamped at each end by means of two pairs of purpose designed clamping blocks. Locating pins in each pair of clamping blocks ensured that the specimens would not slip against the clamping blocks. Figure 8.2.2.4 shows the method of clamping the specimens in the Tinius Olsen test machine using the wedged grips of the machine during the tension tests.

As in the first series of corner tensile experiments, a 50 mm Denison extensometer was employed to monitor the strains within the gauge length of the specimens during the tests. Load-extension graphs were plotted for each specimen using X-Y plotters which continuously registered the applied tensile forces and extensometer readings as each specimen was tensioned to fracture. Test conditions were kept to that for the tensile testing of standard yield specimens as described in section 6.3 of this thesis.

8.2.2.3 Results (Corner Tensile Tests, Series Two)

Some selected experimental plots of stress versus percentage elongation are shown at the end of this chapter. Figures 8.2.2.5 and 8.2.2.6 shows the typical behaviour of the virgin material and figures 8.2.2.7 to 8.2.2.10 illustrates the findings for the corner specimens.

A summary of all the corner tensile test results is presented in table 8.2.2 where the increase in the average corner yield strength is compared to the theoretical predictions based on the theories of Karren [23] and Lind and Schroff [30]. As in table 8.2.1, only the corner strengths are considered in this table, with the contributions from the flat elements on each side of the corners removed by assuming they yield at the virgin material yield stress.

The full set of experimental plots along with further details of this series of experiments can be found in Han [18].

Test No.	Inside Radius (mm)	Thickness (mm)	Corner Area (mm^2)	Virgin (0.2%) Yield Stress	Ultimate Tensile Stress	Virgin (1%) Yield Stress	Expt (1%) Yield Stress	Expt % Increase	Karren % Increase	Lind % Increase
t1-1	2.50	0.95	4.44	181.99	303.93	201.84	490.80	143.16	63.53	68.09
t2-1	2.50	0.95	4.44	181.99	303.93	201.84	495.83	145.65	63.53	68.09
t3-1	2.50	0.95	4.44	181.99	303.93	201.84	506.77	151.08	63.53	68.09
t2-1	3.00	0.95	5.19	181.99	303.93	201.84	430.89	113.48	56.17	58.30
t2-2	3.00	0.95	5.19	181.99	303.93	201.84	437.19	116.60	56.17	58.30
t2-3	3.00	0.95	5.19	181.99	303.93	201.84	448.07	121.99	56.17	58.30
t4-1	2.25	1.85	9.23	208.21	304.56	212.18	428.21	101.81	77.95	85.82
t4-2	2.25	1.85	9.23	208.21	304.56	212.18	486.12	129.11	77.95	85.82
t4-3	2.25	1.85	9.23	208.21	304.56	212.18	437.86	106.36	77.95	85.82
t5-1	2.75	1.85	10.68	208.21	304.56	212.18	389.30	83.48	70.51	74.15
t5-2	2.75	1.85	10.68	208.21	304.56	212.18	364.28	71.68	70.51	74.15
t5-3	2.75	1.85	10.68	208.21	304.56	212.18	372.62	75.62	70.51	74.15
t6-1	4.00	1.85	14.31	208.21	304.56	212.18	361.53	70.39	57.44	55.33
t6-2	4.00	1.85	14.31	208.21	304.56	212.18	342.86	61.59	57.44	55.33
t6-3	4.00	1.85	14.31	208.21	304.56	212.18	339.75	60.12	57.44	55.33
t7-1	2.50	2	11.00	292.95	357.27	289.48	619.01	113.84	43.78	39.93
t7-2	2.50	2	11.00	292.95	357.27	289.48	566.29	95.62	43.78	39.93
t9-1	2.75	2	11.78	292.95	357.27	289.48	494.42	70.80	41.52	37.27
t9-2	2.75	2	11.78	292.95	357.27	289.48	535.30	84.92	41.52	37.27
t10-1	4.00	2	15.71	292.95	357.27	289.48	460.76	59.17	32.97	27.95
t10-2	4.00	2	15.71	292.95	357.27	289.48	481.17	66.22	32.97	27.95
t11-1	5.00	2	18.85	292.95	357.27	289.48	482.06	66.53	28.13	23.29
t11-2	5.00	2	18.85	292.95	357.27	289.48	474.15	63.79	28.13	23.29
t11-3	5.00	2	18.85	292.95	357.27	289.48	434.93	50.25	28.13	23.29

Table 8.2.2 : Corner Tensile Experiments (Series Two) [Continued on the next page]

Test No.	Inside Radius (mm)	Thickness (mm)	Corner Area (mm^2)	Virgin (0.2%) Yield Stress	Ultimate Tensile Stress	Virgin (1%) Yield Stress	Expt (1%) Yield Stress	Expt % Increase	Karren % Increase	Lind % Increase
t13-1	2.75	2.75	17.82	279.09	408.94	278.84	501.39	79.81	85.84	98.72
t13-2	2.75	2.75	17.82	279.09	408.94	278.84	513.88	84.29	85.84	98.72
t14-1	4.00	2.75	23.22	279.09	408.94	278.84	463.64	66.27	71.57	75.77
t14-2	4.00	2.75	23.22	279.09	408.94	278.84	434.87	55.96	71.57	75.77
t16-1	5.25	2.75	28.62	279.09	408.94	278.84	399.30	43.20	61.90	61.47
t16-2	5.25	2.75	28.62	279.09	408.94	278.84	404.83	45.18	61.90	61.47
t16-3	5.25	2.75	28.62	279.09	408.94	278.84	404.83	45.18	61.90	61.47
t16-4	5.25	2.75	28.62	279.09	408.94	278.84	373.71	34.02	61.90	61.47
t17-1	2.75	3	20.03	309.02	461.22	349.088	685.35	96.33	92.93	110.65
t17-2	2.75	3	20.03	309.02	461.22	349.088	583.17	67.06	92.93	110.65
t18-1	4.00	3	25.92	309.02	461.22	349.088	596.68	70.93	77.76	85.51
t18-2	4.00	3	25.92	309.02	461.22	349.088	596.68	70.93	77.76	85.51
t20-1	5.25	3	31.81	309.02	461.22	349.088	557.82	59.79	67.51	69.67
t20-2	5.25	3	31.81	309.02	461.22	349.088	543.82	55.78	67.51	69.67
t20-3	5.25	3	31.81	309.02	461.22	349.088	564.82	61.80	67.51	69.67
t21-1	7.75	3	43.59	309.02	461.22	349.088	526.96	50.95	53.84	50.84
t21-2	7.75	3	43.59	309.02	461.22	349.088	526.96	50.95	53.84	50.84
t21-3	7.75	3	43.59	309.02	461.22	349.088	516.74	48.03	53.84	50.84

Note : - All Stresses in N/mm^2.
- All Experimental Stresses are compared at the Permanent Set of 1% Plastic Strain.
- % Increases are the improvements in Corner Yield Stresses over the Virgin Yield Strength.

Table 8.2.2 : Corner Tensile Experiments (Series Two)

8.2.2.4 Observations and Comments (Corner Tensile Tests, Series Two)

The experimental results shows that the increase in yield strength at the corners ranged from 34% to 151% over the virgin material yield stress. The increase being higher for the tighter corners with the smaller radius of bends for all the thicknesses examined.

The theoretical predictions using the methods by Karren [23] and Lind and Schroff [30] seem to underestimate the increase in corner strength for the specimens made from the three thinner materials (0.95 mm, 1.85 mm and 2 mm) and overestimate the effect for the thicker materials (2.75 mm and 3 mm), the overestimation being worse for the specimens with tighter bend radii. This is thought to be due to the corner forming process in which the ultimate loads were exceeded for some the thick specimens with tight corners. This was evident from the load-upper roller displacement trace monitored during the cold forming. Hence, for those specimens, it can be said that the corners were 'over-bent', in that the outer fibres were tensioned beyond the ultimate tensile stress which rendered them incapable of maintaining their resistance to subsequent loading.

The rigidity problems encountered with the bending rig described in section 8.2.1 were eradicated in the second bending machine used to produce the specimens in this second series of corner tensile experiments. It may be said that this second bending machine is overly rigid in that it is capable of damaging the specimens when tight corners are bent on thick material, as in some cases of the 2.75 mm and 3 mm specimens examined. This second method of forming the corners on the tensile test pieces also enables the monitoring of the applied forces and reactions during the cold forming process which proved to be useful in recognising over-bending of specimens.

By machining the final shape of the tensile specimens before the cold forming of the corners, originally (before bending) rectangular cross-sections were achieved and the measurement of the cross-sectional areas were more precise. The milling process was also simplified since the specimens were flat at this stage.

The use of clamping blocks and locating pins for holding the ends of the specimens during the tension tests eliminated the problems of rotations in the specimen ends as illustrated in figure 8.2.1.18. In this second series of tests, the ends were securely held in all cases and there was no slippage between the specimens and the clamping blocks, and the locating pins did not cause any bearing problems on the specimens. However, some bending was observed on the specimens as the tensile stresses were applied, these formed half sine-waves within the gauge section of the test specimens, illustrated in figure 8.2.2.11. This effect can now be attributed to the fact that the gauge cross-section is unsymmetrical with the centroid which did not coincide with the line of the applied loading, especially considering the fact that the corner region possessed varying yield strengths. The relatively long elasto-plastic region found in the load-extension plots of the first series of corner tensile experiments which also appeared in this second series of tests, can now be confirmed to be intrinsic to the cross-section of the specimens and not because of bending effects due to bolt bearing problems in the first series of experiments. Since the current study is concerned with the increase in yield strength due to the cold forming of the corners, the use of stresses compared at the permanent set of 1% plastic strain adequately overcomes the problems of having a long elasto-plastic region of material behaviour for this series of experiments, this does not cause much error since the plastic region of material behaviour is rather linear for the specimens tested.

Further discussion of this series of experiments will be presented in chapter 9 of this thesis.

8.3 CORNER HARDNESS EXPERIMENTS

This set of experiments was conducted with the aim of determining the distribution of yield and ultimate strength over the cross-section of mild steel plates containing cold formed corners. The use of static indentation hardness testing enabled detailed mapping of the hardness over the cross-section to be ascertained and by relating these hardness measurements to yield and ultimate strengths, strength variations could be estimated. Average corner yield and ultimate strengths were also calculated from the detailed data and compared with theoretical predictions.

The set of specimens in these experiments consisted of 16 plate samples containing cold formed corners cut from the same pieces which was used in the corner tensile experiments (series one), the material and section properties of the specimens should therefore be identical to those examined by tensile testing (series one) and comparisons of the results could be made in order to verify the findings from both sets of experiments.

In these experiments, 1.5 inch long specimens were moulded in epoxy resin and subsequently milled and ground to expose smooth flat cross-sections with 45° and 90° corners. Location lines were then marked onto each cross-section as illustrated by figure 8.3.1 and hardness readings were taken along each of these lines.

8.3.1 Method of Hardness Measurement

Hardness readings using an Avery-Denison visual hardness testing machine with a Vickers Pyramidal diamond indentor were then measured along the location lines, 4 to 6 readings were taken along each line, depending on the plate thickness. The Vickers hardness number was used to quantify the hardness, and is calculated from the applied load during indentation divided by the pyramidal area of indentation, using Eqn.(8.3.1) shown below.

$$H_v = 1.8544\frac{p}{d^2} \qquad \text{Eqn.(8.3.1)}$$

where H_v is the Vickers hardness number
p is the applied load
and d is the average diagonal length of the pyramidal indentation.

The hardness test procedure was in accordance to BS EN 23878 and consisted of applying a load of between 1 to 120 kg through the diamond tip indentor for a period of between 10 to 15 seconds, removing the indentor and measuring the diagonal lengths of the indentation left on the surface of the specimen. In order to maximise the number of data points in the relatively small cross-sectional area, the load of 10 kg was selected for these experiments.

A full description of these experiments together with a complete set of the plotted results can be found in Sim [69].

8.3.2 Relationship between Hardness number and Yield / Ultimate Strength

The work of Tabor [71] was employed to approximate the local yield and ultimate strengths of the material from the hardness data. Based on the assumption that the strain hardening region of the material stress-strain curve could be described by the power law, Tabor found that the yield strength of most metals could be estimated by Eqn.(8.3.2), which relates the results from the Vickers hardness test to the yield stress.

$$Y_s = \frac{4 \cdot p}{2.8\pi d^2} \qquad \text{Eqn.(8.3.2)}$$

where Y_s is the material yield strength
p is the load applied during indentation
and d is the average diagonal length of the pyramidal indentation.

And Eqn.(8.3.3) was used to relate the Vickers hardness number to the ultimate tensile strength of the material.

$$U_s = H_v \frac{1-x}{2.9}\left(\frac{12.5x}{1-x}\right)^x \qquad \text{Eqn.(8.3.3)}$$

where U_s is the material ultimate tensile strength
H_v is the Vickers hardness number
and x is the material stress-strain index.

From the expressions, it can be seen that both the approximate yield and ultimate estimates are directly proportional to the Vickers hardness number.

8.3.3 Results (Corner Hardness Experiments)

The vast amount of detailed data collected in this set of experiments made it difficult to present the results from all the 16 specimens examined, two sets of results were selected and presented at the end of this chapter. Each set consists of two subsets, one for the corner and the other for the adjacent flat plate element, and each subset contains :-

1) Table of estimated yield strength at each data point
2) Table of estimated ultimate strength at each data point
3) 3 dimensional plot of estimated yield strength
4) 3 dimensional plot of estimated ultimate strength
5) 2 dimensional plot of the average (for each location line) yield strength
6) 2 dimensional plot of the average (for each location line) ultimate strength

Figures 8.3.2 to 8.3.9 shows the complete set of results for the 2 mm thick specimen with a 90° corner of inside radius 2 mm and figures 8.3.10 to 8.3.17 shows the results for the 3 mm thick specimen with a 90° corner of inside radius of 2 mm.

A summary of the average estimated corner yield and ultimate strengths is presented in table 8.3.1, along with experimental increases in average corner yield strength and theoretical predictions using the work of Karren [23] and Lind and Schroff [30].

Table 8.3.1 : Corner Hardness Experiments

Test No.	Inside Radius (mm)	Thickness (mm)	Angle (Deg)	Element of Specimen	Expt. Average Corner Yield Stress	Expt. Average Corner UTS	Virgin Yield Stress from Hardness Est.	Virgin UTS from Hardness Est.	Virgin (2%) Yield Stress from Tensile Test	Virgin UTS from Tensile Test	Expt % Increase	Karren % Increase	Lind % Increase
1	10	2	45	Corner	326.20	426.87	282.27	369.39	230.57	327.37	19.05	29.73	24.30
				Flat	292.45	382.72	282.27	369.39	230.57	327.37	4.42		
2	12	2	45	Corner	376.09	451.19	282.27	369.39	230.57	327.37	40.69	25.02	20.56
				Flat	290.57	380.25	282.27	369.39	230.57	327.37	3.60		
3	15	2	45	Corner	337.98	422.29	282.27	369.39	230.57	327.37	24.16	19.49	13.63
				Flat	294.35	383.84	282.27	369.39	230.57	327.37	5.24		
4	10	3	45	Corner	400.30	561.27	351.55	492.91	300.53	466.30	16.22	52.06	31.81
				Flat	366.93	514.47	351.55	492.91	300.53	466.30	5.12		
5	12	3	45	Corner	408.54	572.81	351.55	492.91	300.53	466.30	18.96	49.42	39.02
				Flat	392.87	551.24	351.55	492.91	300.53	466.30	13.75		
6	15	3	45	Corner	414.43	581.08	351.55	492.91	300.53	466.30	20.92	43.07	31.92
				Flat	388.58	544.03	351.55	492.91	300.53	466.30	12.32		
7	2	2	90	Corner	353.76	462.89	282.27	369.39	230.57	327.37	31.01	71.76	76.36
				Flat	287.32	375.99	282.27	369.39	230.57	327.37	2.19		
8	4	2	90	Corner	353.74	462.94	282.27	369.39	230.57	327.37	31.00	56.16	53.45
				Flat	281.07	367.81	282.27	369.39	230.57	327.37	-0.52		
9	6	2	90	Corner	348.78	457.40	282.27	369.39	230.57	327.37	28.85	43.85	29.45
				Flat	270.27	353.67	282.27	369.39	230.57	327.37	-5.20		
10	2	3	90	Corner	428.71	601.17	351.55	492.91	300.53	466.30	25.67	114.66	91.86
				Flat	369.07	517.48	351.55	492.91	300.53	466.30	5.83		
11	4	3	90	Corner	541.08	780.89	351.55	492.91	300.53	466.30	63.07	85.04	60.46
				Flat	367.39	515.13	351.55	492.91	300.53	466.30	5.27		
12	6	3	90	Corner	439.60	587.31	351.55	492.91	300.53	466.30	29.30	65.93	61.97
				Flat	369.25	517.18	351.55	492.91	300.53	466.30	5.89		
13	12	2	45	Corner	325.53	426.00	282.27	369.39	230.57	327.37	18.76	25.02	20.56
				Flat	295.56	388.09	282.27	369.39	230.57	327.37	5.76		
14	4	2	90	Corner	321.08	440.83	282.27	369.39	230.57	327.37	16.83	56.16	53.45
				Flat	295.74	387.01	282.27	369.39	230.57	327.37	5.84		
15	4	1.6	90	Corner	456.26	661.77	282.27	409.42	444.43	548.76	39.15	16.22	13.60
				Flat	387.32	416.74	282.27	409.42	444.43	548.76	23.64		
16	6	2.5	90	Corner	467.39	634.97	434.37	590.1	486.02	546.26	6.79	16.22	13.80
				Flat	446.38	606.41	434.37	590.1	486.02	546.26	2.47		

Note : - All Stresses in N/mm^2.

- Virgin Stresses from Hardness estimation were derived from Hardness measurements taken in regions of the specimen remote from the cold formed corners.
- All Experimental Corner Stress Increases were calculated taking the Stresses from Hardness estimation as Virgin.
- % Increases are the improvements in Corner Yield Stresses over the Virgin Yield Strength.

8.3.4 Observations and Comments (Corner Hardness Experiments)

The use of hardness measurements to estimate the material strengths achieved the primary objective of harvesting relatively detailed mappings of the distribution of the varying degree of increase in material yield stress due to cold work, the thinness of the plates limited the number of data points across the thickness of the specimens, thus preventing the realisation of the true distribution of strain over the thickness and the location of the neutral fibre, however, the technique served well in obtaining the variations in material properties along the length of the bend and adjacent flats.

The use of the simple expressions of Tabor [71] to approximate the values of the yield and ultimate strength from the hardness numbers may not have given result of high accuracy, this was evident from the differences found comparing the data with that obtained through simple tensile testing of identical material, however, the precision of the expressions used is not critical if data from the hardness tests were used only as a gauge of the amount of increase in strength rather than strength in absolute terms. Taking the estimated yield and ultimate strengths calculated using Eqn.(8.3.2) and Eqn.(8.3.3) of a remote point some distance from the corners of the specimen as the datum, the increases in strengths at various points in the vicinity of the corners can be worked out and this difference can then used to estimate the corner strengths, this method would work well assuming that the hardness numbers are linearly proportional to the yield and ultimate stresses.

It was observed from examining the plots that in both the yield and ultimate strengths, the regions with the elevated strengths tended to end 2 mm to 3 mm from the edge of the bent material, it can also be seen in table 8.3.1 that the average strengths in the 10 mm long flats elements adjacent to the corners are in most cases only slightly above the virgin strengths. It is therefore quite correct to assume that all the effects of cold

working during the forming of the corners are in fact concentrated within the 45° or 90° arc of the corners.

The experimental plots shows that the strengths within the arc of the bend does vary, with the peak strengths occurring at the toe of the corners (mid length on the arc of the bend), the maximum yield stress can reach values of up to 1.8 times the virgin yield strength, which can be much higher than even the ultimate tensile strength of the virgin material. The strengths are also generally higher at the outer fibres of the corners, which is to be expected since the strains applied during cold forming are larger in those regions.

The increases in the yield strength of the corners found in this set of corner hardness experiments are generally smaller than those found in the corner tensile experiments. The corner yield stress estimates were in reasonable agreement with those found in the tensile experiments but by considering the differences between the estimated corner yield strengths and the estimate virgin yield stress (derived by the same method for a point remote to the corner region) as the increase in strength, the percentage increases in yield were rather low.

From the results in table 8.3.1, it can be seen that both the theoretical methods of predicting corner strength by Karren [23] and Lind and Schroff [30] produced some results with large differences from the experimental findings, in a number of cases, the theories overestimates the corner strengths by quite a large margin, this brought about some doubt in the dependability of these two theories in the prediction of the corner strengths.

The findings from this set of corner hardness experiments will be discussed further in chapter 9 of this thesis.

8.4 STRAIN HARDENING IN PLASTIC HINGES

In the plastic mechanism theory presented in chapter 2 of this thesis, the rigid-perfectly plastic material model was employed, in which strain hardening was not accounted for. This assumption is perfectly acceptable if the strains within the beams were relatively small, but during the formation of the plastic collapse mechanisms, the material at the outer fibres of the plastic hinges can experience very high levels of strain, in which case, neglecting the strain hardening effect of the material could lead to significant errors, especially if the margin between the yield and ultimate strength of the actual beam material is large. This section details a simple method of accounting for the additional resisting moment in the plastic hinges due to material strain hardening.

The technique starts off by assuming that the plate material behaviour can be idealised as a rigid-linear strain hardening material with the ultimate tensile stress occurring at approximately 15% strain, as shown in figure 8.4.1. The plastic stress at any strain can then be estimated by Eqn.(8.4.1)

$$\sigma_{sh} = \sigma_o + E_p \cdot \varepsilon \qquad \text{Eqn.(8.4.1)}$$

where the plastic modulus is given by

$$E_p = \frac{(\sigma_{ult} - \sigma_o)}{0.15} \qquad \text{Eqn.(8.4.2)}$$

where σ_{ult} is the material ultimate tensile strength.

It is further assumed that the material behaves in the same manner under compression as it would under tension. Considering the plate bending at the plastic hinges to be purely flexural, the stress distribution across the thickness of the plate can be idealised as that shown in figure 8.4.2. The strain varies linearly across the thickness, maximum strain occurring at the extreme fibres which can be found using Eqn.(8.4.3).

$$\varepsilon_e = \frac{y}{R} = \frac{\left(\frac{t}{2}\right)}{\vartheta \cdot t} = \frac{1}{2\vartheta} \qquad \text{Eqn.(8.4.3)}$$

where y is the distance of the fibre from the neutral axis
and ϑ is the ratio of the mean corner radius of bend to the thickness.

The stress at the extreme fibres can then be found using Eqn.(8.4.1) and the plastic plate bending moment capacity can be estimated by Eqn.(8.4.4).

$$m_{psh} = \frac{\sigma_o \cdot t^2}{4} + (\sigma_e - \sigma_o)\frac{t^2}{6} \qquad \text{Eqn.(8.4.4)}$$

where σ_e is the stress corresponding to ε_e at the extreme fibres.

According to equations presented above, and taking that the ultimate tensile stress of the material occurs at 15% strain, a mean corner radius to thickness ratio of 3.333 would bring the stress at the outer fibres to the ultimate tensile strength. In the experimental investigations, the observed radius to thickness ratios were as small as 2 in some cases and in the mechanism theory presented in chapter 2, it was assumed that the rolling mechanism lines would maintain their original radii (in the manufactured state).

For the purpose of the current work, it was assumed that the extreme fibre stresses at the yield lines of the plastic mechanisms could be estimated to be equal to the ultimate tensile material strength, this would allow Eqn.(8.4.4) to be simplified to :

$$m_{psh} = \frac{\sigma_o \cdot t^2}{4} + (\sigma_{ult} - \sigma_o)\frac{t^2}{6} \qquad \text{Eqn.(8.4.5)}$$

The plate moment capacity found from Eqn.(8.4.5) was used to replace the fully plastic plate moment, m_p in the equations used for the plastic mechanism analysis presented in chapters 2, 3, 4 and 5 of this thesis. This simple approach produced plastic mechanism loads which agreed well with the experimental findings of beam collapse behaviour, this was seen in chapter 7 where the results were compared.

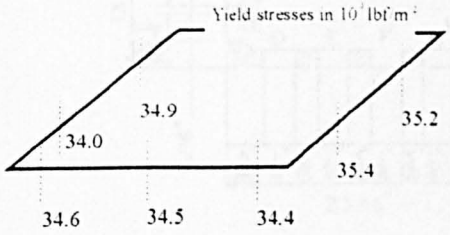

a) Lipped Channel

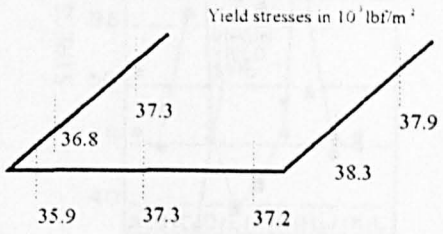

b) Plain Channel

Figure 8.1.1

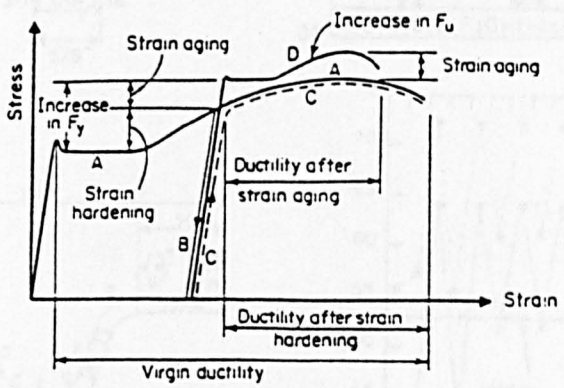

Figure 8.1.3 : Effects of Strain Hardening and Strain Ageing

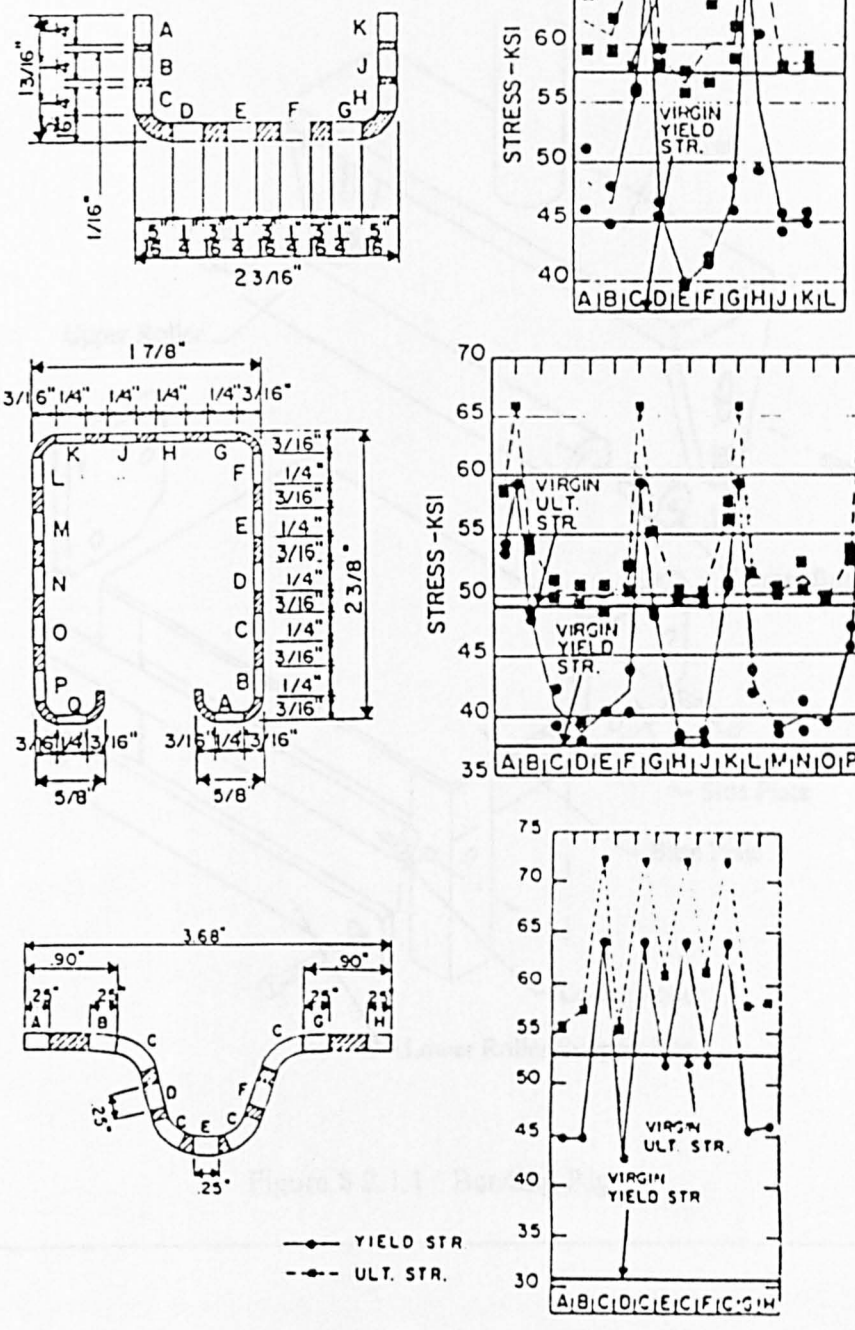
13/16"
1/16"
23/16"
A
B
C
D
E
F
G
H
J
K
STRESS-KSI
VIRGIN ULT. STR.
VIRGIN YIELD STR.
A|B|C|D|E|F|G|H|J|K|L
1 7/8"
3/16" 1/4" 1/4" 1/4" 1/4" 3/16"
23/8"
5/8"
L
M
N
O
P
Q
A|B|C|D|E|F|G|H|J|K|L|M|N|O|P|Q
3.68"
.90"
.25"
YIELD STR
ULT. STR.

Figure 8.1.2

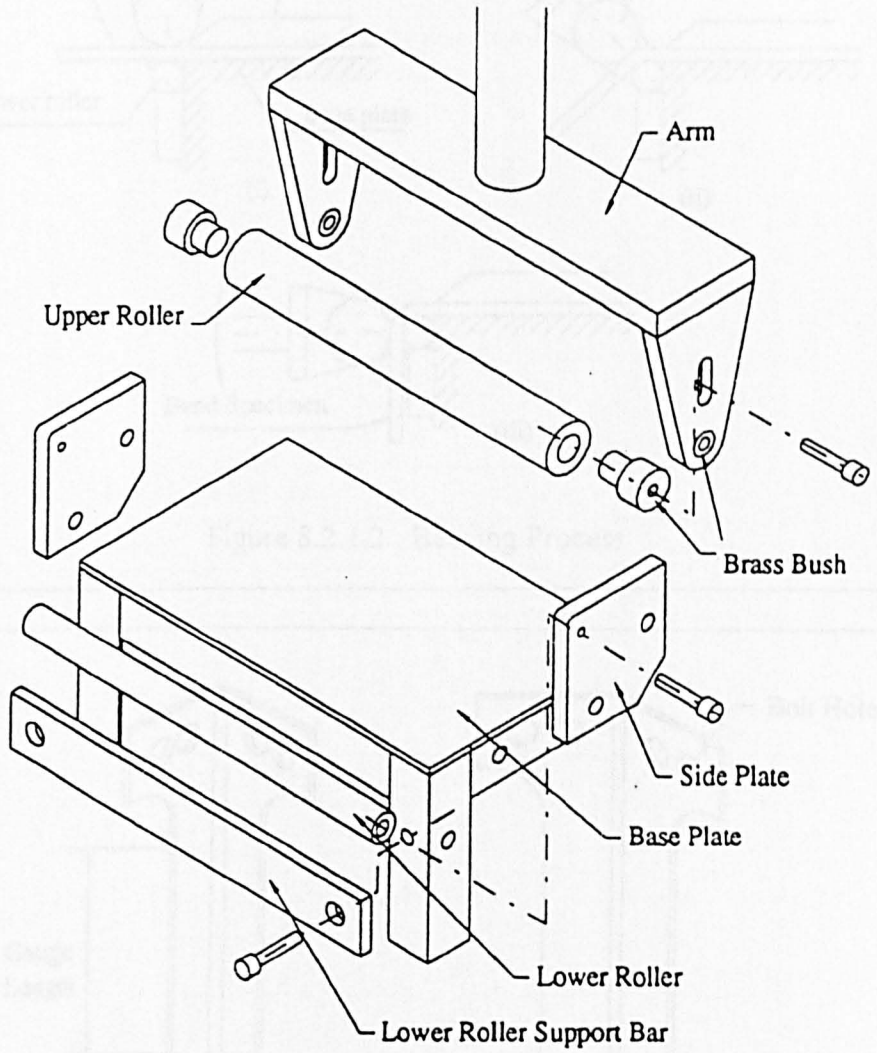

Figure 8.2.1.1 : Bending Rig

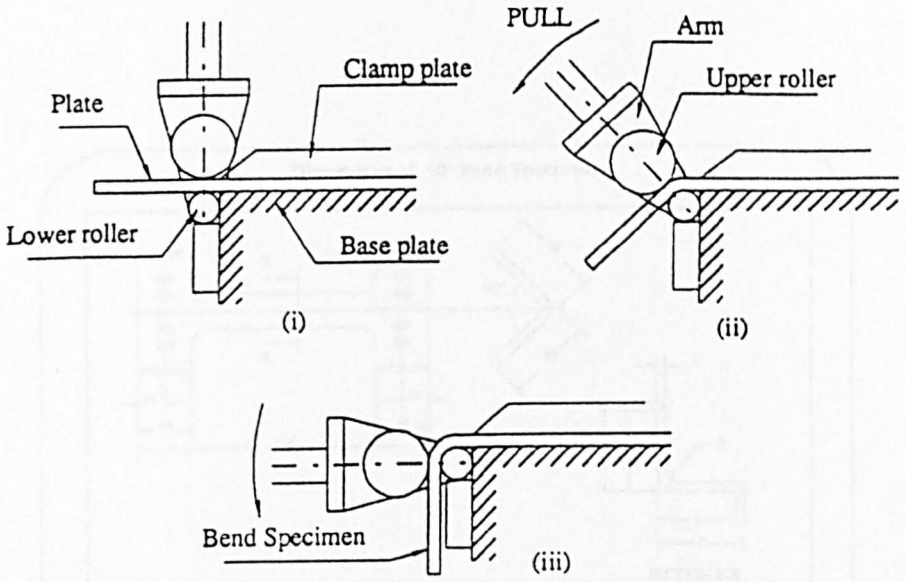

Figure 8.2.1.2 : Bending Process

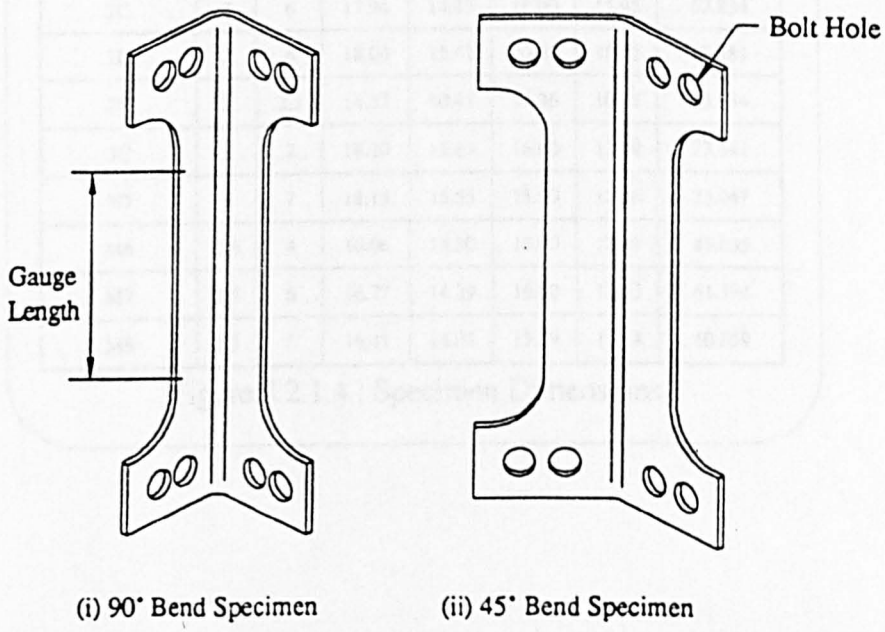

Figure 8.2.1.3 : Corner Specimens (Series One)

Dimensions of 90° Bend Specimens

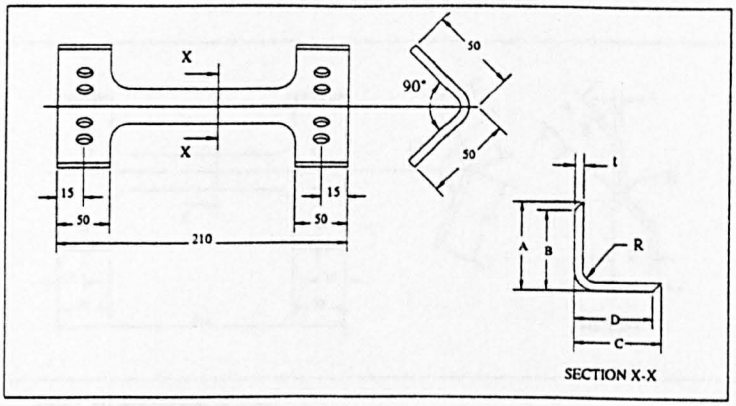

Note : All dimensions in mm

Specimen No.	t	R	A	B	C	D	Area (total)
2A	2	4	16.83	15.76	19.12	17.27	61.834
2B	2	4	17.20	14.94	18.91	16.91	61.212
2C	2	6	17.94	14.87	18.00	15.95	57.834
2D	2	6	18.00	15.62	20.08	18.22	63.181
2E	2	2.5	14.53	10.41	14.36	10.85	53.054
3C	3	7	18.20	15.63	16.00	12.49	73.541
3D	3	7	18.13	15.55	15.90	12.38	73.047
M6	1.6	4	16.06	14.50	15.00	13.19	43.035
M7	2.5	6	16.77	14.39	16.00	13.33	61.594
M8	2.5	6	16.41	14.01	15.79	13.18	60.859

Figure 8.2.1.4 : Specimen Dimensions

Dimensions For 45 ° Bend Specimens

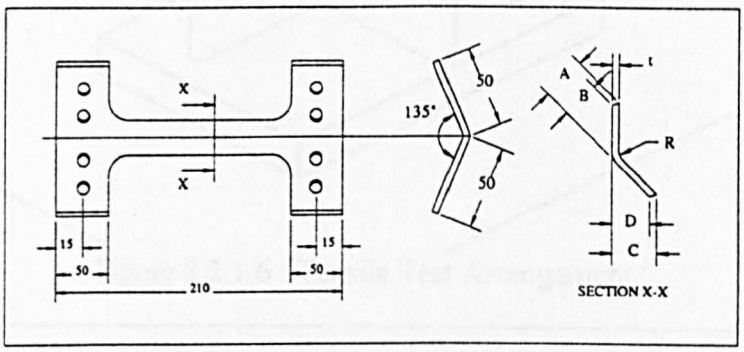

Note : All dimensions in mm

Specimen No.	t	R	A	B	C	D	Area (total)
2H	2	8	11.12	9.11	11.30	9.31	52.137
2I	2	8	12.14	10.22	10.00	7.93	52.383
2J	2	10	12.53	10.63	10.10	8.01	52.791
2K	2	10	11.88	9.92	11.18	8.50	52.157
2L	2	12	12.46	10.53	10.50	8.43	51.891
2M	2	12	12.44	10.51	10.60	8.53	52.141
3G	3	12	13.62	10.69	12.30	9.23	78.921
3H	3	12	13.75	10.82	12.50	7.89	78.743
3I	3	15	13.39	10.43	12.70	9.66	78.111
3J	3	15	14.20	11.38	11.20	8.04	78.526

Figure 8.2.1.5 : Specimen Dimensions

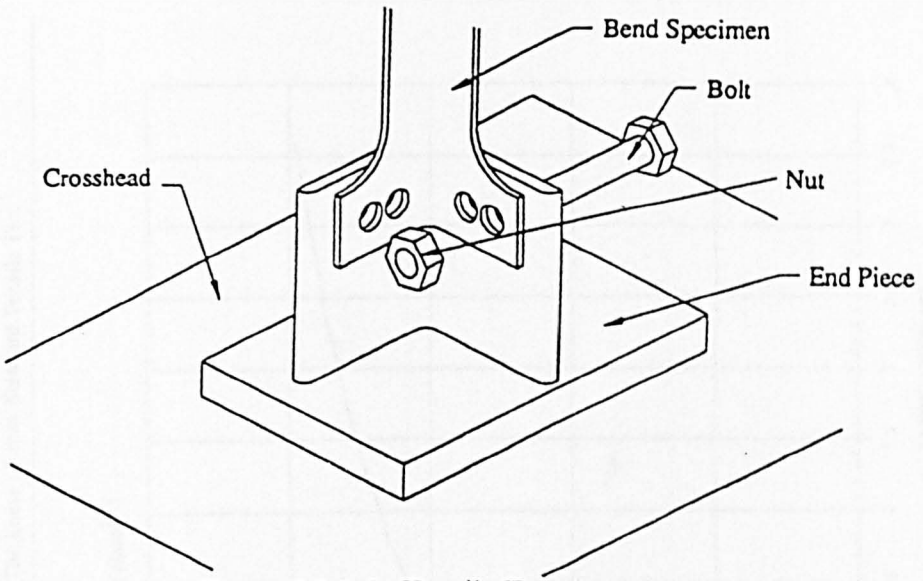

Figure 8.2.1.6 : Tensile Test Arrangement

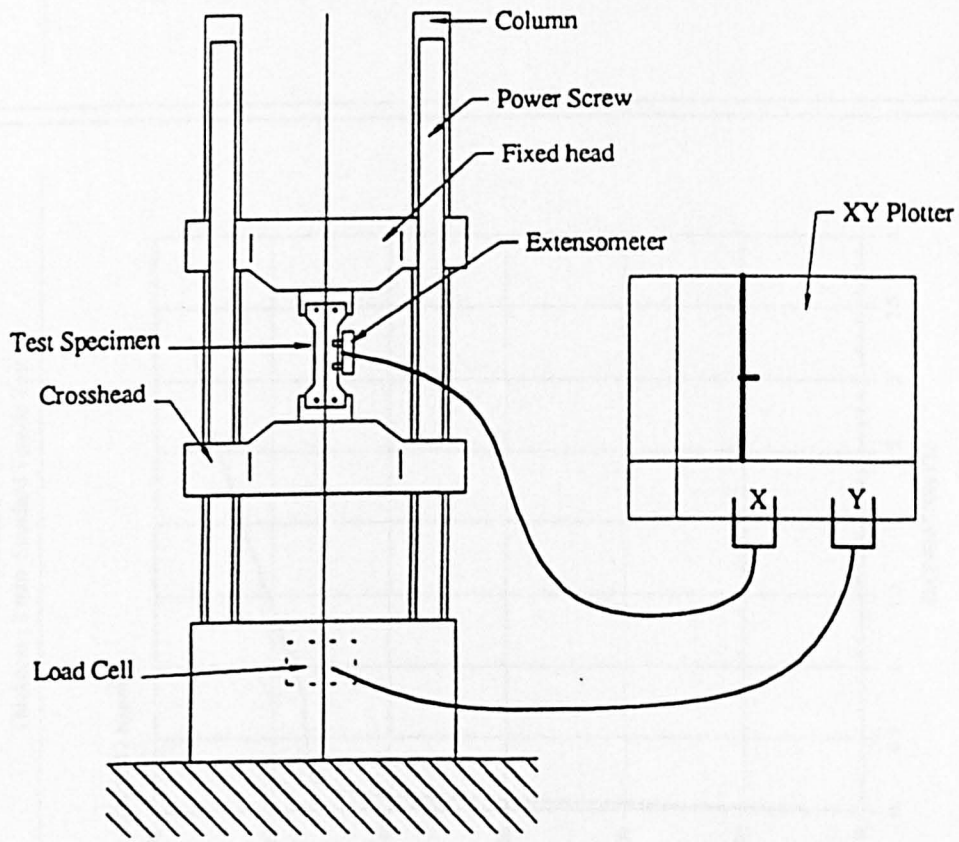

Figure 8.2.1.7 : Instrument Layout

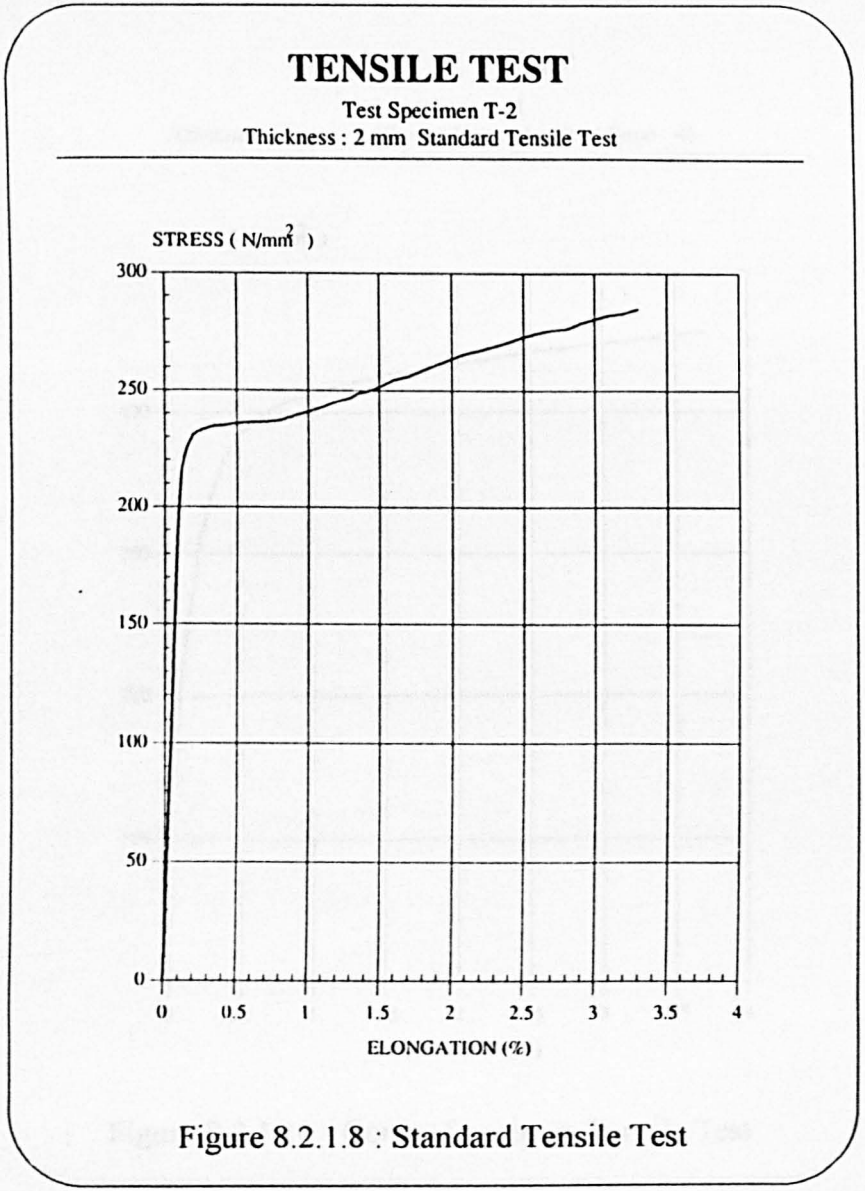

Figure 8.2.1.8 : Standard Tensile Test

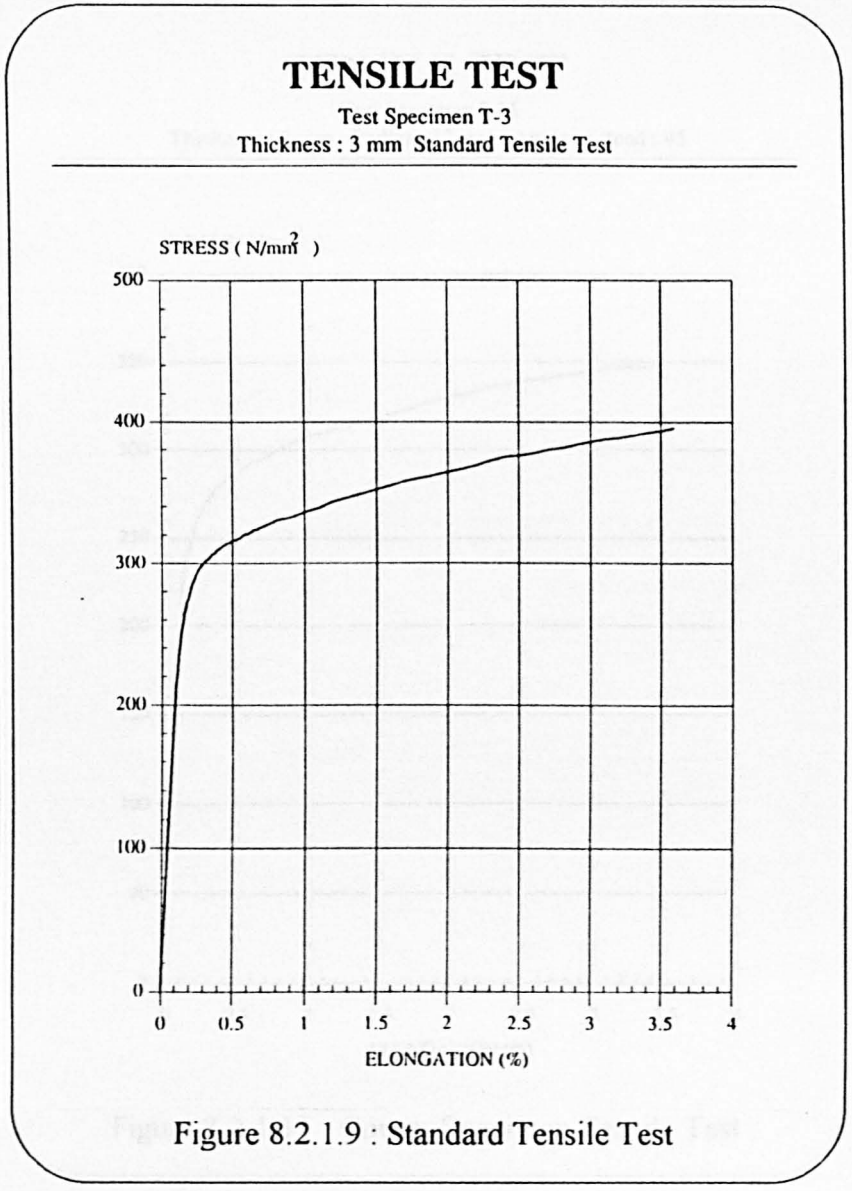

Figure 8.2.1.9 : Standard Tensile Test

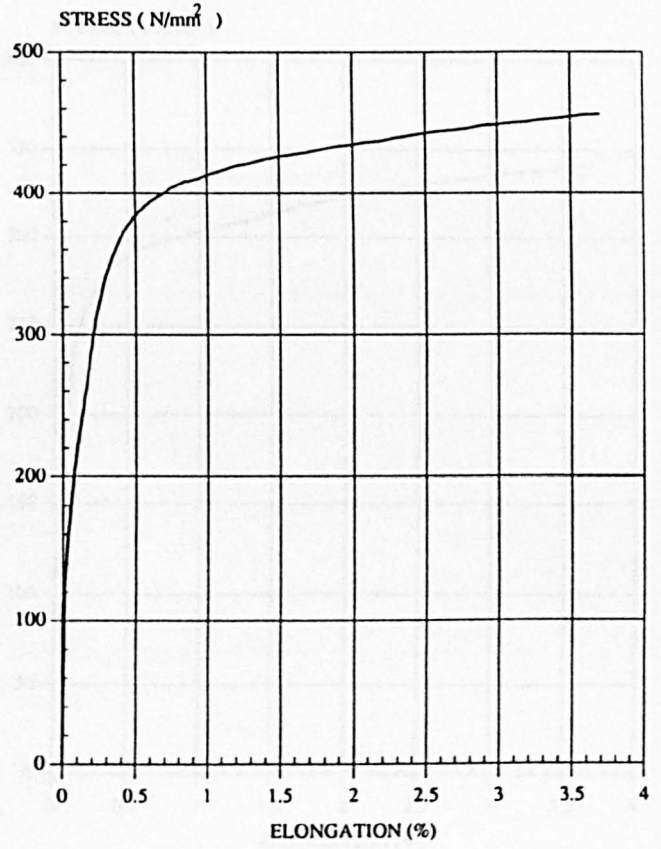

Figure 8.2.1.10 : Corner Specimen Tensile Test

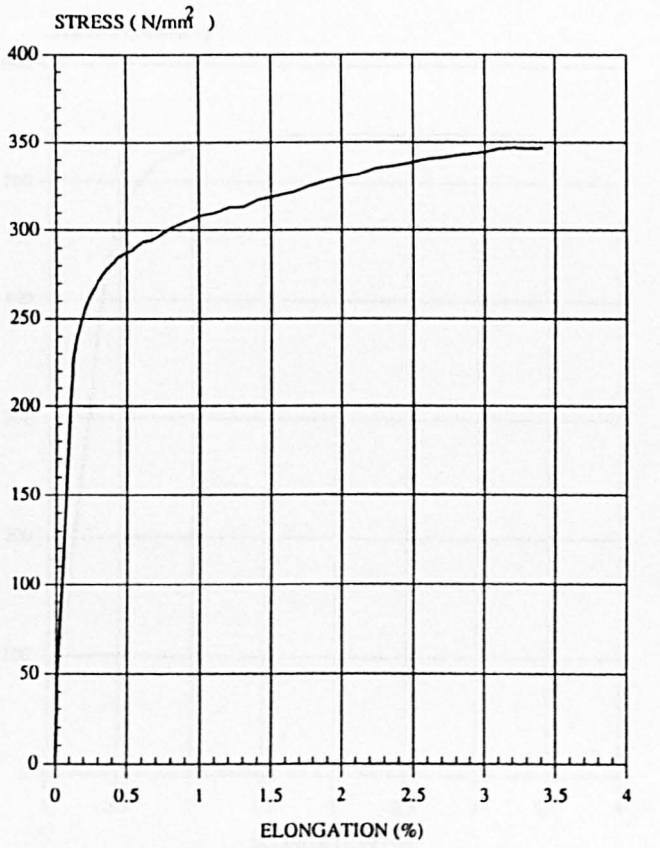

Figure 8.2.1.11 : Corner Specimen Tensile Test

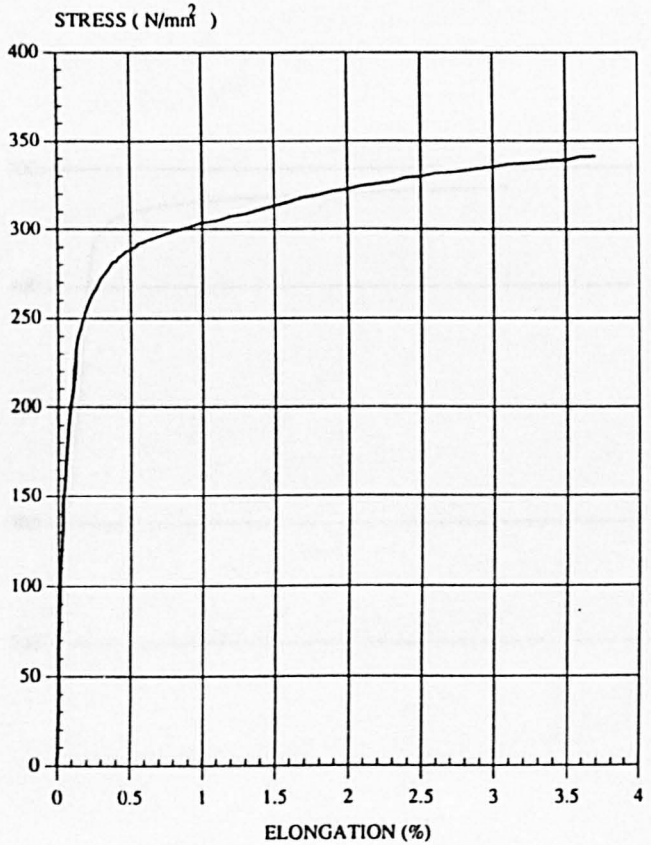

Figure 8.2.1.12 : Corner Specimen Tensile Test

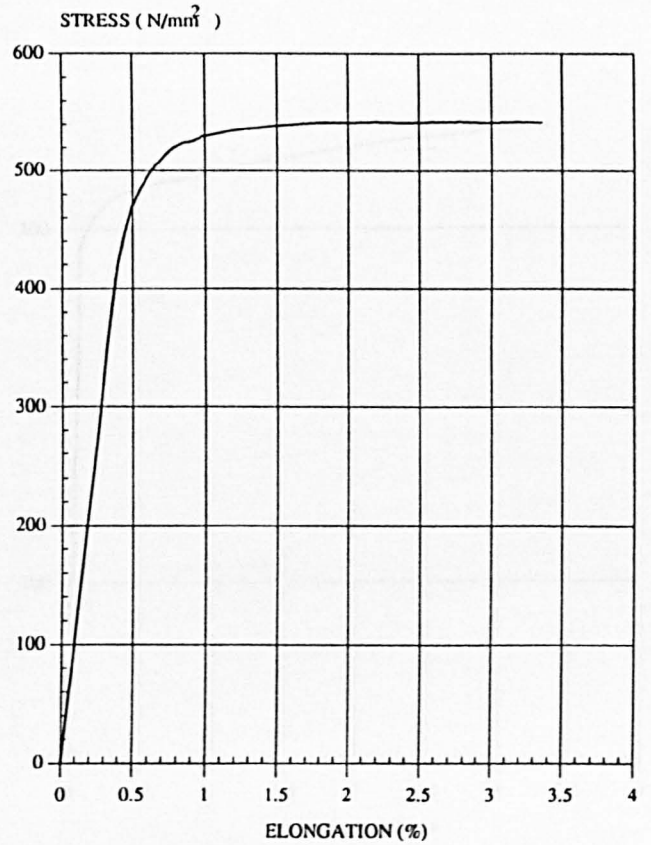

Figure 8.2.1.13 : Corner Specimen Tensile Test

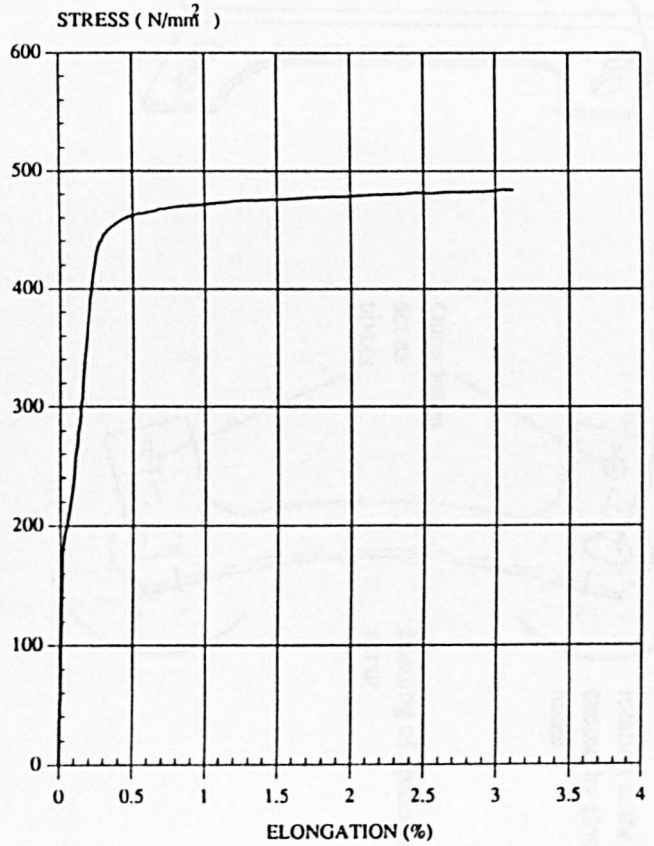

Figure 8.2.1.14 : Corner Specimen Tensile Test

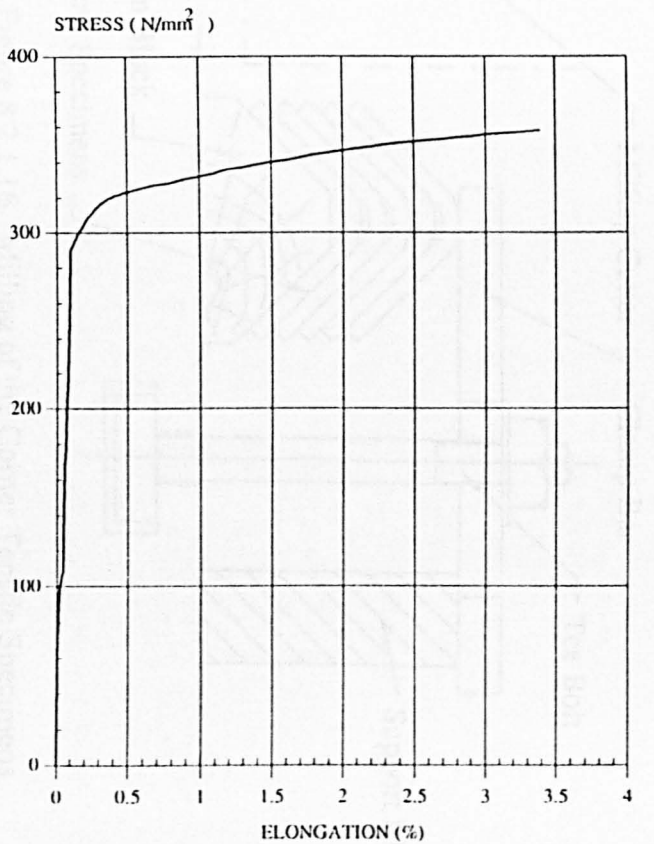

Figure 8.2.1.15 : Corner Specimen Tensile Test

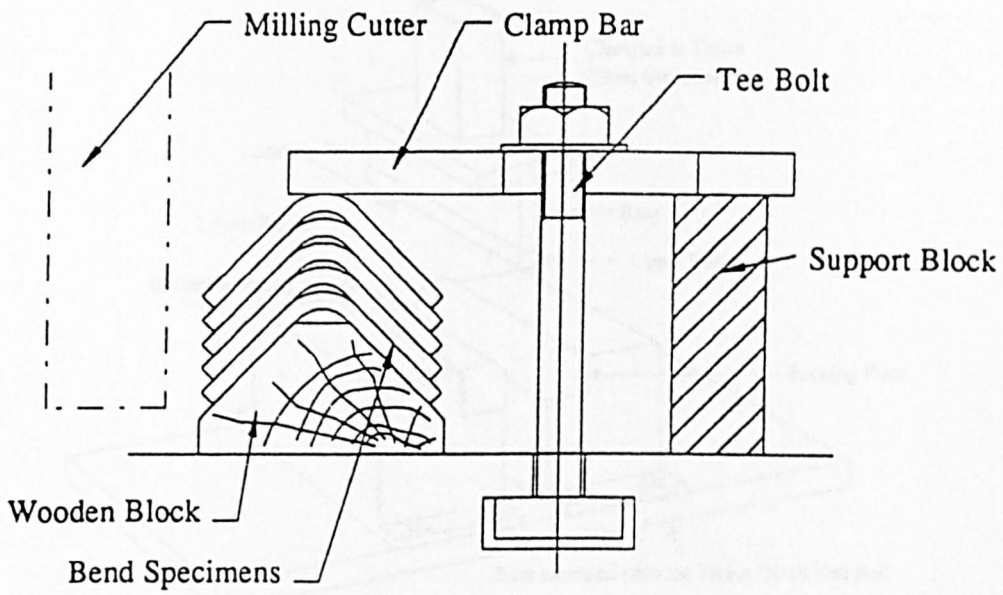

Figure 8.2.1.16 : Milling of the Corner Tensile Specimens

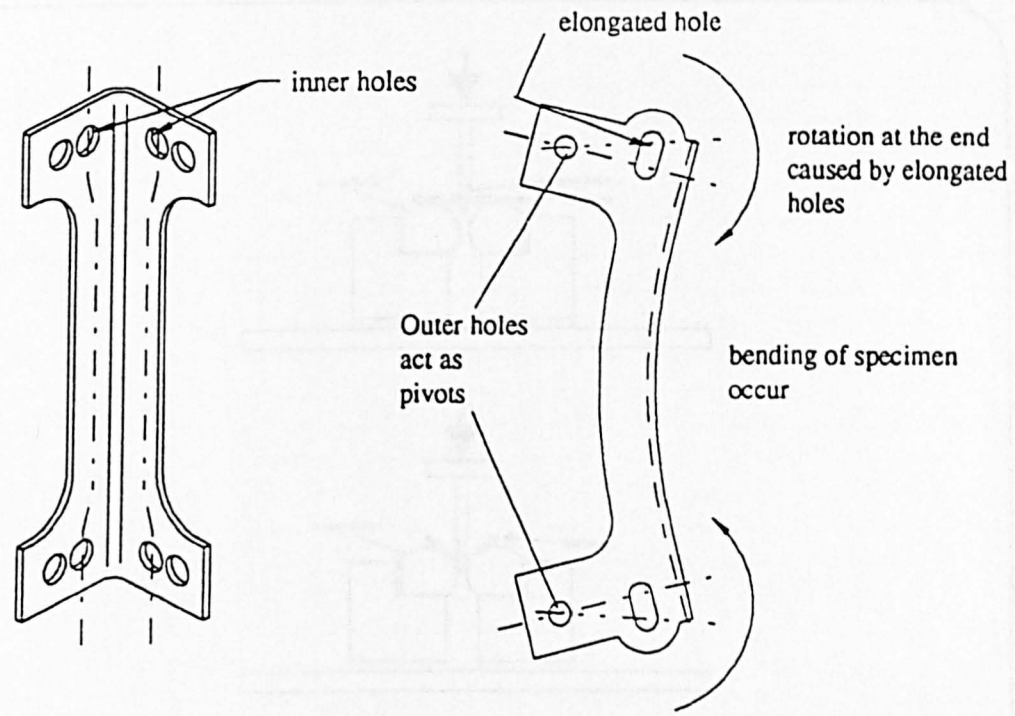

Figure 8.2.1.17 : Bolt Hole Bearing Effect

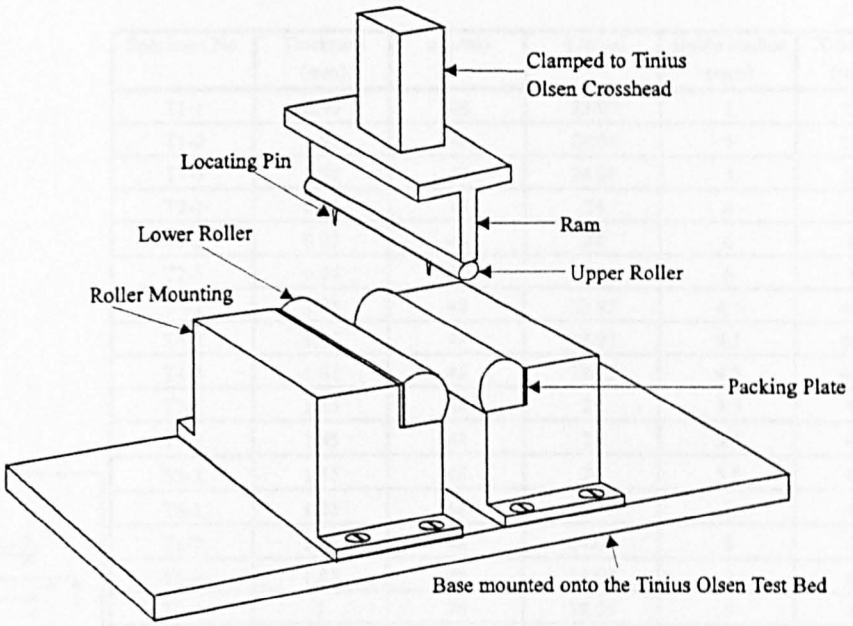

Figure 8.2.2.1 : Air Braking Bending Rig

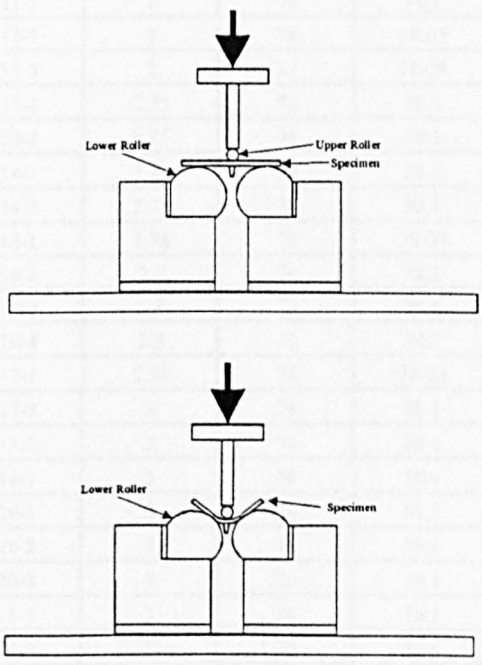

Figure 8.2.2.2 : Air Braking Process

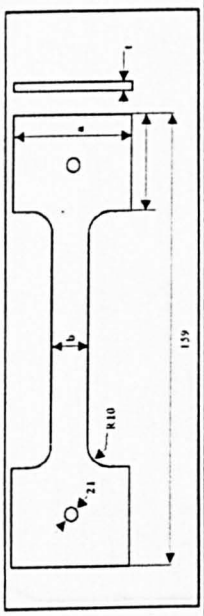

Specimen No.	Thickness (mm)	a (mm)	b (mm)	Inside Radius (mm)	X-Sect Area (mm^2)
T1-1	0.95	48	23.97	5	22.77
T1-2	0.95	48	24.08	5	22.88
T1-3	0.95	48	24.06	5	22.86
T2-1	0.95	48	24	6	22.8
T2-2	0.95	48	24	6	23.3
T2-3	0.95	48	24	6	22.8
T4-1	1.85	48	23.95	4.5	44.34
T4-2	1.85	48	23.95	4.5	44.34
T4-3	1.85	48	23.95	4.5	44.34
T5-1	1.85	48	24	5.5	44.4
T5-2	1.85	48	24	5.5	44.4
T5-3	1.85	48	24	5.5	44.4
T6-1	1.85	48	24.05	8	44.5
T6-2	1.85	48	24.05	8	44.5
T6-3	1.85	48	24.05	8	44.5
T7-1	2	76	38.05	5	76.1
T7-2	2	76	38.05	5	76.1
T9-1	2.05	76	37.7	5.5	77.2
T9-2	2.05	76	37.7	5.5	77.2
T10-1	2.05	76	37.9	8	77.6
T10-2	2.05	76	37.9	8	77.6
T11-1	2	76	38.1	10.5	76.2
T11-2	2	76	38.05	10.5	76.1
T11-3	2	76	38.05	10.5	76.1
T13-1	2.75	76	38.1	5.5	104.77
T13-2	2.75	76	38.1	5.5	104.77
T14-1	2.78	76	38.1	8	106
T14-2	2.78	76	38.1	8	106
T16-1	2.78	76	38.07	10.5	105.83
T16-2	2.8	76	38.1	10.5	106.86
T16-3	2.8	76	38.1	10.5	106.86
T16-4	2.8	76	38.1	10.5	106.86
T17-1	2.98	76	38.05	5.5	113.39
T17-2	3	76	38.1	5.5	114.15
T18-1	3	76	38.1	8	114.3
T18-2	3	76	38.1	8	114.3
T20-1	3	76	38.1	10.5	114.3
T20-2	3	76	38.1	10.5	114.3
T20-3	3	76	38.1	10.5	114.3
T21-1	3	76	38.1	15.5	114.3
T21-2	3	76	38.1	15.5	114.3
T21-3	3	76	38.1	15.5	114.3

Figure 8.2.2.3 : Specimen Dimensions

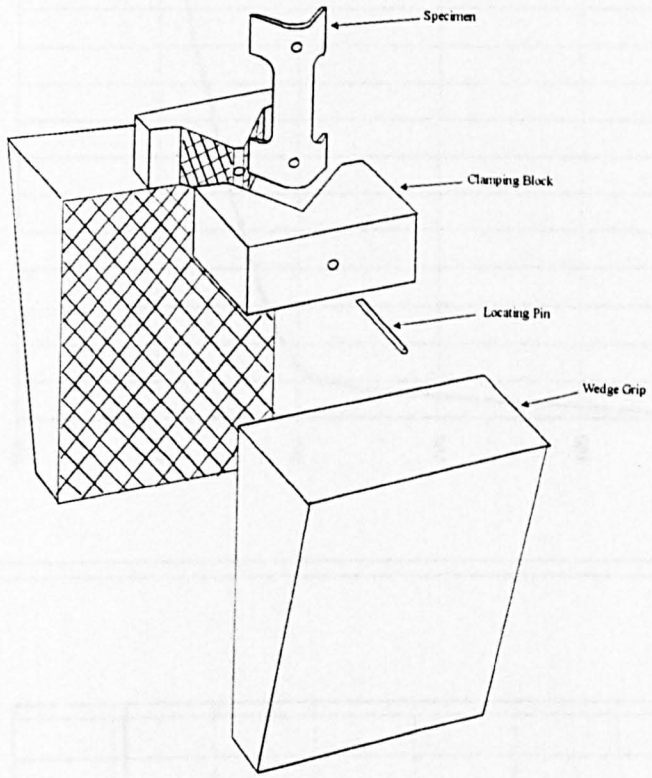

Figure 8.2.2.4 : Clamping Arrangement

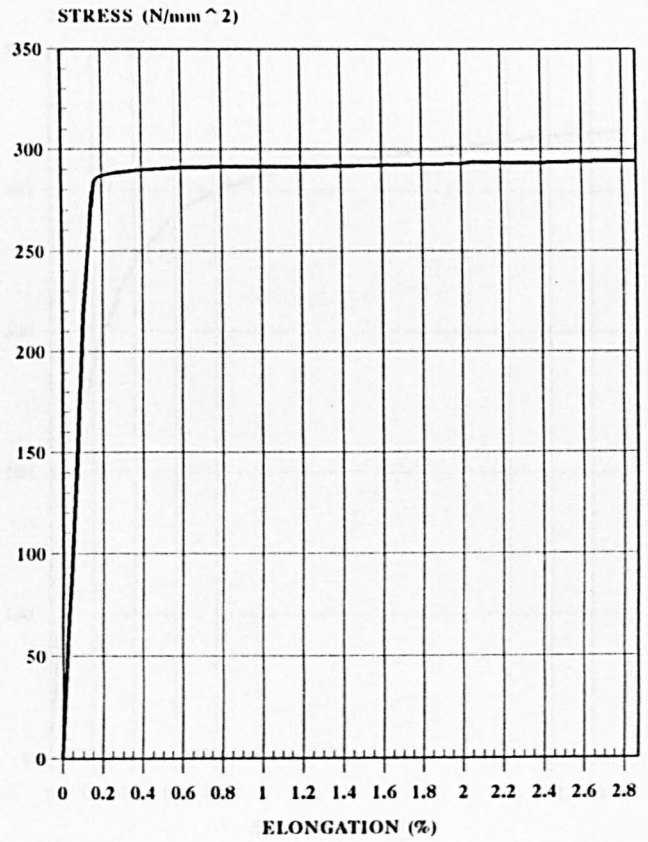

Figure 8.2.2.5 : Standard Tensile Test

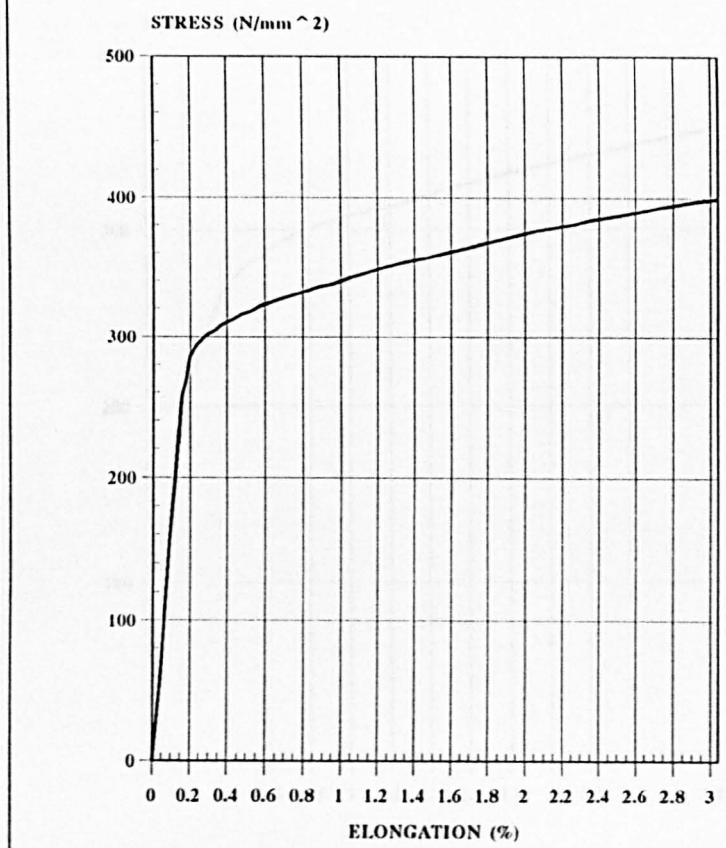

Figure 8.2.2.6 : Standard Tensile Test

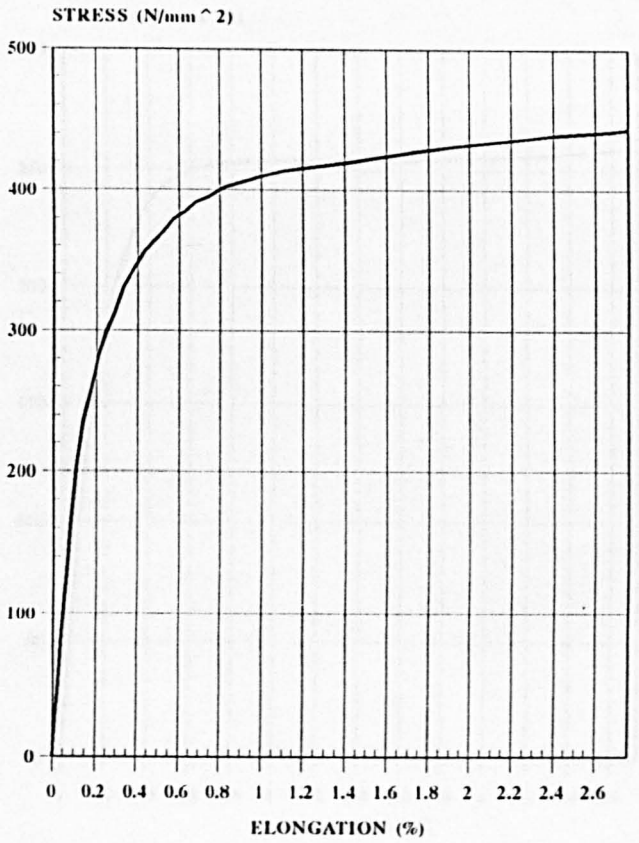

Figure 8.2.2.7 : Corner Specimen Tensile Test

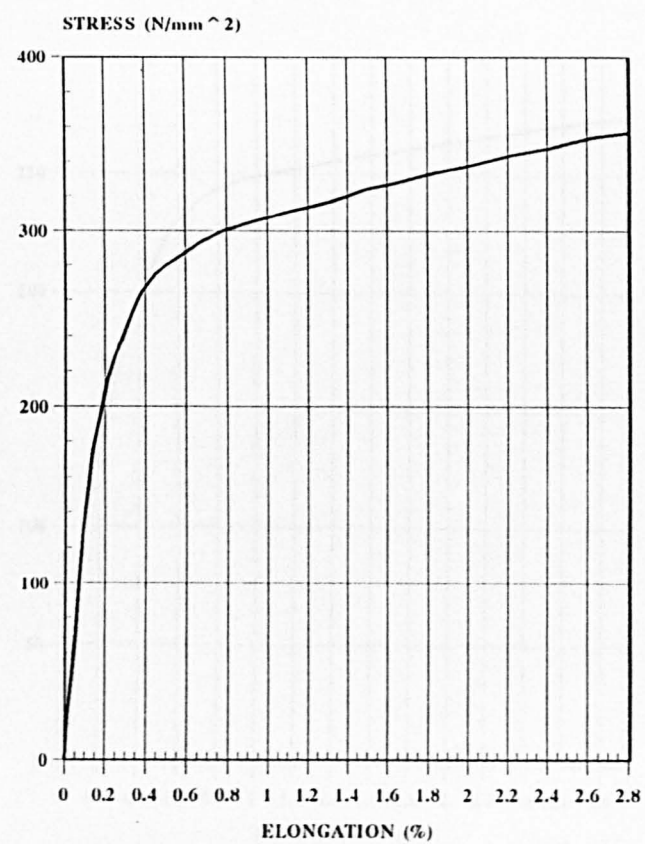

Figure 8.2.2.8 : Corner Specimen Tensile Test

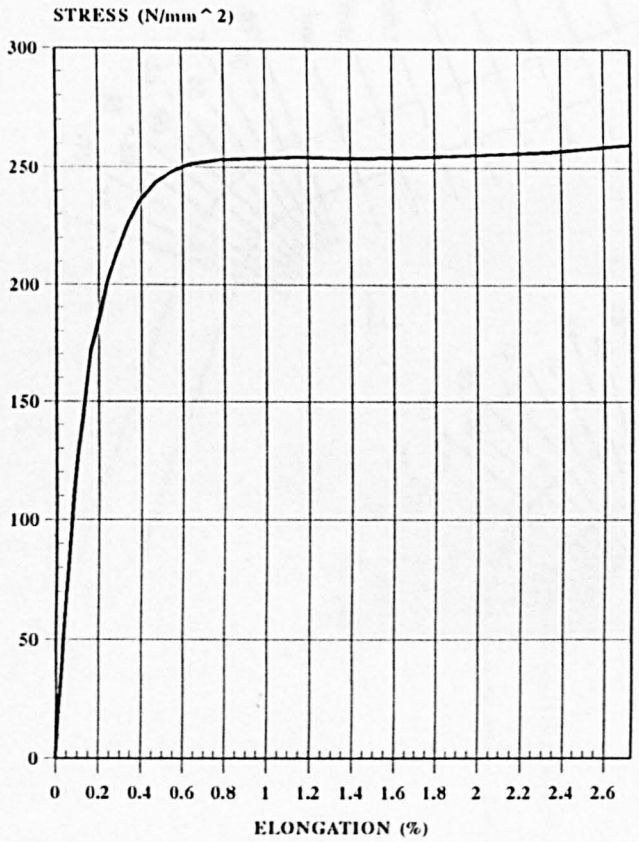

Figure 8.2.2.9 : Corner Specimen Tensile Test

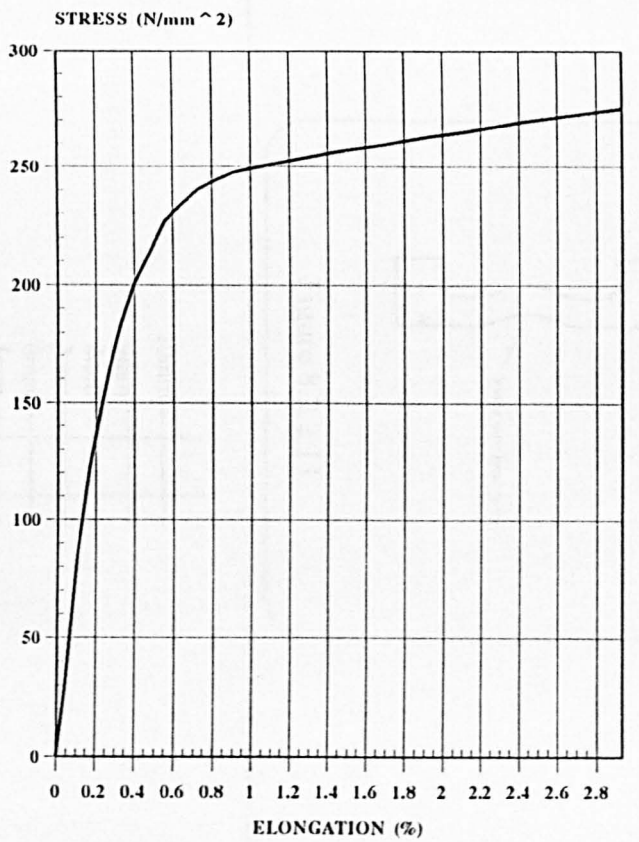

Figure 8.2.2.10 : Corner Specimen Tensile Test

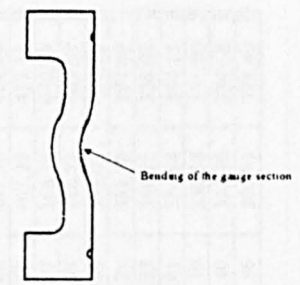

Figure 8.2.2.11

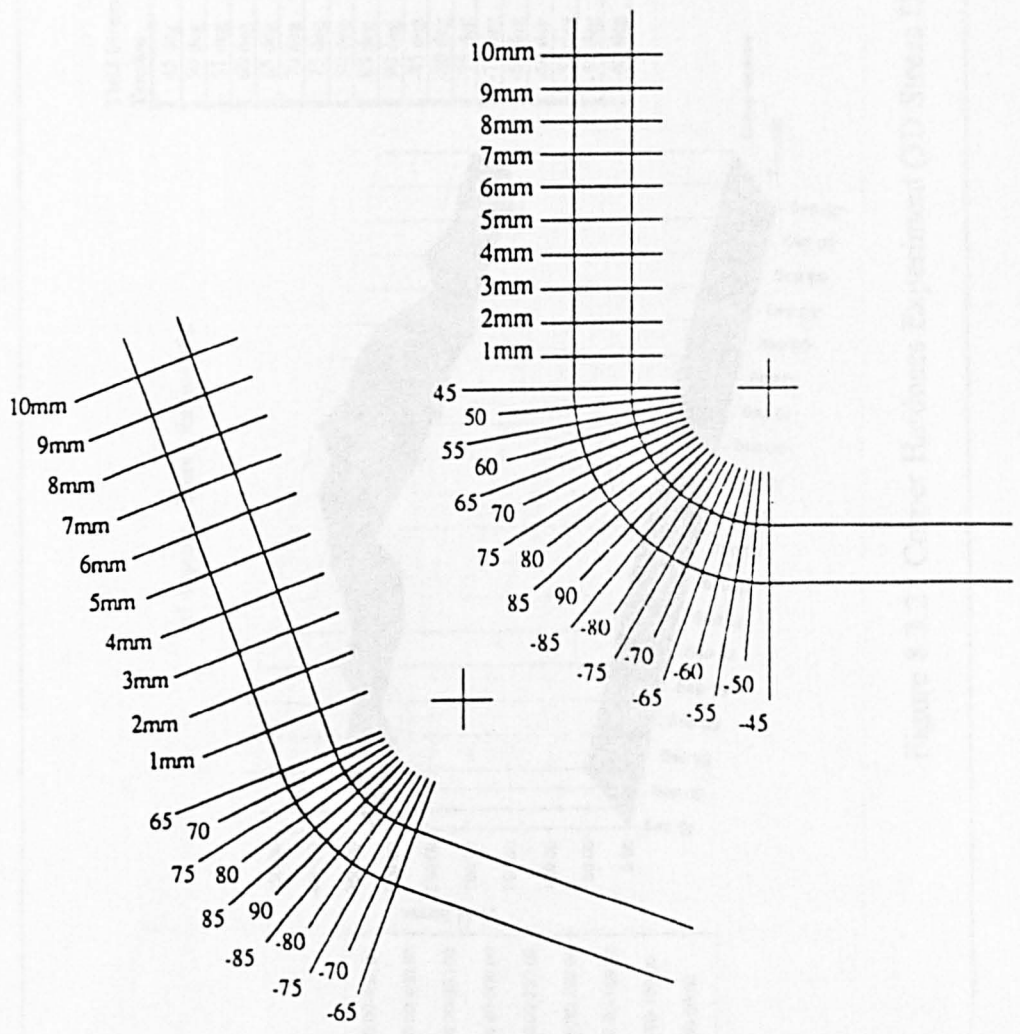

Figure 8.3.1 : Location Lines on Corner Hardness Specimens

Yield Stress (N/mm²)

Tension				Compression
45 deg	324.10	324.10	300.95	313.86
50 deg	317.22	291.79	293.29	313.86
55 deg	340.41	297.85	310.56	315.53
60 deg	364.15	334.84	318.92	344.20
65 deg	351.98	325.85	327.62	338.54
70 deg	351.98	336.68	334.84	360.03
75 deg	346.12	334.84	346.12	388.17
80 deg	399.88	344.20	348.06	402.28
85 deg	414.64	399.88	402.28	424.94
90 deg	430.24	372.62	402.28	417.18
-85 deg	414.64	355.97	366.24	446.73
-80 deg	422.33	351.98	446.73	409.63
-75 deg	362.08	357.99	333.01	417.18
-70 deg	372.62	342.30	331.20	397.49
-65 deg	366.24	320.63	346.12	336.68
-60 deg	353.97	350.01	334.84	364.15
-55 deg	370.48	324.10	338.54	331.20
-50 deg	348.06	329.40	322.36	336.68
-45 deg	333.01	313.86	300.95	329.40

Figure 8.3.2 : Corner Hardness Experiment (3D Stress Distribution)

Ultimate Tensile Strength (N/mm²)

Tension				Compression
45 deg	424.12	424.12	393.84	410.73
50 deg	415.12	381.84	383.80	410.73
55 deg	445.47	389.78	406.40	412.92
60 deg	476.54	438.18	417.34	450.43
65 deg	460.61	426.42	428.73	443.02
70 deg	460.61	440.59	438.18	471.14
75 deg	452.95	438.18	452.95	507.97
80 deg	523.29	450.43	455.48	526.44
85 deg	542.61	523.29	526.44	556.09
90 deg	563.02	487.62	526.44	545.94
-85 deg	542.61	465.83	479.28	584.61
-80 deg	552.68	460.61	584.61	536.05
-75 deg	473.83	468.48	435.79	545.94
-70 deg	487.62	447.94	433.42	520.17
-65 deg	479.28	419.58	452.95	440.59
-60 deg	463.21	458.04	438.18	476.54
-55 deg	484.82	424.12	443.02	433.42
-50 deg	455.48	431.06	421.84	440.59
-45 deg	435.79	410.73	393.84	431.06

Figure 8.3.3 : Corner Hardness Experiment (3D Stress Distribution)

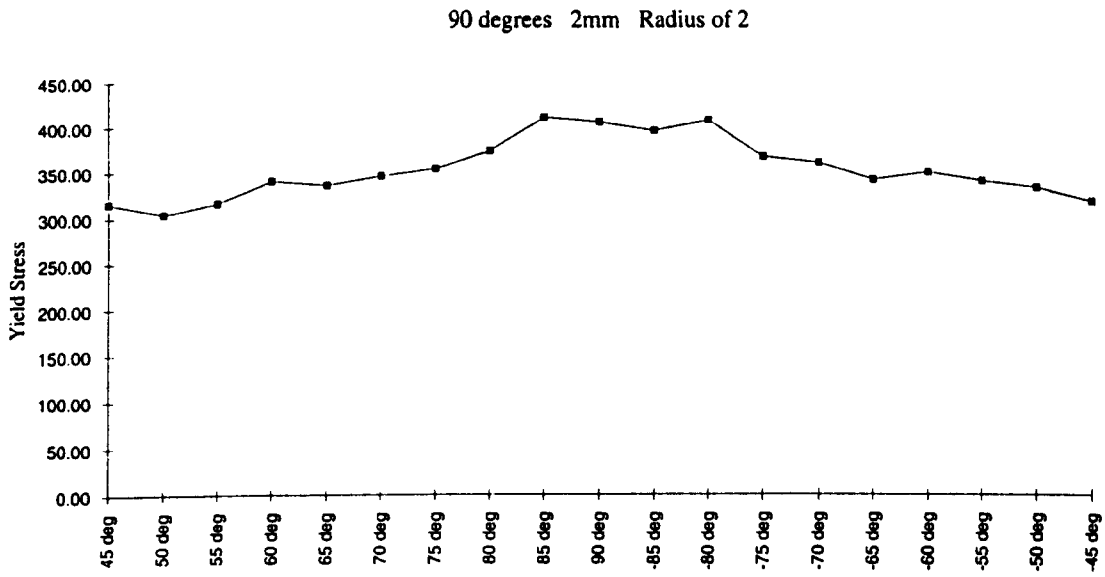

Figure 8.3.4 : Stress Distribution

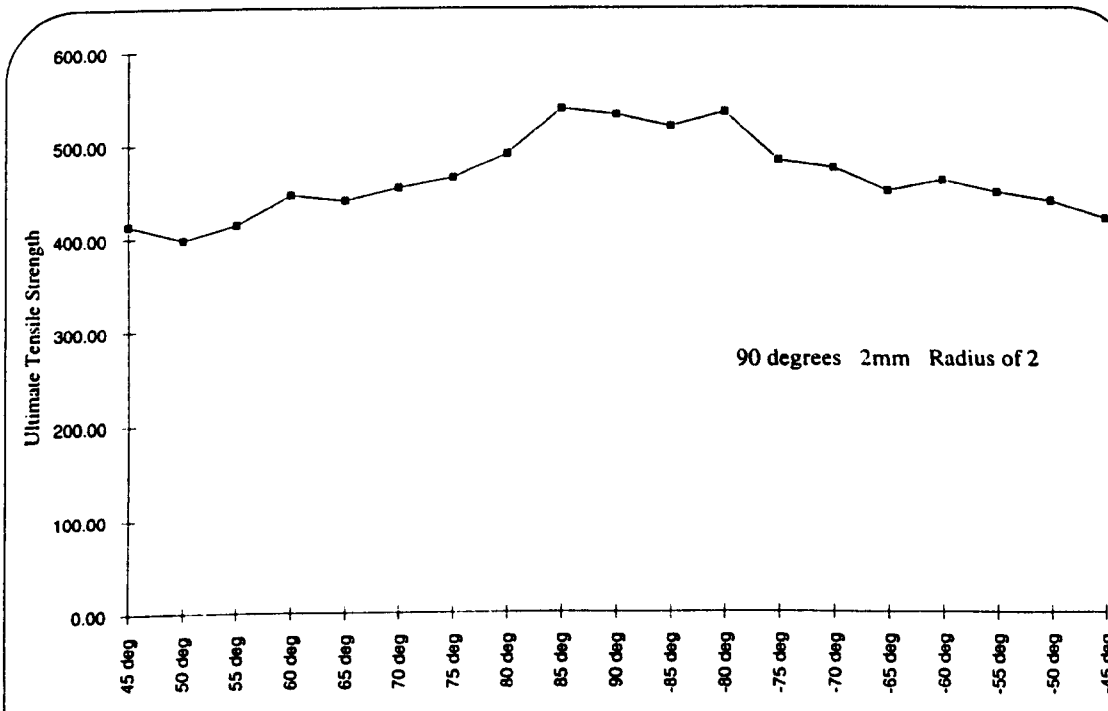

Figure 8.3.5 : Stress Distribution

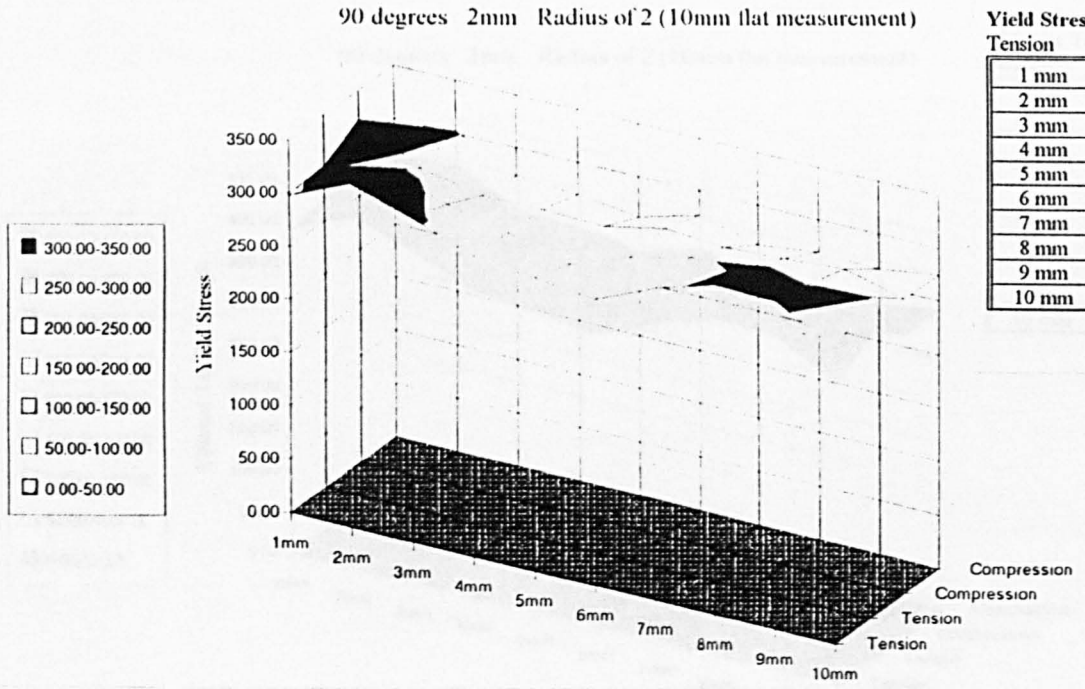

Yield Stress (N/mm²)

Tension				Compression
1 mm	297.85	302.52	322.36	293.29
2 mm	322.36	312.20	290.30	302.52
3 mm	304.10	293.29	277.42	273.31
4 mm	281.61	280.20	278.81	269.30
5 mm	274.67	264.08	276.04	261.53
6 mm	267.98	284.47	287.36	277.42
7 mm	291.79	297.85	284.47	262.80
8 mm	308.93	302.52	287.36	269.30
9 mm	307.31	299.40	290.30	266.67
10 mm	277.42	300.59	276.04	274.67

Figure 8.3.6 : Corner Hardness Experiment (3D Stress Distribution)

Ultimate Tensile Strength (N/mm²)

Tension				Compression
1 mm	389.78	395.89	421.84	383.80
2 mm	421.84	408.56	379.90	395.89
3 mm	397.96	383.80	363.03	357.66
4 mm	368.53	366.68	364.85	352.41
5 mm	359.44	345.58	361.23	342.24
6 mm	350.68	372.26	376.05	363.03
7 mm	381.84	389.78	372.26	343.91
8 mm	404.27	395.89	376.05	352.41
9 mm	402.15	391.80	379.90	348.97
10 mm	363.03	393.84	361.23	359.44

Figure 8.3.7 : Corner Hardness Experiment (3D Stress Distribution)

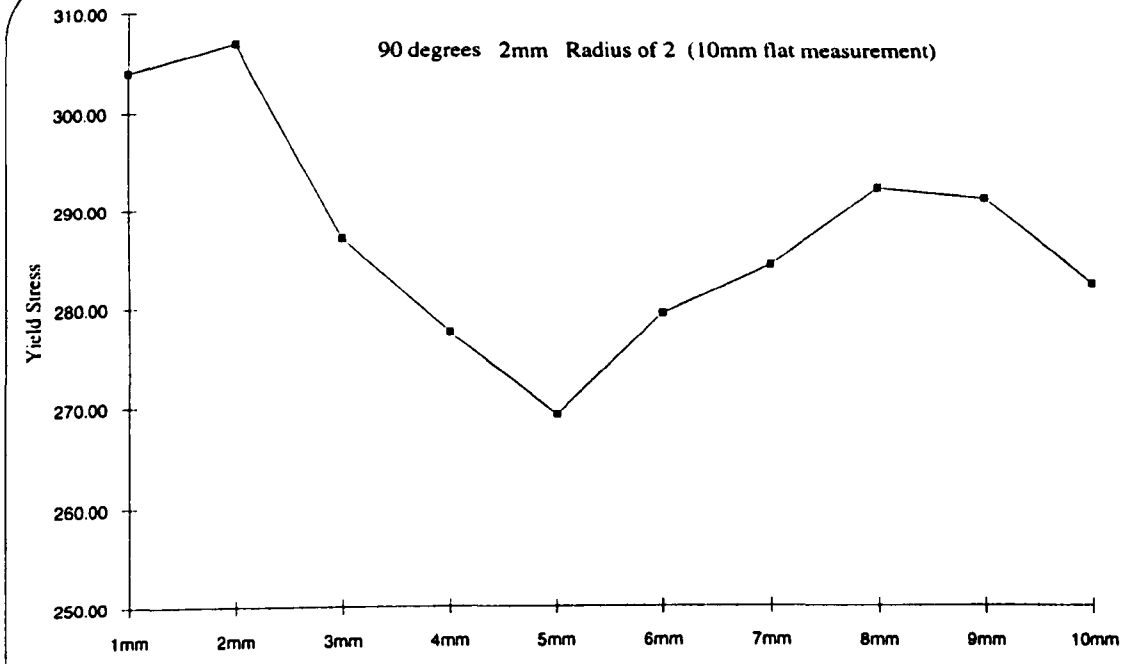

Figure 8.3.8 : Stress Distribution

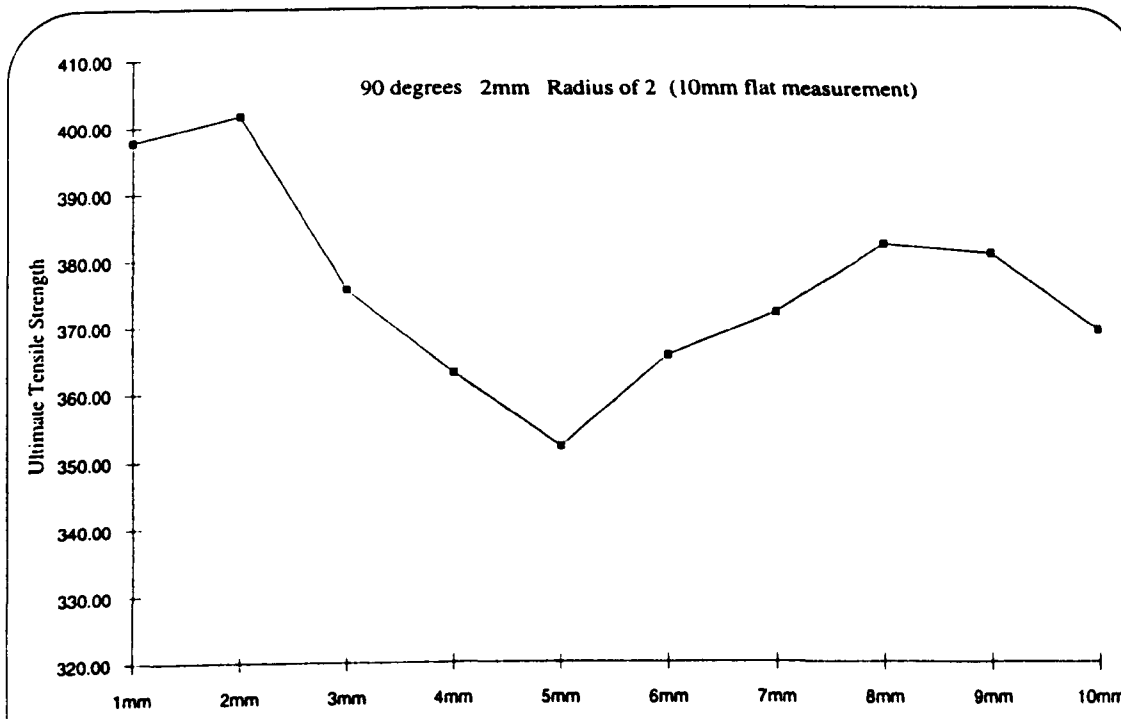

Figure 8.3.9 : Stress Distribution

Yield Stress (N/mm²)

Tension						Compression
45 deg	432.92	407.16	366.24	364.15	412.13	402.28
50 deg	441.13	412.13	372.62	376.97	430.24	432.92
55 deg	422.33	412.13	397.49	399.88	412.13	443.92
60 deg	438.37	422.33	399.88	414.64	412.13	455.34
65 deg	419.75	449.57	414.64	376.97	395.13	458.26
70 deg	458.26	414.64	392.79	390.47	417.18	443.92
75 deg	438.37	430.24	409.63	376.97	419.75	435.63
80 deg	464.19	427.58	381.39	390.47	467.20	485.89
85 deg	530.43	464.19	404.71	407.16	452.44	473.31
90 deg	516.09	476.41	432.92	395.13	482.70	498.97
-85 deg	495.65	461.21	381.39	404.71	438.37	461.21
-80 deg	492.37	438.37	419.75	424.94	455.34	476.41
-75 deg	495.65	438.37	397.49	427.58	452.44	489.11
-70 deg	473.31	441.13	424.94	409.63	427.58	461.21
-65 deg	432.92	409.63	379.17	419.75	446.73	458.26
-60 deg	430.24	424.94	424.94	390.47	430.24	458.26
-55 deg	430.24	441.13	388.17	370.48	417.18	458.26
-50 deg	424.94	417.18	392.79	388.17	412.13	443.92
-45 deg	424.94	419.75	404.71	392.79	432.92	449.57

Figure 8.3.10 : Corner Hardness Experiment (3D Stress Distribution)

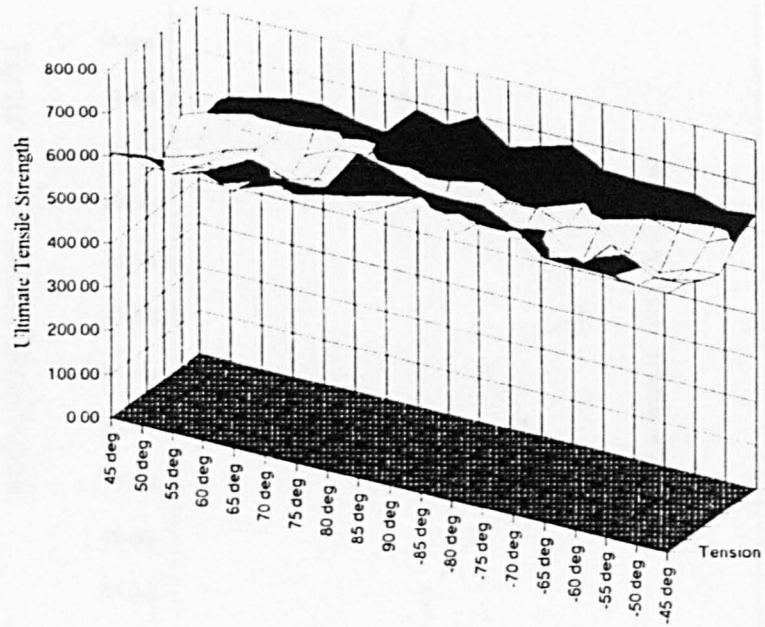

Ultimate Tensile Strength (N/mm²)

Tension						Compression
45 deg	607.01	570.88	513.51	510.58	577.85	564.05
50 deg	618.51	577.85	522.46	528.55	603.24	607.01
55 deg	592.16	577.85	557.33	560.67	577.85	622.42
60 deg	614.64	592.16	560.67	581.37	577.85	638.43
65 deg	588.53	630.35	581.37	528.55	554.02	642.53
70 deg	642.53	581.37	550.74	547.48	584.94	622.42
75 deg	614.64	603.24	574.35	528.55	588.53	610.81
80 deg	650.85	599.51	534.75	547.48	655.07	681.27
85 deg	743.72	650.85	567.45	570.88	634.37	663.63
90 deg	723.62	667.98	607.01	554.02	676.79	699.62
-85 deg	694.96	646.67	534.75	567.45	614.64	646.67
-80 deg	690.35	614.64	588.53	595.82	638.43	667.98
-75 deg	694.96	614.64	557.33	599.51	634.37	685.79
-70 deg	663.63	618.51	595.82	574.35	599.51	646.67
-65 deg	607.01	574.35	531.64	588.53	626.37	642.53
-60 deg	603.24	595.82	595.82	547.48	603.24	642.53
-55 deg	603.24	618.51	544.26	519.45	584.94	642.53
-50 deg	595.82	584.94	550.74	544.26	577.85	622.42
-45 deg	595.82	588.53	567.45	550.74	607.01	630.35

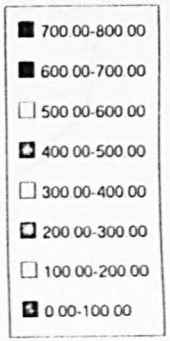

Figure 8.3.11 : Corner Hardness Experiment (3D Stress Distribution)

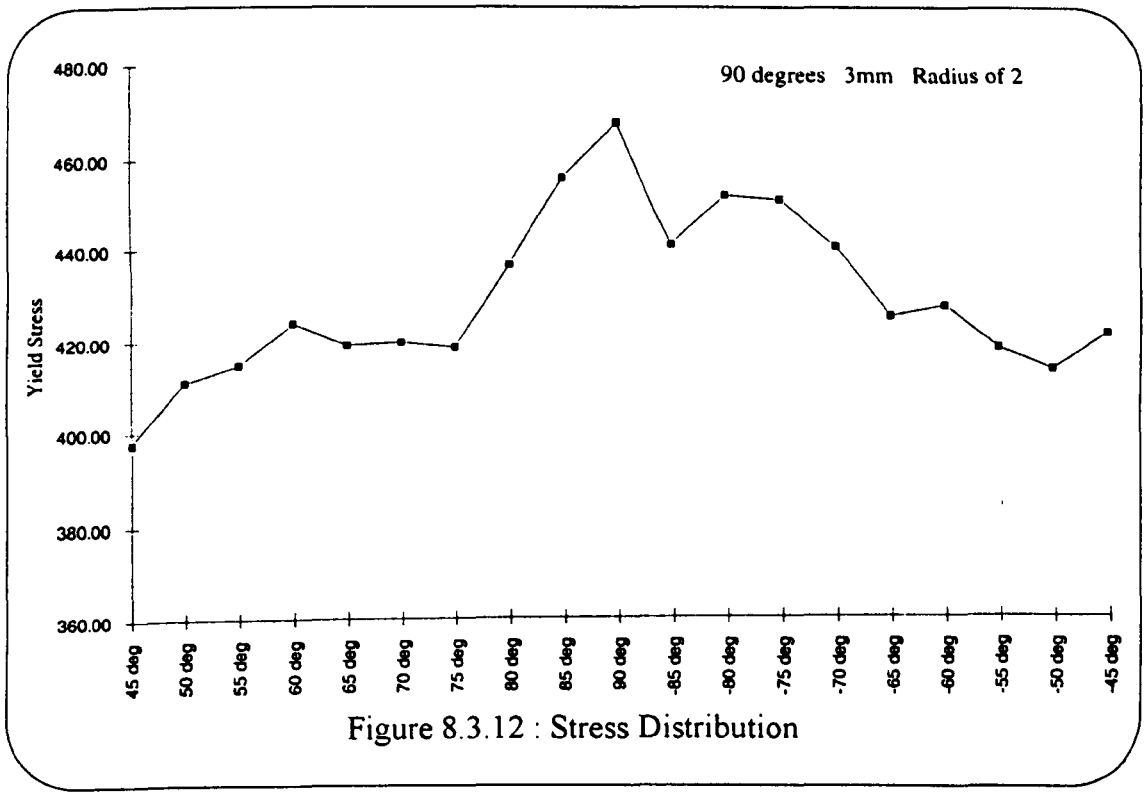

Figure 8.3.12 : Stress Distribution

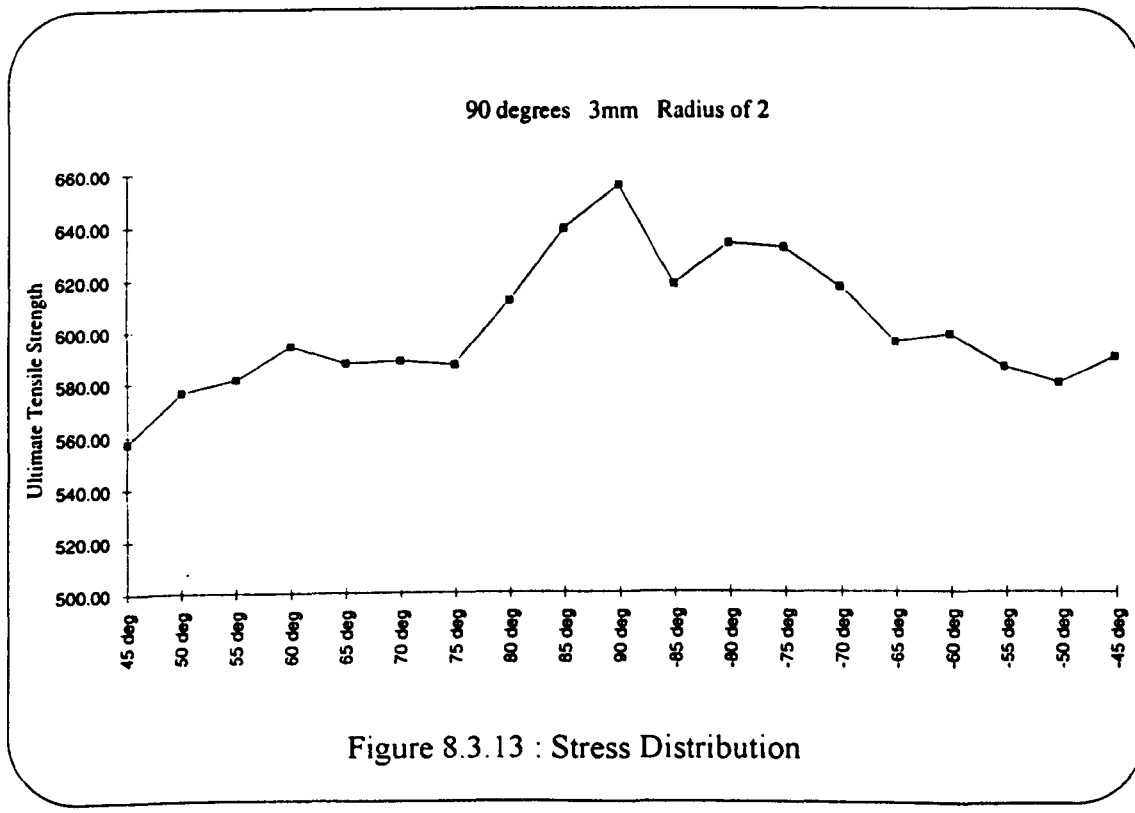

Figure 8.3.13 : Stress Distribution

Yield Stress (N/mm²)

Tension						Compression
1 mm	461.21	427.58	404.71	353.97	385.89	424.94
2 mm	412.13	417.18	360.03	374.79	399.88	402.28
3 mm	407.16	372.62	355.97	362.08	385.89	368.35
4 mm	355.97	357.99	348.06	355.97	368.35	350.01
5 mm	383.63	383.63	355.97	360.03	370.48	353.97
6 mm	357.99	357.99	348.06	368.35	399.88	357.99
7 mm	333.01	350.01	342.30	336.68	372.62	376.97
8 mm	338.54	355.97	355.97	368.35	381.39	374.79
9 mm	336.68	357.99	348.06	364.15	370.48	360.03
10 mm	340.41	350.01	353.97	348.06	372.62	344.20

Figure 8.3.14 : Corner Hardness Experiment (3D Stress Distribution)

Ultimate Tensile Strength (N/mm²)

Tension						Compression
1 mm	646.67	599.51	567.45	496.30	541.06	595.82
2 mm	577.85	584.94	504.80	525.49	560.67	564.05
3 mm	570.88	522.46	499.11	507.68	541.06	516.47
4 mm	499.11	501.94	488.02	499.11	516.47	490.76
5 mm	537.89	537.89	499.11	504.80	519.45	496.30
6 mm	501.94	501.94	488.02	516.47	560.67	501.94
7 mm	466.92	490.76	479.94	472.06	522.46	528.55
8 mm	474.67	499.11	499.11	516.47	534.75	525.49
9 mm	472.06	501.94	488.02	510.58	519.45	504.80
10 mm	477.29	490.76	496.30	488.02	522.46	482.61

Figure 8.3.15 : Corner Hardness Experiment (3D Stress Distribution)

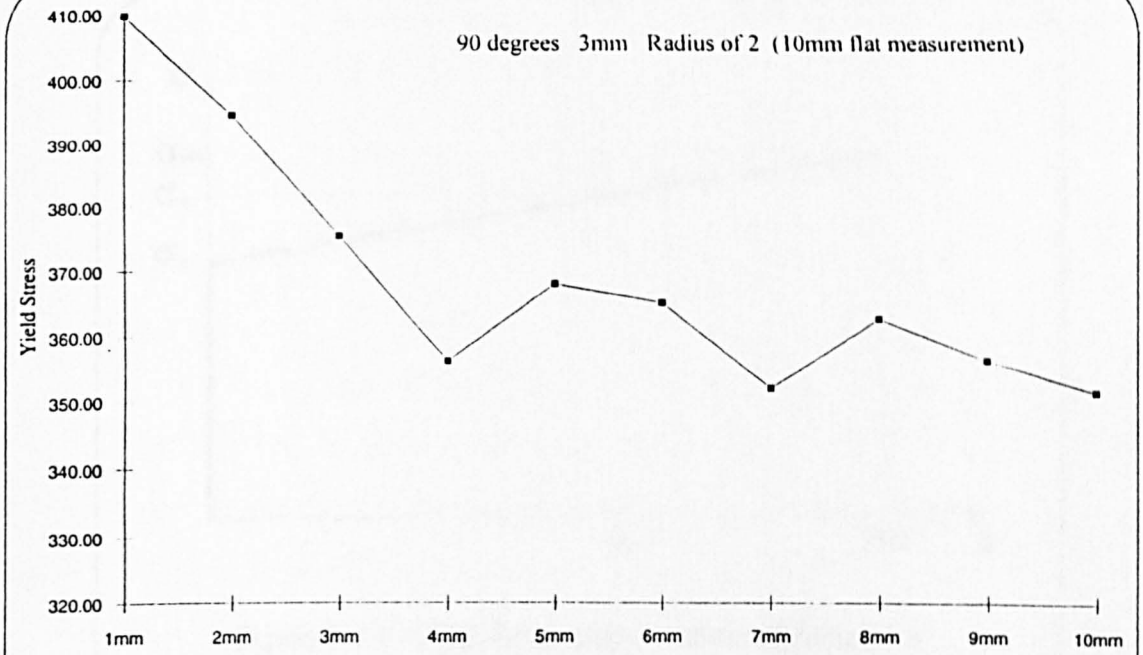

Figure 8.3.16 : Stress Distribution

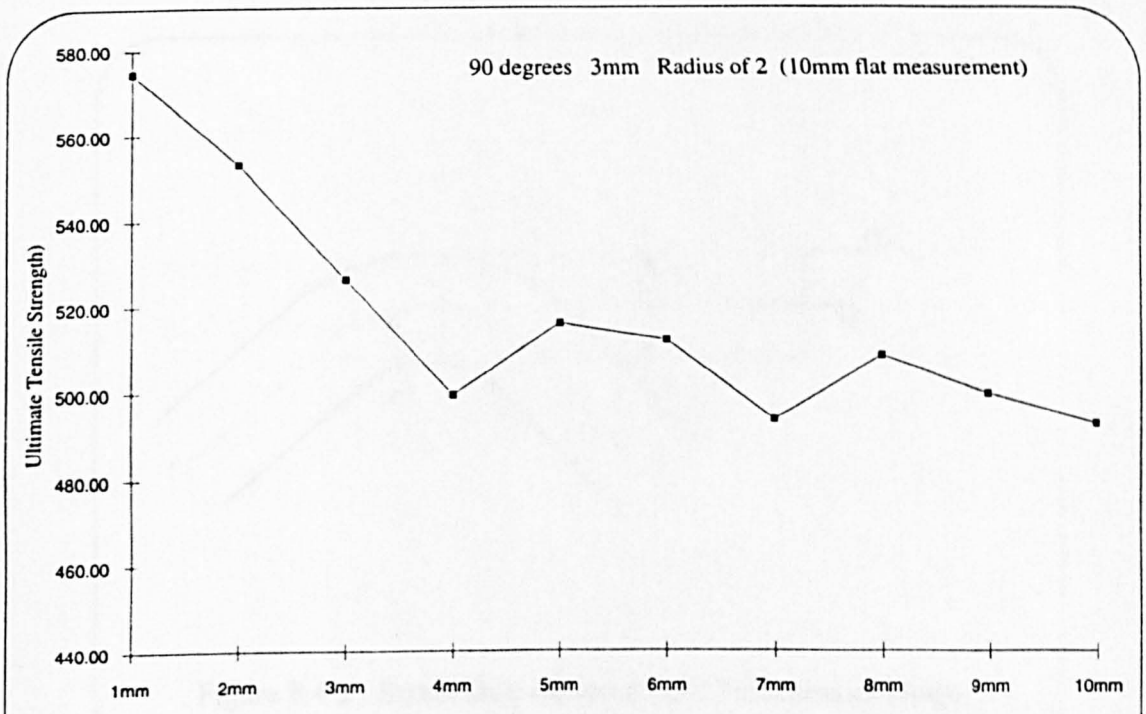

Figure 8.3.17 : Stress Distribution

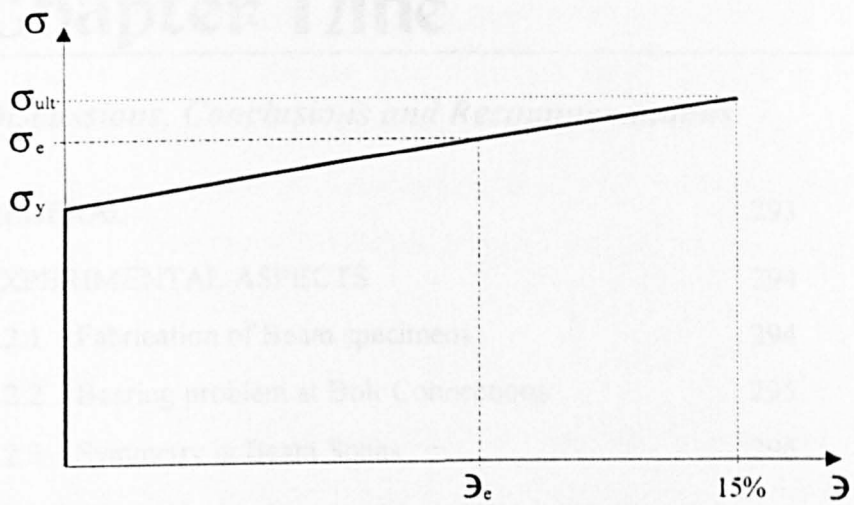

Figure 8.4.1 : Rigid-Linear Plastic Material Behaviour

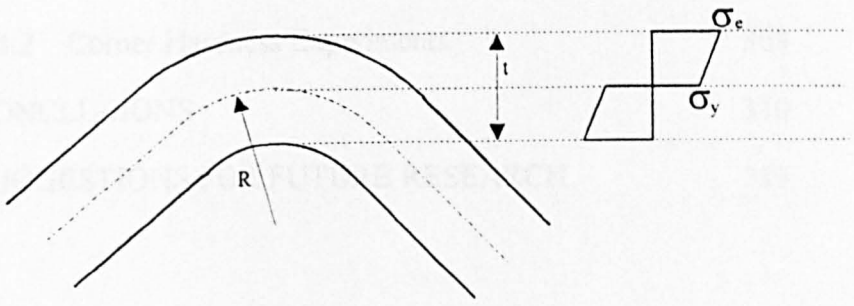

Figure 8.4.2 : Strain Distribution across Thickness of Hinge

Chapter Nine

Discussions, Conclusions and Recommendations

9.1 GENERAL

In the field of engineering research, it is not unusual to find that during the course of an investigation into a subject, the researcher finds a string of related subjects which are in need of attention and each investigative project can lead to several others. It is therefore very difficult to absolutely complete research work in any one general topic without confining the final recommendations to specific situations in which the conditions have been considered.

In chapter 2, the method of utilising separate elastic and plastic solutions to estimate the ultimate load carrying capacity of thin-walled beams that fails due to the infestation of local buckling was introduced. The analytical techniques were then applied in theoretical models for plain channels, lipped channels and zed sections in chapters 3, 4 and 5 respectively. The theoretical predictions based on these models were then compared with the results from reasonably extensive experimental investigations in chapter 7 of this thesis. Experimental work on the effects of strain hardening on the yield strength of thin-walled sections was presented in chapter 8. This chapter aims to discuss the findings of the theoretical and experimental studies of the previous chapters and highlight the conditions under which the present theories are applicable. The thesis ends with a number of conclusions which have been drawn from the current work and a few recommendations which are hoped to be of value to other workers in the field of thin-walled structures and future investigations.

9.2 EXPERIMENTAL ASPECTS

The main objectives of the beam experimental investigations of the current study were to provide insight into the behaviour of the selected beams as they are subjected to loads beyond the ultimate load carrying capacity and experimental data to verify and assess the performance of the theoretical models. These objectives were achieved by the experimental program described in chapter 6, within reasonable laboratory standards. From the observations made during the beam tests, the assumptions made in the development of the theoretical analysis methods presented in this thesis did not violate any major rules that govern the behaviour of the physical beam specimens. There are however, a number of observations that suggest reasons for minor discrepancies between the theoretical and experimental results for the beam tests which have been deemed to be successful, these will be highlighted in this chapter.

The following sections presents discussions of some problems encountered during the execution of the experimental program and how these affected the results.

9.2.1 Fabrication of the Beam specimens

Some of the beam specimens described in chapter 6 were produced in the laboratories of the University of Strathclyde. The fabrication process included the shearing of mild steel sheets to the required dimensions and cold folding right angled corners to form the final plain and lipped channel cross-sections. The guillotine and folding machine available for the task limited the total length of each beam specimen to a maximum of 2 m, which limited the span length for the double spanning beams to approximately 0.975 m. This presented no problems for the plain channels as the cross-sectional dimensions could be reduced so that the ratio of beam span to the maximum cross-sectional dimension remains above 8 (design rule for the specimens). In the case

of the lipped channels however, in which the minimum width of the flanges was limited by the size of the fixed folding blade of the folding machine, in order to adhere to the design rule on the minimum span length, meant that the final cross-section of the lipped channels had flanges which were only slightly smaller than the webs. These cross-sections are not of much practical use since the BS 5950 : Part 5 : 1987 [8] limits the stiffened flange width to 60 times the thickness (section 4.2 of the code). As a result, all the fabricated lipped channel beams tested were considered to be of secondary importance in the current study as such cross-sections are unlikely to be adopted for use in practical structural sections.

9.2.2 Bearing problem at Bolt Connections

Although the beam specimens tested were designed against bolt bearing problems using the recommendations of the BS 5950 : Part 5, the single end bolt holes in some of the beams experienced the 'digging in' of bolts. This was evident from the observed elongation of these holes after the beam tests. There are two reasons for this phenomenon, the first is the fact that all end bolts were only hand tightened during the experiments so that relatively free rotation was allowed at the ends and the second relates to the difference in size between the bolts used and the corresponding bolt holes. Following the excepted standard adopted by the cold formed steel industry, all bolt holes were bored 2 mm larger than the nominal bolt diameters, this resulted in very small actual bearing areas for these bolts, as illustrated by figure 9.2.1, which promoted the 'digging in' of the bolts. Although this effect caused only very small downward displacements (typically 1 mm to 2 mm) of the entire beam which added to the beam deflections monitored during the tests, the difference between the elastic deflections of the experimental results and the theoretical elastic lines is quite obviously noticeable (see graphs in chapter 7, figures 7.2.1 to 7.2.4).

9.2.3 Symmetry along the Beam Spans

In the beam experiments, symmetry was not always achieved between the two halves of the single span beams and between the two spans of the double span specimens. This effect resulted in the failure mechanisms developing along the beams which were not symmetrical about the centre of the beam specimens, however, this did not critically affect the experimental results. In the single spanning beams which are not symmetrical, 'half-mechanisms' developed as illustrated by some of the photographs presented in chapters 4 and 5, figures 4.2.2, 5.2.1 and 5.2.2, in which obvious yield lines developed only on one side of the loading cleat, the overall effect of this is to approximately double the global hinge angle on one half of the plastic collapse mechanism while reducing the hinge angle on the other side to a negligible value, as demonstrated by figure 9.2.2. This causes almost the same net energy dissipation in the overall mechanism as in the case of the development of a complete plastic mechanism. There are a few possible causes for this effect, these being errors in the position of the bored bolt holes, misalignment of the loading cleat, unequal height of the end supports and the contact at the bolt connections being different on each half of the beam. In beams where ultimate failure is followed by collapse with reducing moment capacity at the failure section, it can be shown that non-symmetrical failure mechanisms actually dissipate slightly less energy than complete mechanisms. It is therefore likely that 'half- mechanisms' tend to develop whenever possible.

Similar causes also resulted in the failure of only one span in the double spanning beams but again, this did not affect the comparison of results since the theoretical analysis examines each span of the beams separately. The beam tests were conducted on a displacement controlled test machine and the applied loads were transmitted to the loading cleats through a roller / lever system which always applied equal loads on each span. As soon as one span fails and begin to shed load, the other span would not be able to attain it's ultimate load. It is therefore very rare to fail both spans simultaneously since the two spans of the beams are rarely completely identical.

9.3 Verification of Theoretical Results

The topic of elasto-plastic behaviour has received much attention from researchers in recent years. A number of authors have found that the use of plastic collapse characteristics from analysis using the plastic mechanism approach in conjunction with a suitable elastic buckling formulation can produce rather satisfactory estimates of the ultimate loads of thin-walled structural members which buckle locally. Methods based purely on the elastic theory of material behaviour tend to result in rather conservative approximations. The plastic mechanism approach provides a relatively simple means of estimating the plastic strength of structures. This approach has been adopted in the current study and the results have proven to be generally satisfactory for the thin-walled beam sections examined.

9.3.1 The Plastic Mechanisms

In the theoretical plastic mechanism analyses presented in this thesis, bending energy of the plastic hinges were calculated using the reduced moment capacity of the hinges which took into consideration the inclination of the hinges to the bending axis and the effects of the axial compression. In addition, the use of the modified plate plastic bending moment capacity in the formulation, presented in section 8.4 of this thesis, enabled the utilisation of the strain hardened strength of the material. The theoretical plastic collapse mechanisms presented in chapters 3, 4 and 5 are based on the yield line patterns observed during the experimental investigation of the beam sections and are kinematically admissible mechanisms which satisfies the equilibrium and mechanism conditions, introduced in chapter 2, section 2.4.3. The theoretical collapse characteristic obtained are therefore theoretical upper bound solutions, however, the mechanism load minimisation procedures used to determine the final geometry of the plastic mechanisms seem to have oversimplified the theoretical mechanisms.

The general belief that since the energy involved in the bending of plates about the plastic hinges is lower than the membrane straining effects, true mechanisms (as defined by Murray [44]), would theoretically occur whenever possible, may not be universally true. In the plastic mechanisms examined in the current study, the outer hinges on the compression flanges of the tested beams were inclined at an angle of between 30° to 60° to the bending axis of the beam cross-section. In the theoretical models, this inclination could not be justified since it will not only increase the length of the outer hinges but it would also require additional membrane straining on the adjacent platelets to maintain kinematic admissivity. In keeping with the adopted theoretical assumptions, the inclination of these hinges was ignored to minimise the mechanism loads.

In all the presented mechanisms, the independent mechanism size 'c' was found by means of a mechanism load minimisation process and considering the mechanism lock-up conditions, the value of 0.145 times the web depth was adopted for all the mechanisms according to this approach which enabled the maximum hinge rotations before lock-up occurred. This assumption was supported by experimental findings, the experimental mechanism size 'c' ranged between 0.145 to 0.2 times the web depth. For the lipped sections, the second independent variable was the inclination angle of the outer hinges of the lip mechanisms which was taken as 50° as suggested by load minimisation procedures. This angle was also found to produce the minimum loads in a similar situation encountered by Sin [70] for a plain channel mechanism.

The current method of mechanism analysis reacts to increases in compression flange width by increasing the plastic hinges length for the flange hinge lines which ultimately increases the mechanism loads. In the experimental investigations, it was observed that in some cases, the ultimate load carrying capacity of the beam can actually be reduced by a wide flange, since the critical buckling stress is reduced. The current theories were deemed to be satisfactory for the practical ranges of the compression

flange width, and had the tendency to overestimate the loads when the flange ratio of width to thickness exceeded 40.

9.3.2 The Single Span Beams

For the plain channel sections examined, the current theory produced beam ultimate moment capacity predictions that compared well with the experimental results. The maximum bending moment capacity evaluated using the recommendations of the BS 5950 : Part 5 seem to work better for the very slender sections (with 203 mm webs) while underestimating the ultimate loads for the more practical sections.

The fabricated single span lipped channel beams examined were observed to experience some degree of flange curling due to the relatively wide flanges. The theoretical deflection estimates, in which no account for such effects were taken therefore did not compare very well with the experimental results. In spite of this, most of the theoretical predictions were rather good for the sections which did fail mainly due to the local plastic mechanisms.

The single span zed sections were not as predictable as the plain channels, due to the shape of the cross-section, the restraining of the tendency for the section to deflect sideways at mid span (along the cross-sectional bending axis) as the loads were applied, caused the compression flanges to curl in some of the specimens, especially for the deeper and thicker sections. This effect caused the elastic behaviour of the theoretical beams to stray from the experimental loading lines which subsequently may have affected the ultimate loads. The discrepancy generally became larger for the beams with longer spans since the deflections involved were larger. Nevertheless, the theoretical results from the presented analyses using the modified plastic mechanism for the lipped channels were generally in good agreement with the experimental findings.

The zed sections examined had relatively narrow flanges and for these cross-sections, the presented predictions based on the BS 5950 recommendations overestimated the ultimate moment capacity of a number of the beam specimens. This can be observed from figures 7.4.1 to 7.4.8 and table 7.4.1 presented in chapter 7. In the calculations presented in this thesis which adopted formulations from BS 5950 : Part 5, the bi-axial bending effects of these non doubly symmetrical cross-sections were not considered. This caused the overestimation of the maximum moment capacity of a number of the single span zed section beams.

The relatively small amounts of flange curling in some of the tested beams had the effect of reducing the effective second moment of area of the experimental beam sections, this in turn caused the experimental deflections to become larger than the theoretical behavioural predictions. This phenomenon, together with the effects of bolt bearing at the ends of the beam and the possible elastic compression of the supports under the supporting cleats, caused the experimental deflections of a majority of the beams to be greater than the theoretical deflections. This can be seen in the plots presented in chapter 7 (figures 7.2.1 to 7.2.4, 7.3.1 to 7.3.4 and 7.4.1 to 7.4.8) for the single span beams of all three cross-sections examined. The theoretical load predictions are generally good, and the difference of deflection between the experimental and theoretical collapse curves does not affect ultimate load predictions for the double span beams.

9.3.3 The Double Span Beams

Two theories have been presented for the evaluation of double span beam load-deflection behaviour, the results from both of these methods have been presented in chapter 7 for the double spanning beams tested. From the comparison of the results, it is immediately obvious that both methods are suitable for the double span beams tested on the Tinius Olsen machine, see figures 7.2.5 to 7.2.8, where the loads were applied by means of loading cleats. However, for the more practical specimens tested in the vacuum box, see figures 7.3.9 to 7.3.12 and 7.4.9 to 7.4.12, where the span lengths were much longer and uniformly distributed loads were applied, the first method (introduced in chapter 2) based purely on the energy method, proved to be inferior to the more generally applicable method (introduced in chapter 3) of using two stages of elastic beam solutions with the energy method to construct the entire range of loading behaviour in multi-spanning beams. The reasons for this relates to the way in which the elastic deflections were accounted for in the theories. Since the elastic deflections in the first method (energy approach) were estimated from the single span loading line, the span length for the double span beams has to be similar to the span length of the single span beam from which the collapse characteristics are taken for the double span analysis. For the specimens tested in the vacuum box, the spans of the double spanning beams were much longer than the sample beams tested in single span configuration, the second method which considered the initial stages of the loading of those beams by means of elastic beam solutions could therefore predict the larger elastic deflections which were found in the experiments more closely. The second theory is therefore recommended for general use.

In all cases, the current theory predicted the ultimate loads of the double span beams examined reasonably accurately. The theoretical maximum loads based on the BS 5950 : Part 5 recommendations always underestimated the experimental ultimate loads, this is to be expected since these solutions did not account for the effects of plastic moment redistribution.

For the lipped channel beams tested in the vacuum box, it may be realised that the experimental loads were a little higher than the theoretical estimates in some cases, figures 7.3.9 to 7.3.12, this was thought to be due to the use of 38 mm thick (clipboard) floorboards to cover the floor beams during the tests. As these boards were screwed onto the beams, they would have possibly strengthened the beams against bending, especially at the region of the central supports where the beam bending deformations during collapse were large. This would account for the discrepancies between the theoretical and experimental results for these beams.

For the double span zed sections tested, two of the tests were conducted with the system set up for up-lift experiments in which the roof sheeting were fitted onto the tension flange (between supports). In view of the beam cross-section and the fact that the compression flanges were not prevented from sideway movements by the roof sheeting, as in the download tests, sideway deflections developed as local buckling set in causing the beams to twist. This explains the difference in the shape of the theoretical and experimental load-deflection plots presented in chapter 7, figures 7.4.11 and 7.4.12, however, the theoretical ultimate load predictions were very close to the experimental ultimate loads.

9.3.4 Alternative Failure Mode in the Lipped Channels

The high proportion of the flange width to web depth ratio for the fabricated lipped channels caused a set of 0.775 mm thick single span beams and most of the double span specimens tested in the Tinius Olsen to fail with extreme amounts of flange curling which did not allow regular plastic mechanisms such as those described in this thesis to form. The beams were deemed to fail in a mode which is quite different from that found in the other beams examined in the current study. No attempt was made to analyse these beams theoretically since these were not typical of the practical sections which are likely to be used in practice. As mentioned in section 9.2.1, the flanges of these beams violated the maximum width provisions of BS 5950 : Part 5 and as such could only be considered to be of secondary importance in the current study.

On examination of the presented double span lipped channel results which were deemed to have failed by the alternative mode, it can be observed that the shapes of the load-deflection behaviour are rather different from the other beams examined, see figures 7.3.5 to 7.3.8. The elastic deformations on these plots are much greater before the ultimate loads are reached, the elasto-plastic regions stretches over a larger span of beam deflections and the drop off in load following the ultimate load point is much more gradual. These characteristics seem to accompany this mode of beam failure.

9.4 EFFECTS OF STRAIN HARDENING IN COLD FORMED SECTIONS

A number of researchers have uncovered evidence that the cold forming processes employed in the fabrication of thin-walled sections have the effect of work hardening the steel so that the strength of the material in the formed corners is increased. The research on this topic is still far from completion, in the author's opinion, there is much to be learnt in the behaviour of the cold formed section and how the valuable additional strength can be effectively accounted for in design. This section of the thesis discusses the observations and findings brought into focus by the author's experimental investigations into this topic.

From observing tests on stub columns, Karren and Winter [24] realised that the flat regions of the columns, having a lower yield point, started to buckle locally at an average cross-sectional stress at or slightly above their own lower yield point thus preventing the higher yield strength of the corners to be fully effective. This casts some doubt on the use of the full effect of the work hardened corner strength in the elastic analysis of locally buckled structures. As such, no attempt was made at this stage to incorporate cold forming effects in the analysis of the thin-walled beams examined in this thesis.

9.4.1 Corner Tensile Experiments

In an attempt to discover the relationship between the corner radius to thickness ratio and the increase in strength imparted in the corner material of cold formed sections, mild steel plates were formed into test specimens containing 90° and 45° bends for tensile and hardness testing. From the results of the experiments, it was noticed that the 2.75 mm and 3 mm thick specimens, especially those with tight corners, displayed relatively lower increases in corner strength compared to the thinner specimens. On examining the load-deformation data collected during the fabrication of the second series of corner tensile test specimens, it was realised that those 2.75 mm and 3 mm specimens had been subjected to bending loads beyond the ultimate loading capacities to various degrees. It was therefore concluded that those pieces had been 'over-bent' and portions of the cross-section must have sustained irrecoverable damage during the cold forming process. Assuming a simple strain situation depicted by figure 8.4.2, the outer fibres of the corner section would theoretically sustain damage when

$$\vartheta \leq \frac{1}{2 \cdot \varepsilon_{ult}} \qquad \text{Eqn.(9.4.1)}$$

where ϑ is the mean corner radius to thickness ratio
and ε_{ult} is the strain at which the ultimate tensile stress occurs.

For a material that attains ultimate tensile stress at 15% strain, damage according to this simple model is theoretically possible when the mean radius to thickness falls below 3.33, which is not rare in commercial sections. The actual ratio of course depends on the ductility of the material used for the section and the actual strain model is more complex, but this exercise demonstrates the possibility of causing damage to the corner material by over-bending.

From the corner tensile experimental results, there is evidence to show that reducing the corner radius to thickness ratio (within the ranges of between approximately 1.8 to 3) does not have a great net effect on the overall average strength of the corner specimens. Although the maximum strength and the average corner strength for tight corners are higher, the corner cross-sectional area in which the elevated strength is present is relatively smaller for the tighter corners and hence the overall effect for the entire section is not improved by much.

The maximum increase in the yield strength of the corner material found in the corner tensile specimens is approximately 150% over the virgin yield strength. Comparing the experimentally derived increase in yield strength to the theoretical predictions based on the formulations by Karren [23] and Lind and Schroff [30], both the theories tend to underestimate the increase in yield for all the specimens which were deemed to be undamaged during the cold forming process (all except the 2.75 mm and 3 mm thick specimens). There is therefore more potential in corner strength than the theories predict.

During the tensile testing of the corner specimens, it was discovered that the stress-strain behaviour of the cross-sections with cold formed corners could be quite different from that of the virgin material from which the corner specimens were made. The stress-strain plots for the corner specimens, see figures 8.2.1.10 to 8.2.1.15 and 8.2.2.7 to 8.2.2.10, generally exhibited relatively more gradual transition from linear elastic to stabilised plastic behaviour. With the larger region of elasto-plastic material behaviour, the technique of taking the stress that occurs at 0.2% plastic strain as the estimated yield point for flat tensile test specimens is not suitable for the specimens containing corners. Higher values of permanent set were used to assess the relative increase in the average overall yield strength of the corner specimens, these were chosen so that the stresses were measured at stabilised regions of plastic behaviour whereby the stresses were approximately linearly proportional to the plastic strains.

During the tensile straining of the corner test specimens, it was observed that the sections tended to bend with the free edges experiencing larger tensile strains than the corner regions, this was accompanied by some 'flattening out' at mid-length of the angled sections, these behaviours are demonstrated in figure 9.4.1. These effects were more obvious in the first series of corner tensile experiments due to the bearing problems in the bolted connections that secured the ends of the specimens. The clamping technique used in the second series of corner tensile experiments worked well and effectively applied tensile stresses relatively uniformly distributed over the test cross-section, see figure 9.4.2, the bending and flattening effects could therefore be attributed to the natural mechanical behaviour of the test sections. Considering the fact that the corner specimens consisted of flat elements which behaved like the virgin material and corner elements which had a higher yield point and relatively lower ductility, the tensile stresses and strains carried by the two types of elements would be different during the tension tests. The corner specimens could therefore be thought of as a composite of two metals and as the tensile stresses were applied, the flat elements exhibited a higher level of axial strain in order to sustain a stress level equivalent to that carried by the stiffer corner elements. In addition to this, the corner elements have a strength distribution such that the centre of the bends had the highest strength, the strength reduced towards the flat elements and this elevated strength due to cold forming reducing to that of the virgin material 2 mm to 3 mm into the flat element. Hence, as the tension test progressed, the free edge of the flat elements eventually yielded first at the virgin yield stress, the yielding then spread towards the corners until ultimate failure. This would explain the bending and flattening effects in the cross-section since the free edges experienced higher strains than the corners. The progressive yielding which starts at the free edges working it way towards the corner produces the gradual transition from linear elastic to stabilised plastic behaviour which was observed in the stress-strain plots.

9.4.2 Corner Hardness Experiments

The increase in yield and ultimate strength of the cold formed corners were assessed by comparing the Vickers' hardness measurements in the corner region of the specimens with that taken at a remote point where the material could be assumed to behave like the virgin material. Generally, the average increases in strength of the corners found in these experiments were smaller than those found in the tensile experiments, with a maximum average corner yield strength of 163% of the virgin yield point.

The distribution of strength over the cold formed corner specimens were established, yield and ultimate strength peaked at the 'toe' of the corners (mid way through the arc of the bends) with values of yield up to 1.8 times the virgin. The elevated strength levels reduced towards the flat elements until approximately 2 mm to 3 mm into the flats where the strengths were equivalent to the virgin strengths. Measurements were taken 10 mm into the flat elements, and the average yield strength over this 10 mm length of flats was found to be approximately 5% over the virgin yield stress.

In the other direction of the cross-section, higher strengths were found in the outer fibres of the thickness where the plastic strains experienced during the cold forming process were relatively larger than those at the core.

From these findings, it can therefore be confirmed that plastic bending effects does not occur evenly over the arc length of the corners, maximum strains are experienced at the centre of the bends, at the outer fibres, and the effects diminish towards the flat elements. It would not be unreasonable to assume that work hardening only affected the immediate vicinity of the corners over the arc of the bend.

Although the evidence suggests that there is a definite relationship between the hardness and the yield / ultimate strength of the material, the results evaluated using the formulations of Tabor [71] did not compare very well with those from the tensile experiments. Nevertheless, the experiments conducted using this technique successfully established the relatively detailed distribution of work hardening effects on the material in the cold formed corners.

9.5 CONCLUSIONS

Theoretical and experimental investigations on the behaviour of some thin-walled beams, which focused on the ultimate carrying capacity and collapse behaviour, have been presented. The subject of the effects of plastic moment redistribution on the behaviour of indeterminate beams have also been examined as part of the beam studies. Experimental work relating to the effects of strain hardening on the strength of thin-walled sections with cold formed corners was performed and the findings have been detailed in this thesis. This section summarises the conclusions that can be drawn from the studies in the following paragraphs :

The method of combining an elastic analysis with a plastic mechanism analysis to estimate ultimate load carrying capacity and to describe the behaviour before and after the ultimate load of beams composed of thin plates which buckle locally has been proven to be able to provide good approximations through relatively simple analysis. The initial yielding which usually occurs at the surface of locally formed buckles is followed shortly after by through thickness yielding which leads to the formation of the yield lines which make up plastic mechanisms. The initiation and growth of plasticity in the thin-walled beam, which invalidates the elastic theory, occurs within a relatively short elasto-plastic region. The theoretical collapse curves from plastic mechanism analysis therefore intersects the elastic loading lines within a narrow transition region in which neither of the theories are governing and with care, rather good ultimate load predictions are possible.

The plain channel mechanism presented in chapter 3 has proven to be a rather versatile theoretical model, the pattern of yield lines in the flanges and web of this idealised plastic mechanism works well in the simulation of the consistently observed pattern of yield lines found in the plain channel beam experiments. With minor

modifications, this theoretical mechanism can be used to model collapse in lipped channels and lipped zed sections, with reasonable accuracy, as demonstrated by the models presented in chapters 4 and 5.

The general approach described in the previous two paragraphs is suitable for sections which do not have excessively wide flanges. When the width of the flanges approaches or exceeds 60 times the thickness of the section, the failure mode which accompanies the collapse of the beam section is rather unpredictable, and may include relatively large amounts of flange curling with unsymmetrical patterns of yield lines. Within the range of flange widths examined in this study, the theoretical predictions of beam behaviour are generally most accurate for sections with flanges of width less than 40 times the material thickness.

The consideration of axial compression, hinge inclination to the cross-sectional bending axis and strain hardening strength in plastic moment capacity, in the energy dissipation in the yield lines of plastic mechanisms seem to have worked well with the postulated theoretical mechanisms presented in this thesis. The results generated by the current theoretical models are generally in good agreement with the experimental findings. In comparison with the recommendations of BS 5950 : Part 5, the code is only more accurate for extremely slender sections, while it underestimates moment capacities of the more practically proportioned cross-sections (used by cold formed steel manufacturers). The code also does not provide for plasticity in indeterminate beams except for compact sections and can hence severely underestimate ultimate loads in multi-span beams which buckle locally.

The experiments on double spanning beams have revealed that the effects of plastic moment redistribution can contribute substantially to further load carrying capacity after the first collapse mechanisms have developed along the beams. Simple design methods which do not take such moment redistribution into account could severely

underestimate the ultimate beam loads. Although the full ultimate load capacity of such beams is not likely to be used in design since the beam deflections may become quite large after the initiation of failure, the additional capacity may go into reducing the safety factor of such beams in some applications.

The theoretical method of using two stages of elastic beam analysis along with a final collapse stage based on the energy approach, first introduced in section 3.5.4 of this thesis, has proven to be give good approximations of multi-spanning beam behaviour. For beams with relatively short spans for which the collapse behaviour of a single failure point in a beam of similar span is known, the simpler method based purely on energy considerations, introduced in section 2.5, can also provide good multi-span load predictions.

There is enough evidence from this study to suggest that with further refinements to the analytical techniques presented in this thesis, this method of beam analysis could become a very powerful tool for the designers of thin-walled beams.

The study on the effects of strain hardening on cold formed sections described in this thesis have not reached a theoretical conclusion, however, the experimental findings have shown that the theories by Karren [23] and Lind and Schroff [30] (which was adopted by BS 5950 : Part 5 : 1987) tends to underestimate the increases in the yield strength of the corner material. The distribution of the increased strength derived from strain hardening effects over the cross-section of the cold formed corner has been determined.

9.6 SUGGESTIONS FOR FUTURE RESEARCH

The study of the elasto-plastic behaviour of thin-walled beams is by no means complete, however, the author hopes that the work presented in this thesis will add to the useful knowledge on the subject and perhaps inspire others to carry out further research in order to gain greater understanding of the elasto-plastic and collapse behaviour of thin-walled structures which are prone to local buckling. Such knowledge would enable reliable plastic design procedures to be developed for this class of structures which has much potential. The following paragraphs list the aspects of the work that have not been covered by the current study, in which the author feels further research may be needed.

In the current work on the behaviour of locally buckled beams, much attention was focused onto the theoretical derivation of the plastic collapse curve, however, the approximation of the ultimate beam loads using the current analysis method depends also on the elastic solution. It may therefore be appropriate to improve the elastic analyses of the problems, the presented theory only accounts for the local elastic buckling effects through the use of the effective width approach, it may be advantageous to extend the elastic analysis to include the effects of flange curling and perhaps twisting of the elastic beams for the lipped sections, particularly for the zed section beams which tend to exhibit these behaviours. It is the opinion of the author that these effects would reduce the elastic bending stiffness of the beams which may improve the accuracy of the ultimate load predictions.

The beam tests conducted in the Tinius Olsen test machine for the current study did not anticipate the importance of the small amounts of beam movement due to the effects of bolt bearing problems and perhaps support deformation at the ends of the beams, although these effects does not affect the theoretical predictions of beam

behaviour, they contributed to the deflections which were measured at the load points and made the experimental results appear to be further from the theoretical plots than they should, it may be worthy to refer to Eurocode 3 (Draft). [85] before conducting similar beam experiments. This document recommends the measuring of the end deflections of the beam so that they may be eliminated in subsequent presentation of the experimental results.

The work presented on the effects of strain hardening on the strength of sections containing cold formed corners only covers the preliminary experimental findings on this topic and there is much work to be done before the additional material strength can be effectively utilised in the design of cold formed sections. As the increase in the average strength in the corners could be as high as 250% of the virgin yield stress, a reliable theory that could accurately predict such increases could prove to be extremely useful towards economical designs of cold formed steels. However, it should be cautioned that the theory would need to consider the interactions between the elements which behave as the virgin material and the strain hardened corner elements and the full effect of the increased corner strength may not be usable in practical load carrying members. The use of the finite element approach may be considered for this problem but the analysis would require the development of perhaps a subroutine within the solution procedure which would take into account the cold work that have been applied in forming the corners and it's effects on the subsequent yielding of the strain hardened corner material in a direction perpendicular to the initial strains applied during the cold forming process.

The current study on thin-walled beams has only considered plain channels, lipped channels and zed sections, it may be useful to attempt similar analysis on beams of other cross-sections. Some work on box sections have been performed by the author and it was found that the plastic mechanism developed by Kecman [25] for

the collapse of square section tubes compares well with the typical pattern of yield lines found in the collapse of rectangular and trapezoidal box section beams.

The work presented in this thesis have been focused on the static loading of thin-walled beams, with some refinements, the postulated plastic mechanisms could be applied to similar beams under dynamic loading situations.

The author would like to conclude this chapter by expressing a sincere hope that the work presented in this thesis will contribute to the useful knowledge of the behaviour of thin-walled structures.

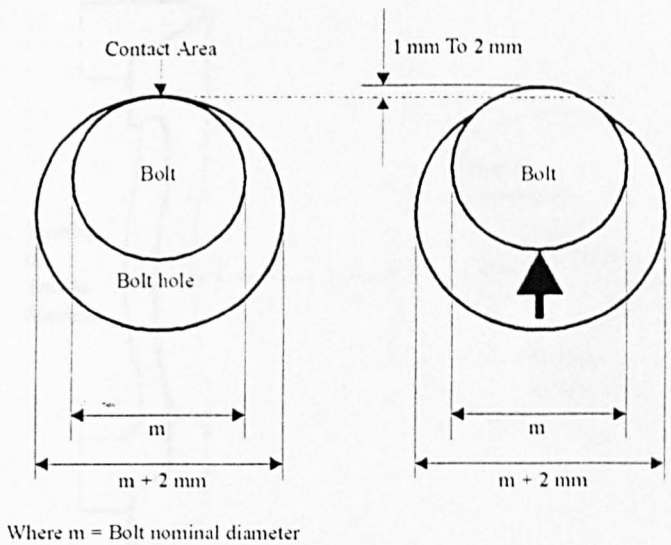

Figure 9.2.1 : Bolt Bearing

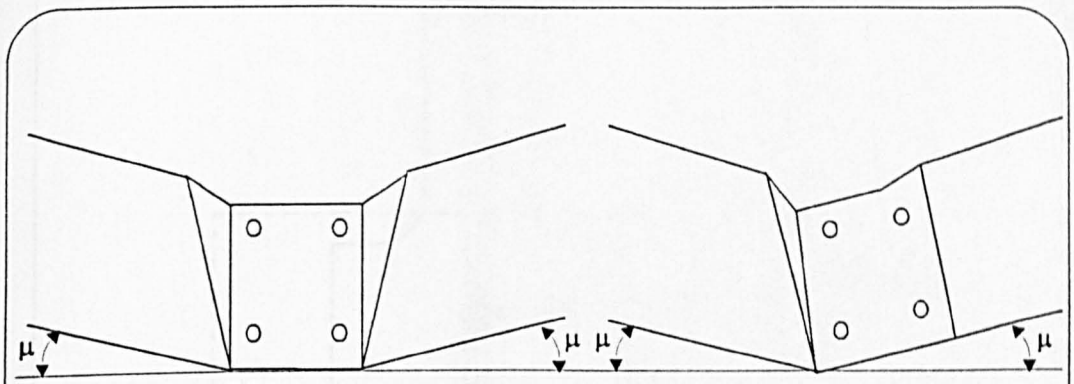

Figure 9.2.2 : Half Mechanism

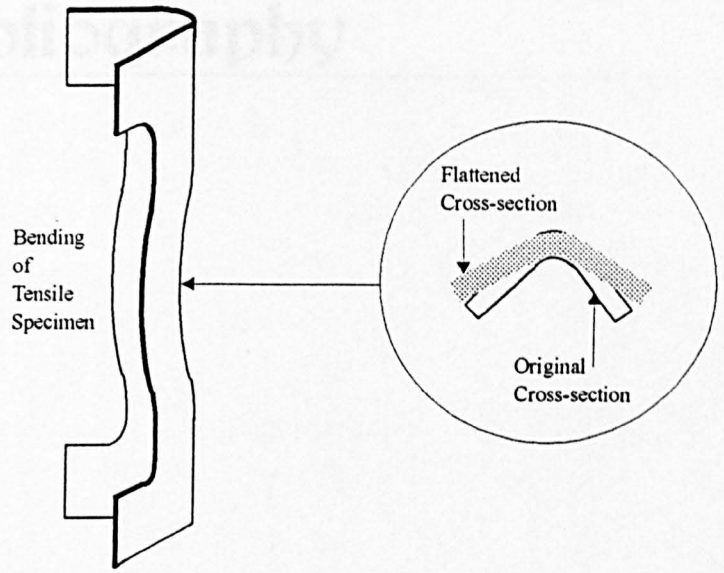

Figure 9.4.1 : Deformation of Corner Tensile Specimens

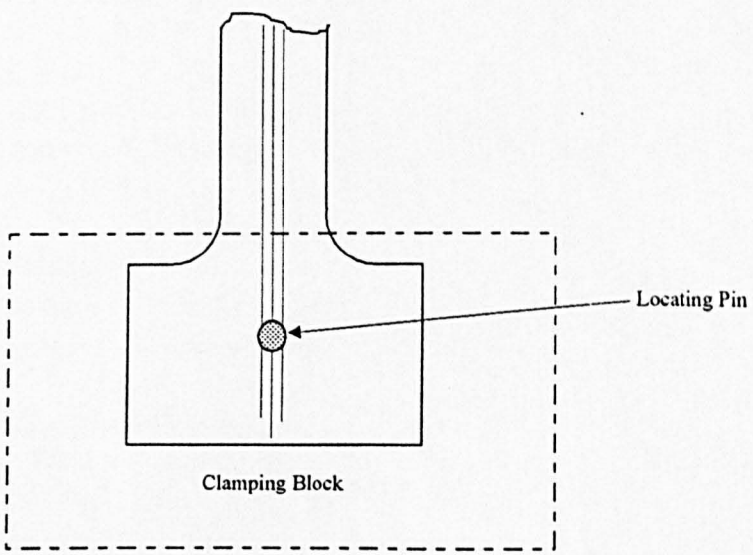

Figure 9.4.2 : Clamping Position for Corner Tensile Tests (Series Two)

Bibliography

1. Baker, J.F., Horne, M.R. and Heyman, J.
"The Steel Skeleton -vol 2- Plastic Behaviour and design.", Cambridge University Press, [1956]

2. Bakker, M., Peköz, T. and Stark, j.
"A model of the behaviour of thin-walled flexural members under concentrated load.", Proc. Tenth Int. Specialty Conf. on Cold-formed Steel Struct., St.Louis, Missouri, U.S.A., [1990]

3. Bakker, M.C.M.
"Web Crippling of Cold-formed Steel Members.", PhD Thesis, Technischt Universiteit Eindhoven., [1992]

4. Bakker, M.C.M. and Stark, J.W.B.
"Theoretical and Experimental Research on Web Crippling of Cold-formed Flexural Steel Members.", Thin-walled Struct., v.18(1994), Elsevier Appl.Sci., pp. 261-290, [1994]

5. Benson, R.C.
"Nonlinear Bending and Collapse of Long, Thin Open Section Beams and Corrugated Panels.", J. of Appl. Mech. Sci., March 1984, v. 51, pp. 141-145, [1984]

6. Bleich, F.
"Buckling Strength of Metal Structures.", McGraw Hill, [1952]

7. Bradfield, C.D.
"An Evaluation of the Elastic-Plastic Analysis of Steel Plates Loaded by Uniaxial In-plane Compression.", Int. J. Mech. Sci., v. 24(3), pp. 127-146, [1982]

8. British Standards Institude.
"Code of practice for design of cold formed sections.", BS 5950, Structural use of steelwork in building, Part 5, [1987]

9. British Standards Institude.
"Method of test at ambient temperature.", BS EN 10 002-1, Tensile testing of metallic materials, Part 1, [1990]

10. Bryan, G.H.
"On the Stability of Plane Plate under Thrust in it's own Plane with Applications on the Buckling of the Sides of a Ship.", Proc., London Math. Soc., 22, pp. 54., [1891]

11. Chajes, A., Britvec, S.J. and Winter, G.
"Effects of Cold Straining on Structural Sheet Steel.", J. of the Struct. Div., Proc. A.S.C.E., v. 89, No. ST2, pp. 1-32, Apr., [1963]

12. Chua, C.Y.
"To study the effects of cold forming on the material properties of thin-gauge steel. (By Tensile Test)", BEng(hons) thesis, Dep. of Mech. Eng., University of Strathclyde, [1994]

13. Crisfield, M.A.
"Large-Deflection Elasto-Plastic Buckling Analysis of Plates using Finite Elements.", Dep. of Environment, Transport and Road Research Lab. Report No. LR593, [1973]

14. Crisfield, M.A.
"Full-range Analysis of Steel Plates and Stiffened Plating under Axial Compression.", Proc. Instn. Civil Engrs., Part 2, 59, pp. 595-624, Dec.,[1975]

15. Davies, P., Kemp, K.O. and Walker, A.C.
"An analysis of the Failure Mechanism of an Axially Loaded Simply Supported Steel Plate.", Proc. Instn. Civil Engrs., Part 2, 59, pp. 645-658, Dec., [1975]

16. Frieze, P.A., Dowling, P.I. and Hobbs, R.E.
"Ultimate Behaviour of Plates in Compression.", Proc. Int. Conf. on Steel Plated Structure, Imperial College, London, Crosby Lockwood Staples, London, [1977]

17. Graves-Smith, T.R.
"The Post-Buckling of a Thin-Walled Box Beam in Pure Bending.", Int. J. Mech. Sci., v. 14, pp. 711-722, [1972]

18. Han, F.S.
"To study the effects of cold forming on the material properties of thin-gauge steel. (By Tensile Test)", BEng(hons) thesis, Dep. of Mech. Eng., University of Strathclyde, [1995]

19. Hancock, G.J.
"Non-Linear Analysis of Thin-Walled I-Sections in Bending.", Aspects of the Analysis of Plate Structures, Clarendon Press, Oxford, [1985]

20. Harvey, J.M.
"Studies on the Interactions of Plate Components of Structural Sections under Selected Load Conditions.", PhD Thesis, University of Glasgow, [1952]

21. Hetrakul, N. and Yu, W.W.
"Cold-formed Steel I Beams Subjected to Combined Bending and Web Crippling.", Proc. Int. Conf. on Thin-Walled Structures, Recent Technical Advances and Trends in Design, Research and Construction, University of Strathclyde, 3-6 April, [1979]

22. Horne, M.R.
"Plastic Theory of Structures.", Thomas Nelson and sons, [1971]

23. Karren, K.W.
"Corner Properties of Cold-formed Steel Shapes.", J. of the Struct. Div., Proc. A.S.C.E., v. 93, No. ST1, pp. 401-432, Feb., [1967]

24. Karren, K.W. and Winter, G.
"Effects of Cold-forming on Light-gauge Steel Members.", J. of the Struct. Div., Proc. A.S.C.E., v. 93, No. ST1, pp. 433-469, Feb., [1967]

25. Kecman, D.
"Bending Collapse of Rectangular and Square Section Tubes.", Int. J. Mech. Sci., v. 25, No. 9-10, pp. 623-636, [1983]

26. Key, P.W. and Hancock, G.J.
"Non-Linear Analysis of Cold-formed Sections Using the Finite Strip Method.", Proc. Ninth Int. Specialty Conf. on Cold-formed Steel Struct., St.Louis, Missouri, U.S.A., [1988]

27. Korol, R.M. and Sherbourne, A.N.
"Strength Prediction of Plates in Uniaxial Compression.", J. of the Struct. Div., Proc. A.S.C.E., v. 98, No. ST9, pp. 1965-1986, Sept., [1972]

28. Kótelko, M. and Królak, M.
"Collapse Behaviour of Triangular Cross-Section Girders Subject to Pure Bending.", Thin-Walled Struct., v. 15-2, Elsevier Appl. Sci., pp. 127-141, [1993]

29. Levy, S.
"Bending of Rectangular Plates with Large Deflections.", 28th Annual Report, N.A.C.A., No. 737, [1942]

30. Lind, N.C. and Schroff, D.K.
"Utilization of Cold Work in Cold-formed Steel.", J. of the Struct. Div., Proc. A.S.C.E., v. 101, No. ST4, pp. 67-78, Jan., [1975]

31. Little, G.H.
"Rapid Analysis of Plate Collapse by Live-Energy Minimisation.", Int. J. Mech. Sci., v. 19, Pergamon Press, pp. 725-744, [1977]

32. Little, G.H.
"The Collapse of Rectangular Steel Plates Under Uniaxial Compression.", The Structural Engineer, v. 58b, No. 3, pp. 45-61, Sept., [1980]

33. Loughlan, J. and Rhodes, J.
"Interaction Buckling of Lipped Channel Columns.", Stability Problems in Engineering Structures and Components, Edited by T.H. Richards and P. Stanley, Applied Science Publishers, pp. 179-198, [1979]

34. Loughlan, J. and Rhodes, J.
"The Interaction Buckling of Lipped Channels under Concentric or Eccentric Loading.", Thin-Walled Structures, Edited by J. Rhodes and A.C. Walker, Granada Publications, [1980]

35. Loughlan, J. and Upadhya, A.R.
"Locally Imperfect Plain Channel Columns.", Proc. of the J.M. Harvey Conf., University of Strathclyde, Behaviour of Thin-walled Structures, edited by J. Rhodes and J. Spence, London, Elsevier Appl. Sci. Publishers, pp. 47-67, [1984]

36. Loughlan, J. and Nabavian, M.
"The Behaviour of Thin-walled I-Section Columns after Local Buckling.", Proc. Eighth Int. Specialty Conf. on Cold-formed Steel Structures, St. Louis, Missouri, U.S.A., pp. 189-216, Nov., [1986]

37. Mahendran, M. and Murray, N.W.
"Effect of Initial Imperfections on Local Plastic Mechanisms in Thin Steel plates with In-plane Compression." , Proc. Int. Conf. on Steel and Aluminium Structures, ICSAS 91, Singapore, 22-24 May, [1991]

38. Mofflin, D.S. and Dwight, J.B.
"Buckling of Aluminium Plates in Compression.", Proc. of the J.M. Harvey Conf., University of Strathclyde, Behaviour of Thin-walled Structures, eds. J. Rhodes and J. Spence, London, Elsevier Appl. Sci. Publishers, pp. 399-427, [1984]

39. Moxham, K.E.
"Theoretical Prediction of the Strength of Welded Steel Plates in Compression.", Cambridge University, Report No. CUED/C-Struct/TR2., [1971]

40. Murray, N.W.
"The Behaviour of Thin Stiffened Steel Plates.", Memoires Abhandlungen Publications, Int. Ass. for Bridge and Structural Engs., 33-I, pp. 191-201, [1973]

41. Murray, N.W.
"Buckling of Stiffened Panels Loaded Axially and in Bending.", The Structural Engineer, Aug. 1973, No. 8, v. 51, pp. 285-301, [1973]

42. Murray, N.W.
"Analysis and Design of Stiffened Plates for Collapse Load.", The Structural Engineer, Mar. 1975, No. 3, v. 53, pp. 153-158, [1975]

43. Murray, N.W.
"The Static Approach to Plastic Collapse and Energy Dissipation in Some Thin-walled Steel Structures.", Chapter 2, Structural Crashworthiness, pp. 44-65, Butterworths, [1983]

44. Murray, N.W.
"Introduction to the Theory of Thin-walled Structures.", Clarendon Press, Oxford, [1984]

45. Murray, N.W.
"The Elastic Buckling and Collapse Behaviour of Thin-walled Structures.", Proc. Int. Conf. on Steel and Aluminium Structures, ICSAS 91, Singapore, 22-24 May, [1991]

46. Murray, N.W. and Khoo, P.S.
"Some Basic Plastic Mechanisms in the Local Buckling of Thin-walled Steel Structures.", Int. J. Mech. Sci., v. 23, No. 12, pp. 703-713, [1981]

47. Narayanan, R. and Chow, F.Y.
"Strength of Biaxially Compressed Perforated Plates.", Proc. Seventh Int. Specialty Conf. on Cold-formed Steel Structures, St. Louis, Missouri, U.S.A., pp. 55-73, Nov., [1984]

48. Rasmussen, K.J.R.
"The Behaviour of Thin-walled Channel Columns.", PhD Thesis, University of Sydney, School of Civil and Mining Engineering, [1988]

49. Rasmussen, K.J. and Hancock, G.J.
"Nonlinear Analysis of Thin-walled Channel Section Columns.", Thin-walled Structures, v. 13, Elsevier Appl. Sci., pp. 145-176, [1992]

50. Ratliff, G.D.
"Interaction of Concentrated Loads and Bending in C-Shaped Beams.", Proc. Third Int. Specialty Conf. on Cold-formed Steel Structures, St. Louis, Missouri,U.S.A., pp. 337-356, Nov., [1975]

51. Rawlings, B. and Shapland, P.
"The Behaviour of Thin-walled Box Sections under Gross Deformation.", The Structural Engineer, Apr. 1975, No. 4, v. 53. pp. 181-186, [1975]

52. Rhodes, J.
"The Non-Linear Behaviour of Thin-walled Beams subjected to Pure Moment Loading.", PhD Thesis, University of Strathclyde, Dept. of Mech. Eng., [1969]

53. Rhodes, J.
"On the Approximation Prediction of Elasto-Plastic Plate Behaviour.", Proc. Instn. Civ. Engrs., Part 2, v. 71, Mar. 1981, pp. 165-183, [1981]

54. Rhodes, J.
"Effective Width in Plate Buckling.", Developments in Thin-walled Structures, Applied Science, London, [1982]

55. Rhodes, J.
"The Post Buckling Behaviour of Bending Elements.", Proc. Sixth Int. Specialty Conf. on Cold-formed Steel Structures, St. Louis, Missouri, pp. 135-155, Nov., [1982]

56. Rhodes, J.
"Behaviour of Thin-walled Channels in Bending.", Dynamics of Structures, ASCE, [1987]

57. Rhodes, J.
"The Design of Cold Formed Steel Structural Members.", Elsevier, Appl. Sci. Publishers, [1990]

58. Rhodes, J. and Harvey, J.M.
"Design of Thin-walled Beams.", Proc. Fourth Int. Conf. on Stress Analysis, Apr., [1970]

59. Rhodes, J. and Harvey, J.M.
"The Local Buckling and Post Local Buckling Behaviour of Thin-walled Beams.", Aeronautical Quarterly, v. XIX, pp. 363-388, Nov., [1971]

60. Rhodes, J. and Harvey, J.M.
"The Post Buckling Behaviour of Thin-flat Plates in Compression with Unloaded Edges Elastically Restrained against Rotation.", Int. J. of Mech. Eng. Sci., v. 13, pp. 82-91, [1971]

61. Rhodes, J. and Harvey, J.M.
"Plates in Uniaxial Compression with Various Support Conditions at the Unloaded Edges.", Int. J. of Mech. Sci., v. 13, pp. 787-802, [1971]

62. Rhodes, J. and Harvey, J.M.
"Effects of Eccentricity of Load or Compression on the Buckling and Post-buckling Behaviour of Plates.", Int. J. of Mech. Sci., v. 13, pp. 867-879, [1971]

63. Rhodes, J. and Walker, A.C.
"Current Problems in the Design of Cold-formed Steel Sections.", Aspects of the Analysis of Plate Structures, Clarendon Press, Oxford, [1985]

64. Roberts, T.M. and Azizian, Z.G.
"Nonlinear Analysis of Thin-walled Bars of Open Section.", Int. J. of Mech. Sci., v. 25, No. 8, pp. 565-577, [1983]

65. Seki, N. and Sunami, Y.
"Energy Absorption of Thin-walled Box Beam subjected to Combination of Bending with Axial Compression.", Proc. XVII Int. Congr., Fisita, Budapest, pp. 1435-1446, [1978]

66. Sherbourne, A.N. and Haydl, H.M.
"Carrying Capacity of Edge-compressed Rectangular Plates.", Can. J. Civ. Eng., v. 7, pp. 19-26, [1980]

67. Sherbourne, A.N. and Korol, R.M.
"Postbuckling of Axially Compressed Plates.", J. of the Struct. Div., Proc. ASCE, v. 98, No. ST10, pp. 2223-2234, Oct., [1972]

68. Sherbourne, A.N. and Korol, R.M.
"Ultimate Strength of Plates in Uniaxial Compression.", IABSE Proc., Apr. [1974]

69. Sim, C.N.
"To study the effects of cold forming on the material properties of thin-gauge steel. (Hardness Test Approach)", BEng(hons) thesis, Dep. of Mech. Eng., University of Strathclyde, [1994]

70. Sin, K.W.
"The Collapse Behaviour of Thin-walled Sections.", PhD Thesis, University of Strathclyde, Dept. of Mech. Eng., [1984]

71. Tabor, D.
"The Hardness of Metals.", Oxford University Press, [1951]

72. Tidbury, G.H. and Kecman, D.
"Investigation into the Behaviour of Hinges produced by Bending Collapse of Vehicle Structural Components.", XVII Int. Congr., Fisita, Budapest, pp. 849-864, [1978]

73. Timoshenko, S.P. and Gere, J.M.
"Theory of Elastic Stability.", McGraw Hill, [1982]

74. Timoshenko. S.P. and Woinowsky-Krieger, S.
"Theory of Plates and Shells.", McGraw Hill, Kogakusha, [1959]

75. Venant, M. St-.
"Discussion in Theorie de l'Elasticite des Corp Solids.", Clebsch, p. 704, [1883]

76. Walker, A.C.
"Thin-Walled Structural Forms under Eccentric Compressive Load Actions.", PhD thesis, University of Glasgow, [1964]

77. Walker, A.C.
"A Brief Review of Plate Buckling.", Contribution to Behaviour of Thin-walled Structures, Appl. Sci., London, [1983]

78. Walker, A.C., Dawson, R.G., Harvey, J.M., Rhodes, J., Black,M.M. and Morrell, P.J.B.
"Design and Analysis of Cold-formed Sections.", Intertext Books-London and Heath & Reach in association with the Cold Rolled Sections Association, [1975]

79. Walker, A.C. and Murray, N.W.
"A Plastic Collapse Mechanisms for Compressed Plates.", IABSE, v. 35, pp. 217-236, [1975]

80. Winter, G.
"Four Papers on the Performance of Thin-walled Steel Structures.", Cornell Univ. Eng. Expt. Station, Reprint No. 33, Nov. 1, [1950]

81. Yamaki, N.
"Post-Buckling Behaviour of Rectangular Plates with Small Initial Curvature Loaded in Edge Compression.", J. Appl. Mech., v. 26, pp. 407-414, Sept., [1959]

82. Zhao, X.L. and Hancock, G.J.
"A Theoretical Analysis of the Plastic-Moment Capacity of an Inclined Yield Line under Axial Force.", Thin-walled Structures, v. 15, Elsevier Appl. Sci., pp. 185-207, [1993]

83. Zhao, X.L. and Hancock, G.J.
"Experimental Verification of the Theory of Plastic-Moment Capacity of an Inclined Yield Line under Axial Force.", Thin-walled Structures, v. 15, Elsevier Appl. Sci. pp. 209-233, [1993]

84. Zienkiewicz
"The Finite Element Method in Engineering Science.", McGraw Hill, London, [1971]

The following document which was not formerly published was used as a reference:

85. Eurocode
"Cold Formed Steel Sheeting and Members.", Appendix A, Eurocode 3, Part 1.3, (Draft), March, [1989]

Appendices

Appendix I

LOCAL BUCKLING COEFFICIENT

According to BS 5950 : Part 5 : 1987

The following local buckling coefficient expressions are extracted from Appendix B of the British Standard 5950 : Part 5 : 1987, and are applicable to the compression elements of beams.

A) Stiffened Elements connected to webs on both sides

$$K \approx 7 - \frac{1.8h}{0.15+h} - 0.091h^3 \qquad \text{Eqn.(AI.1)}$$

where $h = \frac{B_2}{B_1}$ (See figure AI.1 for B_1 and B_2)

B) Stiffened Elements connected to a web on one edge and a lip on the other

$$K \approx 5.4 - \frac{1.4h}{0.6+h} - 0.02h^3 \qquad \text{Eqn.(AI.2)}$$

where $h = \frac{B_2}{B_1}$ (See figure AI.1 for B_1 and B_2)

C) Unstiffened Elements

$$K \approx 1.28 - \frac{0.8h}{2+h} - 0.0025h^2 \qquad \text{Eqn.(AI.3)}$$

where $h = \frac{B_2}{B_1}$ (See figure AI.2 for B_1 and B_2)

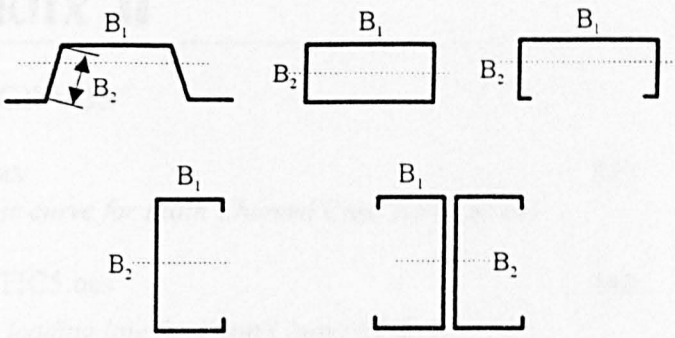

Figure AI.1

Figure AI.2

Appendix II

BASIC PROGRAMS

PC8.bas

This program calculates the data points for the collapse curve of Plain Channel beams using the PC8 plastic mechanism.

```
DECLARE SUB ACOS (value AS DOUBLE, angle AS DOUBLE)
DECLARE SUB ASIN (value AS DOUBLE, angle AS DOUBLE)
DECLARE SUB ATE (c#, d#, amax#, mu#, af#, adiffin#)
DIM pt(5), diff(5)
DEFDBL A-Z

10 CLS
ON ERROR GOTO 199
INPUT "YIELD STRESS OF BEAM MAT'L (N/mm^2)        "; ys
INPUT "ULTIMATE STRESS OF BEAM MAT'L (N/mm^2) "; us
INPUT "THICKNESS OF CHANNEL MAT'L (mm)            "; t
INPUT "FLANGE WIDTH (mm)(centre-line dim)         "; b
INPUT "CHANNEL DEPTH (mm)(centre-line dim)        "; d
INPUT "MECHANISM SIZE c (mm)                      "; c
' *mu BEING THE ANGLE OF BEND OF THE BUCKLED BEAM *
INPUT "LAST POINT FOR mu in (deg)                 "; mul
mul = mul / 180 * 3.141593
INPUT "INTERVAL FOR MU in (deg)                   "; muintv
muintv = muintv / 180 * 3.141593
INPUT "DISTANCE BETWEEN HORIZONTAL BOLTS  "; lb
INPUT "DISTANCE BETWEEN TOP AND TOP BOLTS  "; amax
INPUT "RADIUS-to-THICKNESS RATIO FOR HINGES  "; brtr
INPUT "SPAN LENGTH in (mm)                        "; sl
INPUT "FILENAME FOR THE DATA POINTS               "; file$
file$ = "a:" + file$ + ".DAT"
OPEN file$ FOR OUTPUT AS #1
PRINT #1, "SECTION DETAILS"
PRINT #1, "--------------------------"
PRINT #1, "YIELD STRESS OF BEAM MAT'L (N/mm^2)       :"; ys
PRINT #1, "ULTIMATE STRESS OF BEAM MAT'L (N/mm^2) :"; us
PRINT #1, "THICKNESS OF CHANNEL MAT'L (mm)           :"; t
PRINT #1, "FLANGE WIDTH (mm)                         :"; b
PRINT #1, "CHANNEL WEB DEPTH (mm)                    :"; d
PRINT #1, "MECHANISM SIZE c (mm)                     :"; c
PRINT #1, "INTERVALS FOR mu (deg)                 :"; muintv / 3.141593 * 180
PRINT #1, "DISTANCE BETWEEN HORIZONTAL BOLTS  :"; lb
PRINT #1, "DISTANCE BETWEEN TOP AND TOP BOLTS  :"; amax
PRINT #1, "RADIUS-to-THICKNESS RATIO                 :"; brtr
PRINT #1, "SPAN LENGTH (mm)                          :"; sl
PRINT #1, "      "
```

```
PRINT #1, " Angle     Moment Cap.   Load    Defln      Diff'       adif"
PRINT #1, "mu(deg)      (Nmm)       (kN)    (mm)     (Nmmrad)     (mm)"
PRINT #1, "---------  ---------------  -------  --------  ------------  ------"


REM ***********************************
REM *      Calculation of the data points        *
REM ***********************************


'The ultimate moment :-
mult = ys * t * ((b * d) + (d ^ 2) / 4)

'The rolling radius :-
rr = brtr * t

'Calculation of the mpsh (Considering strain hardening)
mp = ys * (t ^ 2) / 4
ssh = us
mpsh = mp + (ssh - ys) * (t ^ 2) / 6
mp = mpsh

FOR mu = (muintv + (.001 / 180 * 3.141593)) TO mul STEP muintv

mu1 = mu - muintv
mu2 = mu + muintv

CALL ATE(c, d, amax, mu, a, adiffin)
CALL ATE(c, d, amax, mu1, a1, adiffin1)
CALL ATE(c, d, amax, mu2, a2, adiffin2)

' Check for lock-up condition
teta2 = ATN((a / d))
mulu = ATN((c / (d * COS(teta2))))
IF (mu = mulu) OR (mu > mulu) THEN
    PRINT "LOCK UP CONDITION 2"
    PRINT #1, "LOCK UP CONDITION 2 at mu = "; mu / 3.141593 * 180
    GOTO 201
END IF
```

```
REM* MARGIN HALVING IS USED TO FIND THE m DATA POINTS.*

pt(1) = 1
pt(5) = mult
pt(3) = ((pt(5) - pt(1)) / 2) + pt(1)
count = 1
20 count = count + 1
  pt(4) = ((pt(5) - pt(3)) / 2) + pt(3)
  pt(2) = ((pt(3) - pt(1)) / 2) + pt(1)

FOR I = 1 TO 5
      I = INT(I)
      m = pt(I)

'START OF ENERGY EQUATION

      ' Left hand side expression
      lhs = 4 * m * muintv

      ' Right hand side of the work equation

'When a = amax, lock-up also occurs
      IF (a2 > amax) THEN GOTO 200
      teta21 = ATN((a1 / d))
      teta22 = ATN((a2 / d))

      'Right side first expression
      hm1 = 2 * mp * (1 - (m / mult) ^ 2) * b
      f3 = c * SIN(mu1) + d * COS(mu1) * COS(teta21) - d + a1 * (1 + SIN(teta21))
      CALL ASIN((f3 / c), f4)
      eta11 = ATN(((TAN((f4 - mu1))) / COS(teta21)))
      f5 = c * SIN(mu2) + d * COS(mu2) * COS(teta22) - d + a2 * (1 + SIN(teta22))
      CALL ASIN((f5 / c), f6)
      eta12 = ATN(((TAN((f6 - mu2))) / COS(teta22)))
      rhs1 = hm1 * eta12 - hm1 * eta11

      'Right side second expression
      hm2 = 2 * mp * (1 - (m / mult) ^ 2) * (b + a)
      eta21 = ATN(((TAN(f4)) / COS(teta21)))
      eta22 = ATN(((TAN(f6)) / COS(teta22)))
      rhs2 = hm2 * eta22 - hm2 * eta21
```

```
'Right side third expression
rhs3 = hm1 * mu2 - hm1 * mu1

'Right side forth expression
hm4 = 2 * mp * (1 - (m / mult) ^ 2) * (d - a)
f7 = (d - a1) / (SIN(mu1) + (d * COS(mu1) * COS(teta21)) / c)
f8 = f7 * d * COS(teta21) / c
teta41 = ATN((f8 * a1 / (d * (f7 * COS(mu1) - f8 * SIN(mu1)))))
f9 = (d - a2) / (SIN(mu2) + (d * COS(mu2) * COS(teta22)) / c)
f10 = f9 * d * COS(teta22) / c
teta42 = ATN((f10 * a2 / (d * (f9 * COS(mu2) - f10 * SIN(mu2)))))
rhs4 = hm4 * teta42 - hm4 * teta41

'Right side fifth expression
zeta2 = ATN((c / d))
f11 = SQR((c ^ 2 + d ^ 2))
hm5 = 2 * mp * (1 - (m / mult) ^ 2) / (SQR(1 - .75 * ((m / mult) ^ 2) *
      ((SIN(zeta2)) ^ 2) * (4 - 3 * ((SIN(zeta2)) ^ 2)))) * f11
f12 = (a1 / c) * COS(zeta2)
CALL ASIN(f12, teta51)
f13 = (a2 / c) * COS(zeta2)
CALL ASIN(f13, teta52)
rhs5 = hm5 * teta52 - hm5 * teta51

'Right side sixth expression
hm6 = mp * lb * (1 - (m / mult) ^ 2) / (SQR((1 - .75 * ((m / mult) ^ 2))))
eta61 = 2 * a1 / rr + teta21
eta62 = 2 * a2 / rr + teta22
rhs6 = hm6 * eta62 - hm6 * eta61

'Right side seventh expression
hm7 = 2 * mp * (1 - (m / mult) ^ 2) / (SQR((1 - .75 * ((m / mult) ^ 2))))
eta71 = c * a1 / rr
eta72 = c * a2 / rr
rhs7 = hm7 * eta72 - hm7 * eta71

'Right side First membrane strain expression
mem11 = ys * b * c * t * (SQR((1 + ((b ^ 2) / (c ^ 2)) * (SIN(teta21) ^ 2))) - 1)
mem12 = ys * b * c * t * (SQR((1 + ((b ^ 2) / (c ^ 2)) * (SIN(teta22) ^ 2))) - 1)
rhs8 = mem12 - mem11


rhs = rhs1 + rhs2 + rhs3 + rhs4 + rhs5 + rhs6 + rhs7 + rhs8
```

```
'END OF ENERGY EQUATION

      diff(I) = rhs - lhs
      diff(I) = ABS(diff(I))
NEXT I
IF diff(3) < .0000001 OR count = 500 THEN
      m = pt(3)
      GOTO 100
END IF
IF diff(2) < diff(4) THEN
      pt(5) = pt(3)
      pt(3) = pt(2)
ELSE
      pt(1) = pt(3)
      pt(3) = pt(4)
END IF

GOTO 20

100
PRINT "BINGO !"

'TO CONVERT MOMENT-ANGLE DATA TO MID SPAN LOAD-DEFLECTION
load = (4 * m / sl) / 1000
defln = sl / 2 * SIN(mu)


PRINT TAB(2); : PRINT USING "##.####"; (mu * 180 / 3.141593);
PRINT TAB(11); : PRINT USING "#########.##"; m;
PRINT TAB(25); : PRINT USING "###.#########"; diff(3);
PRINT TAB(40); : PRINT USING "###.#########"; adiffin
PRINT #1, TAB(1); : PRINT #1, USING "##.#######"; (mu * 180 / 3.141593);
PRINT #1, TAB(12); : PRINT #1, USING "#########.##"; m;
PRINT #1, TAB(28); : PRINT #1, USING "###.####"; load;
PRINT #1, TAB(38); : PRINT #1, USING "###.####"; defln;
PRINT #1, TAB(50); : PRINT #1, USING "###.############"; diff(3);
PRINT #1, TAB(70); : PRINT #1, USING "###.############"; adiffin


NEXT mu

CLOSE #1
GOTO 201
199 PRINT "ERROR IN FILE OR PROGRAM"
GOTO 300
```

```
200 PRINT "MECHANISM LOCKED UP (CONDITION 1) ! "
   PRINT #1, "MECHANISM LOCK UP  CONDITION 1 AT MU="; mu2 /
                                                    3.141593 * 180
201 PRINT "FINISHED "
202 INPUT "TRY AGAIN "; resp$
IF resp$ = "Y" OR resp$ = "y" THEN GOTO 10
PRINT "PROGRAM TERMINATED"
300 END


SUB ACOS (value AS DOUBLE, angle AS DOUBLE)
x = value
angle = ATN((-x) / SQR((-x) * x + 1)) + 1.5708
END SUB


SUB ASIN (value AS DOUBLE, angle AS DOUBLE)
x = value
angle = ATN(x / SQR((-x) * x + 1))
END SUB


SUB ATE (c, d, amax, mu, af, adiffin)
DIM q(5), adif(5)
'Trial and Error routine for finding a2
REM* MARGIN HALVING IS USED TO FIND THE a2 DATA POINTS.*
q(1) = .000001
q(5) = amax + 1
q(3) = ((q(5) - q(1)) / 2) + q(1)
qcount = 1
12 qcount = qcount + 1
  q(4) = ((q(5) - q(3)) / 2) + q(3)
  q(2) = ((q(3) - q(1)) / 2) + q(1)

FOR J = 1 TO 5
      J = INT(J)
      a = q(J)

      ls1 = d * COS(mu) * COS((ATN((a / d))))
      ls2 = a * (1 + SIN((ATN((a / d)))))
      f14 = (c * COS(mu) - d * SIN(mu) * COS((ATN((a / d))))) / c
      CALL ACOS(f14, f15)
      ls3 = c * SIN(f15)
      rs = d - c * SIN(mu)
      adif(J) = ABS((ls1 + ls2 - ls3 - rs))
```

```
NEXT J
IF adif(3) < .0000001 OR qcount = 1000 THEN
      af = q(3)
      adiffin = adif(3)
      GOTO 14
END IF
IF adif(2) < adif(4) THEN
      q(5) = q(3)
      q(3) = q(2)
ELSE
      q(1) = q(3)
      q(3) = q(4)
END IF

GOTO 12
14
PRINT "MAGIC !"
END SUB
```

ELASTIC5.bas

This program calculates the elastic loading line for Plain Channel beams.

```
DEFDBL A-Z
10 CLS
ON ERROR GOTO 200
INPUT "MAT'L YIELD STRESS (N/mm^2)                 "; ys
INPUT "THICKNESS OF THE BEAM MAT'L (N/mm^2)  "; t
INPUT "FLANGE WIDTH (mm)                           "; b
INPUT "WED DEPTH (mm)                              "; d
INPUT "FULL SPAN LENGTH (mm)                       "; l
INPUT "FILENAME FOR DATA                           "; FILE$

FILE$ = "a:" + FILE$ + ".dat"
OPEN FILE$ FOR OUTPUT AS #1
PRINT #1, "MAT'L YIELD STRESS (N/mm^2)  :"; ys
PRINT #1, "MAT'L THICKNESS (mm)          :"; t
PRINT #1, "FLANGE WIDTH (mm)             :"; b
PRINT #1, "WEB DEPTH (mm)                :"; d
PRINT #1, "SPAN (mm)                     :"; l
PRINT #1, "DEFLECTN(mm)   LOAD(kN)"
PRINT #1, "----------------------  --------------"

young = 207000
pratio = .3

' Convert to centre line dimension
d = d - t
b = b - (t / 2)

q = d / b
k = 1.28 - ((.8 * q) / (2 + q)) - .0025 * (q ^ 2)
IF k < .425 THEN k = .425
Pcr = k * ((t / b) ^ 2) * (3.141593 ^ 2) * young / (12 * (1 - (pratio ^ 2)))

IF (ys < Pcr) THEN
    PRINT "THIS BEAM DOES NOT BUCKLE ELASTICALLY !"
    GOTO 201
END IF
```

```
FOR avstr = 0 TO ys STEP 2

IF (avstr < Pcr) THEN
' No Buckling
      h = d / 2
      beu = b

ELSE
' Elastic Buckling
      beff = b * (1 + 14 * (((avstr / Pcr) ^ .5) - .35) ^ 4) ^ (-.2)
      beu = .89 * beff + .11 * b
      h = (((d ^ 2) / 2) + (d * b)) / (beu + d + b)

END IF


I1 = beu * (t ^ 3) / 12 + beu * t * (h ^ 2)
I2 = t * (h ^ 3) / 12 + t * (h ^ 3) / 4
I3 = t * ((d - h) ^ 3) / 12 + (d - h) * t * ((d - h) ^ 2) / 4
I4 = b * (t ^ 3) / 12 + b * t * ((d - h) ^ 2)
Ixx = I1 + I2 + I3 + I4

f1 = avstr * beu * t
f2 = avstr / 2 * h * t
f3 = avstr * ((d - h) ^ 2) * t / (2 * h)
f4 = avstr * (d - h) * b * t

m = f1 * h + f2 * 2 * h / 3 + f3 * 2 / 3 * (d - h) + f4 * (d - h)
load = 4 * m / l
defln = load * (l ^ 3) / (48 * young * Ixx)

PRINT TAB(2); : PRINT USING "##.####"; defln;
PRINT TAB(12); : PRINT USING "###.####"; (load / 1000)
PRINT #1, TAB(2); : PRINT #1, USING "##.####"; defln;
PRINT #1, TAB(12); : PRINT #1, USING "###.####"; (load / 1000)

NEXT avstr

CLOSE #1
GOTO 201
200 PRINT "ERROR IN PROGRAM OR FILENAME"
GOTO 300
201 PRINT "FINISHED"
300 END
```

DSB3.bas

This program was designed to calculate load-deflection data for double span beams from single beam moment-mu data (based purely on the energy approach).

```
DECLARE SUB asin (value, angle)
DECLARE SUB intp (file$, mu, m)
2 CLS
ON ERROR GOTO 30
INPUT "Input single span Moment-mu data filename (Forget a: & .dat)    "; f$
INPUT "New data filename for the load-deflection data (Forget a: & .dat)"; newf$
file$ = "a:" + f$ + ".dat"
newf$ = "a:" + newf$ + ".dat"
OPEN newf$ FOR OUTPUT AS #2

INPUT "Enter Span length L1 (mm) [Central sup to load pt] "; l1
INPUT "Enter Span length (mm)                              "; sl
l2 = sl - l1
PRINT "Analysing "; file$; "AND STORING IN "; newf$

PRINT #2, "Double Span load-deflection (kN-mm) constructed from "; f$

FOR defln = 0 TO 70 STEP .1

    vmu1 = defln / l1
    CALL asin(vmu1, mu1)
    mu1 = mu1 / 3.14159 * 180

    vmu2 = defln / l2
    CALL asin(vmu2, mu2)
    mu2 = mu2 / 3.14159 * 180

    mu3 = (mu1 + mu2) / 2

    CALL intp(file$, mu1, m1)
    CALL intp(file$, mu3, m2)

    f1 = l1 * (SQR((1 - ((defln ^ 2) / (l1 ^ 2)))))
    f2 = l2 * (SQR((1 - ((defln ^ 2) / (l2 ^ 2)))))
    p = ((m1 / f1) + (m2 * ((1 / f1) + (1 / f2)))) / 1000
```

```
        PRINT TAB(2); : PRINT USING "###.###"; defln;
        PRINT TAB(12); : PRINT USING "#######.######"; p;
        PRINT TAB(29); : PRINT USING "##.##"; mu1;
        PRINT TAB(36); : PRINT USING "##.##"; mu3;
        PRINT TAB(43); : PRINT USING "########.#"; m1;
        PRINT TAB(55); : PRINT USING "########.#"; m2

        PRINT #2, TAB(2); : PRINT #2, USING "###.###"; defln;
        PRINT #2, TAB(12); : PRINT #2, USING "#######.######"; p;
        PRINT #2, TAB(29); : PRINT #2, USING "##.##"; mu1;
        PRINT #2, TAB(36); : PRINT #2, USING "##.##"; mu3;
        PRINT #2, TAB(43); : PRINT #2, USING "########.#"; m1;
        PRINT #2, TAB(55); : PRINT #2, USING "########.#"; m2


NEXT defln

30      PRINT "Error in filename or program"
GOTO 201
200     PRINT "EOF encountered"
        PRINT "CONVERTED DATA STORED IN "; g$
201     CLOSE #2
        INPUT "RUN THIS PROGRAM AGAIN "; b$
        IF b$ = "Y" OR b$ = "y" THEN GOTO 2
END


SUB asin (value, angle)
x = value
angle = ATN(x / SQR((-x) * x + 1))
END SUB
```

```
SUB intp (file$, angle, moment)
     OPEN file$ FOR INPUT AS #1

     INPUT #1, line$
     INPUT #1, x1, y1

1000   INPUT #1, x2, y2

     IF line$ = "" OR line$ = "EOF" THEN GOTO 20000

     IF angle > x1 AND angle < x2 THEN GOTO 2000
     IF angle = x1 THEN
          moment = y1
          GOTO 2500
     END IF
     IF angle = x2 THEN
          moment = y2
          GOTO 2500
     END IF

     x1 = x2
     y1 = y2
     GOTO 1000

2000     moment = (((angle - x1) / (x2 - x1)) * (y2 - y1)) + y1

2500     CLOSE #1
     GOTO 20010
20000 PRINT "Error in interpolation"
20010
END SUB
```

MSBPC.bas

This program was designed to calculate load-deflection data for double span Plain Channel beams from collapse characteristics derived from single span beam moment-mu data (based on two stages of elastic beam solutions and the energy approach).

```
DEFDBL A-Z
DECLARE SUB asin (value, angle)
DECLARE SUB intp (f$, angle, moment)

10 CLS
ON ERROR GOTO 200
INPUT "MAT'L YIELD STRESS (N/mm^2)              "; ys
INPUT "THICKNESS OF THE BEAM MAT'L (mm)     "; t
INPUT "FLANGE WIDTH (mm)                        "; b
INPUT "WED DEPTH (mm)                           "; d
INPUT "FULL SPAN LENGTH (mm)                    "; sl
INPUT "LOAD POINT DISTANCE (mm)                 "; ll
INPUT "FILENAME FOR DATA                        "; file$
file$ = "a:" + file$ + ".dat"
INPUT "FILENAME FOR THE COLLAPSE DATA     "; cdfile$
cdfile$ = "a:" + cdfile$ + ".dat"
OPEN file$ FOR OUTPUT AS #1
PRINT #1, "MAT'L YIELD STRESS (N/mm^2)      :"; ys
PRINT #1, "MAT'L THICKNESS (mm)             :"; t
PRINT #1, "FLANGE WIDTH (mm)                :"; b
PRINT #1, "WEB DEPTH (mm)                   :"; d
PRINT #1, "SPAN (mm)                        :"; sl
PRINT #1, "LOAD POINT DISTANCE              :"; ll
PRINT #1, "CONSTRUCTED FROM                 :"; cdfile$
PRINT #1, "DEFLECTN(mm)  LOAD(kN)"
PRINT #1, "--------------------  -------------"

' Convert d to centre line dimension
d = d - t
b = b - (t / 2)

young = 207000

OPEN cdfile$ FOR INPUT AS #2
INPUT #2, line$
INPUT #2, mum, mmax
CLOSE #2
```

```
pratio = .3
q = d / b
k = 1.28 - ((.8 * q) / (2 + q)) - .0025 * (q ^ 2)
IF k < .425 THEN k = .425
Pcr = k * ((t / b) ^ 2) * (3.141593 ^ 2) * young / (12 * (1 - (pratio ^ 2)))

FOR avstr = 0 TO (10 * ys) STEP 1

IF (avstr < Pcr) THEN
' No Buckling
      h = d / 2
      beu = b

ELSE
' Elastic Buckling
      beff = b * (1 + 14 * (((avstr / Pcr) ^ .5) - .35) ^ 4) ^ (-.2)
      beu = .89 * beff + .11 * b
      h = (((d ^ 2) / 2) + (d * b)) / (beu + d + b)

END IF


I1 = beu * (t ^ 3) / 12 + beu * t * (h ^ 2)
I2 = t * (h ^ 3) / 12 + t * (h ^ 3) / 4
I3 = t * ((d - h) ^ 3) / 12 + (d - h) * t * ((d - h) ^ 2) / 4
I4 = b * (t ^ 3) / 12 + b * t * ((d - h) ^ 2)
Ixx = I1 + I2 + I3 + I4

f1 = avstr * beu * t
f2 = avstr / 2 * h * t
f3 = avstr * ((d - h) ^ 2) * t / (2 * h)
f4 = avstr * (d - h) / h * b * t

M = f1 * h + f2 * 2 * h / 3 + f3 * 2 / 3 * (d - h) + f4 * (d - h)

p = -M / ((sl / 2) * ((3 * (l1 / sl) ^ 2) - ((l1 / sl) ^ 3)) - l1)
ra = p / 2 * (3 * ((l1 / sl) ^ 2) - ((l1 / sl) ^ 3))
c = ra * (sl ^ 2) / 6 - p / 6 * (l1 ^ 3) / sl
load = p
defln = (1 / (young * Ixx)) * (c * (sl - l1) - ra / 6 * ((sl - l1) ^ 3))
mb = M
IF (mb = mmax) OR (mb > mmax) THEN GOTO 100
```

```
PRINT TAB(2); : PRINT USING "####.####"; defln;
PRINT TAB(16); : PRINT USING "###.####"; (load / 1000)
PRINT #1, TAB(2); : PRINT #1, USING "####.####"; defln;
PRINT #1, TAB(16); : PRINT #1, USING "###.####"; (load / 1000)

NEXT avstr

' Mid support collapsed
100
FOR mu = 0 TO .174533 STEP .000174533#
mub = mu / 3.141593 * 180
CALL intp(cdfile$, mub, mb)

load = (young * Ixx * mu + mb * sl / 3) / (((sl - l1) * sl / 6) - (((sl - l1) ^ 3) / (6 * sl)))

d1 = mb / 2 * (l1 ^ 2)
d2 = mb * (l1 ^ 3) / (6 * sl)
d3 = load * (sl - l1) * (l1 ^ 3) / (6 * sl)
d4 = mb * sl * l1 / 3
d5 = load * l1 / 6 * (((sl - l1) * sl) - (((sl - l1) ^ 3) / sl))
defl1 = (d1 - d2 - d3 - d4 + d5) / (young * Ixx)

IF (mu = 0) THEN ddif = defl1
defl1 = defl1 - ddif

p = load
ra = p / 2 * (3 * ((l1 / sl) ^ 2) - ((l1 / sl) ^ 3))
c = ra * (sl ^ 2) / 6 - p / 6 * (l1 ^ 3) / sl
defl2 = (1 / (young * Ixx)) * (c * (sl - l1) - ra / 6 * ((sl - l1) ^ 3))

defln = defl1 + defl2

rb = (mb + load * (sl - l1)) / sl
md = (rb * l1 - mb)
IF (md = mmax) OR (md > mmax) THEN GOTO 150

PRINT TAB(2); : PRINT USING "####.####"; defln;
PRINT TAB(16); : PRINT USING "###.####"; (load / 1000)
PRINT #1, TAB(2); : PRINT #1, USING "####.####"; defln;
PRINT #1, TAB(16); : PRINT #1, USING "###.####"; (load / 1000)

NEXT mu
```

```
' Collapsed at b and d
150     dlast = defln

l2 = sl - l1

FOR dinc = 0 TO 100 STEP .1

        vmu1 = dinc / l1
        CALL asin(vmu1, mu1)
        mu1 = mu1 / 3.14159 * 180

        vmu2 = dinc / l2
        CALL asin(vmu2, mu2)
        mu2 = mu2 / 3.14159 * 180

        mu3 = (mu1 + mu2) / 2

        CALL intp(cdfile$, mu1, m1)
        CALL intp(cdfile$, mu3, m2)

        f1 = l1 * (SQR((1 - ((dinc ^ 2) / (l1 ^ 2)))))
        f2 = l2 * (SQR((1 - ((dinc ^ 2) / (l2 ^ 2)))))
        p = ((m1 / f1) + (m2 * ((1 / f1) + (1 / f2))))
        load = p

ra = p / 2 * (3 * ((l1 / sl) ^ 2) - ((l1 / sl) ^ 3))
c = ra * (sl ^ 2) / 6 - p / 6 * (l1 ^ 3) / sl
de = (1 / (young * Ixx)) * (c * (sl - l1) - ra / 6 * ((sl - l1) ^ 3))
dec = de - dp
IF (dinc = 0) THEN dec = 0

        defl = dinc + dlast + dec

PRINT TAB(2); : PRINT USING "####.####"; defl;
PRINT TAB(16); : PRINT USING "###.####"; (load / 1000)
PRINT #1, TAB(2); : PRINT #1, USING "####.####"; defl;
PRINT #1, TAB(16); : PRINT #1, USING "###.####"; (load / 1000)

175
dp = de
NEXT dinc
```

```
CLOSE #1
GOTO 201
200 PRINT "ERROR IN PROGRAM OR FILENAME"
GOTO 300
201 PRINT "FINISHED"
300 END

SUB asin (value, angle)
x = value
angle = ATN(x / SQR((-x) * x + 1))
END SUB

SUB intp (f$, angle, moment)
      OPEN f$ FOR INPUT AS #2
      INPUT #2, line$
      INPUT #2, x1, y1
      x0 = x1
      x1 = x1 - x0
1000   INPUT #2, x2, y2
      x2 = x2 - x0
      IF angle > x1 AND angle < x2 THEN GOTO 2000
      IF angle = x1 THEN
            moment = y1
            GOTO 2500
      END IF
      IF angle = x2 THEN
            moment = y2
            GOTO 2500
      END IF
      x1 = x2
      y1 = y2
      GOTO 1000
2000     moment = (((angle - x1) / (x2 - x1)) * (y2 - y1)) + y1
2500
CLOSE #2
     GOTO 20010
20000 PRINT "Error in interpolation"
20010
END SUB
```

LC8.bas

This program calculates the data points for the collapse curve of Lipped Channel beams using the LC8 plastic mechanism.

```
DECLARE SUB ACOS (value AS DOUBLE, angle AS DOUBLE)
DECLARE SUB ASIN (value AS DOUBLE, angle AS DOUBLE)
DECLARE SUB ATE (c#, d#, amax#, mu#, af#, adiffin#)
DIM pt(5), diff(5)
DEFDBL A-Z

10 CLS
ON ERROR GOTO 199
INPUT "YIELD STRESS OF BEAM MAT'L (N/mm^2)          "; ys
REM INPUT "YIELD STRAIN OF BEAM MAT'L (10^-6 st)  "; sty
INPUT "ULTIMATE STRESS OF BEAM MAT'L (N/mm^2)   "; us
INPUT "THICKNESS OF CHANNEL MAT'L (mm)          "; t
INPUT "FLANGE WIDTH                             "; b
INPUT "CHANNEL DEPTH (mm)                       "; d
INPUT "LIP SIZE (mm)                            "; w
INPUT "MECHANISM SIZE c (mm)                    "; c
INPUT "LIP MECHANISM ANGLE, beta (deg)          "; beta
REM* mu BEING THE ANGLE OF BEND OF THE BUCKLED BEAM *
INPUT "LAST POINT FOR MU in (deg)               "; mul
mul = mul / 180 * 3.141593
INPUT "INTERVAL FOR MU in (deg)                 "; muintv
muintv = muintv / 180 * 3.141593
INPUT "DISTANCE BETWEEN HORIZONTAL BOLTS        "; lb
INPUT "DISTANCE BETWEEN TOP AND TOP BOLTS       "; amax
INPUT "RADIUS-to-THICKNESS RATIO FOR HINGES     "; brtr
INPUT "SPAN LENGTH in (mm)                      "; sl
INPUT "FILENAME FOR THE DATA POINTS             "; file$
file$ = "a:" + file$ + ".DAT"
OPEN file$ FOR OUTPUT AS #1
PRINT #1, "SECTION DETAILS"
PRINT #1, "------------------------"
PRINT #1, "YIELD STRESS OF BEAM MAT'L (N/mm^2)          :"; ys
REM PRINT #1, "YIELD STRAIN OF BEAM MAT'L (10^-6 st) :"; sty
PRINT #1, "ULTIMATE STRESS OF BEAM MAT'L (N/mm^2)  :"; us
PRINT #1, "THICKNESS OF CHANNEL MAT'L (mm)          :"; t
PRINT #1, "FLANGE WIDTH (mm)                        :"; b
PRINT #1, "CHANNEL WEB DEPTH (mm)                   :"; d
PRINT #1, "LIP SIZE (mm)                            :"; w
PRINT #1, "MECHANISM SIZE c (mm)                    :"; c
PRINT #1, "LIP MECHANISM ANGLE, beta (deg)          :"; beta
```

```
PRINT #1, "INTERVALS FOR mu (deg)                    :"; muintv / 3.141593 * 180
PRINT #1, "DISTANCE BETWEEN HORIZONTAL BOLTS         :"; lb
PRINT #1, "DISTANCE BETWEEN TOP AND TOP BOLTS        :"; amax
PRINT #1, "RADIUS-to-THICKNESS RATIO                 :"; brtr
PRINT #1, "SPAN LENGTH (mm)                          :"; sl
PRINT #1, "      "
PRINT #1, " Angle     Moment Cap.    Load    Defln      Diff          adif"
PRINT #1, "mu(deg)     (Nmm)         (kN)    (mm)    (Nmmrad)       (mm)"
PRINT #1, "---------  ------------   ------  -------  ------------   --------"

REM ***********************************
REM *      Calculation of the data points      *
REM ***********************************

beta = beta / 180 * 3.141593

'The ultimate moment :-
d = d - t
w = w - (t / 2)
b = b - t
mult = ys * t * ((b * d) + (d ^ 2) / 4 + w * (d - w))

'The rolling radius :-
rr = brtr * t

'Calculation of the mpsh (Considering strain hardening)
mp = ys * (t ^ 2) / 4
ssh = us
mpsh = mp + (ssh - ys) * (t ^ 2) / 6
mp = mpsh

FOR mu = (muintv + (.001 / 180 * 3.141593)) TO mul STEP muintv

mu1 = mu - muintv
mu2 = mu + muintv

CALL ATE(c, d, amax, mu, a, adiffin)
CALL ATE(c, d, amax, mu1, a1, adiffin1)
CALL ATE(c, d, amax, mu2, a2, adiffin2)

' Check for lock-up condition
teta2 = ATN((a / d))
mulu = ATN((c / (d * COS(teta2))))
IF (mu = mulu) OR (mu > mulu) THEN
    PRINT "LOCK UP CONDITION 2"
```

```
      PRINT #1, "LOCK UP CONDITION 2 at mu = "; mu / 3.141593 * 180
      GOTO 201
END IF


REM* MARGIN HALVING IS USED TO FIND THE m DATA POINTS.*
pt(1) = 1
pt(5) = mult
pt(3) = ((pt(5) - pt(1)) / 2) + pt(1)
count = 1
20 count = count + 1
  pt(4) = ((pt(5) - pt(3)) / 2) + pt(3)
  pt(2) = ((pt(3) - pt(1)) / 2) + pt(1)

FOR I = 1 TO 5
      I = INT(I)
      m = pt(I)

'START OF ENERGY EQUATION

      ' Left hand side expression
      lhs = 4 * m * muintv

      ' Right hand side of the work equation

'When a = amax, lock-up also occurs
      IF (a2 > amax) THEN GOTO 200
      teta21 = ATN((a1 / d))
      teta22 = ATN((a2 / d))

      'Right side first expression
      hm1 = 2 * mp * (1 - (m / mult) ^ 2) * b
      f3 = c * SIN(mu1) + d * COS(mu1) * COS(teta21) - d + a1 * (1 + SIN(teta21))
      CALL ASIN((f3 / c), f4)
      eta11 = ATN(((TAN((f4 - mu1))) * COS(teta21)))
      f5 = c * SIN(mu2) + d * COS(mu2) * COS(teta22) - d + a2 * (1 + SIN(teta22))
      CALL ASIN((f5 / c), f6)
      eta12 = ATN(((TAN((f6 - mu2))) * COS(teta22)))
      rhs1 = hm1 * eta12 - hm1 * eta11

      'Right side second expression
       hm2 = 2 * mp * (1 - (m / mult) ^ 2) * (b + a)
       eta21 = ATN(((TAN(f4)) * COS(teta21)))
       eta22 = ATN(((TAN(f6)) * COS(teta22)))
       rhs2 = hm2 * eta22 - hm2 * eta21
```

```
'Right side third expression
rhs3 = hm1 * mu2 - hm1 * mu1

'Right side forth expression
hm4 = 2 * mp * (1 - (m / mult) ^ 2) * (d - a)
f7 = (d - a1) / (SIN(mu1) + (d * COS(mu1) * COS(teta21)) / c)
f8 = f7 * d * COS(teta21) / c
teta41 = ATN((f8 * a1 / (d * (f7 * COS(mu1) - f8 * SIN(mu1)))))
f9 = (d - a2) / (SIN(mu2) + (d * COS(mu2) * COS(teta22)) / c)
f10 = f9 * d * COS(teta22) / c
teta42 = ATN((f10 * a2 / (d * (f9 * COS(mu2) - f10 * SIN(mu2)))))
rhs4 = hm4 * teta42 - hm4 * teta41

'Right side fifth expression
zeta2 = ATN((c / d))
f11 = SQR((c ^ 2 + d ^ 2))
hm5 = 2 * mp * (1 - (m / mult) ^ 2) / (SQR(1 - .75 * ((m / mult) ^ 2) *
      ((SIN(zeta2)) ^ 2) * (4 - 3 * ((SIN(zeta2)) ^ 2)))) * f11
f12 = (a1 / c) * COS(zeta2)
CALL ASIN(f12, teta51)
f13 = (a2 / c) * COS(zeta2)
CALL ASIN(f13, teta52)
rhs5 = hm5 * teta52 - hm5 * teta51

'Right side sixth expression
hm6 = mp * lb * (1 - (m / mult) ^ 2) / (SQR((1 - .75 * ((m / mult) ^ 2))))
eta61 = 2 * a1 / rr + teta21
eta62 = 2 * a2 / rr + teta22
rhs6 = hm6 * eta62 - hm6 * eta61

'Right side seventh expression
hm7 = 2 * mp * (1 - (m / mult) ^ 2) / (SQR((1 - .75 * ((m / mult) ^ 2))))
eta71 = c * a1 / rr
eta72 = c * a2 / rr
rhs7 = hm7 * eta72 - hm7 * eta71

'Right side First membrane strain expression
mem11 = ys * b * c * t * (SQR((1 + ((b ^ 2) / (c ^ 2)) * (SIN(teta21) ^ 2))) - 1)
mem12 = ys * b * c * t * (SQR((1 + ((b ^ 2) / (c ^ 2)) * (SIN(teta22) ^ 2))) - 1)
rhs8 = mem12 - mem11

'Right side lip membrane expression at B and C
lmem1 = ys * t * eta21 * (w ^ 2) / 2
lmem2 = ys * t * eta22 * (w ^ 2) / 2
rhs9 = lmem2 - lmem1
```

```
'Right side lip mechanism at A and D
lhm1 = 4 * mp * (1 - (m / mult) ^ 2) * w
lhm2 = 4 * mp * (1 - (m / mult) ^ 2) / (SQR(1 - .75 * ((m / mult) ^ 2) *
      ((SIN(beta)) ^ 2) * (4 - 3 * ((SIN(beta)) ^ 2)))) * w / (COS(beta))
f14 = COS((eta11 / 2)) - (SIN((eta11 / 2))) / TAN(beta)
CALL ACOS(f14, eta1011)
f15 = COS((eta12 / 2)) - (SIN((eta12 / 2))) / TAN(beta)
llup = f15 * w * TAN(beta)

IF (llup = 0) OR (llup < 0) THEN GOTO 198
    CALL ACOS(f15, eta1012)

    f16 = 1 / (COS((eta11 / 2)) + SIN((eta11 / 2)) * (TAN(beta)))
    CALL ACOS(f16, f17)
    f18 = (SIN(f17)) / (SIN(beta))
    CALL ASIN(f18, eta1021)
    f19 = 1 / (COS((eta12 / 2)) + SIN((eta12 / 2)) * (TAN(beta)))
    CALL ACOS(f19, f20)
    f21 = (SIN(f20)) / (SIN(beta))
    CALL ASIN(f21, eta1022)
    rhs10 = (lhm1 * eta1012 - lhm1 * eta1011) + (lhm2 * eta1022 - lhm2 * eta1021)

    'Right side lip mechanism at K and L
    f22 = COS((mu1 / 2)) - (SIN((mu1 / 2))) / TAN(beta)
    CALL ACOS(f22, eta1111)
    f23 = COS((mu2 / 2)) - (SIN((mu2 / 2))) / TAN(beta)
    llup2 = f23 * w * TAN(beta)

IF (llup2 = 0) OR (llup2 < 0) THEN GOTO 198
    CALL ACOS(f23, eta1112)

    f24 = 1 / (COS((mu1 / 2)) + SIN((mu1 / 2)) * (TAN(beta)))
    CALL ACOS(f24, f25)
    f26 = (SIN(f25)) / (SIN(beta))
    CALL ASIN(f26, eta1121)
    f27 = 1 / (COS((mu2 / 2)) + SIN((mu2 / 2)) * (TAN(beta)))
    CALL ACOS(f27, f28)
    f29 = (SIN(f28)) / (SIN(beta))
    CALL ASIN(f29, eta1122)
    rhs11 = (lhm1 * eta1112 - lhm1 * eta1111) + (lhm2 * eta1122 - lhm2 * eta1121)


rhs = rhs1 + rhs2 + rhs3 + rhs4 + rhs5 + rhs6 + rhs7 + rhs8 + rhs9 + rhs10 + rhs11

'END OF ENERGY EQUATION
```

```
        diff(I) = rhs - lhs
        diff(I) = ABS(diff(I))
    NEXT I
    IF diff(3) < .0000001 OR count = 500 THEN
        m = pt(3)
        GOTO 100
    END IF
    IF diff(2) < diff(4) THEN
        pt(5) = pt(3)
        pt(3) = pt(2)
    ELSE
        pt(1) = pt(3)
        pt(3) = pt(4)
    END IF
    GOTO 20
    100
    PRINT "BINGO !"

    'TO CONVERT MOMENT-ANGLE DATA TO MID SPAN LOAD-DEFLECTION
    load = (4 * m / sl) / 1000
    defln = sl / 2 * SIN(mu)

    PRINT TAB(2); : PRINT USING "##.####"; (mu * 180 / 3.141593);
    PRINT TAB(11); : PRINT USING "#########.##"; m;
    PRINT TAB(25); : PRINT USING "###.#########"; diff(3);
    PRINT TAB(40); : PRINT USING "###.#########"; adiffin
    PRINT #1, TAB(1); : PRINT #1, USING "##.#######"; (mu * 180 / 3.141593);
    PRINT #1, TAB(12); : PRINT #1, USING "#########.##"; m;
    PRINT #1, TAB(28); : PRINT #1, USING "###.####"; load;
    PRINT #1, TAB(38); : PRINT #1, USING "###.####"; defln;
    PRINT #1, TAB(50); : PRINT #1, USING "####.###########"; diff(3);
    PRINT #1, TAB(70); : PRINT #1, USING "###.###########"; adiffin

    NEXT mu

    CLOSE #1
    GOTO 201
    198 PRINT "LIP MECHANISM LOCK UP !"
      PRINT #1, "LIP MECHANISM LOCK UP AT MU = "; mu2 / 3.141593 * 180
    GOTO 201
    199 PRINT "ERROR IN FILE OR PROGRAM"
    GOTO 300
    200 PRINT "MECHANISM LOCKED UP (CONDITION 1) ! "
```

```
   PRINT #1, "MECHANISM LOCK UP  CONDITION 1 AT MU="; mu2 /
                                                    3.141593 * 180
201 PRINT "FINISHED "
202 INPUT "TRY AGAIN "; resp$
IF resp$ = "Y" OR resp$ = "y" THEN GOTO 10
PRINT "PROGRAM TERMINATED"
300 END


SUB ACOS (value AS DOUBLE, angle AS DOUBLE)
x = value
angle = ATN((-x) / SQR((-x) * x + 1)) + 1.5708
END SUB


SUB ASIN (value AS DOUBLE, angle AS DOUBLE)
x = value
angle = ATN(x / SQR((-x) * x + 1))
END SUB


SUB ATE (c, d, amax, mu, af, adiffin)
DIM q(5), adif(5)
'Trial and Error routine for finding a2
REM* MARGIN HALVING IS USED TO FIND THE a2 DATA POINTS.*
q(1) = .000001
q(5) = amax + 1
q(3) = ((q(5) - q(1)) / 2) + q(1)
qcount = 1
12 qcount = qcount + 1
  q(4) = ((q(5) - q(3)) / 2) + q(3)
  q(2) = ((q(3) - q(1)) / 2) + q(1)

FOR J = 1 TO 5
      J = INT(J)
      a = q(J)

      ls1 = d * COS(mu) * COS((ATN((a / d))))
      ls2 = a * (1 + SIN((ATN((a / d)))))
      f14 = (c * COS(mu) - d * SIN(mu) * COS((ATN((a / d))))) / c
      CALL ACOS(f14, f15)
      ls3 = c * SIN(f15)
      rs = d - c * SIN(mu)
      adif(J) = ABS((ls1 + ls2 - ls3 - rs))
```

```
NEXT J
IF adif(3) < .0000001 OR qcount = 1000 THEN
      af = q(3)
      adiffin = adif(3)
      GOTO 14
END IF
IF adif(2) < adif(4) THEN
      q(5) = q(3)
      q(3) = q(2)
ELSE
      q(1) = q(3)
      q(3) = q(4)
END IF

GOTO 12
14
PRINT "MAGIC !"
END SUB
```

ELASTIC8.bas

This program calculates the elastic loading line for Lipped Channel beams.

```
DEFDBL A-Z
10 CLS
ON ERROR GOTO 200
INPUT "MAT'L YIELD STRESS (N/mm^2)                "; ys
INPUT "THICKNESS OF THE BEAM MAT'L (N/mm^2)  "; t
INPUT "FLANGE WIDTH (mm)                          "; b
INPUT "WED DEPTH (mm)                             "; d
INPUT "LIP SIZE (mm)                              "; w
INPUT "FULL SPAN LENGTH (mm)                      "; l
INPUT "FILENAME FOR DATA                          "; FILE$

FILE$ = "a:" + FILE$ + ".dat"
OPEN FILE$ FOR OUTPUT AS #1
PRINT #1, "MAT'L YIELD STRESS (N/mm^2)  :"; ys
PRINT #1, "MAT'L THICKNESS (mm)         :"; t
PRINT #1, "FLANGE WIDTH (mm)            :"; b
PRINT #1, "WEB DEPTH (mm)               :"; d
PRINT #1, "LIP SIZE (mm)                :"; w
PRINT #1, "SPAN (mm)                    :"; l
PRINT #1, "DEFLECTN(mm)   LOAD(kN)"
PRINT #1, "----------------------  --------------"

' Convert d to centre line dimension
b = b - t
d = d - t
w = w - (t / 2)

mult = ys * t * ((b * d) + (d ^ 2) / 4 + w * (d - w))
young = 207000
pratio = .3

q = d / b
IF (w = (b / 5)) OR (w > (b / 5)) THEN
      k = 5.4 - ((1.4 * q) / (.6 + q)) - (.02 * (q ^ 3))
      IF (k < 4) THEN k = 4
ELSE
      k = 1.28 - ((.8 * q) / (2 + q)) - .0025 * (q ^ 2)
      IF k < .425 THEN k = .425
END IF

Pcr = k * ((t / b) ^ 2) * (3.141593 ^ 2) * young / (12 * (1 - (pratio ^ 2)))
```

```
FOR avstr = 0 TO (10 * ys) STEP 1

IF (avstr < Pcr) THEN
' No Buckling
      h = d / 2
      bef = b

ELSE
' Elastic Buckling
      beff = b * ((1 + 14 * (((avstr / Pcr) ^ .5) - .35) ^ 4) ^ (-.2))
      beu = .89 * beff + .11 * b

      IF (w = (b / 5)) OR (w > (b / 5)) THEN
            bef = beff
      ELSE
            bef = beu
      END IF

h = (((d ^ 2) / 2) + (d * b) + (w * d)) / (bef + (2 * w) + d + b)

END IF

I1 = bef * (t ^ 3) / 12 + bef * t * (h ^ 2)
I2 = t * (h ^ 3) / 12 + t * (h ^ 3) / 4
I3 = t * ((d - h) ^ 3) / 12 + (d - h) * t * ((d - h) ^ 2) / 4
I4 = b * (t ^ 3) / 12 + b * t * ((d - h) ^ 2)
I5 = t * (w ^ 3) / 12 + w * t * ((h - (w / 2)) ^ 2)
I6 = t * (w ^ 3) / 12 + w * t * ((d - h - (w / 2)) ^ 2)
Ixx = I1 + I2 + I3 + I4 + I5 + I6

f1 = avstr * bef * t
f2 = (avstr / 2) * h * t
f3 = avstr * ((d - h) ^ 2) * t / (2 * h)
f4 = avstr * ((d - h) / h) * b * t
f5 = avstr * w * t * ((h - w) / h)
f6 = (avstr / 2) * w * t * (w / h)
f7 = avstr * w * t * ((d - h - w) / h)
f8 = f6

M = f1 * h + f2 * 2 * h / 3 + f3 * (2 / 3) * (d - h) + f4 * (d - h) + f5 * (h - (w / 2)) +
    f6 * (h - (w / 3)) + f7 * (d - h - (w / 2)) + f8 * (d - h - (w / 3))

IF (M > mult) THEN M = mult
load = 4 * M / l
```

```
defln = load * (l ^ 3) / (48 * young * Ixx)

strdif = ABS((ys - avstr))
IF (strdif < 1) THEN yload = load

PRINT TAB(2); : PRINT USING "##.####"; defln;
PRINT TAB(12); : PRINT USING "###.####"; (load / 1000)
PRINT #1, TAB(2); : PRINT #1, USING "##.####"; defln;
PRINT #1, TAB(12); : PRINT #1, USING "###.####"; (load / 1000)
IF (M = mult) THEN GOTO 199

NEXT avstr

199    PRINT #1, "First Yield Load : "; yload
       PRINT #1, "Mult             : "; mult

CLOSE #1
GOTO 201
200 PRINT "ERROR IN PROGRAM OR FILENAME"
GOTO 300
201 PRINT "FINISHED"
300 END
```

MSBLC.bas

This program was designed to calculate load-deflection data for double span Lipped Channel beams from collapse characteristics derived from single span beam moment-mu data (based on two stages of elastic beam solutions and the energy approach).

```
DEFDBL A-Z
DECLARE SUB asin (value, angle)
DECLARE SUB intp (f$, angle, moment)

10 CLS
ON ERROR GOTO 200
INPUT "THICKNESS OF THE BEAM MAT'L (N/mm^2)  "; t
INPUT "FLANGE WIDTH (mm)                     "; b
INPUT "WED DEPTH (mm)                        "; d
INPUT "LIP SIZE (mm)                         "; w
INPUT "FULL SPAN LENGTH (mm)                 "; sl
INPUT "LOAD POINT DISTANCE (mm)              "; ll
INPUT "FILENAME FOR DATA                     "; file$
file$ = "a:" + file$ + ".dat"
INPUT "FILENAME FOR THE COLLAPSE DATA        "; cdfile$
cdfile$ = "a:" + cdfile$ + ".dat"
OPEN file$ FOR OUTPUT AS #1
PRINT #1, "MAT'L THICKNESS (mm)      :"; t
PRINT #1, "FLANGE WIDTH (mm)         :"; b
PRINT #1, "WEB DEPTH (mm)            :"; d
PRINT #1, "LIP SIZE (mm)             :"; w
PRINT #1, "SPAN (mm)                 :"; sl
PRINT #1, "LOAD POINT DISTANCE       :"; ll
PRINT #1, "CONSTRUCTED FROM          :"; cdfile$
PRINT #1, "DEFLECTN(mm)  LOAD(kN)"
PRINT #1, "--------------------  -------------"

' Convert d to centre line dimension
d = d - t
b = b - t
w = w - (t / 2)

young = 207000
```

```
h = d / 2
I1 = b * (t ^ 3) / 12 + b * t * (h ^ 2)
I2 = t * (h ^ 3) / 12 + t * (h ^ 3) / 4
I3 = t * ((d - h) ^ 3) / 12 + (d - h) * t * ((d - h) ^ 2) / 4
I4 = b * (t ^ 3) / 12 + b * t * ((d - h) ^ 2)
I5 = t * (w ^ 3) / 12 + w * t * ((h - (w / 2)) ^ 2)
I6 = t * (w ^ 3) / 12 + w * t * ((d - h - (w / 2)) ^ 2)
Ixx = I1 + I2 + I3 + I4 + I5 + I6

OPEN cdfile$ FOR INPUT AS #2
INPUT #2, line$
INPUT #2, mum, mmax
CLOSE #2

FOR p = 0 TO 100000 STEP 50
ra = p / 2 * (3 * ((l1 / sl) ^ 2) - ((l1 / sl) ^ 3))
c = ra * (sl ^ 2) / 6 - p / 6 * (l1 ^ 3) / sl
load = p
defln = (1 / (young * Ixx)) * (c * (sl - l1) - ra / 6 * ((sl - l1) ^ 3))
mb = p * l1 - ra * sl

IF (mb = mmax) OR (mb > mmax) THEN GOTO 100

PRINT TAB(2); : PRINT USING "####.####"; defln;
PRINT TAB(16); : PRINT USING "###.####"; (load / 1000)
PRINT #1, TAB(2); : PRINT #1, USING "####.####"; defln;
PRINT #1, TAB(16); : PRINT #1, USING "###.####"; (load / 1000)

NEXT p

' Mid support collapsed
100
FOR mu = 0 TO .174533 STEP .000174533#
mub = mu / 3.141593 * 180
CALL intp(cdfile$, mub, mb)

load = (young * Ixx * mu + mb * sl / 3) / (((sl - l1) * sl / 6) - (((sl - l1) ^ 3) / (6 * sl)))

d1 = mb / 2 * (l1 ^ 2)
d2 = mb * (l1 ^ 3) / (6 * sl)
d3 = load * (sl - l1) * (l1 ^ 3) / (6 * sl)
d4 = mb * sl * l1 / 3
d5 = load * l1 / 6 * (((sl - l1) * sl) - (((sl - l1) ^ 3) / sl))
defl1 = (d1 - d2 - d3 - d4 + d5) / (young * Ixx)
```

```
IF (mu = 0) THEN ddif = defl1
defl1 = defl1 - ddif

p = load
ra = p / 2 * (3 * ((l1 / sl) ^ 2) - ((l1 / sl) ^ 3))
c = ra * (sl ^ 2) / 6 - p / 6 * (l1 ^ 3) / sl
defl2 = (1 / (young * Ixx)) * (c * (sl - l1) - ra / 6 * ((sl - l1) ^ 3))

defln = defl1 + defl2

rb = (mb + load * (sl - l1)) / sl
md = (rb * l1 - mb)
IF (md = mmax) OR (md > mmax) THEN GOTO 150

PRINT TAB(2); : PRINT USING "####.####"; defln;
PRINT TAB(16); : PRINT USING "###.####"; (load / 1000)
PRINT #1, TAB(2); : PRINT #1, USING "####.####"; defln;
PRINT #1, TAB(16); : PRINT #1, USING "###.####"; (load / 1000)

NEXT mu

' Collapsed at b and d
150    dlast = defln

l2 = sl - l1

FOR dinc = 0 TO 100 STEP .1

    vmu1 = dinc / l1
    CALL asin(vmu1, mu1)
    mu1 = mu1 / 3.14159 * 180

    vmu2 = dinc / l2
    CALL asin(vmu2, mu2)
    mu2 = mu2 / 3.14159 * 180

    mu3 = (mu1 + mu2) / 2

    CALL intp(cdfile$, mu1, m1)
    CALL intp(cdfile$, mu3, m2)

    f1 = l1 * (SQR((1 - ((dinc ^ 2) / (l1 ^ 2)))))
    f2 = l2 * (SQR((1 - ((dinc ^ 2) / (l2 ^ 2)))))
    p = ((m1 / f1) + (m2 * ((1 / f1) + (1 / f2))))
    load = p
```

```
ra = p / 2 * (3 * ((l1 / sl) ^ 2) - ((l1 / sl) ^ 3))
c = ra * (sl ^ 2) / 6 - p / 6 * (l1 ^ 3) / sl
de = (1 / (young * Ixx)) * (c * (sl - l1) - ra / 6 * ((sl - l1) ^ 3))
dec = de - dp
IF (dinc = 0) THEN dec = 0

    defl = dinc + dlast + dec

PRINT TAB(2); : PRINT USING "####.####"; defl;
PRINT TAB(16); : PRINT USING "###.####"; (load / 1000)
PRINT #1, TAB(2); : PRINT #1, USING "####.####"; defl;
PRINT #1, TAB(16); : PRINT #1, USING "###.####"; (load / 1000)

175
dp = de
NEXT dinc

CLOSE #1
GOTO 201
200 PRINT "ERROR IN PROGRAM OR FILENAME"
GOTO 300
201 PRINT "FINISHED"
300 END


SUB asin (value, angle)
x = value
angle = ATN(x / SQR((-x) * x + 1))
END SUB


SUB intp (f$, angle, moment)
    OPEN f$ FOR INPUT AS #2

    INPUT #2, line$
    INPUT #2, x1, y1
    x0 = x1
    x1 = x1 - x0

1000   INPUT #2, x2, y2
    x2 = x2 - x0

    IF line$ = "" OR line$ = "EOF" THEN GOTO 20000

    IF angle > x1 AND angle < x2 THEN GOTO 2000
```

```
        IF angle = x1 THEN
            moment = y1
            GOTO 2500
        END IF
        IF angle = x2 THEN
            moment = y2
            GOTO 2500
        END IF

        x1 = x2
        y1 = y2
        GOTO 1000

2000    moment = (((angle - x1) / (x2 - x1)) * (y2 - y1)) + y1

2500
CLOSE #2
        GOTO 20010
20000 PRINT "Error in interpolation"
20010
END SUB
```

Z1.bas

This program calculates the data points for the collapse curve of Zed section beams using the Z1 plastic mechanism which applies to failure sections along the span of beams subjected to Uniformly Distributed Loads.

```
DECLARE SUB ACOS (value AS DOUBLE, angle AS DOUBLE)
DECLARE SUB ASIN (value AS DOUBLE, angle AS DOUBLE)
DIM pt(5), diff(5)
DEFDBL A-Z

10 CLS
ON ERROR GOTO 199
INPUT "YIELD STRESS OF BEAM MAT'L (N/mm^2)          "; ys
INPUT "ULTIMATE STRESS OF BEAM MAT'L (N/mm^2)  "; us
INPUT "THICKNESS OF CHANNEL MAT'L (mm)              "; t
INPUT "COMPRESSION FLANGE WIDTH (mm)                "; b
INPUT "TENSION FLANGE WIDTH (mm)                    "; b2
INPUT "CHANNEL DEPTH (mm)                           "; d
INPUT "COMPRESSION FLANGE LIP SIZE (mm)             "; w
INPUT "TENSION FLANGE LIP SIZE (mm)                 "; w2
INPUT "MECHANISM SIZE c (mm)                        "; c
INPUT "LIP MECHANISM ANGLE, beta (deg)              "; beta
REM* mu BEING THE ANGLE OF BEND OF THE BUCKLED BEAM *
INPUT "LAST POINT FOR MU in (deg)                   "; mul
mul = mul / 180 * 3.141593
INPUT "INTERVAL FOR MU in (deg)                     "; muintv
muintv = muintv / 180 * 3.141593
'INPUT "DISTANCE BETWEEN HORIZONTAL BOLTS     "; lb
'INPUT "DISTANCE BETWEEN TOP AND TOP BOLTS    "; amax
INPUT "RADIUS-to-THICKNESS RATIO FOR HINGES    "; brtr
INPUT "SPAN LENGTH in (mm)                          "; sl
INPUT "FILENAME FOR THE DATA POINTS                 "; file$
file$ = "a:" + file$ + ".DAT"
OPEN file$ FOR OUTPUT AS #1
PRINT #1, "SECTION DETAILS"
PRINT #1, "--------------------------"
PRINT #1, "YIELD STRESS OF BEAM MAT'L (N/mm^2)        :"; ys
PRINT #1, "ULTIMATE STRESS OF BEAM MAT'L (N/mm^2) :"; us
PRINT #1, "THICKNESS OF CHANNEL MAT'L (mm)            :"; t
PRINT #1, "FLANGE WIDTH [comp,ten] (mm)               :"; b, b2
PRINT #1, "CHANNEL WEB DEPTH (mm)                     :"; d
PRINT #1, "LIP SIZE [comp,ten] (mm)                   :"; w, w2
PRINT #1, "MECHANISM SIZE c (mm)                      :"; c
PRINT #1, "LIP MECHANISM ANGLE, beta (deg)      :"; beta
```

```
PRINT #1, "INTERVALS FOR mu (deg)                    :"; muintv / 3.141593 * 180
PRINT #1, "DISTANCE BETWEEN HORIZONTAL BOLTS         :"; lb
PRINT #1, "DISTANCE BETWEEN TOP AND TOP BOLTS        :"; amax
PRINT #1, "RADIUS-to-THICKNESS RATIO                 :"; brtr
PRINT #1, "SPAN LENGTH (mm)                          :"; sl
PRINT #1, "      "
PRINT #1, " Angle      Moment Cap.    Load     Defln       Diff        adif"
PRINT #1, "mu(deg)       (Nmm)        (kN)     (mm)      (Nmmrad)    (mm)"
PRINT #1, "----------  ---------------  ------  -------  ------------  ------"


REM ***********************************
REM *       Calculation of the data points       *
REM ***********************************

beta = beta / 180 * 3.141593

'The ultimate moment :-
d = d - t
w = w - (t / 2)
b = b - t
b2 = b2 - t
w2 = w2 - (t / 2)

n = (d + b2 + w2 - b - w) / 2
mult = ys * t * (b * n + (n ^ 2) / 2 + ((d - n) ^ 2) / 2 + b2 * (d - n) + w * (n - (w / 2))
        + w2 * (d - n - (w2 / 2)))

'The rolling radius :-
rr = brtr * t

'Calculation of the mpsh (Considering strain hardening)
mp = ys * (t ^ 2) / 4
ssh = us
mpsh = mp + (ssh - ys) * (t ^ 2) / 6
mp = mpsh

FOR mu = (muintv + (.001 / 180 * 3.141593)) TO mul STEP muintv

mu1 = mu - muintv
mu2 = mu + muintv
```

```
a = ((d ^ 2) - (c * SIN(mu) + d * COS(mu) - SQR((c ^ 2 - (c * COS(mu) - d *
SIN(mu)) ^ 2))) ^ 2) / (2 * d)
a1 = ((d ^ 2) - (c * SIN(mu1) + d * COS(mu1) - SQR((c ^ 2 - (c * COS(mu1) - d *
SIN(mu1)) ^ 2))) ^ 2) / (2 * d)
a2 = ((d ^ 2) - (c * SIN(mu2) + d * COS(mu2) - SQR((c ^ 2 - (c * COS(mu2) - d *
SIN(mu2)) ^ 2))) ^ 2) / (2 * d)

REM* MARGIN HALVING IS USED TO FIND THE m DATA POINTS.*
pt(1) = 1
pt(5) = mult
pt(3) = ((pt(5) - pt(1)) / 2) + pt(1)
count = 1
20 count = count + 1
  pt(4) = ((pt(5) - pt(3)) / 2) + pt(3)
  pt(2) = ((pt(3) - pt(1)) / 2) + pt(1)

FOR I = 1 TO 5
    I = INT(I)
    m = pt(I)

'START OF ENERGY EQUATION

    ' Left hand side expression
    lhs = 4 * m * muintv

    ' Right hand side of the work equation

    'Right side first expression
    hm1 = 2 * mp * (1 - (m / mult) ^ 2) * b2
    f3 = c * SIN(mu1) + d * COS(mu1) - SQR((d ^ 2 - 2 * a1 * d))
    CALL ASIN((f3 / c), f4)
    eta11 = f4 - mu1
    f5 = c * SIN(mu2) + d * COS(mu2) - SQR((d ^ 2 - 2 * a2 * d))
    CALL ASIN((f5 / c), f6)
    eta12 = f6 - mu2
    rhs1 = hm1 * eta12 - hm1 * eta11

    'Right side second expression
    hm2 = 2 * mp * (1 - (m / mult) ^ 2) * (b2 + a)
    eta21 = f4
    eta22 = f6
    rhs2 = hm2 * eta22 - hm2 * eta21
```

```
'Right side third expression
hm3 = 2 * mp * (1 - (m / mult) ^ 2) * b
rhs3 = hm3 * mu2 - hm3 * mu1

'Right side forth expression
hm4 = 2 * mp * (1 - (m / mult) ^ 2) * (d - a)
f7 = a1 / (d - a1)
CALL ASIN(f7, teta21)
f8 = a1 * COS(teta21)
teta41 = ATN((f8 / (SQR((d ^ 2 - 2 * a1 * d)) * TAN((ATN((c / d)) - mu1)))))
f9 = a2 / (d - a2)
CALL ASIN(f9, teta22)
f10 = a2 * COS(teta22)
teta42 = ATN((f10 / (SQR((d ^ 2 - 2 * a2 * d)) * TAN((ATN((c / d)) - mu2)))))
rhs4 = hm4 * teta42 - hm4 * teta41

'Right side fifth expression
zeta2 = ATN((c / d))
f11 = SQR((c ^ 2 + d ^ 2))
hm5 = 2 * mp * (1 - (m / mult) ^ 2) / (SQR(1 - .75 * ((m / mult) ^ 2) *
      ((SIN(zeta2)) ^ 2) * (4 - 3 * ((SIN(zeta2)) ^ 2)))) * f11
f12 = a1 / ((d - a) * SIN(zeta2))
CALL ASIN(f12, teta51)
f13 = a2 / ((d - a) * SIN(zeta2))
CALL ASIN(f13, teta52)
rhs5 = hm5 * teta52 - hm5 * teta51

'Right side sixth expression
hm6 = 2 * mp * (1 - (m / mult) ^ 2) / (SQR((1 - .75 * ((m / mult) ^ 2))))
eta61 = c * a1 / rr
eta62 = c * a2 / rr
rhs6 = hm6 * eta62 - hm6 * eta61

'Right side lip membrane expression at B
lmem1 = ys * t * eta21 * (w2 ^ 2) / 2
lmem2 = ys * t * eta22 * (w2 ^ 2) / 2
rhs7 = lmem2 - lmem1

'Right side lip mechanism at A and D
lhm1 = 4 * mp * (1 - (m / mult) ^ 2) * w2
lhm2 = 4 * mp * (1 - (m / mult) ^ 2) / (SQR(1 - .75 * ((m / mult) ^ 2) *
      ((SIN(beta)) ^ 2) * (4 - 3 * ((SIN(beta)) ^ 2)))) * w2 / (COS(beta))
f14 = COS((eta11 / 2)) - (SIN((eta11 / 2))) / TAN(beta)
CALL ACOS(f14, eta1011)
f15 = COS((eta12 / 2)) - (SIN((eta12 / 2))) / TAN(beta)
```

```
        llup = f15 * w * TAN(beta)

IF (llup = 0) OR (llup < 0) THEN GOTO 198
        CALL ACOS(f15, eta1012)

        f16 = 1 / (COS((eta11 / 2)) + SIN((eta11 / 2)) * (TAN(beta)))
        CALL ACOS(f16, f17)
        f18 = (SIN(f17)) / (SIN(beta))
        CALL ASIN(f18, eta1021)
        f19 = 1 / (COS((eta12 / 2)) + SIN((eta12 / 2)) * (TAN(beta)))
        CALL ACOS(f19, f20)
        f21 = (SIN(f20)) / (SIN(beta))
        CALL ASIN(f21, eta1022)
        rhs8 = (lhm1 * eta1012 - lhm1 * eta1011) + (lhm2 * eta1022 - lhm2 * eta1021)

        'Right side lip mechanism at K
        f22 = COS((mu1 / 2)) - (SIN((mu1 / 2))) / TAN(beta)
        CALL ACOS(f22, eta1111)
        f23 = COS((mu2 / 2)) - (SIN((mu2 / 2))) / TAN(beta)
        llup2 = f23 * w * TAN(beta)

IF (llup2 = 0) OR (llup2 < 0) THEN GOTO 198
        CALL ACOS(f23, eta1112)

        f24 = 1 / (COS((mu1 / 2)) + SIN((mu1 / 2)) * (TAN(beta)))
        CALL ACOS(f24, f25)
        f26 = (SIN(f25)) / (SIN(beta))
        CALL ASIN(f26, eta1121)
        f27 = 1 / (COS((mu2 / 2)) + SIN((mu2 / 2)) * (TAN(beta)))
        CALL ACOS(f27, f28)
        f29 = (SIN(f28)) / (SIN(beta))
        CALL ASIN(f29, eta1122)
        lhm3 = 4 * mp * (1 - (m / mult) ^ 2) * w
        lhm4 = 4 * mp * (1 - (m / mult) ^ 2) / (SQR(1 - .75 * ((m / mult) ^ 2) *
                ((SIN(beta)) ^ 2) * (4 - 3 * ((SIN(beta)) ^ 2)))) * w / (COS(beta))
        rhs9 = (lhm3 * eta1112 - lhm3 * eta1111) + (lhm4 * eta1122 - lhm4 * eta1121)


        rhs = rhs1 + rhs2 + rhs3 + rhs4 + rhs5 + rhs6 + rhs7 + rhs8 + rhs9


'END OF ENERGY EQUATION
```

```
        diff(I) = rhs - lhs
        diff(I) = ABS(diff(I))
NEXT I
IF diff(3) < .0000001 OR count = 500 THEN
        m = pt(3)
        GOTO 100
END IF
IF diff(2) < diff(4) THEN
        pt(5) = pt(3)
        pt(3) = pt(2)
ELSE
        pt(1) = pt(3)
        pt(3) = pt(4)
END IF

GOTO 20
100
PRINT "BINGO !"

'TO CONVERT MOMENT-ANGLE DATA TO MID SPAN LOAD-DEFLECTION
load = (4 * m / sl) / 1000
defln = sl / 2 * SIN(mu)


PRINT TAB(2); : PRINT USING "##.####"; (mu * 180 / 3.141593);
PRINT TAB(11); : PRINT USING "#########.##"; m;
PRINT TAB(25); : PRINT USING "###.#########"; diff(3);
PRINT TAB(40); : PRINT USING "###.#########"; adiffin
PRINT #1, TAB(1); : PRINT #1, USING "##.#######"; (mu * 180 / 3.141593);
PRINT #1, TAB(12); : PRINT #1, USING "#########.##"; m;
PRINT #1, TAB(28); : PRINT #1, USING "###.####"; load;
PRINT #1, TAB(38); : PRINT #1, USING "###.####"; defln;
PRINT #1, TAB(50); : PRINT #1, USING "####.###########"; diff(3);
PRINT #1, TAB(70); : PRINT #1, USING "###.###########"; adiffin

NEXT mu

CLOSE #1
GOTO 201
198 PRINT "LIP MECHANISM LOCK UP !"
  PRINT #1, "LIP MECHANISM LOCK UP AT MU = "; mu2 / 3.141593 * 180
GOTO 201
199 PRINT "ERROR IN FILE OR PROGRAM"
GOTO 300
```

```
   PRINT #1, "MECHANISM LOCK UP  CONDITION 1 AT MU="; mu2 /
                                                    3.141593 * 180
201 PRINT "FINISHED "
202 INPUT "TRY AGAIN "; resp$
IF resp$ = "Y" OR resp$ = "y" THEN GOTO 10
PRINT "PROGRAM TERMINATED"
300 END


SUB ACOS (value AS DOUBLE, angle AS DOUBLE)
x = value
angle = ATN((-x) / SQR((-x) * x + 1)) + 1.5708
END SUB


SUB ASIN (value AS DOUBLE, angle AS DOUBLE)
x = value
angle = ATN(x / SQR((-x) * x + 1))
END SUB
```

MSBZ2.bas

This program was designed to calculate load-deflection data for double span Zed section beams subjected to Uniformly Distributed Loads from collapse characteristics derived from single span beam moment-mu data (based on two stages of elastic beam solutions and the energy approach).

```
DEFDBL A-Z
DECLARE SUB asin (value, angle)
DECLARE SUB intp (f$, angle, moment)

10 CLS
ON ERROR GOTO 200
INPUT "MAT'L YIELD STRESS (N/mm^2)                 "; ys
INPUT "THICKNESS OF THE BEAM MAT'L (N/mm^2)  "; t
INPUT "TOP FLANGE WIDTH (mm)                       "; b
INPUT "BOTTOM FLANGE WIDTH (mm)                    "; b2
INPUT "WED DEPTH (mm)                              "; d
INPUT "TOP LIP SIZE (mm)                           "; w
INPUT "BOTTOM LIP SIZE (mm)                        "; w2
INPUT "FULL SPAN LENGTH (mm)                       "; sl
INPUT "FILENAME FOR DATA                           "; file$
file$ = "a:" + file$ + ".dat"
INPUT "FILENAME FOR THE CENTRAL SUP COLLAPSE DATA "; cfile$
cfile$ = "a:" + cfile$ + ".dat"
INPUT "FILENAME FOR SPAN COLLAPSE DATA       "; mfile$
mfile$ = "a:" + mfile$ + ".dat"
OPEN file$ FOR OUTPUT AS #1
PRINT #1, "MAT'L YIELD STRESS (N/mm^2)   :"; ys
PRINT #1, "MAT'L THICKNESS (mm)          :"; t
PRINT #1, "FLANGE WIDTH (mm)             :"; b
PRINT #1, "BOTTOM FLANGE WIDTH (mm)      :"; b2
PRINT #1, "WEB DEPTH (mm)                :"; d
PRINT #1, "LIP SIZE (mm)                 :"; w
PRINT #1, "BOTTOM LIP SIZE (mm)          :"; w2
PRINT #1, "SPAN (mm)                     :"; sl
PRINT #1, "CONSTRUCTED FROM              :"; cdfile$
PRINT #1, "DEFLECTN(mm)   LOAD(kN)"
PRINT #1, "----------------------  --------------"

' Convert d to centre line dimension
d = d - t
b = b - t
b2 = b2 - t
w = w - (t / 2)
```

```
w2 = w2 - (t / 2)

young = 207000

OPEN cfile$ FOR INPUT AS #2
INPUT #2, line$
INPUT #2, mum, mmax
CLOSE #2

OPEN mfile$ FOR INPUT AS #3
INPUT #3, line$
INPUT #3, mudm, mdmax
CLOSE #3

pratio = .3
q = d / b
IF (w = (b / 5)) OR (w > (b / 5)) THEN
      k = 5.4 - ((1.4 * q) / (.6 + q)) - (.02 * (q ^ 3))
      IF (k < 4) THEN k = 4
ELSE
      k = 1.28 - ((.8 * q) / (2 + q)) - .0025 * (q ^ 2)
      IF k < .425 THEN k = .425
END IF

Pcr = k * ((t / b) ^ 2) * (3.141593 ^ 2) * young / (12 * (1 - (pratio ^ 2)))

FOR avstr = 0 TO (10 * ys) STEP 1

IF (avstr < Pcr) THEN
' No Buckling
      bef = b

ELSE
' Elastic Buckling
      beff = b * ((1 + 14 * (((avstr / Pcr) ^ .5) - .35) ^ 4) ^ (-.2))
      beu = .89 * beff + .11 * b

      IF (w = (b / 5)) OR (w > (b / 5)) THEN
            bef = beff
      ELSE
            bef = beu
      END IF
END IF
```

```
h = (((d ^ 2) / 2) + (d * b2) + (w2 * d) - ((w2 ^ 2) / 2) + ((w ^ 2) / 2)) / (bef + d + b2
    + w + w2)

I1 = bef * (t ^ 3) / 12 + bef * t * (h ^ 2)
I2 = t * (h ^ 3) / 12 + t * (h ^ 3) / 4
I3 = t * ((d - h) ^ 3) / 12 + (d - h) * t * ((d - h) ^ 2) / 4
I4 = b2 * (t ^ 3) / 12 + b2 * t * ((d - h) ^ 2)
I5 = t * (w ^ 3) / 12 + w * t * ((h - (w / 2)) ^ 2)
I6 = t * (w2 ^ 3) / 12 + w2 * t * ((d - h - (w2 / 2)) ^ 2)
Ixx = I1 + I2 + I3 + I4 + I5 + I6

f1 = avstr * bef * t
f2 = (avstr / 2) * h * t
f3 = avstr * ((d - h) ^ 2) * t / (2 * h)
f4 = avstr * ((d - h) / h) * b2 * t
f5 = avstr * w * t * ((h - w) / h)
f6 = (avstr / 2) * w * t * (w / h)
f7 = avstr * w2 * t * ((d - h - w2) / h)
f8 = avstr / 2 * w2 * t * (w2 / h)

M = f1 * h + f2 * 2 * h / 3 + f3 * (2 / 3) * (d - h) + f4 * (d - h) + f5 * (h - (w / 2)) +
    f6 * (h - (w / 3)) + f7 * (d - h - (w2 / 2)) + f8 * (d - h - (w2 / 3))

wload = 8 * M / (sl ^ 2)
defln = (1 / (young * Ixx)) * wload * (sl ^ 4) / 192
mb = M
IF (mb = mmax) OR (mb > mmax) THEN GOTO 100

PRINT TAB(2); : PRINT USING "####.####"; defln;
PRINT TAB(16); : PRINT USING "###.####"; (wload / 1)
PRINT #1, TAB(2); : PRINT #1, USING "####.####"; defln;
PRINT #1, TAB(16); : PRINT #1, USING "###.####"; (wload / 1)

NEXT avstr

' Mid support collapsed
100

dinc = 0
xmax = (mmax / (wload * sl)) + (sl / 2)
l1 = xmax
l2 = sl - l1
    vmu1 = dinc / l1
    CALL asin(vmu1, mu1)
    mu1 = mu1 / 3.14159 * 180
```

```
        vmu2 = dinc / l2
        CALL asin(vmu2, mu2)
        mu2 = mu2 / 3.14159 * 180

        mu3 = (mu1 + mu2) / 2

        CALL intp(cfile$, mu1, m1)
        CALL intp(mfile$, mu3, m2)

        f1 = l1 * (SQR((1 - ((dinc ^ 2) / (l1 ^ 2)))))
        f2 = l2 * (SQR((1 - ((dinc ^ 2) / (l2 ^ 2)))))
        wloadf = ((m1 / f1) + (m2 * ((1 / f1) + (1 / f2)))) / (sl / 2)


FOR mu = 0 TO .174533 STEP .000174533#
mub = mu / 3.141593 * 180
CALL intp(cfile$, mub, mb)

wload = 24 * (young * Ixx * mu + mb * sl / 3) / (sl ^ 3)

defl1 = ((5 * wload * (sl ^ 4) / 384) - (mb * (sl ^ 2) / 16)) / (young * Ixx)

IF (mu = 0) THEN ddif = defl1
defl1 = defl1 - ddif
defl2 = (1 / (young * Ixx)) * wload * (sl ^ 4) / 192
defln = defl1 + defl2
xmax = (mb / (wload * sl)) + (sl / 2)

PRINT TAB(2); : PRINT USING "####.####"; defln;
PRINT TAB(16); : PRINT USING "###.####"; (wload / 1)
PRINT #1, TAB(2); : PRINT #1, USING "####.####"; defln;
PRINT #1, TAB(16); : PRINT #1, USING "###.####"; (wload / 1)

IF (wload = wloadf) OR (wload > wloadf) THEN GOTO 150

NEXT mu

' Collapsed at b and d
150     dlast = defln

l1 = xmax
l2 = sl - l1

PRINT l1
INPUT vynx
```

```
FOR dinc = .5 TO 1000 STEP .5

      vmu1 = dinc / l1
      CALL asin(vmu1, mu1)
      mu1 = mu1 / 3.14159 * 180

      vmu2 = dinc / l2
      CALL asin(vmu2, mu2)
      mu2 = mu2 / 3.14159 * 180

      mu3 = (mu1 + mu2) / 2

      CALL intp(cfile$, mu1, m1)
      CALL intp(mfile$, mu3, m2)

      f1 = l1 * (SQR((1 - ((dinc ^ 2) / (l1 ^ 2)))))
      f2 = l2 * (SQR((1 - ((dinc ^ 2) / (l2 ^ 2)))))
      wload = ((m1 / f1) + (m2 * ((1 / f1) + (1 / f2)))) / (sl / 2)

IF (l1 = (sl / 2)) OR (l1 > (sl / 2)) THEN
      dms = (sl / 2) / l1 * dinc
ELSE
      dms = (1 - ((sl / 2) - l1) / l2) * dinc
END IF

de = (1 / (young * Ixx)) * wload * (sl ^ 4) / 192
dec = de - dp
IF (dinc = .5) THEN dec = 0

      defl = dms + dlast + dec

PRINT TAB(2); : PRINT USING "####.####"; defl;
PRINT TAB(16); : PRINT USING "###.####"; (wload / 1)
PRINT #1, TAB(2); : PRINT #1, USING "####.####"; defl;
PRINT #1, TAB(16); : PRINT #1, USING "###.####"; (wload / 1)

dp = de
NEXT dinc

CLOSE #1
GOTO 201
200 PRINT "ERROR IN PROGRAM OR FILENAME"
GOTO 300
201 PRINT "FINISHED"
300 END
```

```
SUB asin (value, angle)
x = value
angle = ATN(x / SQR((-x) * x + 1))
END SUB


SUB intp (f$, angle, moment)
     OPEN f$ FOR INPUT AS #2

     INPUT #2, line$
     INPUT #2, x1, y1
     x0 = x1
     x1 = x1 - x0

1000   INPUT #2, x2, y2
     x2 = x2 - x0

     IF line$ = "" OR line$ = "EOF" THEN GOTO 20000

     IF angle > x1 AND angle < x2 THEN GOTO 2000
     IF angle = x1 THEN
          moment = y1
          GOTO 2500
     END IF
     IF angle = x2 THEN
          moment = y2
          GOTO 2500
     END IF

     x1 = x2
     y1 = y2
     GOTO 1000

2000     moment = (((angle - x1) / (x2 - x1)) * (y2 - y1)) + y1

2500
CLOSE #2
     GOTO 20010
20000 PRINT "Error in interpolation"
20010
END SUB
```

Appendix III

MAXIMUM BENDING MOMENT CAPACITY

According to BS 5950 : Part 5 : 1987

The following guidelines for the calculation of the bending capacity of thin-walled beam sections are based on the recommendations of BS 5950 : Part 5 : 1987, Section 5, for the design of members subject to bending.

For the sections examined in the current study, the moment capacity is determined on the basis of the limiting compressive stress in the stiffened webs, which is estimated from,

$$P_o = \left\{ 1.13 - 0.0019 \frac{d}{t} \left(\frac{\sigma_o}{280} \right)^{\frac{1}{2}} \right\} \sigma_o \qquad \text{Eqn.(A3.1)}$$

where P_o is the limiting compressive stress in the web
d is the overall web depth
t is the material thickness
and σ_o is the material yield strength.

The effective width of the compression flange of the beam is then worked out using Eqn.(2.3.2.3) or Eqn.(2.3.2.4), by substituting

$$f_c = P_o \qquad \text{Eqn.(A3.2)}$$

The second area of moment for the section is then calculated using the effective cross-sectional dimensions and the moment capacity is determined using

$$M_c = \frac{I_{eff}}{y_c} P_o \qquad \text{Eqn.(A3.3)}$$

where M_c is the bending moment capacity (BS 5950 : Part 5 : 1987)

I_{eff} is the effective section second area of moment

and y_c is the distance of the neutral axis of bending from the compression edge in the effective section.

For sections which satisfy the conditions stated in section 5.2.3.1 of the BS 5950 : Part 5, the plastic bending capacity is utilised according to the following criterion.

For sections with stiffened compression elements,

(a) for $\frac{b}{t} \le 25\left(\frac{280}{\sigma_o}\right)^{\frac{1}{2}}$ (plastic cross section)

$$M'_c = Mp$$

(b) for $\frac{b}{t} \ge 40\left(\frac{280}{\sigma_o}\right)^{\frac{1}{2}}$

$$M'_c = Mc$$

(c) for $25\left(\frac{280}{\sigma_o}\right)^{\frac{1}{2}} \le \frac{b}{t} \le 40\left(\frac{280}{\sigma_o}\right)^{\frac{1}{2}}$

$$M'_c = M_c + \frac{40\left(\frac{280}{\sigma_o}\right)^{\frac{1}{2}} - \frac{b}{t}}{15\left(\frac{280}{\sigma_o}\right)^{\frac{1}{2}}}(M_p - M_c)$$

Eqn.(A3.4)

where b is the full width of the compression flange
M_p is the fully plastic bending capacity
and M'_c is the modified moment capacity which includes plastic effects.

For sections with unstiffened compression elements

(a) for $\frac{b}{t} \leq 8\left(\frac{280}{\sigma_o}\right)^{\frac{1}{2}}$ (plastic cross section)

$$M'_c = M_p$$

(b) for $\frac{b}{t} \geq 13\left(\frac{280}{\sigma_o}\right)^{\frac{1}{2}}$

$$M'_c = M_c$$

(c) for $8\left(\frac{280}{\sigma_o}\right)^{\frac{1}{2}} \leq \frac{b}{t} \leq 13\left(\frac{280}{\sigma_o}\right)^{\frac{1}{2}}$

$$M'_c = M_c + \frac{13\left(\frac{280}{\sigma_o}\right)^{\frac{1}{2}} - \frac{b}{t}}{5\left(\frac{280}{\sigma_o}\right)^{\frac{1}{2}}}(M_p - M_c)$$

Eqn.(A3.5)